PLIOCENE STRATIGRAPHY AND THE IMPACT OF PANAMA UPLIFT ON CHANGES IN CARIBBEAN AND TROPICAL EAST PACIFIC UPPER OCEAN STRATIFICATION (6 – 2.5 MA)

PLIOZÄNE STRATIGRAPHIE UND DER EINFLUSS DES PANAMA-SEEWEGES AUF DIE STRATIFIZIERUNG DER OBERFLÄCHEN-WASSERMASSEN IN DER KARIBIK UND IM TROPISCHEN OST-PAZIFIK
(6 – 2.5 MA)

Kumulative Dissertation

zur Erlangung des Doktorgrades
der Mathematisch-Naturwissenschaftlichen Fakultät
der Christian-Albrechts-Universität
zu Kiel

vorgelegt
von

Silke Steph

Kiel, 2005

PLIOCENE STRATIGRAPHY AND THE IMPACT OF PANAMA UPLIFT ON CHANGES IN CARIBBEAN AND TROPICAL EAST PACIFIC UPPER OCEAN STRATIFICATION (6 – 2.5 MA)

PLIOZÄNE STRATIGRAPHIE UND DER EINFLUSS DES PANAMA-SEEWEGES AUF DIE STRATIFIZIERUNG DER OBERFLÄCHEN-WASSERMASSEN IN DER KARIBIK UND IM TROPISCHEN OST-PAZIFIK
(6 – 2.5 MA)

Kumulative Dissertation

zur Erlangung des Doktorgrades
der Mathematisch-Naturwissenschaftlichen Fakultät
der Christian-Albrechts-Universität
zu Kiel

vorgelegt
von

Silke Steph

Kiel, 2005

158 pages	52 figures	10 tables	8 appendices

Referent: _____

Koreferent: _____

Tag der Disputation: _____

Zum Druck genehmigt, Kiel, den: _____

Der Dekan: _____

ABSTRACT

This thesis examines the closure history of the Central American Seaway (CAS) and its effect on changes in ocean circulation and climate during the time interval from ~6 – 2.5 Ma. It was accomplished within the DFG Research Unit "Impact of Gateways on Ocean Circulation, Climate and Evolution" at the University of Kiel. Proxy records from Ocean Drilling Program (ODP) Sites 999 and 1000 (Caribbean), and from ODP Sites 1237, 1239 and 1241 (low-latitude east Pacific) are developed and examined. In addition, previously established proxy data from Atlantic Sites 925/926 (Ceara Rise) and 1006 (western Great Bahama Bank) and from two east Pacific sites (851, 1236) are included for interpretations. The main objectives of this study are (1) to acquire a consistent stratigraphic framework for all sites, (2) to reconstruct Pliocene changes in Caribbean and tropical east Pacific upper ocean water masses (i.e. temperature, salinity, thermocline depth), and (3) to identify potential underlying forcing mechanisms.

The stratigraphic framework was established by tuning benthic stable isotope records to orbitally tuned reference records (Sites 1241, 925/926). The orbital tuning procedure (Sites 1241, 1237) is based on matching cyclic variations in proxy records like benthic stable isotopes, percentage sand of the carbonate fraction, and shipboard logging data to the orbital solution of Laskar et al. (1993). The tuning results add up to one consistent benthic $\delta^{18}O$ stratigraphy for all Pliocene Caribbean and tropical east Pacific sediment sections. Accordingly, they provide an excellent opportunity for comparisons of Pliocene proxy records from different oceanic areas.

The assessment of Pliocene changes in Caribbean and tropical east Pacific upper ocean water mass signatures is achieved by a comparison of $\delta^{18}O$ records from shallow- and deep-dwelling planktonic foraminifers, indicative of salinity and temperature changes. These $\delta^{18}O$ records are partly combined with Mg/Ca-derived temperature records from the same foraminiferal species.

Pronounced sea surface salinity (SSS) gradients between the two Caribbean sites (999, 1000) after 4.7 – 4.2 Ma with lower salinities closer to the final gateway region indicate that the lateral expansion of the Pacific low salinity tongue into the Caribbean was strongly reduced. Besides, the inner-Caribbean SSS gradients reveal a strong variability on precessional time scales after 4.4 Ma, with higher SSS gradients during northern hemisphere summer insolation maxima. This suggests that the volume transport through the CAS varied on precession cycles, implying higher contributions of low-salinity Pacific inflow during northern hemisphere summer insolation minima, and a stronger influence of high-salinity Atlantic water masses during northern hemisphere summer insolation maxima.

With $\delta^{18}O_{G.\ sacculifer}$ values being significantly lower in the equatorial western Atlantic (Site 925, Ceara Rise) than at the Caribbean sites after 4.4 Ma, the possibility of a transfer of high-salinity water masses from the South Atlantic to the Caribbean can be excluded. Similar $\delta^{18}O_{G.\ sacculifer}$ values in the central Caribbean (Site 1000) and the Caribbean outflow region (Site 1006) indicate that high-salinity water masses left the Caribbean *via* the Florida Current, thereafter feeding the Gulf Stream. The combination of both results suggests the North Atlantic subtropical gyre as a possible source for Caribbean high-salinity surface waters during the Pliocene.

A warming and/or deepening of the Caribbean thermocline after 4.5 Ma indicates a strengthening of the Caribbean/West Atlantic Warm Pool. Concomitant to the thermocline-deepening in the Caribbean, the tropical east Pacific thermocline shoaled with a major subsurface cooling step between 4.5 and 4.0 Ma (Site 1241). Temperatures within the thermocline, though, remained relatively stable throughout the Pliocene, as indicated by Mg/Ca temperature reconstructions from Site 1241. The observed changes are in good agreement with numerical modeling results adressing the closure of the CAS that were carried out within the framework of the Research Unit "Ocean Gateways".

Strong mixed-layer temperature and/or salinity ($\delta^{18}O$) and nutrient ($\delta^{13}C$) gradients between the equatorial east Pacific (Site 1239) and the east Pacific North Equatorial Counter Current region (Site 1241), especially after 4.5 Ma, do not support the scenario of a "permanent El Niño-like state" during the Pliocene.

KURZFASSUNG

Die Auswirkungen der Schließung des Panama-Seeweges auf Ozeanzirkulation und Klima für den Zeitabschnitt von ~6 – 2.5 Mio. J.v.h. (Millionen Jahren vor heute) stehen im Mittelpunkt dieser Studie, die innerhalb der DFG Forschergruppe "Ozeanpassagen" an der Universität Kiel durchgeführt wurde. Im Rahmen dieser Arbeit wurden Proxy-Kurven von Ocean Drilling Program (ODP) Sites 999 und 1000 (Karibik) und von ODP Sites 1237, 1239 und 1241 (tropischer Ost-Pazifik) erstellt und untersucht. Bereits vorhandene Proxy-Daten vin den atlantischen ODP Sites 925/926 (Ceara Rise) und 1006 (Bahama-Bank) sowie von zwei ost-pazifischen Sites (851, 1236) wurden für Vergleiche und Interpretationen herangezogen. Die wesentlichen Zielsetzungen umfassten: (1) die Erarbeitung einer einheitlichen Stratigraphie, (2) die Rekonstruktion von pliozänen Veränderungen in den oberflächennahen Wassermassen der Karibik und des tropischen Ost-Pazifiks (z.B. Temperatur, Salzgehalt, Thermoklinentiefe) und (3) die Abschätzung der Steuerungsmechanismen für diese Veränderungen.

Das stratigraphische Gerüst wurde durch die Anpassung benthischer Sauerstoff-Isotopenkurven an astronomisch kalibrierte Referenzkurven (Sites 1241, 925/926) erstellt. Die astronomische Kalibrierung (Sites 1237, 1241) basiert auf der Anpassung von Proxy-Daten (z.B. benthischen $\delta^{13}C$ Kurven, Sandgehalten (%) der Karbonatfraktion und Kernlogging-Daten) an berechnete Orbitalparameter. Die daraus resultierende einheitliche Stratigraphie ergab die Möglichkeit, die pliozänen Sedimentkerne der Karibik und des Pazifiks direkt miteinander zu vergleichen.

Die Rekonstruktion pliozäner Veränderungen in den oberflächennahen Wassermassen basiert auf einem Vergleich von $\delta^{18}O$-Kurven für flach- und tieflebende planktonische Foraminiferen (Anzeiger für Temperatur und Salzgehalt). Diese wurden zum Teil mit Mg/Ca-Temperatur-Rekonstruktionen für die gleichen Foraminiferenarten kombiniert.

Nach 4.7 – 4.2 Mio. J.v.h. entwickelten sich ausgeprägte Unterschiede im Salzgehalt der oberflächennahen Wassermassen zwischen den karibischen Sites 999 und 1000. Höhere Salzgehalte in größerer Entfernung zu den letzten Öffnungen des Panama-Seeweges weisen darauf hin, dass die laterale Ausdehnung der salzärmeren pazifischen Wassermassen in die Karibik hinein zu dieser Zeit stark eingeschränkt war. Außerdem zeigen die inner-karibischen Unterschiede im Salzgehalt der oberflächennahen Wassermassen nach 4.4 Mio. J.v.h. eine ausgeprägte Variabilität auf Präzessions-Zyklen. Dabei gehen höhere Unterschiede im Salzgehalt zwischen Sites 999 und 1000 in der Regel mit Maxima in der Nordhemisphären-Sommerinsolation einher. Dies deutet auf einen stärkeren Einstrom von salzärmeren pazifischen Oberflächen-Wassermassen während Minima – und auf einen verstärkten Einfluss von salzreicheren atlantischen Wassermassen während Maxima in der Nordhemisphären-Sommerinsolation hin.

Ein Transfer von salzreicheren Wassermassen aus dem Südatlantik in die Karibik nach etwa 4.4 Mio. J.v.h. kann ausgeschlossen werden, da die $\delta^{18}O$-Werte von *G. sacculifer* im äquatorialen West-Atlantik (Ceara Rise, Site 925) deutlich geringer waren als in der Karibik (Site 1000). Ähnliche $\delta^{18}O$-Werte von *G. sacculifer* in der zentralen Karibik (Site 1000) und in der karibischen Ausstrom-Region (Site 1006) zeigen jedoch, dass salzreiche Oberflächen-Wassermassen aus der Karibik den Golfstrom speisten. Eine Verknüpfung dieser Ergebnisse schlägt die nordatlantische subtropische Gyre als Quellregion für salzreiche karibische Oberflächen-Wassermassen vor.

Eine Erwärmung der karibischen Thermokline nach 4.5 Mio. J.v.h. deutet auf eine Verstärkung des atlantisch-karibischen Warmwasser-Pools hin. Gleichzeitig zeigt eine starke Abkühlung am Fuß der photischen Zone zwischen 4.5 Ma und 4.0 Ma eine Verflachung der Thermokline im tropischen Ost-Pazifik (Site 1241). Mg/Ca-Temperatur-Rekonstruktionen deuten jedoch darauf hin, dass die Thermoklinen-Temperatur im Ost-Pazifik im Verlauf des Pliozäns relativ konstant war. Diese Beobachtungen stimmen gut mit Modellierungsergebnissen der Forschergruppe "Ozeanpassagen" überein.

Unterschiede im $\delta^{18}O$ und $\delta^{13}C$ von *G. sacculifer* zwischen Site 1239 (äquatorialer Ost-Pazifik) und Site 1241 (nord-äquatorialer Gegenstrom), speziell im Zeitabschnitt von 4.5 – 2.5 Mio. J.v.h., weisen auf Unterschiede in der Temperatur und im Nährstoffgehalt der oberflächennahen Wassermassen hin. Die Annahme eines permanenten El Niño-Zustandes im Pliozän wird durch diese Hinweise nicht unterstützt.

Danksagung

Ohne die Hilfe und Unterstützung vieler freundlicher Menschen wäre diese Arbeit nicht möglich gewesen. Ihnen und euch allen möchte ich an dieser Stelle ein Dankeschön sagen.

Herrn Prof. W.-Chr. Dullo möchte ich herzlich dafür danken, dass er mir ermöglicht hat, diese Promotion am IFM-GEOMAR durchzuführen. Ein weiterer Dank gilt natürlich Herrn Prof. Wolfgang Kuhnt und Priv. Doz. Dr. Dirk Nürnberg, die sich zur Übernahme des Koreferates bereit erklärt haben.

Dr. Ralf Tiedemann und Dr. Dirk Nürnberg sei dafür gedankt, dass sie dieses Projekt im Rahmen der DFG Forschergruppe "Ozeanpassagen" ins Leben gerufen haben. Hier auch ein herzlicher Dank an Herrn Prof. M. Sarnthein. Ohne Ihr Zutun und Engagement gäbe es keine Forschergruppe "Ozeanpassagen"!

Das größte Dankeschön geht hier natürlich an Dr. Ralf Tiedemann für die intensive Betreuung und Unterstützung, sowie für zahlreiche Ratschläge, Hilfestellungen, Tips und Tricks. Vor allem danke ich dir für die Zeit und Energie, die du in so manch eine engagierte Diskussion gesteckt hast!

An dieser Stelle auch nochmals vielen Dank an Dr. Dirk Nürnberg für die Unterstützung und für viele Anregungen. Ein besonderer Dank an Dr. Joachim Schönfeld für viele gute Ideen und manch eine kritische Anmerkung.

Ich bedanke mich ganz herzlich bei Lulzim Haxhiaj für die große Unterstützung im Isotopenlabor. Silvia Koch danke ich für die Hilfe bei Reinigung und Messung der Mg/Ca-Proben. Für das gute Gelingen der Mg/Ca-Messungen auch ein herzlicher Dank an Dr. Dieter Garbe-Schönberg. Nicht zu vergessen sind hier natürlich die studentischen Hilfskräfte: Anna Jesußek, Ulrike Nielsen, Kerrin Wittmaack, und Nicole Gau und deren freundliche und tatkräftige Mitarbeit bei der Probenaufbereitung.

Ein Dank auch an alle Kollegen der Forschergruppe – sowohl am IFM-GEOMAR, als auch "drüben" an der Uni. Jeroen Groeneveld möchte ich für die erfolgreiche Zusammenarbeit während der letzten drei Jahre danken. Ein herzliches Dankeschön an Dr. Hanno Kinkel – nicht nur für die Erstellung der REM-Bilder, sondern auch für viele Diskussionen. Dr. Andreas Schmittner sei für die produktive Zusammenarbeit und für die Bereitstellung der Modellierungsergebnisse gedankt. A big 'thank you' also to Daniela Crudeli for the discussions and the exchange of ideas. Hier geht außerdem auch ein Dankeschön an Jenny Lezius, Prof. John Reijmer und Dr. Mara Weinelt.

Die Diskussion und der Ideenaustausch mit meinen Kollegen und Mit-Doktoranden am IFM-GEOMAR war sehr wichtig für das Gelingen dieser Arbeit. Ich bedanke mich besonders bei Dr. Lars Reuning für die freundschaftliche und konstruktive Zusammenarbeit – und für Diskussionen über Präzessions- und Semi-Präzessionszyklen von **I** bis **Z**. Dr. Arne Sturm möchte ich an dieser Stelle einen lieben Dank für all die kleinen und großen Hilfestellungen im Laufe der Jahre sagen. An Marcus Regenberg ein Dank für viele Diskussionen über die Habitattiefen von planktischen Foraminiferen. Danke auch an Lester Lembke-Jene dafür, dass er mir manch einen Messtag überlassen hat – und dafür, dass du immer Zeit für Diskussionen hattest.

Thanks to Dr. W.P. Chaisson and Dr. Ann Holbourn for your help with the species determination – I would never have been able to distinguish all those forams without your knowledge.

Ein besonderer Dank auch an Prof. Gerald Haug für die gute Zusammenarbeit, sowie an Dr. Stefan Mulitza und Dr. Carsten Rühlemann für aufschlussreiche Diskussionen und viele wertvolle Hinweise.

Ein großes Dankeschön auch an meine Freunde am IFM-GEOMAR für die Unterstützung: Arne Sturm, Lars Reuning, Oliver Bartdorff, Peter Thierer (Peter, ein spezieller Dank natürlich auch für all das Korrekturlesen in den letzten Wochen!) Reinhard Kozdon, Silke Hauff und Thor Hansteen. Dafür natürlich auch einen lieben Dank an all die "fernab vom IFM-GEOMAR" – speziell an Martina Halmer (auch fürs Türschild, gell?), Shungo Kawagata, Hiroshi Kawamura, Burkhard Schramm, Andreas Klügel, André Kaiser und Nick Krmek.

The samples for this study were provided by the Ocean Drilling Program (ODP).

Diese Arbeit wurde von der DFG im Rahmen der Forschergruppe "Ocean Gateways" finanziell unterstützt (Projekt FOR 451, Ti240/12-1 und 12-2).

Meinem Vater Heinz-Henning Steph kann ich für die Unterstützung während meines gesamten Studiums gar nicht oft genug danken. Für die finanzielle Unterstützung auch ein besonderer Dank an meine Großeltern in Braunschweig und in Seesen.

CONTENTS

APPENDICES A

CHAPTER 1

INTRODUCTION

The opening and closure of oceanic gateways have long been considered as important mechanisms that altered ocean circulation and affected global climate (e.g. Weyl, 1968; Berggren and Hollister, 1974; Berger et al., 1981; Haq, 1981; Keigwin, 1982a). During the nineties, simulations with ocean general circulation models that tested the effects of oceanic gatways on ocean circulation (e.g. Drake Passage, Panama Gateway, Indonesian Gateway) highlighted the need for a more detailed understanding of gateway dynamics in order to determine their role for climate change (e.g. Maier-Reimer et al., 1990; Mikolajewicz et al., 1993; Hirst and Godfrey, 1993; Heinze and Crowley, 1997; Mikolajewicz and Crowley, 1997). By the same time, theoretical considerations suggested that the opening of high-latitude gateways (e.g. Drake Passage, Tasman Gateway, Bering Strait) and the closure of low-latitude gateways (e.g. Indonesian Gateway, Panama Gateway) during the last ~50 million years contributed to the long-term Cenozoic cooling trend (e.g. Berger and Wefer, 1996). This significantly stimulated the paleoceanographic community to further examine the role of changes in the configuration of oceanic gateways. In this context, the Kiel paleoceanographic research group provided basic insights into the impact of the closure of the Central American Seaway (CAS) on ocean circulation and climate (e.g. Tiedemann and Franz, 1997; Haug and Tiedemann, 1998; Haug et al., 2001a). In 2001, further call for paleoceanographic evidence resulted in the formation of the DFG Research Unit "Impact of Gateways on Ocean Circulation, Climate and Evolution" at the University of Kiel. This thesis was accomplished within the sub-project "Impact of low-latitude Gateways on the formation of Warm Water Pools, Ocean Circulation, and Climate". The overall goal of the study was to gain further insights into Pliocene ocean-atmosphere processes that were associated with the closure of the CAS.

1.1 Aim of the study, strategy, and structure of the thesis

1.1.1 Aim of the study

The major aims of this thesis were: (1) the identification of Pliocene changes in Pacific and Caribbean upper ocean water mass signatures (temperature, salinity, thermocline depth) that probably resulted from the shoaling of the CAS, (2) to detect linkages between Pacific and Caribbean changes in oceanography, and (3) to identify potential forcing mechanisms. The study focused on the time interval from ~6 – 2.5 Ma. This period includes a critical threshold in the closure history of the CAS when surface water exchange between the Pacific and the Caribbean became significantly restricted (e.g. Keigwin, 1982a; Haug et al., 2001a; see chapter 1.2 for background information).

More specifically, this thesis focused on the following goals:

- to generate an orbitally tuned stratigraphic framework for sediment cores that are relevant for examining the Pliocene closure history of the CAS,
- to detect changes in Pacific-Caribbean and Atlantic-Caribbean surface water exchange during the Pliocene shoaling of the CAS, and to identify the Pliocene source regions of Atlantic inflow into the Caribbean,
- to evaluate potential forcing mechanisms that controlled variations in Caribbean sea surface salinity (SSS) and sea surface temperature (SST) on orbital timescales, before and after the major restriction of Pacific-Caribbean surface water exchange,
- to reconstruct the formation and thermal evolution of the Caribbean/Atlantic Warm Water Pool in response to the shoaling of the CAS,
- to determine Pliocene variations in tropical east Pacific upper ocean water mass signatures and thermocline depth, and to identify the link between the observed changes and the shoaling of the CAS,
- to differentiate between the impact of the shoaling of the CAS and the impact of changes in the configuration of the Indonesian Gateway on changes in tropical east Pacific upper ocean circulation,
- to test the hypothesis of a Pliocene "permanent El Niño-like state" in the tropical east Pacific,
- to examine changes in Caribbean/Atlantic intermediate water ventilation (probably resulting from the restriction of Pacific-Caribbean surface water exchange).

1.1.2 Strategy

- Selection of site locations

Four ODP sites from key positions were chosen for this study: Two ODP sites from the Caribbean (Sites 999, 1000), and two ODP sites from the tropical east Pacific (Sites 1239, 1241). In addition, southeast Pacific Site 1237 was incorporated in establishing an orbitally tuned Pliocene age model. These sites offer a temporal resolution suffiscient for examining orbital-scale variations, as well as complete, or nearly complete Pliocene sediment sections. In addition, existing paleoceanographic data from other site locations, especially from Sites 925/926 (tropical west Atlantic), Site 1006 (western Great Bahama Bank), and from Sites 851 (equatorial east Pacific) and 1236 (central east Pacific) were taken into account for the interpretations. More detailed information about the selection of sites and the quality of sample material is given in chapter 2.

- Establishment of consistent age models

For comparisons of proxy records from different site locations it is essential to establish a consistent high-resolution stratigraphic framework. The age models are either based on tuning cyclic variations in proxy records (e.g. benthic stable isotopes, percentage sand of the carbonate fraction, shipboard logging data) to the orbital solution of Laskar et al. (1993), or on the correlation of benthic stable isotope records to the already orbitally tuned benthic stable isotope records from Sites 925/926 or 1241. Chapter 3 provides basic information about the tuning methods and the quality of the resulting age models. A detailed description of the age models and the tuning procedure is given in chapters 4 (Pacific sites) and 5 (Caribbean sites).

- Reconstruction of upper water column characteristics

To determine paleotemperatures and salinities in the upper water column, a combined approach of measuring Mg/Ca ratios (proxy for temperature) and $\delta^{18}O$ (proxy for temperature, salinity and global ice volume) on the same planktonic foraminiferal species was used (Shackleton, 1974; Nürnberg et al., 1996; Lea et al., 1999; Elderfield and Ganssen, 2000). Measuring both proxies on the same taxa excluded interfering seasonality and/or habitat effects that may occur if proxy data from different faunal groups are used. The combination of both geochemical tracers allows to seperate the temperature signal from the $\delta^{18}O$ signal, and to extract the residual $\delta^{18}O_{water}$ record indicative of changes in salinity and ice volume (Nürnberg et al., 1996).

The thermal structure within the upper water column was determined by the comparison of $\delta^{18}O$ and Mg/Ca records from planktonic foraminifers with different preferred habitat depths (*G. sacculifer*, *G. limbata*, *N. dutertrei*, *G. tumida*; **Fig. 1-1**). Several studies demonstrated that the isotopic offset between different species of planktonic foraminifers reflects the temperature range within the photic zone in the tropics (e.g. Ravelo and Fairbanks, 1992; Ravelo and Shackleton, 1995; Cannariato and Ravelo, 1997; Ravelo and Andreasen, 1999; Chaisson and Ravelo, 2000; Faul et al., 2000). This approach was suggested to provide information about the depth of the thermocline. In general, the temperature range, and thus the isotopic offset in $\delta^{18}O$, should be large when the thermocline is shallow, and small when the thermocline is deep. Since oxygen isotopes are biased by both, temperature changes and variations in $\delta^{18}O_{seawater}$, it is important to include

Mg/Ca ratios into the interpretations in order to differentiate the temperature signal from the salinity signal (for further information see chapter 6).

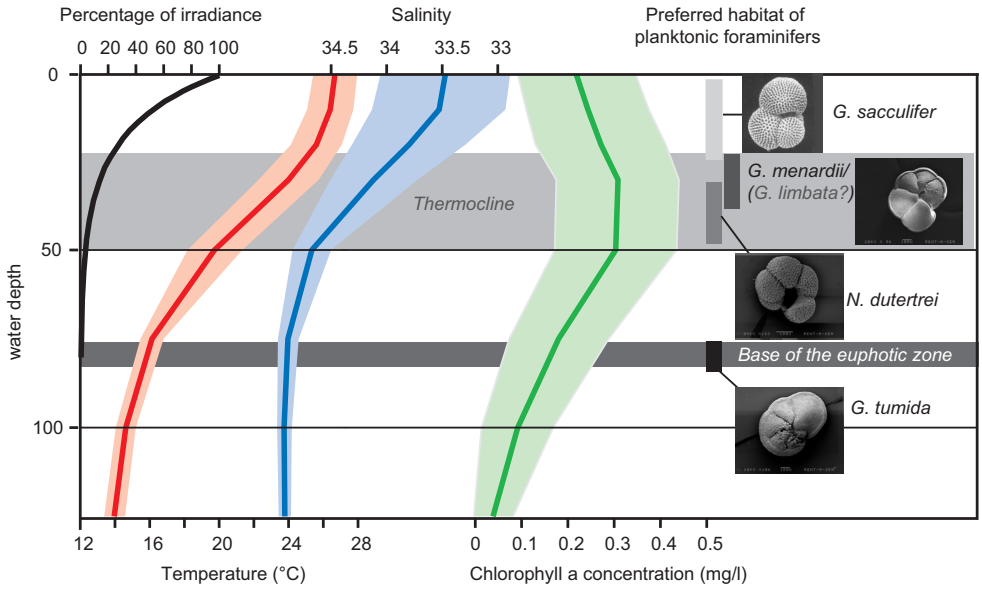

Fig. 1-1 Modern annual-average properties of the upper water column for the tropical east Pacific and assumed habitat depths for the species used in this study. Atlas data on physical and chemical properties are from Ocean Climate Laboratory (2001), squares 7008 and 7009 (10°N/100°W-0°N, 80°W). Data from the Caribbean were excluded. Thick lines indicate the mean values, and shaded areas show the range of standard devitation. Red: temperature, blue: salinity, green: chlorophyll a concentration. Black line: percentage of irradiance, data taken from Enfield and Lee (submitted); the 0.1 % irradiance level is defined as the base of the euphotic zone. The gray area indicates the thermocline as zone with the highest vertical temperature gradient. Bars to the right indicate the range of preferred habitat depths for *G. sacculifer* (mixed-layer), *G. menardii* (*G. limbata*?) (upper thermocline), *N. dutertrei* (lower thermocline) and *G. tumida* (bottom of the photic zone).

- Comparisons with numerical model results

The comparison of proxy data (Mg/Ca and $\delta^{18}O$) to numerical modeling studies with the UVic Earth System Climate Model (ESCM) allows to further evaluate the impact of the Panama closure on Pliocene changes in Caribbean and tropical east Pacific upper ocean stratification. The modeling study provided simulations for different sill depths of the CAS (without considering changes in the Indonesian throughflow) (A. Schmittner, pers. comm.). This comparison is especially important for the interpretation of Pliocene paleoceanographic proxy records from the tropical east Pacific, as it gives additional information about possible overlapping effects caused by other forcing mechanisms (including e.g. Pliocene changes in the configuration of the Indonesian Gateway). Chapter 7 gives information about the model setup used for the simulations.

- Assessment of changes in intermediate and deep water ventilation

Several studies have documented that $\delta^{13}C$ values of the epibenthic foraminifer *C. wuellerstorfi* approximately equal bottom water $\delta^{13}C_{DIC}$ (dissolved inorganic carbon), and are thus a valuable proxy for the reconstruction of deep water ventilation (e.g. McCorkle and Keigwin, 1994). High $\delta^{13}C$ values indicate low nutrient and low CO_2 concentrations and well ventilated (high O_2) water

masses. This signature is typical for young intermediate and deep water masses. With increasing age, the $\delta^{13}C$ values of sub-surface water masses continually decrease due to the oxidation of ^{12}C-rich organic matter. Organic matter with low $\delta^{13}C$ from surface waters is subsequently oxidized and remineralized in the deeper ocean, leaving high $\delta^{13}C$ values in nutrient-poor surface waters and lowering $\delta^{13}C$ values in deep, nutrient-rich waters. Information about the $\delta^{13}C$ signatures of modern Atlantic intermediate and deep water masses is provided in chapter 9.

1.1.3 Structure of the thesis

This thesis has been divided into three main parts:

The first part serves as an introduction (chapters 1 – 3). Chapter 1.2 provides background information about Pliocene climate and ocean circulation, and about the closure history of the CAS. Chapter 2 gives a short overview about site locations and quality of the sample material, and chapter 3 includes a general introduction into sample treatment, analytical methods and stratigraphy. An outline about the modern oceanographic setting of the study area is included in chapters 5 (Caribbean) and 6 (tropical east Pacific).

The second part (chapters 4 – 9) presents and discusses the results of this thesis. Chapters 4 – 6 are manuscripts submitted to scientific journals. Chapters 7 – 9 review the actual state of research and provide an extended summary of planned publications.

- Chapter 4 focusses on the orbitally tuned stratigraphy of Pliocene sediment records from the tropical east Pacific (including Sites 1237, 1241, and 1239).
- Chapter 5 evaluates changes in Caribbean surface hydrography during the Pliocene shoaling of the CAS, and discusses possible forcing mechanisms. Furthermore, this chapter includes the Pliocene benthic $\delta^{18}O$ stratigraphy for Caribbean Site 1000.
- Chapter 6 discusses Pliocene changes in tropical east Pacific upper ocean stratification and possible linkages to tropical gateway dynamics (Site 1241).
- Chapter 7 combines proxy evidence for changes in Caribbean and tropical east Pacific upper ocean water mass signatures with numerical model results for different stages in the shoaling of the CAS.
- Chapter 8 presents the actual state of work with regard to testing the Pliocene "permanent El Niño-hypothesis".
- Chapter 9 provides new information concerning Pliocene changes in Caribbean/Atlantic intermediate water ventilation.

The third part (chapter 10) summarizes the main conclusions of the previous chapters (4 – 9).

The references cited in chapters 1 – 10 are listed in a combined reference chapter at the end of the thesis (chapter 11). All data that were generated by the author within the framework of this thesis are provided in the appendices (A1 – A7).

1.2 Background information

1.2.1 Pliocene climate and ocean circulation

The Pliocene is the most recent interval in Earth's history in which oceanographic and climatic conditions can be studied in context of global warmth relative to today. Evidence is abundant that Pliocene global surface temperatures were on average 3.5 °C warmer than modern ones (e.g. Sloan et al., 1996), and therefore comparable to those predicted for the 21st century (2.1 – 4.6 °C warming, Houghton et al., 1996; Houghton, 1997). High-latitude sea-surface temperatures (SSTs) may have been elevated by as much as 7 °C, and mid-latitude SSTs by about 3 – 4 °C with respect to the modern values. Interestingly, estimates of low-latitude SSTs show no significant difference from the present (Dowsett and Poore, 1991; Dowsett et al., 1992; 1994; 1999). Global ice volume was significantly reduced during the Pliocene warm period (sea-level was about 25 – 30 m higher than modern; Dowsett and Cronin, 1990, Dowsett et al., 1999), and the northern hemisphere lacked a permanent ice cap. $\delta^{18}O$ records of benthic foraminifers indicate that the amplitude of early-middle Pliocene ice volume fluctuations was significantly smaller than during the latest Pliocene and Pleistocene (e.g. Shackleton et al., 1995; Tiedemann et al., 1994) (**Fig. 1-2**).

Even though past warm periods are no direct analogs for future transient climate change, they are indicative of oceanic and cryospheric equilibrium responses and feedbacks in in a warm world.

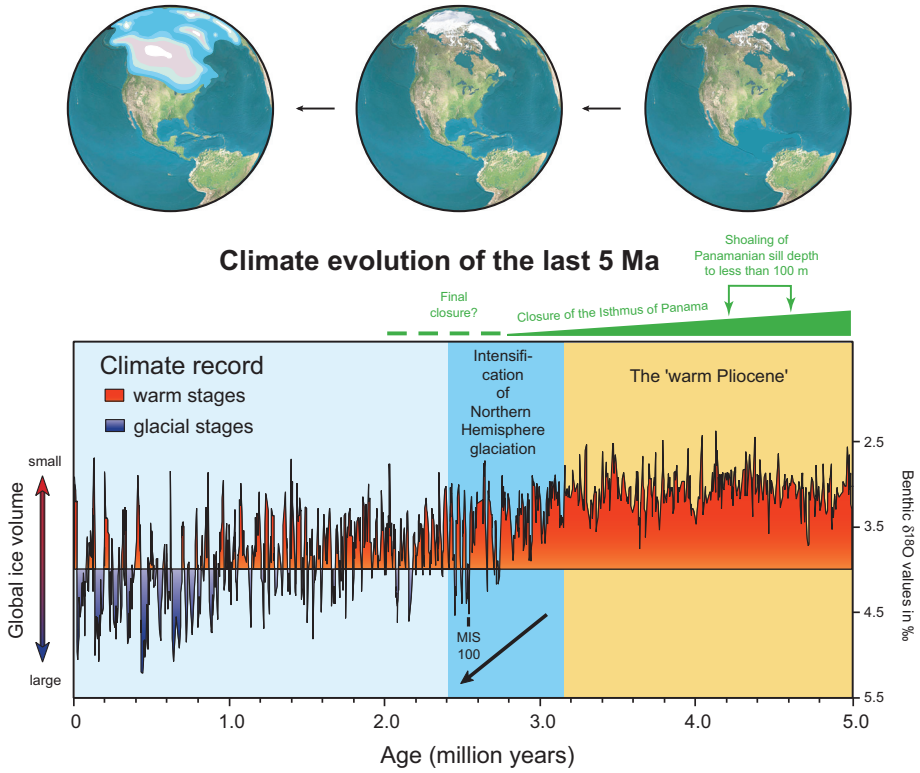

Fig. 1-2 Climate record of the last 5 Ma as indicated by benthic $\delta^{18}O$ isotope values (Tiedemann et al., 1994). The Pliocene closure history of the Isthmus of Panama, the warm Pliocene, and the onset of the Northern Hemisphere glaciation are highlighted (by courtesy of Ralf Tiedemann).

The reasons for early to middle Pliocene global warmth are not yet clear. In a review paper, Crowley (1996) summarized several possible forcing factors, such as changing atmospheric CO_2 levels, orographic effects related to late Cenozoic uplift, and/or changes in meridional heat transport (Rind and Chandler, 1991). Each of these mechanisms is not necessarily exclusive, as, for example, thermohaline circulation (THC) plays a significant role in regulating global climate by redistributing heat and influencing the rate of CO_2 exchange between the ocean surface and the deep ocean (Broecker, 1997).

Although a doubling of the preindustrial atmospheric CO_2 level from 280 ppm to 560 ppm may account for a global temperature increase of 2.1 – 4.6 °C (Houghton et al., 1996), which is comparable to the temperature increase during the Pliocene warm period, there are two important points that argue against significantly higher Pliocene atmospheric CO_2 levels. (1) Paleo-reconstructions based on interpretations from the carbon isotopic composition of organic matter (Raymo et al., 1996) and from stomatal counts on Pliocene leafs (van der Burgh et al., 1993) suggest that Pliocene atmospheric CO_2 was not dramatically elevated with respect to the modern. The average Pliocene CO_2 level of 380 ppm (peaking at 425 ppm) that was suggested by Raymo et al. (1996) is only 35 % higher than preindustrial levels (280 ppm), and less than 10 % higher than the present level (360 ppm; Intergovernmental Panel on Climate Change, 2001). (2) An increase in atmospheric CO_2 is expected to cause a global increase in SSTs (including the tropics) as suggested by model results. Such an increase in tropical SSTs, however, has not been documented for the Pliocene warm period.

In the absence of large changes in radiative forcing directly due to CO_2, Pliocene warmth was alternatively explained by enhanced oceanic heat transport (e.g. Rind and Chandler, 1991; Dowsett et al., 1992; Raymo et al., 1996; Billups et al., 1998), whereas Kim and Crowley (2000) hypothesize that enhanced THC was rather a consequence of Pliocene warming than a primary cause. In general, Ocean General Circulation Models (OGCMs) have shown that North Atlantic Deep Water (NADW) production would rather decrease when atmospheric CO_2 increases (Mikolajewicz et al., 1990; Manabe et al., 1991). In contrast to these modeling studies, proxy data indicate that the relative abundance of NADW in the ocean basins was high during the middle Pliocene, although the atmospheric CO_2 level was probably slightly elevated (Raymo et al., 1992; 1996; Ravelo and Andreasen, 2000). This is corroborated by studies that show an increase in Northern Component Deep Water (NCDW) formation during the early Pliocene (e.g. Haug and Tiedemann, 1998) that was attributed to the concomitant shoaling of the Central American Seaway (CAS) and a related strengthening of the Gulf Stream system (see chapter 1.2.2). Stronger thermohaline overturn has been proposed to reduce the equator-to-pole temperature gradient during the Pliocene by increasing the meridional heat transport to high latitudes (Dowsett et al., 1992; 1994; Chandler et al., 1994). The associated increase in high-latitude SSTs may then have provided a feedback mechanism that kept climate warm by inhibiting the formation of sea ice and thus reducing sea-ice albedo (Raymo et al., 1996). Indeed, faunal assemblages indicate ice-free conditions over most or all of the Arctic Ocean (Cronin et al., 1993; Dowsett et al., 1999). Furthermore, modeling studies imply that surface wind strength over the North Atlantic, North

Pacific, and Southern Ocean was probably higher than today, suggesting that the geostrophic gyre circulation may have been enhanced during the middle Pliocene (Haywood et al., 2000; 2002).

Another mechanism to maintain a weaker meridional temperature gradient during the early Pliocene can be inferred from intensification of the Hadley Circulation as suggested by Molnar and Cane (2002). They argued that a "permanent El Niño-like state" in the Pacific might have led to a spin-up of atmospheric heat transport to northern high latitudes during the early Pliocene, resulting in a warmer climate, especially in Alaska and Canada. Proposing a "permanent El Niño-like state" for the Pacific makes the Pliocene time interval even more interesting, as the current rise in the concentration of greenhouse gases may cause a return to such permanent El Niño conditions (Philander and Fedorov, 2003). This state would *i.a.* be characterized by a relatively warm equatorial east Pacific, a strongly reduced temperature gradient between the West Pacific Warm Pool (WPWP) and the equatorial east Pacific, a possible relaxation of the southeast trade winds, and a relatively deep thermocline in the east Pacific (Wallace, 1998) (**Fig.1-3**). However, the paleoceanographic evidence for a Pliocene El Niño-like state is controversial.

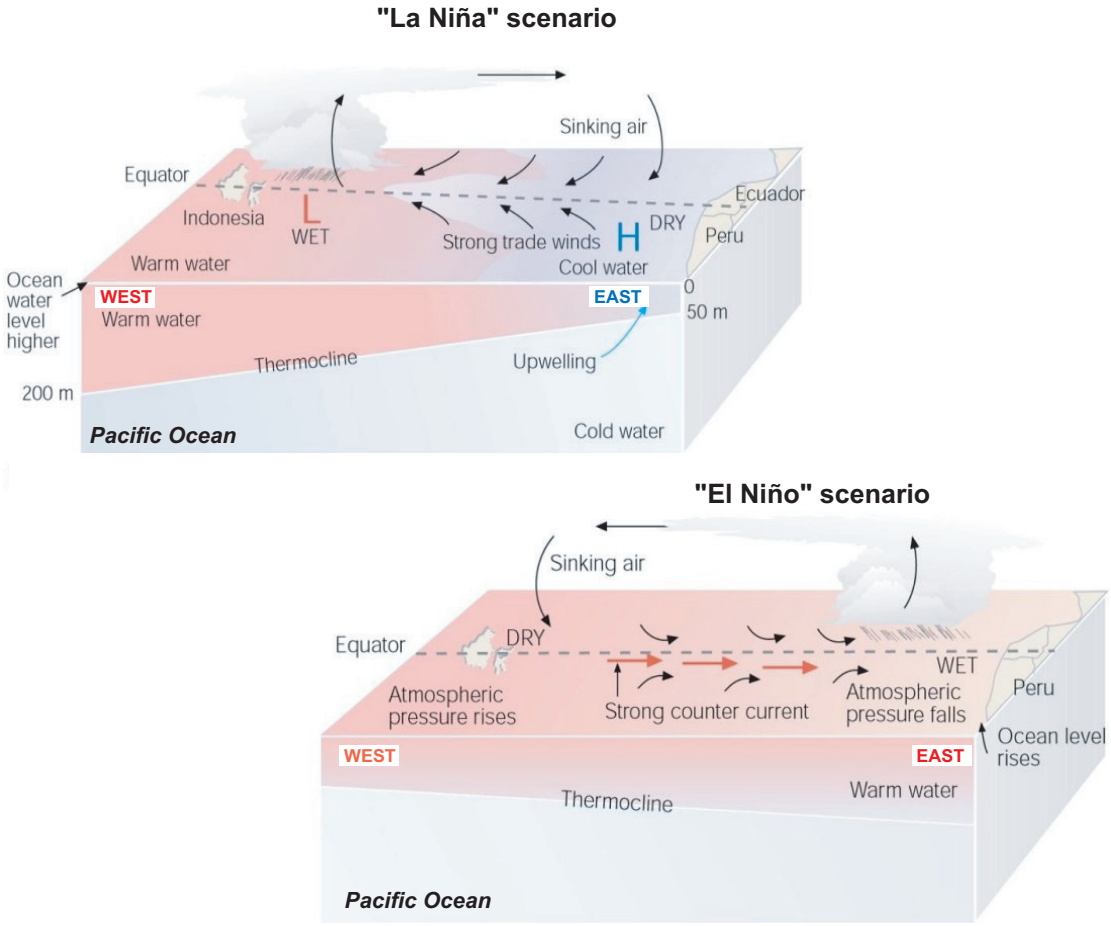

Fig. 1-3 East-west transect across the tropical Pacific during La Niña (top) and El Niño (bottom), showing major oceanographic and atmospheric changes (Figure modified from Ahrens et al., 2001). Note the decrease in the trans-Pacific sea surface temperature gradient and thermocline slope during an El Niño scenario.

A comparison of planktonic $\delta^{18}O$ records from the tropical east and west Pacific suggests that before ~4.0 Ma, SSTs in the WPWP were cooler than in the tropical east Pacific. The development of a more modern-like trans-equatorial SST gradient with higher temperatures in the WPWP and lower temperatures in the tropical east Pacific was not observed to start before 1.5 Ma (Cannariato and Ravelo, 1997; Ravelo et al., 2004). Hovan (1995) examined Neogene variations in dust flux and eolian grain sizes at sediment records from the equatorial east Pacific and inferred a decrease in southeast trade wind strength from 5 Ma to 4 Ma with a prounounced minimum around 4 Ma, and a related southward shift of the ITCZ. These studies may argue for an El Niño-like state.

In contrast, other studies of Wang (1994) and Andersson (1997) examined the Pliocene evolution of SSTs in the WPWP by applying planktonic foraminiferal transfer functions. Their results suggest that early Pliocene SSTs in the WPWP were similar or only slightly cooler than modern ones. Studies of Lawrence et al. (2004), and Groeneveld et al. (submitted a) examined SSTs in the equatorial eastern Pacific by using planktonic Mg/Ca-paleothermometry and ^{37}Uk-temperature reconstructions. Their findings suggest sea-surface and mixed-layer temperatures that were similar to modern ones. The combined evidence would argue for a modern-style east-west temperature gradient during the Pliocene and thus against an El Niño-like state. Furthermore, faunal assemblages and planktonic $\delta^{18}O$ records from tropical Pacific Sites 806 and 847 indicate that the development of the modern trans-Pacific thermocline slope already crossed a critical threshold between 5.0 Ma and 4.0 Ma (Chaisson and Ravelo, 2000). This change was characterized by a shoaling of the thermocline in the eastern tropical Pacific that was also recorded in multispecies planktonic stable isotope records from tropical east Pacific Site 851 as documented by Cannariato and Ravelo (1997). An early Pliocene thermocline shoaling in the tropical east Pacific would either infer a strengthening of the trade winds or might be associated with an increase in the rate of North Atlantic Deep Water (NADW) formation, as oceanographers more recently suggested that changes in NADW formation trigger global adjustments of the thermocline depth (e.g. Huang et al., 2000). The signal is carried from ocean to ocean by Kelvin and Rossby waves inducing an upward (downward) movement of the thermocline, when NADW formation is strong (weak). Model results indicate a 50 m change in the Pacific for a 10 Sverdrup change (1 Sverdrup = $10^6 m^3/s$) in the rate of NADW formation. Indeed, considerable evidence exists for enhanced NADW formation after 4.6 Ma that has been ascribed to the shoaling of the CAS (e.g. Haug and Tiedemann, 1998).

The Pliocene warm period was terminated by an irreversible cooling trend after ~3.2 Ma that was associated with the intensification of Northern Hemisphere Glaciation (NHG), which at 2.5 Ma culminated with significant ice growth in the circum-North Atlantic region after marine isotope stage (MIS) 100 (**Fig. 1-1**). This climate transition towards NHG led to the well-known and pronounced glacial-interglacial fluctuations that characterize the time interval of the last 2.5 Ma. Earth scientists generally agree that overall climate cooling is associated with decreasing levels of atmospheric CO_2 (e.g. Pearson and Palmer, 2000), and that ice sheet build-up is only possible if suffiscient moisture is available and winter snow survives the summer heat (Milankovitch, 1941). But what triggered the detoriation of Earth's climate during the late Pliocene? Many studies consider the late Pliocene/Pleistocene climate transition as a consequence of a long-term global

cooling trend that started about 55 Ma ago (e.g. Berger and Wefer, 1996), and that was probably caused by tectonic processes (e.g. Hay, 1996). For the last 15 Ma to 3 Ma, topographic changes like mountain uplift in Tibet and western America are discussed to have played a major role for global climate change by modulating atmospheric circulation and weathering rates (e.g. Ruddiman et al., 1986; Ruddiman and Raymo, 1988; Raymo and Ruddiman, 1992). Furthermore, two recent hypotheses link the major onset of the NHG to modifications in ocean heat transport and thermohaline circulation that were attributed to the constriction of low-latitude ocean gateways as the Indonesian Gateway and/or the CAS. On one hand, it was suggested that the progressive closure of the CAS has been the cause either for the onset (Berggren and Hollister, 1974), or for the delay (Berger and Wefer, 1996) or for setting preconditions for the NHG (Haug and Tiedemann, 1998; Driscoll and Haug, 1998, see chapter 1.2.2). On the other hand, Cane and Molnar (2001) identified the narrowing of the Indonesian Gateway and associated changes in tropical Pacific oceanography as a mechanism that may have contributed to the Pliocene cooling. The ultimate causes for the late Pliocene-Pleistocene climate transition, however, are still under debate (e.g. Ravelo et al., 2004). For example, the most recent work of Haug et al. (2005) points to the subarctic North Pacific as a major player in the development of NHG. The authors show that the onset of permanent stratification enhanced the seasonality in the North Pacific after 2.7 Ma (warmer summer SSTs, cooler winter SSTs). An extension of the summer warming into the autumn, and a warmer atmosphere that can hold more moisture provided additional water vapour to North America, where it accumulated as snow and thus allowed the build-up of ice sheets.

1.2.2 Closure of the Central American Seaway

Oceanic gateways, such as the once-open Panama gateway, are thought to have acted as critical thresholds in the evolution of ocean circulation and global climate. From all gateways, the Neogene closure history of the CAS is best examined and has become a model system for studying the importance of oceanic gateways for global climate change. The geologic history of Panama uplift has been reconstructed from pelagic sediment records (e.g. Saito, 1976; Keigwin, 1978; 1982a, 1982b; Keller et al., 1989; Moore et al., 1993; Haug and Tiedemann, 1998; Haug et al., 2001a, Lear et al., 2003), marine sediment records exposed on land (e.g. Duque-Caro, 1990; Coates et al., 1992; Collins et al., 1996), and terrestrial environments (e.g. Lundelius, 1987; Marshall, 1988). One question of particular interest remains the role of the final phase of the closure of the CAS and its potential to alter ocean circulation and hence affect global climate, since it was previously often considered as a candidate for being involved into one of the most significant climate changes observed in Earth's history, the transition from pronounced Pliocene warmth to the onset of Northern Hemisphere Glaciation (e.g. Berggren and Hollister, 1974; Berger and Wefer, 1996; Haug and Tiedemann, 1998; Driscoll and Haug, 1998). The following two paragraphs provide an overview about the uplift history of the CAS (paragraph 1.2.2.1) and possible effects of the gateway closure on ocean circulation and climate (paragraph 1.2.2.2). All data were adjusted to the astronomically dated timescale (e.g. Hilgen, 1991a,b; Tiedemann et al., 1994; Shackleton et al., 1995). A summary of important events in the geologic history of the Panama seaway (in chronological order) is given in **Table 1-1** at the end of this chapter.

1.2.2.1 Uplift history of the CAS

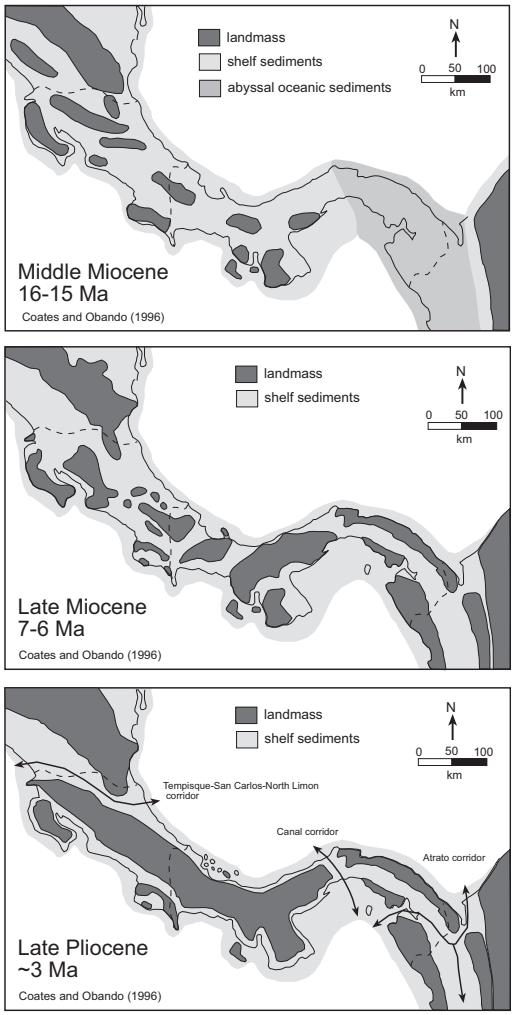

Fig. 1-4 The progressive closure of the Central American Isthmus, as inferred from near-shore marine faunas (after Coates and Obando, 1996.)

The Neogene tectonic closure of the CAS from 13 – 1.8 Ma resulted from the subduction of the Pacific Cocos- and Nazca plates underneath the North and South American plates and later the Caribbean plate (Meschede and Frisch, 1998; Meschede et al., 1999).

During the early Miocene pre-isthmian phase, paleo-bathymetrical reconstructions from benthic foraminiferal assemblages suggest a sill depth of about 2000 m (Duque-Caro, 1990), allowing a free exchange between Pacific and Atlantic water masses down to intermediate depths (Keller and Barron, 1983). From the middle to late Miocene (after 13 – 12 Ma), the Panama sill shoaled to a depth of about 1000 m (Duque-Caro, 1990; Coates et al., 1992). The intermediate water connection between Pacific and Caribbean was broken during this time, as indicated by the diversification of benthic foraminiferal fauna. From about 12 – 6 Ma, the Panamanian sill was elevated to a water depth of about 200 m (Duque-Caro, 1990), but assemblages of bathyal benthic foraminifera from sections of uplifted hemipelagic slope sediments on the Panamanian land bridge indicate that deeper incisions from 500 –200 m water depth still existed (Collins et al., 1996). A first exchange of terrestrial fauna (raccoons) between North and South America is recorded at 9.3 – 8 Ma (Webb, 1985; Marshall, 1988), and indicates the existence of an extended archipelago in Central America since the late Miocene (**Fig. 1-4**). Subsequent uplift resulted in changes of planktonic foraminiferal assemblages at 6.8 Ma and 4.6 Ma (Keller et al., 1989; Chaisson and Ravelo, 2000). Jackson et al. (1993) reported a substantial evolutionary change in Caribbean mollusks during the early Pliocene. After about 5 Ma, the subduction of the Cocos Ridge, that formed during the passage of the Cocos Plate over the Galapagos Hotspot, dramatically elevated the Central American volcanic arc and led to the final phase of the closure (Dengo, 1985). From 4.6 – 4.2 Ma, the restriction of the Panamanian sill reached a critical threshold for upper ocean water mass exchange. During this time, surface water salinity increased in the Caribbean as indicated by the $\delta^{18}O$ values of planktonic foraminifera (Keigwin, 1982a; Haug et al., 2001a; **Fig. 1-5**). Coates et al. (1992) examined the Pacific-Caribbean evolutionary divergence of near-shore marine faunas and concluded that the closure was almost complete since 3.6 – 3.5 Ma. The "great American interchange" of vertebrates that likely

required a land bridge between the Americas appeared at about 3 – 2.7 Ma (Lundelius, 1987; Marshall, 1982; 1988), and marked a final step in the closure of the Isthmus of Panama that was coincident with the glacial-induced sea level drop during the main intensification of the northern hemisphere ice-sheet growth. Keller et al. (1989) suggested that the maximum divergence of Pacific-Caribbean faunal provinces finally began at about 1.9 Ma ago, and that at least a littoral-neritic leakage still persisted until 1.8 Ma.

1.2.2.2 Possible effects of the gateway closure on ocean circulation and climate: Numerical model results and paleoceanographic evidence

The relevance of changes in the gateway configuration of the Panama Seaway for ocean circulation and climate has been subject to several theoretical and modeling studies. Using the theory of 'Island Rule', Nof and van Gorder (2003) suggested that with an open isthmus, a closed Bering Strait, and in the absence of NADW formation the flow through the gateway should be directed from the Atlantic into the Pacific. The results from different three-dimensional ocean circulation models, however, found the opposite. Driven by the hydrostatic head in the Pacific, the main transport of water masses in these models is directed from the Pacific into the Atlantic, particularly in the upper water column (e.g. Maier-Reimer et al., 1990; Mikolajewicz et al., 1993; Mikolajewicz and Crowley, 1997; Murdock et al., 1997; Nisancioglu et al., 2003; Prange and Schulz, 2004). In addition, a small amount of wind-driven transport from the Atlantic into the Pacific was found at the sea surface (e.g. Maier-Reimer et al., 1990). Only with a sill depth well below the depth of NADW (> 1000 m), a certain amount of NADW, or all of it, may escape from the Atlantic into the Pacific (Nisancioglu et al., 2003). In consequence, model results show that the salinity difference between Pacific and Caribbean was greatly reduced with respect to the modern in case of an open isthmus. As the production of NADW largely depends on the transport of high-salinity waters into the North Atlantic, the low current velocities in the Gulf Stream, and the northward transport of relatively fresh (Pacific) water masses lead to a reduction of NADW formation prior to the closure (Mikolajewicz et al., 1993; Mikolajewicz and Crowley, 1997; Nisancioglu et al., 2003; Prange and Schulz, 2004), whereas in some model simulations the meridional overturning circulation even collapses (Maier-Reimer et al., 1990; Murdock et al., 1997). In most of the numerical models, the closure of the Panamanian Gateway is therefore associated with a salinity increase in the tropical Atlantic and with an intensification of the Gulf Stream system that introduces warm and saline waters to high northern latitudes, thereby favoring the production of NADW and strengthening the meridional overturning (Maier-Reimer et al., 1990; Mikolajewicz and Crowley, 1997; Nisancioglu et al., 2003, Prange and Schulz, 2004). The resulting changes in thermohaline circulation have profound implications for the global climate system, including e.g. ocean heat transfer and atmospheric moisture transport.

Although the geological evidence for this chain of causal links is still marked by several gaps, many paleoceanographic studies clearly observe a close connection between the formation of the Isthmus and major oceanographic changes during the early Pliocene (e.g. Keigwin, 1982a; Burton et al., 1997; Haug and Tiedemann, 1998; Haug et al., 2001a).

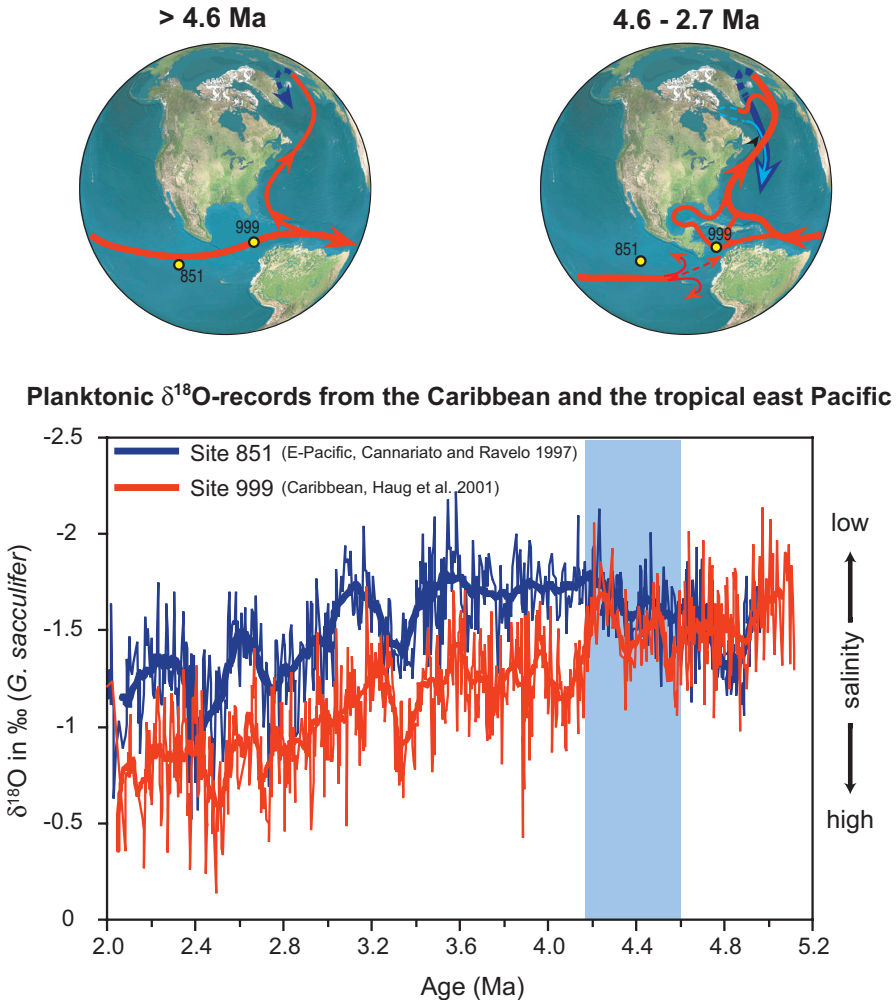

Fig. 1-5 Planktonic $\delta^{18}O$ records (*G. sacculifer*) from tropical east Pacific Site 851 (Cannariato and Ravelo, 1997) and Caribbean Site 999 (Haug et al., 2001a). Figure modified from Haug et al. (2001a). The divergence of Pacific-Caribbean $\delta^{18}O_{G.\ sacculifer}$ records after 4.7 – 4.2 Ma has been interpreted to reflect an increase in Caribbean sea surface salinity due to the restriction of Pacific-Caribbean surface water exchange through the CAS (by courtesy of Ralf Tiedemann).

Haug et al. (2001a) documented a salinity increase in Caribbean surface waters after 4.6 – 4.2 Ma as indicated by a first high-resolution comparison of planktonic $\delta^{18}O$ records from the Caribbean and the tropical east Pacific (**Fig. 1-5**). Less precise, this salinity increase has been shown earlier by Keigwin (1982a). According to these authors, the modern Atlantic-Pacific salinity contrast became fully established at ~4.2 Ma, as indicated by the 0.5 ‰ planktonic $\delta^{18}O$ enrichment in the southern Caribbean Sea (ODP Site 999). The Caribbean salinity increase was interpreted to reflect the restriction of surface water exchange between tropical Pacific and Atlantic in response to the shoaling of the CAS, as also predicted by OGCMs (e.g. Maier-Reimer et al., 1990) and theoretical studies (Weyl, 1968). Diminished surface water exchange influenced sea surface salinity by changing the freshwater balance between the two major ocean basins, with enhanced evaporation in the Caribbean and enhanced precipitation in the Pacific. Today, the salinity

difference between the Pacific and the Atlantic is linked to the net atmospheric transport of water vapor (about 0.2 Sverdrups) by warm and vapor-rich trade winds that blow across the low-lying Central American land bridge (e.g Weyl et al., 1968; Joussaumme et al., 1986). Concomitant to the attainment of a critical threshold for surface water exchange, distinct erosion horizons at the Great Bahama Bank document the intensification of the Gulf Stream (Reijmer et al., 2002).

Paleoceanographic evidence for closure-induced changes in deep-ocean circulation are inferred from foraminiferal stable isotope and Mg/Ca data (see below), and are in good agreement with results from model simulations (Maier-Reimer et al., 1990; Mikolajewicz and Crowley, 1997). Benthic $\delta^{18}O$ values and Mg/Ca temperature reconstructions show a significant warming of deep-water masses formed in the north Atlantic after 6 – 5 Ma that may point to enhanced heat transfer to the North Atlantic *via* a strengthened Gulf Stream (Lear et al., 2003). So far, however, no direct evidence exists for a warming of subarctic surface waters at about 4.6 Ma.

Several studies (e.g. Tiedemann and Franz, 1997; Haug and Tiedemann, 1998) document an enhancement of Atlantic thermohaline circulation concomitant to the observed increase in Caribbean suface salinity after 4.6 Ma (e.g. Keigwin, 1982a; Haug et al., 2001a). An increase in the carbon isotopic composition of the epibenthic foraminifera *C. wuellerstorfi* was observed at deep Caribbean Site 999 after 4.6 Ma (Haug and Tiedemann, 1998). The $\delta^{13}C$ values of *C. wuellerstorfi* serve as a proxy for deep-water ventilation, whereas higher $\delta^{13}C$ values indicate lower nutrient concentrations and better ventilation. Today, the deep Caribbean basins are filled with the good ventilated upper part of NADW (UNADW), as the maximum sill depth of Atlantic-Caribbean passages is about 1900 m. The early Pliocene increase in deep Caribbean $\delta^{13}C$ values was thus interpreted to reflect the initiation of Upper North Atlantic Deep Water (UNADW) formation in the Labrador Sea, whereas Caribbean deep water was dominated by a more $\delta^{13}C$-depleted Southern Ocean water mass before 4.6 Ma (**Fig. 1-6**, Haug and Tiedemann, 1998). This increase in deep-water production in the North Atlantic also led to the modern Atlantic-Pacific chemical asymmetry, which is reflected by a distinct increase in Caribbean carbonate preservation (Site 999) and remaining strong carbonate dissolution in the Pacific (Site 846) since 4.6 Ma (**Fig. 1-6**; Haug and Tiedemann, 1998). The enhancement of Atlantic thermohaline circulation after 4.6 Ma is also reflected by a depression of the lysocline in the equatorial W-Atlantic (Ceara Rise) and a related increase in carbonate preservation (Tiedemann and Franz, 1997), as well as by changes in Atlantic Nd isotope signatures (Burton et al., 1997; Frank et al., 1999). Although deep Atlantic carbonate preservation increased dramatically, an increase in the formation of Lower North Atlantic Deep Water (LNADW) is still discussed controversially (Tiedemann et al., 1997; Raymo, 1997), since benthic $\delta^{13}C$ records from the deep Atlantic (below 2500 m water depth) indicate no clear enhancement of deep water ventilation after 4.6 Ma.

The closure-induced enhancement of Atlantic thermohaline circulation was suggested to have favored the onset of the NHG by influencing the freshwater balance in the Arctic Ocean (Haug and Tiedemann, 1998). The intensification of the Gulf Stream increased the transport of warm, saline surface waters to high northern latitudes. The associated increase in evaporation provided additional atmospheric moisture at high latitudes, which is a substantial requirement for ice sheet

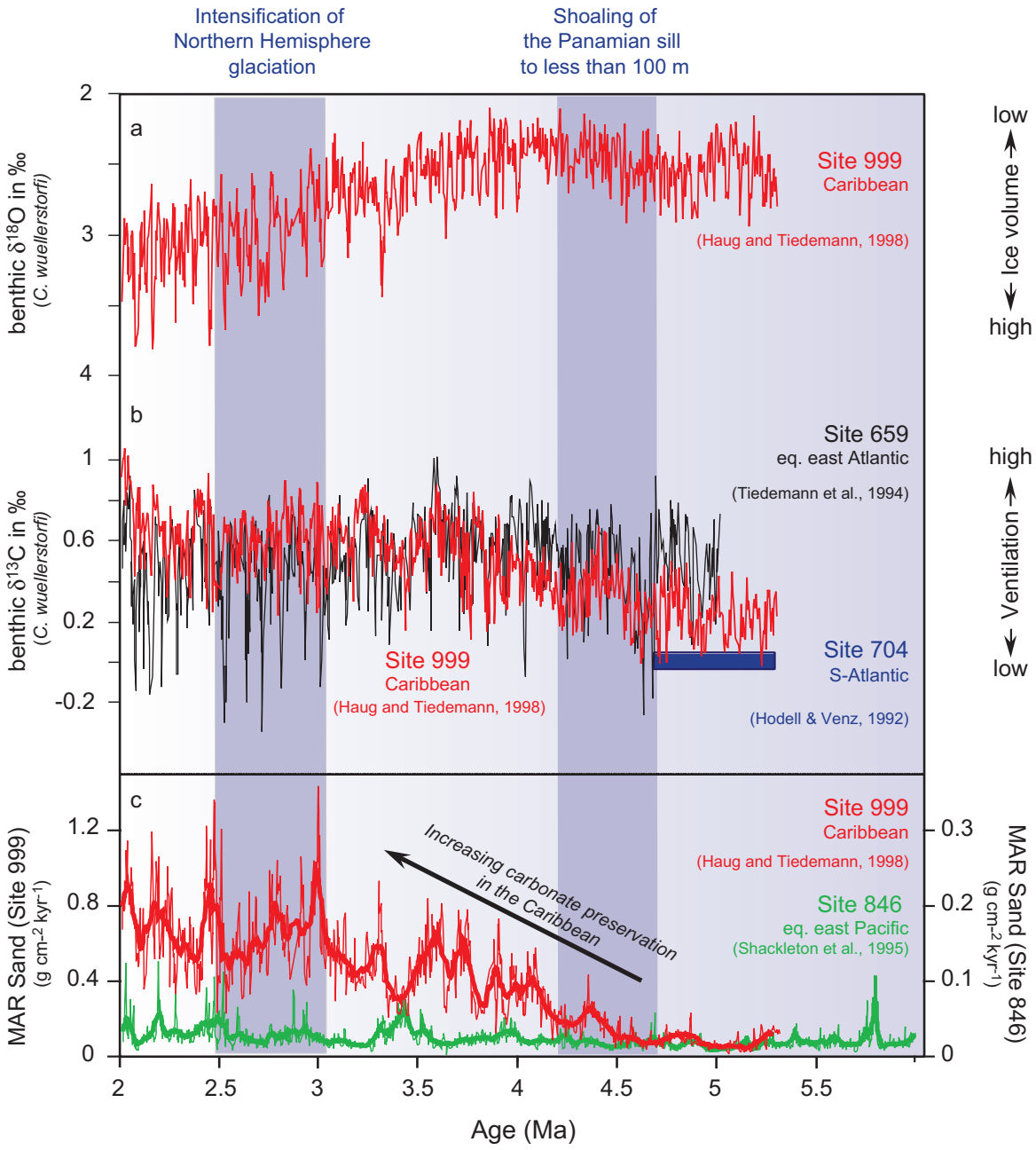

Fig. 1-6 Paleoceanographic records spanning the time interval from 5.3 – 2 Ma (Figure modified from Haug and Tiedemann, 1998). **a**: Benthic $\delta^{18}O$ record (*C. wuellerstorfi*) from Caribbean Site 999 (2828 m water depth; Haug and Tiedemann, 1998). **b**: $\delta^{13}C$ records from Caribbean Site 999 (Haug and Tiedemann, 1998, red), equat. east Atlantic Site 659 (3070 m water depth, Tiedemann et al., 1994). The blue bar indicates the average $\delta^{13}C$ values from South Atlantic Site 704 (2532 m water depth, Hodell and Venz, 1992). **c**: Comparison of carbonate sand fraction mass accumulation rates (MAR sand) at Sites 999 (left axis, red curve, Haug and Tiedemann, 1998) and 846 (right axis, green curve, Shackleton et al., 1995). MAR were calculated using GRAPE density values (Sigurdsson et al., 1997, Haug and Tiedemann, 1998). Thin lines are original data, and thick lines are data smoothed by a 20-point running mean.

growth (Haug and Tiedemann, (1998). Moreover, enhanced moisture delivery to the Eurasian continent *via* atmospheric transport by the westerlies would have increased the freshwater input of Siberian rivers into the Arctic Ocean. This would then have facilitated sea ice formation, increased the albedo, and isolated the high heat capacity of the ocean from the atmosphere (Driscoll and Haug, 1998). Another effect of the closure of the Central American Seaway was predicted by OGCM's that might alter the freshwater balance in the Arctic Ocean, and could thus be critical for ice sheet growth: A reversed flow direction through the Bering Strait (Maier-Reimer et al., 1990). Geologic data indeed support these results. Marincovich and Gladenkov (1998) documented the presence of Atlantic bivalves in the Pacific at about 4.8 Ma and found a widespread occurrence of North Pacific mollusks in the North Atlantic since 3.6 Ma. This suggests a change from a southward flow through the Bering Strait (from the Arctic Ocean into the north Pacific) to a northward flow (from the north Pacific into the Arctic Ocean) between 4.8 and 3.6 Ma.

Other changes in low-latitude atmospheric and upper ocean circulation between 5 Ma and 4 Ma may also relate to the progressive closure of the CAS. For example, shifts towards lower salinity in surface and thermocline waters at the location of Ceara Rise and in the eastern tropical Atlantic around 4.4 Ma were interpreted to reflect a southward shift of the Atlantic ITCZ, a zone of high precipitation (Billups et al., 1998; 1999). Such a shift would move the tropical rain belt away from the Caribbean and could thus possibly contribute to the development of high Caribbean SSS. A southward shift of the ITCZ between 5 Ma and 4 Ma has also been suggested for the tropical east Pacific as deduced from latitudinal changes in the eolian dust flux and grain size spectrum (Hovan, 1995), although the exact age of the transition is not well defined. Farrell et al. (1995) documented an eastward shift in the locus of maximum opal accumulation in the tropical east Pacific ~4.5 Ma ago, probably as a result of a major reorganization in tropical east Pacific upper ocean circulation in response to the progressive closure of the CAS. Furthermore, multispecies planktonic $\delta^{18}O$ records indicate a shoaling of the thermocline in the eastern tropical Pacific at 4.2 Ma (Cannariato and Ravelo, 1997; Chaisson and Ravelo, 2000). The development of the trans-equatorial Pacific east-west thermocline slope crossed a critical threshold by the same time, as indicated by planktonic foraminiferal assemblages and isotopic evidence (Chaisson and Ravelo, 2000). A modest but significant early Pliocene trend towards lower planktonic $\delta^{18}O$ values at Pacific Site 851 is also observed in stacked bulk $\delta^{18}O$ records from the equatorial east Pacific (Shackleton and Hall, 1995), and may indicate a slight warming or a net freshening of equatorial Pacific surface waters between 4.7 Ma and 4.2 Ma. A net freshening seems an obvious consequence of warm and vapor-rich trade winds transporting moisture across Central America, while oceanic mixing with the tropical Atlantic became severely restricted. The observed changes in the geographical patterns of biogenic sediment accumulation and the depth of the thermocline may, among other mechanisms, be indicative of changes in the tropical wind field. The fact that all these changes occurred parallel to the establishment of the salinity gradient between Pacific and Caribbean suggests that the restriction of the Panama seaway led also to profound changes in tropical Pacific surface circulation.

Tab. 1-1 Summary of events that were possibly linked to the closure of the CAS. Table from Farrell et al., 1995, modified and supplemented.

Age (Ma)	Event	Interpretation	Citations
13-12	First diversification of benthic foraminiferal fauna between Pacific and Caribbean.	Shoaling of the sill to mid-bathyal depths (1000 m) with first restriction of deep-and intermediate water connections.	Duque Caro, 1990; Keller and Barron, 1983
12-7.5	„Carbonate Crash", Carbonate dissolution event in the Pacific and Caribbean, (in the Caribbean, this event was terminated by 10 Ma ago).	Subsequent shoaling of the CAS prevents inflow of less carbonate corrosive Atlantic/Caribbean intermediate and deep water into the Pacific.	Lyle et al., 1995; Roth et al., 2000
9.9-8.7	First interchange of some North- and South American mammals („island hoppers") overlaps with carbonate crash.	Development of first islands in the gateway region. Eventually full closure during the middle to late Miocene? (Roth et al., 2000).	Webb, 1985; Marshall, 1988
9.3-4.0	Further steps in the diversification of benthic foraminiferal fauna between Pacific and Caribbean.	9.3 – 7.8 Ma: Shoaling of the sill to upper bathyal depths. The shallow water connection was open. 7.8 – 6.9 Ma: Shoaling of the CAS to 150 m water depth. Pacific-Caribbean shallow water connection was restricted. 6.9 – 4.0 Ma: The sill shoaled to less than 50 m water depth.	Duque-Caro, 1990
8-5	Changes in the Nd and Pb isotopic composition of hydrogenous ferromanganese crusts in the Atlantic (Gulf Stream).	Diminished supply of Pacific water into the Atlantic (850 m water depth).	Frank et al., 1999
6.8-6.6	Increasing difference in benthic foraminiferal $\delta^{13}C$ values between Pacific and Caribbean.	Termination of deep- to intermediate water exchange through the gateway.	Keigwin, 1982a
6.8-6.6	Planktonic foraminiferal assemblages indicate that significant upwelling began in the western Caribbean Basin.	Indication of restricted intermediate water flow through the gateway.	Keller et al., 1989
6-5	Changes in the physical characteristics of proto-NADW (became saltier and warmer as indicated by benthic foraminiferal $\delta^{18}O$ and Mg/Ca).	Subsequent restriction of the CAS, first enhancement of heat- and salt transport to high northern latitudes.	Lear et al., 2003
5-4	Development of an „east-west temperature gradient" in the tropical Pacific upper water column.	Shoaling of the thermocline in the tropical east Pacific was linked to the shoaling of the CAS and indicates changes in the tropical wind field (and/or changes in the amount of NADW-formation that lead to a global adjustment of the thermocline (Huang et al., 2000)).	Chaisson and Ravelo, 2000
5-4	Eolian grain size records indicate a decrease in the trade wind strength (and a related southward shift of the ITCZ) over the tropical east Pacific.	Changes in the wind field over the tropical east Pacific were attributed to the shoaling of the CAS.	Hovan, 1995
4.6	Gradual increase of benthic $\delta^{13}C$ values at deep Caribbean Site 999.	Enhancement of NADW-formation in the North Atlantic, stronger supply of good ventilated water masses into the Caribbean. (UNADW).	Haug and Tiedemann, 1998
4.6	Distinct increase in the Carbonate preservation at Ceara Rise, equat. W-Atlantic.	Deepening of the lysocline due to enhancement of NADW-formation.	Tiedemann and Franz, 1997
4.6-4.2	Caribbean suface salinity increased with respect to the Pacific, based on the ^{18}O enrichment of Caribbean planktonic foraminifers. Changes in in the planktonic foraminiferal fauna (higher contents of *G. sacculifer*) also indicate higher salinity in the Caribbean.	Restriction of surface water exchange between the Pacific and Caribbean; diminished inflow of low-salinity Pacific surface waters.	Keigwin, 1982a; Keller et al., 1989; Haug et al., 2001a
4.6-4.2	Shoaling of the thermocline in the tropical east Pacific as indicated by multispecies planktonic $\delta^{18}O$ records	Was interpreted to reflect changes in the tropical wind field.	Cannariato and Ravelo, 1997
4.4	The locus of maximum opal accumulation in the tropical east Pacific abruptly shifted eastward.	Reorganization of tropical east Pacific surface circulation.	Farrell et al., 1995
4.4-4.3	Decrease in planktonic $\delta^{18}O$ values at Ceara Rise (tropical W-Atlantic) was interpreted to reflect a southward shift of the ITCZ.	Changes in the atmospheric circulation and/or pole-to equator-temperature gradients were related to the shoaling of the CAS.	Chaisson and Ravelo, 1997; Billups et al., 1999
4.2	Cooling of Southern Ocean surface waters, based on diatom assemblages.	Increased heat piracy (trans-equatorial heat transport into the North Atlantic) *via* an enhanced Gulf Stream; stronger thermohaline circulation.	Whitehead and Bohaty, 2003
4.4-2.6	The divergence and provinciality of near-shore and open-ocean faunas increased significantly. Initiation of the „Great American Interchange" of vertebrates over the Central American Landbridge at about 2.7 Ma.	First indications of a final closure of the CAS.	e.g. Kaneps, 1970; Saito, 1976; Keigwin 1978, 1982b; Lundelius, 1987; Marshall, 1988; Coates et al., 1992
2.5-1.9	Permanent divergence of Pacific and Caribbean faunas and floras.	Cessation of sustained surface current flow through the gateway.	Crouch and Poag, 1979; Gartner et al., 1987; Keller et al., 1989
1.9	Maximum divergence of faunal provinces began.	„At least incipent littoral-neritic leakage" occurred across the seaway until 1.8 Ma.	Keller et al., 1989

CHAPTER 2

SITE LOCATIONS AND QUALITY OF SAMPLE MATERIAL

This study focused on Pliocene sediment sections (~6 – 2.5 Ma) of three ODP sites from the tropical east Pacific (Sites 1237, 1239, 1241) and two ODP sites from the Caribbean (Sites 999 and 1000) (**Tab. 2-1**). The following paragraphs provide basic information about the significance of these site locations for the paleoceanographic reconstructions aimed at in this study, and about the quality of their Pliocene sediment records. Furthermore, this study considered already existing proxy records from east Pacific ODP Sites 851 and 1236, and from west Atlantic Sites 925 and 1006 for paleoceanographic interpretations. **Figure 2-1** indicates the site locations, including the plate tectonic backtrack paths of east Pacific sites.

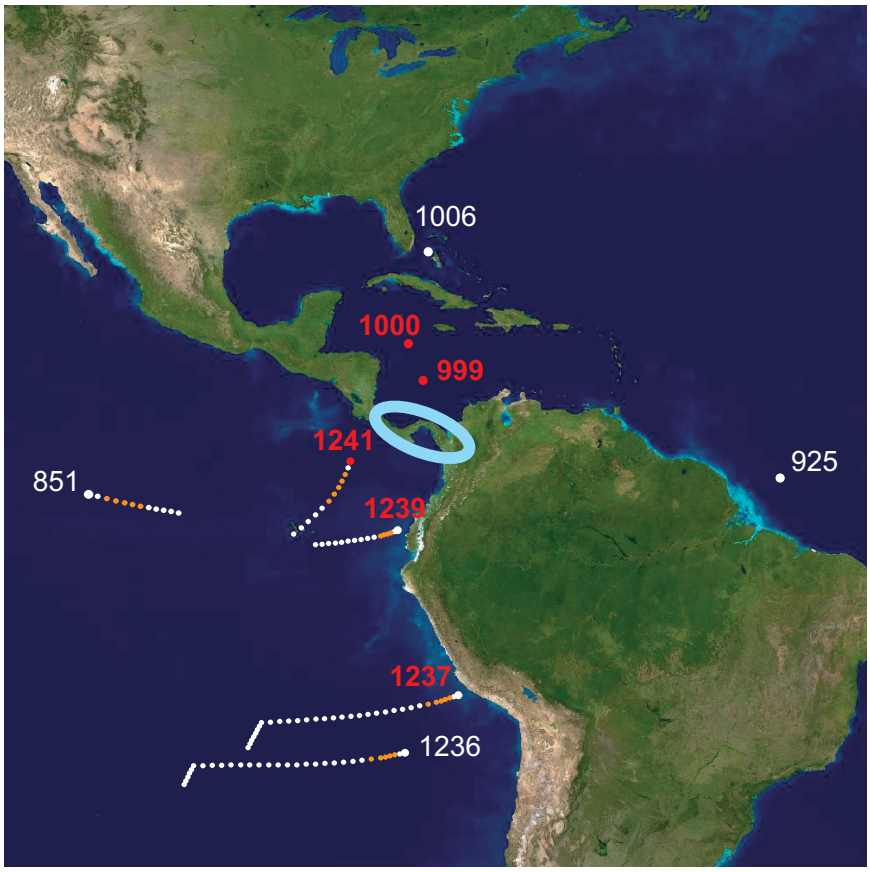

Fig. 2-1 Map of the tropical east Pacific and the Caribbean, showing the locations of ODP sites considered in this study. Plate tectonic backtracks of tropical east Pacific sites are indicated by white and orange dots (1 m.y. steps, Pisias et al., 1995; Mix et al., 2003). The orange dots indicate the paleo-positions between 6 – 2 Ma ago. Sites marked in red were used for the establishment of the stratigraphy and/or proxy records, sites indicated in white provided already existing proxy records. The light blue area shows the suggested final gateway region of the CAS (e.g. Duque-Caro, 1990; Collins et al., 1996).

Tab. 2-1: ODP Sites examined in this study.

ODP Site/(Leg)	Region	Position (Latitude, Longitude)	Water depth
999 (165)	Caribbean, Colombian Basin	12° 44'N, 78°44'W	2828 m
1000 (165)	Caribbean, Nicaraguan Rise	16°33'N, 79°52'W	916 m
1237 (202)	SE-Pacific, Nazca Ridge	16°0.421´S, 76°22.685´W	3212 m
1239 (202)	equat. E-Pacific, Carnegie Ridge	0°40.32´S, 82°4.86´W	1414 m
1241 (202)	tropical E-Pacific, Cocos Ridge	5°50.570'N, 86°26.676'W	2027 m

Site 1241 (tropical east Pacific)

Site 1241 is located in the Guatemala Basin on the north flank of Cocos Ridge at 2027 m water depth (Mix et al., 2003; **Fig. 2-1**). A tectonic backtrack path on the Cocos Plate moves the site location southward and slightly to the west relative to South America (Pisias et al., 1995). Site 1241 was thus probably located close to the equator and at shallower depths during the late Miocene (Mix et al., 2003; see chapter 6 for additional information). Up to now, this work mainly focused on Site 1241 to investigate the impact of the closure of the CAS on tropical east Pacific upper ocean stratification. As Site 1241 was located fairly close to the final gateway region throughout the Pliocene, it was considered as an ideal position to examine closure-related changes in tropical east Pacific surface hydrography.

At this site, three holes were cored with the Advanced Hydraulic Piston Corer (APC) technique to reconstruct a composite depth that demonstrates complete recovery for the Pliocene sediment sequence. This was achieved by detailed inter-hole correlations using closely spaced core logging data (color, sediment density), which allowed to splice across coring-gaps and to replace drilling disturbed sediment sequences (Mix et al., 2003). The time interval from 2.4 – 5.7 Ma, equivalent to the depth interval from 58 mcd to 178 mcd, was sampled at a mean distance of 10 cm above 162 mcd and at a mean distance of 15 cm below. The time resolution of the series is thus generally better than 3 k.y. The relatively shallow water depth of the site resulted in a good preservation of the carbonate shells. Pliocene sediments are dominated by nannofossil ooze with varying amounts of foraminifers, diatoms, clay, and micrite, whereas the carbonate content of the sediment varies between 70 – 90 wt%.

Site 1239 (equatorial east Pacific)

Site 1239 is located ~120 km off the coast of Ecuador, near the crest of Carnegie Ridge at a water depth of 1414 m (Mix et al., 2003; **Fig. 2-1**). The plate tectonic backtrack path moves this site westward almost parallel to the equator, suggesting that it remained within the highly productive equatorial upwelling zone throughout the Pliocene (Mix et al., 2003). Thus, the position of Site 1239 offers the opportunity to test the hypothesis of a permanent El Niño-like state in the tropical east Pacific during the Pliocene.

At this site, two holes that cover the Pliocene interval were drilled with the XCB (extended coring barrel). In addition, Hole A was logged with the triple combo and the FMS-sonic tool strings (Mix et al., 2003). The core logging data from Holes 1239A and 1239B in combination with the

borehole logging data will enable the establishment of a composite depth for the Pliocene interval (Mix et al., 2003). So far, only Hole 1239A was sampled for the time interval from 2.7 – 5.0 Ma, referring to the depth interval from 150 mbsf to 390 mbsf. The establishment of a benthic stable isotope stratigraphy detected several gaps at core breaks (Tiedemann et al., submitted; see chapter 4) that will later be replaced by sediment sections from Hole B. High sedimentation rates of up to 10 cm/k.y. made a sample spacing of 30 cm above 289 mbsf and of 20 cm below suffiscient to obtain a temporal resolution of ~3 k.y. The carbonate contents of the sediment are on average 70 wt% during the Pliocene interval (Sturm et al., in prep.), whereas the content of planktonic foraminifers is relatively low (Mix et al., 2003).

Site 1237 (southeast Pacific)

Site 1237 is located ~140 km off the coast of Peru, situated on a relatively flat bench on the easternmost flank of Nazca Ridge at a water depth of 3212 m (Mix et al., 2003; **Fig. 2-1**). This site was selected in order to develop a Pliocene astronomically tuned stratigraphic reference section for the east Pacific, as it provided an excellent paleomagnetic stratigraphy with clear definitions of all chrons and subchrons over the last 5 m.y. (Mix et al., 2003). This allowed an independent comparison to the Pliocene astronomical polarity time scale (Hilgen, 1991a,b; Shackleton, 1995; Lourens et al., 1996), and demonstrates its global importance.

Three boreholes that cover the Pliocene interval were cored with the APC. The composite depth scale documented complete recovery. For the establishment of the age scale, high-resolution core logging shipboard data (color, sediment density) were available at intervals of 2.5 cm, corresponding to a temporal resolution of 1000 – 2500 yrs (Mix et al., 2003). The Pliocene interval from 4.2 – 5.9 Ma, equivalent to the depth interval from 75 mcd to 113 mcd, was sampled with a spacing of 5 cm for benthic isotope measurements, providing a temporal resolution of ~3 – 4 k.y (Tiedemann et al., submitted, see chapter 4). The carbonate content of the sediment is generally higher than 90 wt% (Mix et al., 2003).

Site 999 (Caribbean)

Southern Caribbean Site 999 is located on the Kogi Rise within the Colombian Basin at a water depth of 2828 m (Sigurdsson et al., 1997; **Fig. 2-1**). This site offers an excellent opportunity to study changes in Caribbean upper ocean water mass signatures during the final phase of the closure of the CAS, since it is positioned relatively close to the final gateway region. Furthermore, the water depth of Site 999 at 2828 m is appropriate to monitor changes in the nutrient concentration (ventilation) of Upper North Atlantic Deep Water (UNADW), as Atlantic water masses have to enter the Caribbean above a sill depth of 1600 – 1900 m to fill the deep Caribbean basins.

Pliocene sediment sequences were only recovered at Hole 999A, which was drilled with the APC technique. Therefore, Site 999 has no composite depth that would ensure the completeness of the sediment sequence. Accordingly, coring gaps may occur at core breaks between succeeding cores. The benthic $\delta^{18}O$ stratigraphy for Site 999 (Haug and Tiedemann, 1998; modified in chapter 5), however, detected no significant stratigraphic gaps in the Pliocene section that may have resulted from core breaks. The time interval from 2.5 – 5.2 Ma, corresponding to the depth interval

from 55 – 160 mbsf, was sampled with a spacing of 10 cm that equals a temporal resolution of ~3 k.y. The completeness of the Pliocene sediment interval, the high carbonate content of the sediment (40 – 72 wt%; Sigurdsson et al., 1997), and the good preservation of foraminiferal shells especially qualified Site 999 for this study.

Site 1000 (Caribbean)

Central Caribbean ODP Site 1000 is located within the Pedro Channel on the Northern Nicaraguan Rise (NNR), 265 km westward of Jamaica, at a water depth of 916 m (Sigurdsson et al., 1997; **Fig. 2-1**). Site 1000 is positioned farther north than Site 999, and thus at a greater distance to the final gateway region. Hence, the comparison of proxy records between these two sites is valuable for examining inner-Caribbean gradients in surface water signatures that were possibly related to changes in the volume transport of the Panamanian throughflow. In addition, the shallow water depth of Caribbean Site 1000 provides a window into the Atlantic intermediate water level, and thus allows for the reconstruction of Pliocene changes in Atlantic intermediate water circulation.

Two holes were drilled at the site location. The late Miocene-Pliocene interval was completely recovered with the APC technique at Hole 1000A. However, cores 1000A–10H and –13H were highly drilling disturbed upon recovery. These intervals were later cored in Hole 1000B (cores 1R and 2R) with the RCB (rotary core barrel) system. It was suggested that the correlation between the two holes is offset by no more than 70 cm, as illustrated by the occurrence of the same turbidite layer at 78.9 mbsf in Hole A and at 79.6 mbsf at Hole B (Sigurdsson et al., 1997). All sections of cores 1000B–1R and –2R that were suggested not to be drilling disturbed were included to close the gaps within Hole A. The comparison of benthic $\delta^{18}O$ records, however, provided no convincing match between holes A and B. This may indicate that the drilling disturbance of cores 1000B–1R and –2R was larger than expected, or that the turbidite layers at both holes are not identical. The fact that no composite depth exists at Site 1000 resulted in larger stratigraphic gaps of the Pliocene sediment sequence. This has been suggested by the comparison of benthic $\delta^{18}O$ records from Site 1000 and Site 925/926 (stratigraphic reference record) (see chapter 5). The time interval from 2.2 – 5.6 Ma, corresponding to the interval from 51 mbsf to 175 mbsf, has been sampled every 10 cm. This yielded a temporal resolution generally better than 3 k.y.

Pliocene sediments deposited in the intervening seaway of the Pedro Channel are a mixture of pelagic and bank-derived neritic carbonates with a minor component of terrigenous sediments. Due to the shallow water depth of the site well above the lysocline, the preservation of foraminiferal shells is excellent. Carbonate contents of the sediment range between 77 and 93 wt% (Sigurdsson et al., 1997). Aragonite (mostly in form of fine, platform-derived needles) is observed across the interval from cores 1000A-15H to 1000A-7H. The high aragonite contents (up to 60 %, Groeneveld et al., submitted b), however, increase the diagenetic potential of the sediment, as aragonite can be dissolved and recrystallized after burial. Chalky parts that hint to such recrystallization were detected in cores 1000A–11H to 1000A–14H, as well as in 1000B–1R and 1000B–2R. The diagenetic overprint from secondary calcite crusts on foraminiferal shells was considered to be not significant for stable isotope measurements (Groeneveld et al., submitted b).

Additional sites considered in this study

Apart from the ODP sites examined in this study, existing Pliocene proxy records from ODP Sites 851, 925, 1006 and 1236 were considered for paleoceanographic interpretations (**Fig. 2-1**). Tropical West Atlantic ODP Site 925 (Ceara Rise, Leg 154, 4° 12.2'N, 43° 29.3'W; Curry et al., 1995) monitors fluctuations in upper water mass signatures within the North Brazil Current that transports water masses into the Caribbean. Site 1006 (Leg 166; 24° 23.9'N, 79° 27.5'W; Eberli et al., 1997) is located under the Florida Current at the western Great Bahama Bank, and monitors the Caribbean outflow into the North Atlantic. Hence, these two sites in combination with those from the Caribbean (999 + 1000) trace the Pliocene warm water return route of the conveyor belt circulation from the South Atlantic *via* the Caribbean into the North Atlantic (Gulf Stream).

ODP Site 851 (Leg 138, 2° 46.2'N, 110° 34,3'W; Mayer et al., 1992) is located at the boundary between the South Equatorial Current (SEC) and the North Equatorial Counter Current (NECC) in the tropical east Pacific. The comparison to Site 1241, which is located farther to the northeast within the NECC, provides information about changes in latitudinal gradients in Pliocene tropical east Pacific upper ocean hydrography.

The benthic $\delta^{13}C$ record from Site 1236 (Tiedemann et al. submitted, see chapter 4), which is located in the southeast Pacific on the Nazca Ridge (21° 21.4'S, 81° 26,2'W; Mix et al., 2003) in a water depth of 1323 m, reflects changes in intermediate water ventilation. The comparison between the benthic $\delta^{13}C$ record from Site 1236 and planktonic $\delta^{13}C$ records from Site 1241 provided insights into the hypothesis whether changes in Antarctic Intermediate Water ventilation triggered changes in tropical Pacific thermocline ventilation during the Pliocene (Cannariato and Ravelo, 1997).

CHAPTER 3

METHODS

3.1 Sample processing

Figure 3-1 summarizes the individual steps of sample processing. After freeze-drying, the original samples were split into a main sample and a sub-sample (ca. 2 cm^3). The sub-samples were homogenized and analyzed for total carbon (TC) to calculate the carbonate contents (see paragraph 3.4). The main sample was first weighed and then washed through a 63 μm mesh, the remainder was oven dried at 60 °C and weighed again. This residue represents the dry sand fraction, which typically consists of nearly 100 % carbonate in the investigated samples. After weighing, the sand fraction was separated in different size fractions by dry sieving (63 – 125 μm, 125 – 250 μm, 250 – 315 μm, 315 – 400 μm, and > 400 μm at Sites 999 and 1000; 63 – 125 μm, 125 – 250 μm, 250 – 355 μm, 355 – 400 μm, and > 400 μm at Site 1241, and 0 – 125 μm, 125 – 250 μm and > 250 μm at Sites 1237 and 1239).

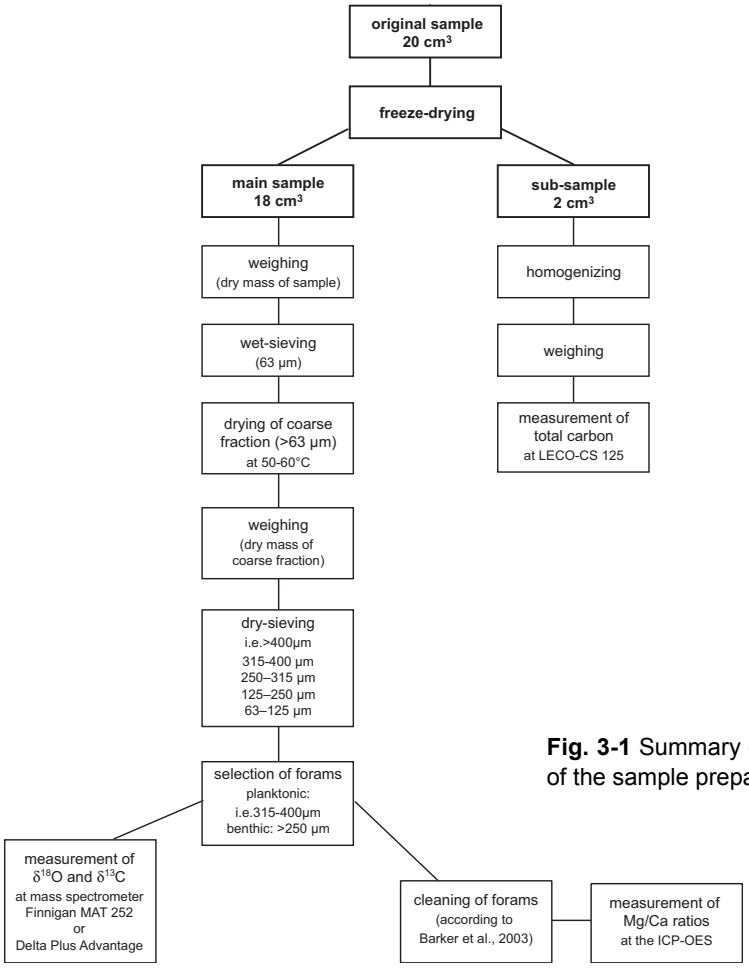

Fig. 3-1 Summary of individual steps of the sample preparation.

3.2 Stable isotope measurements

For each stable isotope measurement ($\delta^{18}O$ and $\delta^{13}C$) 10 to 15 specimens of the planktonic foraminifers *G. sacculifer, G. limbata* (dextral variety), *N. dutertrei, G. tumida* were selected from the following size fractions: for Sites 999 and 1000 from the 315 – 400 μm fraction, for Site 1241 from the 355 – 400 μm fraction (250 – 355 μm for *N. dutertrei*) and for Site 1239 from the > 250 μm fraction. For benthic isotope records, 1-5 tests of the epibenthic species *C. wuellerstorfi* or *C. mundulus* (> 250 μm) were analyzed. Prior to analysis, contaminated specimens were slightly crushed and ultrasonically cleaned with methanol. The excess liquid and mud were siphoned off and the samples were dried at 60°C.

The determination of oxygen and carbon isotopes on planktonic and epibenthic foraminifers was routinely carried out at the laboratory of IFM-GEOMAR (Kiel), using a either a Finnigan Delta-Plus-Advantage mass spectrometer coupled to a Finnigan Gas Bench II (with analytical precision better than ± 0.07 ‰ for $\delta^{18}O$ and better than ± 0.05 ‰ for $\delta^{13}C$; ± 1σ), or a Finnigan MAT 252 mass spectrometer with automated Kiel carbonate preparation device (with analytical precision better than ± 0.07 ‰ for $\delta^{18}O$ and ± 0.04 ‰ for $\delta^{13}C$; ± 1σ). Both machines were intercalibrated using a house standard. The ratios of $^{18}O/^{16}O$ and $^{13}C/^{12}C$ are reported as relative deviations (δ-notation) from a laboratory standard, here with reference to the Pee Dee Belemnite (PDB) standard (Craig, 1957). The calibration to the PDB standard was calculated *via* the National Bureau of Standards NBS-19 and an internal laboratory standard of Solnhofen Limestone (Tiedemann, pers. comm.).

3.3 Mg/Ca measurements

For Mg/Ca measurements, 20 – 25 specimens of the deep-dwelling planktonic foraminiferal species *G. tumida, G. limbata* (dextral variety), and *N. dutertrei* were picked from the same size fraction as used for stable isotope analyses. In case of insufficient numbers of specimens, the fraction 250 – 355 μm was used to provide additional material, from which up to 35 specimens were picked. After gentle crushing, the samples were cleaned according to the cleaning protocol for Mg/Ca of Barker et al. (2003). To remove clays, the samples were rinsed 4 – 6 times with distilled deionized water and twice with methanol (suprapure) with ultrasonical cleaning steps (2 – 3 minutes) after each rinse. Subsequently, samples were treated with a hot (97 °C) oxidizing 1 % NaOH/ H_2O_2 solution (10 ml 0.1 N NaOH (analytical grade); 100 μl 30 % H_2O_2 (suprapur)) for 10 minutes to remove organic matter. Every 2.5 minutes, the vials were rapped on the bench top to release any gaseous build-up. After 5 minutes, the samples were placed in an ultrasonic bath for a few seconds in order to maintain contact between reagent and sample. This treatment was repeated after refreshment of the oxidizing solution. The remaining oxidizing solution was removed during three rinsing steps with distilled deionized water. After transferring the samples into clean vials, a weak acid leach with 250 μl 0.001 M HNO_3 (subboiled distilled) was applied with 30 seconds ultrasonic treatment and subsequent two rinses with distilled deionized water. After cleaning, the samples were dissolved in 0.075 M nitric acid (HNO_3) (subboiled distilled) and diluted several

times, until all samples obtained calcium concentrations in the range of 30 – 70 ppm, being the ideal range for analyses (Garbe-Schönberg et al., in prep.).

The analyses were performed on a simultaneous, radially viewing ICP-OES (Ciros CCD SOP, Spectro A.I., Germany) at the Institute of Geosciences (Kiel University, Germany). The analytical error on the analysis of the Mg/Ca ratios was 0.1 % for a total of 600 samples. Replicate analyses on the same samples, which were cleaned and analyzed during different sessions, showed a standard deviation of 0.09 mmol/mol, introducing a temperature error of about 0.5 °C (for additional information see Groeneveld et al., submitted a,b).

For *G. tumida*, *N. dutertrei*, and *G. limbata*, Mg/Ca temperatures were calculated by using the paleotemperature equation of Anand et al. (2003) (SST = (Log(Mg/Ca)-Log 0.38)/0.09). As this equation is based on a multispecies approach, it allowed for the use of the same calibration for the different species of deep-dwelling foraminifers. Mg/Ca analyses of the mixed-layer-dweller *G. sacculifer* (data shown in chapters 5, 6, and 7) were established within the PhD thesis of J. Groeneveld.

3.4 Carbonate measurements, LECO

Weight percent carbonate contents at Site 1241 were determined by infrared absorption of total carbon (TC, organic and inorganic carbon) released by combustion with a LECO-CS 125-analyser (at IFM-GEOMAR, Kiel). Prior to analysis, the bulk sediment was carefully hand-ground in an agate mortar to achieve homogenous material. Double measurements were obtained for each sample. For analyses, china containers were filled with 20 – 30 mg of sediment and weighed. The samples were then burned at 1200 °C in an inductive oven using copper as catalyst. Deviations of 0.5 % TC between double measurements were tolerated. In case of deviations exeeding this value, a third or fourth run was performed. In order to obtain the weight percentage of calcium carbonate, the measured TC values were multiplied by 8.33, according to the ratio of the atomic weight of C to $CaCO_3$ (under the assumption that all carbon is bound as $CaCO_3$). The TC percentages were considered to fully represent carbon bound in $CaCO_3$, because the organic carbon contents are always lower than 0.4 % in the early Pliocene section of Site 1241 (Mix et al., 2003). Hence, carbonate percentages might be overestimated by a maximum of 3.3 % (equal to an organic carbon content of 0.4 %).

3.5 Stratigraphy, orbital tuning

An accurate time calibration of sediment sequences is essential because it provides the basis for all interpretations concerning the history of ocean circulation and climate. At present, the astronomical tuning technique is the best absolute dating method for sediment records spanning the last 35 Ma, for which astronomers provide a valid and precise orbital solution for variations in Earth's orbital parameters (Laskar, 1999). Astronomical tuning is based on the fact that changes in climate proxy records respond statistically convincing to cyclic variations in orbital parameters, like eccentricity (periods of 413 k.y. + 100 k.y.), obliquity (41-k.y. period), and precession (23-k.y. and 19-k.y. periods). Calculated astronomical records for these orbital parameters provide the basis for dating Neogene sediment records by matching patterns of cyclic variation in climate proxy records with patterns of changes in solar radiation that are controlled by cyclic variations in Earth's orbital parameters. The application of this tuning procedure offers the opportunity for a high precision time-calibration, because the "astronomical clock" is very accurate and cyclic changes in orbital parameters provide very small-scale time markers on geological time scales (Laskar, 1990; Berger and Loutre, 1991; Tiedemann et al., 1994). The error of an astronomically tuned time scale is systematic due to a constant, mostly unknown time lag between changes in orbital insolation and following climate response, including a few thousand years. Thus, the orbital tuning method is far more precise than radiometric dating alone (Hilgen et al., 1999). Within this inaccuracy, the tuning approach provides a reliable and absolute time scale for the magnetic reversal stratigraphy, biostratigraphy, oxygen isotope stratigraphy, and, of course, for records of climate and oceanographic variability that transfer the astronomical record of varying insolation into quasi-cyclic sedimentological variability. The orbitally tuned geological time scale already became the standard chronology for the Pleistocene and Pliocene (0 – 5.3 Ma), when the tuned ages of magnetic reversals were adopted to the geological time scale (Cande and Kent, 1995).

Desirable preconditions for the establishment of an orbitally tuned age scale are:

- The completeness of the recovered sediment sequence (e.g. coring of multiple holes at one ODP-Site) and coring with the APC system to avoid drilling disturbance.
- The establishment of a composite depth (mcd) that ensures a complete stratigraphic profile (in absence of hiatuses) and replaces drilling disturbed intervals. Sampling follows the composite depth sections and switches between holes.
- Relatively constant sedimentation rates, allowing a temporal sampling resolution of 2000 – 3000 years to ensure the detection of the full range of orbital cycles (19 – 413 k.y).
- High carbonate concentrations of the sediment that allow the establishment of high-resolution benthic oxygen and carbon isotope records on well preserved foraminifers.
- Additional proxy records that reveal pronounced cyclic variations on orbital time scales, as for example the percentage sand of carbonate record or shipboard logging data like sediment density, color data, or magnetic susceptibility.
- Magnetostratigraphy and high-resolution biostratigraphy to allow global comparisons.

The Pliocene sediment records of tropical east Pacific Sites 1237 and 1241 offered an excellent opportunity for the establishment of astronomically dated age scales (see chapter 4). The age model of tropical east Pacific Site 1241 is based on tuning high frequency variations in the percentage sand of carbonate fraction and in the benthic $\delta^{13}C$ record to the orbital solution of Laskar et al. (1993), whereas at Site 1237, the benthic $\delta^{13}C$ record and shipboard logging data (GRA density and magnetic susceptibility) were most suitable for orbital tuning. The correlation of benthic isotope stratigraphies between Sites 1237 and 1241 demonstrated that their astronomically calibrated age models are in good agreement within an error range of a few thousand years. Furthermore, the comparison of benthic stable isotope stratigraphies from tropical east Pacific Site 1241 and tropical West Atlantic Site 925/926 (Tiedemann and Franz, 1997; Billups et al., 1997; Shackleton and Hall, 1997) showed an excellent agreement of their orbitally tuned age models (for Site 925/926 established by Tiedemann and Franz, 1997; Shackleton and Crowhurst, 1997).

This year in January, Lisiecki and Raymo (2005) published a stack of benthic $\delta^{18}O$ records (the "LR04" stack) for the last 5.3 Ma, using 57 globally distributed sites aligned by an automated graphic correlation algorithm. This dataset includes at least 12 records back to 4.9 Ma, and 5 records from 5.0 – 5.33 Ma, and serves as the latest stratigraphic benthic $\delta^{18}O$ reference record. During the final stage of this work, it was thus possible to compare the "LR04" stack with the benthic $\delta^{18}O$ record from tropical east Pacific Site 1241 (**Fig. 3-2**). This comparison suggests nearly identical ages for the numbered oxygen isotope stages between 2.4 Ma and 5.0 Ma. The good aggreement between these two records provided additional proof for the quality of the orbitally derived age model for the tropical east Pacific Sites 1241 and 1237, but also for the "LR04" stack. However, larger deviations between the "LR04" stack and Pacific/Atlantic reference records (Sites 1241, 1237, and 925/926) occurred in the time interval older than 5.0 Ma.

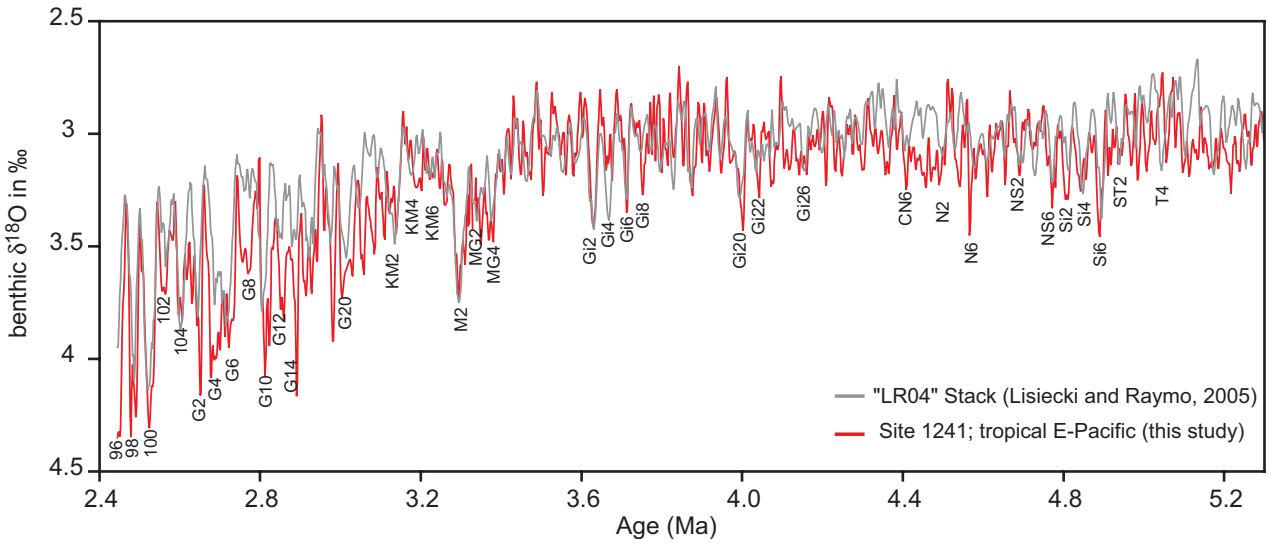

Fig. 3-2 Comparison of the benthic $\delta^{18}O$ record from tropical east Pacific Site 1241 (this study, red line) to the benthic $\delta^{18}O$ stack (gray line) of Lisiecki and Raymo (2005) for the time interval from 2.4 – 5.3 Ma.

The records from east Pacific Sites 1236 and 1239 were not directly tuned to variations in Earth's orbital parameters. At Site 1236, the sedimentation rates are too low to suit for orbital tuning (0.5– 1 cm/k.y.), and Site 1239 still lacks a composite depth scale for the Pliocene interval, which would cover and identify coring gaps that may occur at core breaks. The stratigraphic adjustment of both sites was thus achieved by correlating their benthic $\delta^{18}O$ and $\delta^{13}C$ records to the orbitally tuned isotope record of Site 1241 (chapter 4). The opportunity for an astronomical calibration of the late Miocene to Pliocene time scale was also limited at the Caribbean Sites 999 and 1000, as for both sites no composite depth exists. Their age models are thus based on correlating the benthic $\delta^{18}O$ and $\delta^{13}C$ records to the orbitally tuned benthic isotope stratigraphy from Atlantic Site 925/926 (Leg 154), which is in agreement with that from Site 1237 and 1241. This procedure indirectly resulted in an orbitally tuned age model for the Pliocene sections of Site 999, 1000, 1236, and 1239. This stratigraphic framework finally ensured direct comparisons between Pacific and Caribbean proxy records in the time and frequency domain.

3.5.1 Tuning tools

The software package AnalySeries 1.2 (Paillard et al., 1996) was used for orbital tuning, stratigraphic alignment, and spectral analyses. AnalySeries especially facilitates the transformation of "proxy data versus depth" records into "proxy data versus age" records by graphically adjusting cyclic fluctuations of paleoclimate proxy records to the astronomical tuning target or to reference proxy records. The age of each data point is estimated by linear interpolation between age-depth control points. AnalySeries also provides filters and a set of spectral analysis methods that are partly complementary in terms of robustness versus resolution. The classical Blackman-Tuckey method (Blackman and Tuckey, 1958) was used for spectral analysis in the time and depth domain. Tuckey bandpass filters with a central frequency of 0.0476 cycles/k.y. (bandwidth 0.01) and 0.025 cycles/k.y. (bandwidth 0.009) were used to extract the precession and obliquity-related components from the proxy records, respectively. The orbital solution of Laskar et al. (1993) was used as tuning target for Pliocene variations in northern hemisphere summer insolation, obliquity, and precession.

CHAPTER 4

ASTRONOMICALLY CALIBRATED TIME SCALES FROM 6 – 2.5 MA AND BENTHIC ISOTOPE STRATIGRAPHIES OF SITES 1236, 1237, 1239 AND 1241

Ralf Tiedemann[1], Arne Sturm[1], Silke Steph[1], Steven P. Lund[2], and Joseph S. Stoner[3]

[1]IFM-GEOMAR, Wischhofstr. 1-3, 24148 Kiel, Germany

[2]Department of Earth Sciences, University of Southern California, Los Angeles, USA

[3]COAS, Oregon State University, Corvallis, USA

submitted to ODP Scientific Results, *Volume 202*

Abstract

We present benthic isotope stratigraphies for Sites 1236, 1237, 1239 and 1241 that span the late Miocene to Pliocene time interval from 6 Ma to 2.4 Ma. Orbitally tuned time scales were generated for Sites 1237 and 1241 by correlating the high frequency variations in GRA density, percent sand of the carbonate fraction, and benthic $\delta^{13}C$ to the orbital solution of Laskar et al. (1993). The astronomical time scales for Sites 1237 and 1241 are in agreement with the one from Atlantic Site 925/926 (Leg 154). The comparison of benthic $\delta^{18}O$ and $\delta^{13}C$ records from the east Pacific sites and Atlantic Site 925/926 revealed a surprising clarity of the "41-k.y. signal" in $\delta^{13}C$ records and a remarkably good correlation between their $\delta^{13}C$ records. This suggests that the late Miocene to Pliocene amplitudes of obliquity-related $\delta^{13}C$ cycles reflect a magnitude of global response, often larger than that provided by obliquity-related $\delta^{18}O$ cycles. At Site 1237, the orbitally derived ages of Pliocene magnetic reversal boundaries between the base of Réunion and the top of Thvera confirm earlier astronomical datings of Shackleton et al. (1995) and Lourens et al. (1996), except for the Kaena chron. Our astronomical ages for the base and top of Kaena are one and two obliquity cycles older, respectively. The age models of Sites 1236 and 1239 were established by correlating their benthic $\delta^{18}O$ and $\delta^{13}C$ records directly to the orbitally tuned isotope record of Site 1241.

4.1 Introduction

Our goal is to establish an astronomical time scale (ATS) from 12 Ma to 2.5 Ma at Sites 1237 and 1241 that integrates the framework of magnetostratigraphy, biostratigraphy, tephrachronology and oxygen isotope stratigraphy. Here we present a progress report that documents our results of an orbitally tuned stratigraphy for the early Pliocene time interval from 6 Ma to 2.5 Ma. The tuned ages of magnetic reversals (Site 1237) and oxygen isotope records (1237 and 1241) are directly compared with other orbitally tuned age models from Ceara Rise (Tiedemann and Franz, 1997), the equatorial east Pacific (Shackleton et al., 1995), and the Mediterranean (Lourens et al., 1996).

The astronomical tuning technique is at present the most accurate absolute dating method for sediment records spanning the time interval of the last 35 Ma, for which astronomers provide a valid and precise orbital solution for variations in Earth's orbital parameters (Laskar, 1999). Changes in the eccentricity of the Earth's orbit are marked by main periods of 413 k.y. and 100 k.y., and the tilt and precession of the Earth's axis are dominated by periods of 41 k.y. and 23/19 k.y, respectively. These astronomical records provide the basis to date Neogene sediment records by matching patterns of cyclic variation in climate proxy records with patterns of changes in solar radiation that are controlled by cyclic variations in Earth's orbital parameters. The astronomical tuning method is based on the fact that cyclic changes in climate proxy records respond statistically convincing to variations in insolation. The application of this tuning procedure made a high-precision time-calibration possible, because the "astronomical clock" is very accurate and cyclic changes in orbital parameters give very small-scale time markers on geological time scales (Laskar, 1990; Berger and Loutre, 1991). At best, the ATS could provide an age control point every 10.000 or 20.000 years, corresponding to half of a precession or an obliquity cycle. The orbital tuning method is far more precise than that achievable by radiometric dating alone (Hilgen et al., 1999). The error of an astronomically tuned time scale is systematic and includes a few thousand years, based on the assumption of a constant (mostly unknown) time lag between a change in orbital insolation and the following climate response. Within this inaccuracy, the tuning approach provides a reliable and absolute time scale for the magnetic reversal stratigraphy, the biostratigraphy, the oxygen isotope stratigraphy, and, of course, for records of climate and oceanographic variability that transfer the astronomical record of varying insolation into quasi-cyclic sedimentological variability. The orbitally tuned geological time scale already became the standard chronology for the Pleistocene and Pliocene (0 – 5.3 Ma), when the tuned ages of magnetic reversals were adopted to the geological time scale (Cande and Kent, 1995).

The improvement of the Pleistocene astronomical polarity time scale (APTS) and its expansion into the Miocene has been primarily pushed forward by two scientific groups, using sedimentary cycle patterns in both, marine successions exposed on land in the Mediterranean (Hilgen and co-workers, Utrecht) and marine records from Ocean Drilling Program (ODP) sites located in the equatorial Pacific and Atlantic (Shackleton and co-workers, Cambridge). Hilgen (1991a, b) developed a Pliocene APTS back to 5.3 Ma by correlating sedimentary

cycles from land-based sections to the astronomical record (Berger and Loutre, 1991). Lourens et al. (1996) improved this record by tuning to the astronomical solution of Laskar et al. (1993). The work of Hilgen et al. (1995), Krijgsman et al. (1999) and Hilgen et al. (2003) expanded the Mediterranean APTS back to 13.6 Ma.

Based on marine records from ODP Leg 138 in the eastern equatorial Pacific, Shackleton et al. (1995) developed an APTS for the past 6 Ma by matching cyclic variations in gamma ray attenuation (GRA) density records to the orbital insolation record of Berger and Loutre (1991), and advanced the Pliocene oxygen isotope stratigraphy from 2.5 Ma to 6 Ma. At the same time, Tiedemann et al. (1994) developed an astronomically calibrated oxygen isotope timescale for northeast Atlantic Site 659 off the coast of Africa by tuning Pliocene variations in dust flux (2.5 Ma to 5 Ma) to the astronomical solution of Berger and Loutre (1991). These studies provided a common benthic oxygen isotope stratigraphy and nomenclature for the Pliocene. The work of Shackleton et al. (1995) also provided a preliminary tuning from 6 to 10 Ma by using an astronomically calibrated age of 5.9 Ma for the magnetic reversal C3A.n(t) as a starting point and an age of 9.6 Ma for C5n.1n(t) as a fixed end point that, however, was based on radiometric dating. The APTS from Leg 138 suggests that the ages of the late Miocene reversal boundaries are up to 180 k.y. younger than those derived from the Mediterranean area (Hilgen et al., 1995; Krijgsman et al., 1999). The offset seems to develop in the interval from 5.3 Ma to 6 Ma (Kent, 1999).

More recently, Tiedemann and Franz (1997), Shackleton and Crowhurst (1997), and Shackleton et al. (1999) established an ATS from 2.5 – 34 Ma at sediment records from Leg 154 (Ceara Rise) by tuning sedimentary cycles to the astronomical record of Laskar et al. (1993). The work of Tiedemann and Franz (1997), Billups et al. (1997), and Shackleton and Crowhurst (1997) provided an oxygen isotope stratigraphy for the interval from 2.5 Ma to 7 Ma (Site 925/926). The application of the Laskar solution (instead of Berger and Loutre, 1991) modified the calibration of the early Pliocene isotope stages prior to ~4 Ma to one obliquity cycle older than previously proposed. Unfortunately, the sediment records from Leg 154 provided no magnetostratigraphic information, which complicates comparisons with other time scales.

Rapid progress in advancing the marine APTS to the Neogene/Paleogene boundary is limited by the availability of good reference sections. The sediment record from Site 1237 that was drilled during Leg 202 on Nazca Ridge meets nearly all aspects of providing such a reference section. (1) It comprises a complete Neogene sequence that was drilled by the Advanced Hydraulic Piston Corer Technique (APC). The composite depth section documents complete recovery for the sequence from 0 Ma to ~31.5 Ma without any detectable stratigraphic breaks as indicated by microfossil and magnetic stratigraphy. (2) Various types of data, indicative of changes in chemical sediment composition and physical properties document the evident orbital cycles. (3) High carbonate concentrations allow the establishment of high-resolution benthic oxygen and carbon isotope records and offer an excellent potential for refining the foraminiferal and nannofossil biostratigraphy. (4) The paleomagnetic

stratigraphy at Site 1237 is excellent with clear definitions of all chrons and subchrons over the last 5 Ma as well as from 7 Ma to 13 Ma. The polarity assignments for the interval from 5 – 7 Ma and for the lowermost part of the sequence between 13 Ma and 31 Ma are still preliminary, because the polarity sequence allows several possible interpretations. At Site 1237 so far, we developed an astronomically tuned age model for the time interval from 2.5 Ma to 6 Ma that includes a benthic oxygen isotope stratigraphy from 4 Ma to 6 Ma.

To verify our tuning at Site 1237, we also established an orbitally tuned time scale at Site 1241. Site 1241 yielded a complete and continuous sediment record for the time interval of the last 9 m.y. Here, we measured a benthic isotope record from 2.5 Ma to 5.7 Ma that enables a comparison with that from Site 1237 within the overlapping time interval from 4 Ma to 5.7 Ma.

4.2 Data and Methods

For orbital tuning, we considered shipboard core logging data (magnetic susceptibility, bulk density, color spectra) as well as carbonate percentages, sand fraction percentages of the carbonate fraction and benthic isotope records. Core logging shipboard data (Mix et al., 2003) were measured at intervals of 2.5 cm (Site 1237) and 5 cm (Site 1241) and provide a temporal resolution of 1000 – 2500 years, which corresponds to sedimentation rates ranging from 1 – 3 cm/k.y. at Site 1237 and from 2 – 5 cm at Site 1241. Isotope data, carbonate and sand percentages were measured every 5 cm at Site 1237 and every 10 cm at Site 1241.

Isotope data from Sites 1237 and 1241 were analyzed at the IFM-GEOMAR Institute in Kiel using a Finnigan/MAT-252 mass spectrometer equipped with a fully automated Finnigan/Kiel-Carbo-II carbonate preparation device. For each isotope analysis up to 5 specimens of the epibenthic foraminifers *C. wuellerstorfi* or *C. mundulus* were picked from the 250 – 500 μm fraction. The laboratory standard was calibrated to PDB through NBS 19. Analytical reproducibility of the laboratory standard typically was about ± 0.06 ‰ for $\delta^{18}O$ and ± 0.03 ‰ for $\delta^{13}C$ (± 1σ). Isotope data from Site 1236 were measured at the Leibniz Labor for Radiometric Dating and Isotope Research at Kiel University using a Finnigan/Delta-Plus-XL mass spectrometer coupled to a Finnigan/Gas-Bench-II. Precision of the local carbonate standard was ± 0.07 ‰ for $\delta^{18}O$ and ± 0.05 ‰ for $\delta^{13}C$ (± 1σ) over the period of analyses.

The $CaCO_3$ contents were determined by infrared absorption of total CO_2 (organic and inorganic carbon) released by combustion with a LECO-Analyser. Early Pliocene organic carbon contents are lower than 0.4 % at Sites 1236, 1237 and 1241 (Mix et al., 2003). Hence, carbonate percentages might be overestimated by up to 3.3 % (equal to an organic carbon content of 0.4 %).

The sand fraction represents the wet-sieved residue of the fraction > 63 μm, which consists of nearly 100 % carbonate. The content of the dry sand fraction is given as weight percent of total $CaCO_3$ to compensate for dilution effects caused by noncarbonate dilutants.

For orbital tuning and spectral analyses, we used the software package AnalySeries 1.2 (Paillard et al., 1996). AnalySeries especially facilitates the transformation of "proxy data versus depth" records into "proxy data versus age" records by graphically adjusting cyclic fluctuations of paleoclimatic proxy records to the astronomical target record. The age of each data point was estimated by linear interpolation between age-depth control points. AnalySeries also provides filters and a set of spectral analysis methods that are partly complementary in terms of robustness versus resolution. We preferred to use the classical Blackman-Tukey method (Blackman and Tukey, 1958) for spectral analysis in the time and depth domain. The algorithm computes first the auto-covariance of the data, then applies a window, and finally Fourier-transforms it to compute the spectrum. It is a very robust method, unlikely to present spurious spectral features. The main drawback is its poor resolution in the spectral domain, because sharp features can be considerably smoothed. This method allows to choose a resolution versus confidence parameter: the length of the auto-covariance series, which is generally set to 60 % of the input series. The confidence level associated with the error bar on the spectrum is typically set to 80 %. For filtering and spectral analysis in the time domain, we interpolated each record at equidistant intervals, corresponding to the average time resolution of the proxy record. Tukey bandpass filters with a central frequency of 0.0476 cycles/k.y. (bandwidth: 0.01) and 0.025 cycles/k.y (bandwidth: 0.009) were used to extract the precession and obliquity-related components from the proxy records, respectively.

We used the orbital solution from Laskar et al. (1993) for Pliocene variations in northern hemisphere summer insolation, obliquity, and precession as a tuning target. Until 1996, orbitally derived age models where based on the astronomical solution of Berger and Loutre (1991). Lourens et al. (1996) demonstrated, however, that unrealistic large time lags will occur between obliquity and the obliquity-related variations in the proxy records, if the orbital data from Berger and Loutre (1991) are used as a tuning target. Lourens et al. (1996) pointed out that the geological record can be calibrated most accurately to the summer insolation record calculated from the Laskar et al. (1993) solution $La93_{(1,1)}$ with a dynamically ellipticity of the Earth of 1 and a tidal dissipation term of 1, both close to present day values. Differences between the astronomical solutions of Ber90 and $La93_{(1,1)}$ are small in the middle Pliocene but increase towards the Miocene. For example, the obliquity of Ber90 leads that from $La93_{(1,1)}$ by 22 k.y. at 5 Ma. At precession, Ber90 leads $La93_{(1,1)}$ by 10 k.y. at 5 Ma. More recently, Pälike and Shackleton (2000) showed that using the solution of Laskar (1993) with present day values for dynamically ellipticity and tidal dissipation as a tuning target for the last 25 Ma does not introduce large errors during astronomical tuning.

4.3 Revised composite depth scale at Site 1241

A major precondition for tuning marine paleoclimate records to the astronomical record is to ensure the recovery of complete and undisturbed sediment records. This is achieved by drilling multiple offset-holes at the same site location to splice across coring gaps and distorted sediment sequences through inter-hole correlations using closely spaced core-logging measurements. This strategy (Ruddiman et al., 1987) became a standard on paleoceanographic ODP Legs. At Site 1241, the construction of the composite depth was based on core logging magnetic susceptibility and gamma ray attenuation (GRA) density data. We reinspected the composite depth by considering in addition the core logging color data, which was not possible during the cruise due to time constraints. The correlation of overlapping sections from adjacent holes by means of color data suggests a mismatch between Cores 202-1241C-11H and 202-1241A-16H (**Fig. 4-1**). The former correlation resulted in a doubling of a 63 cm long sediment section. Our new splice suggests a switch point at 175.77 mcd, from 202-1241C-11H-7, 20 cm (same as before) to 202-1241A-16H-4, 72 cm. This deletes 63 cm from the former composite depth (the interval Core 202-1241A-16H-4, 7-72 cm: corresponding to an interval of 65 cm on the mbsf scale). The revision leads to a small reduction of the composite depth scale, as 63 cm are subtracted from the mcd below sample 202-1241A-16H-4, 72 cm.

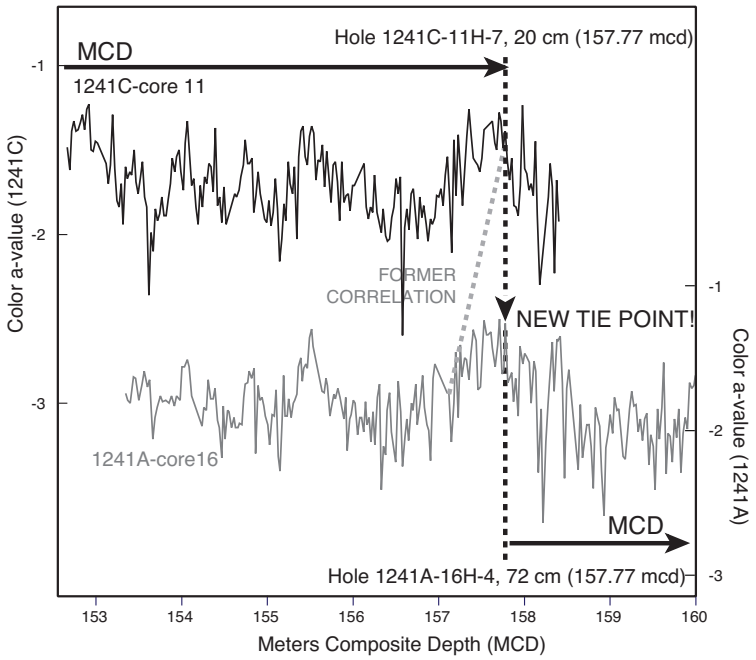

Fig. 4.1 Revision of former MCD-splice at Site 1241. Between - Hole correlations using color a-values suggest a new tie point in the mcd splice at 157.77 mcd (black dotted line). The composite depth switches from Hole 1241C-11H-7, 20 cm to Hole 1241A-16H-4, 72 cm. The former tie point switched from Hole 1241C-11H-7, 20 cm to Hole 1241A-16H-4, 7 cm, which is 65 cm upcore from the new tie point (dotted gray line). As a consequence, the former composite depth (MCD) has to be corrected by -65 cm below 157.77 mcd (by deleting the interval from 1241A-16H-4, 7 cm to 1241A-16H-4, 72 cm).

4.4 Tuning procedure

At best, the tuning medium should be marked by cyclic, high amplitude fluctuations and a high signal-to-noise ratio. From our experience, however, we know that a single climate proxy record mostly includes an interval of low signal-to-noise ratios, where a clear interpretation of the geological record with regard to its orbitally induced variability is difficult to derive. Therefore, we used a multi-proxy approach for orbital tuning to overcome such problems. Discrete ash layers (Mix et al., 2003) were removed from the data sets to avoid misinterpretations of the climate signal and distortions of sedimentation rates. The sediment record from Site 1237 was especially affected by the frequent deposition of ash layers. Fourteen ash layers were identified in the time interval from 2.4 Ma to 6 Ma by the Leg 202 shipboard party, some of them ranging in thickness from 15 cm to 36 cm. Inspection of the sand fraction record indicated that the range with significant amounts of ash often spanned a larger interval than simply suggested by a discrete ash layer. Although we deleted discrete ash layers from the composite depth, the "normal pelagic sedimentation rate" is overestimated by the amount of dispersed ash in such intervals.

The first step toward astronomical calibration was to identify dominant cycles of selected proxy records in the depth domain by means of spectral analyses on succeeding 10 m long intervals. This approach helped to trace long-term changes in sedimentation rates; e.g., an increase in sedimentation rate would move dominant precession or obliquity-related frequencies (cycles/m) to lower frequencies. The spectral comparison between different proxy records also clearly identifies precession and obliquity-related cycles and indicates which of the proxy records are best suited for tuning to the precession and/or obliquity.

In a second step, we extracted the precession and obliquity-related components from the proxy records by bandpass filtering each of the succeeding 10 m long sections. We then used the merged filter outputs for a first tuning. We started with tuning to obliquity for two reasons. First, most proxy records revealed a stronger response to obliquity than to precession. Considering more than one proxy for tuning to obliquity improved the continuous and reliable detection of the 41-k.y. cycle from 2.5 Ma to 6 Ma. Second, the effect of obliquity on insolation is symmetric across hemispheres. That is, cold summers occur in both hemispheres at the same time (in phase). This increases the likelihood that proxy records indicative of global climate change respond to obliquity forcing with possibly different but relatively constant phase lags. Pliocene variations in benthic $\delta^{18}O$ and $\delta^{13}C$ are dominated by 41-k.y. cycles and are thought to respond with relatively constant phase lags to obliquity forcing. Fluctuations in benthic $\delta^{18}O$ records are linked to high latitude processes because they are sensitive to variations in global ice volume and to changes in deep-water temperature/salinity. Provided that the effect of obliquity on insolation is symmetric across hemispheres, the mid-Pliocene shift from unipolar to bipolar glaciations or changes in the location of predominant deep-water formation (Southern Ocean versus North Atlantic) should not have significantly affected the phase of the obliquity-related benthic $\delta^{18}O$ variations (Clemens, 1999). The work of Imbrie and Imbrie (1980) and Imbrie et al. (1984) suggested a lag between obliquity and

obliquity-controlled variations in ice volume of 8 k.y. for the Pleistocene time interval. Their model also implied that the time lag strongly depends on the size of the ice sheet, whereas a smaller ice sheet would result in a smaller phase lag. For the relatively warm Pliocene interval prior to the northern hemisphere glaciation, the true phase lag may have been close to 6 k.y. as suggested by Chen et al. (1995). The disadvantage of solely using Pliocene benthic $\delta^{18}O$ records for orbital tuning is their low signal-to-noise ratio, because the small variability in global ice volume prior to the northern hemisphere glaciation (> 3 Ma) distinctly decreased the $\delta^{18}O$ amplitudes. In some intervals of the early Pliocene, the signal-to noise ratio is so low that it is difficult to decide whether 41-k.y. cycles are registered or not (Tiedemann et al., 1994; Shackleton et al., 1995). In this context, the benthic $\delta^{13}C$ records are an alternative for tuning to obliquity. Obliquity-related fluctuations in benthic $\delta^{13}C$ are thought to be largely controlled by global variations in marine productivity and the mass of organic matter stored in forests, soils and shallow marine sediments (Shackleton, 1977), presumably related to glacial-interglacial climate change. Although the globally correlative nature of the Pliocene benthic $\delta^{13}C$ signal has never been examined in detail, several studies indicated that Pliocene benthic $\delta^{13}C$ maxima lag $\delta^{18}O$ minima in the eastern Pacific with a relatively constant phase of ~2 k.y. at the obliquity band (Mix et al., 1995; Shackleton et al., 1995). Considering a phase difference of 6 k.y. between Pliocene variations in orbital obliquity and benthic $\delta^{18}O$, $\delta^{13}C$ maxima may have lagged obliquity maxima by ~8 k.y. For an unambiguous tracing of 41-k.y. cycles, we also considered other proxy records like GRA density, magnetic susceptibility and color reflectance data. After determining their phase relationships with respect to $\delta^{18}O$ minima (warm stages), we established a preliminary age model that is based on tuning their 41-k.y. components to orbital obliquity. At this stage, the tuning provided constant phase relationships between the proxy records and orbital obliquity, but did not include the possible phase lags for $\delta^{18}O$ and $\delta^{13}C$, as mentioned above. Instead of that, we continued with tuning to precession, because matching the obliquity-related filter output of a proxy record to orbital obliquity is not as easy as tuning to precession, because the amplitudinal variability in orbital obliquity is low and thus provides no eye-catching control points for a correct match.

The advantage of tuning to orbital precession is that the amplitudinal power of orbital precession is well structured by eccentricity-induced packets of 100 k.y. or 400 k.y. intervals. These packets are often easily recognized in proxy records that are dominated by precessional variance (e.g. Tiedemann et al., 1994; Tiedemann and Franz, 1997). Therefore, we also used such packets for aligning climate variables with strong precessional responses. GRA density data from Site 1237 and the sand fraction record from Site 1241 reveal significant response to orbital precession forcing. Their precession-related filter outputs provided a powerful independent check on the correlation initially defined by tuning to obliquity. Nevertheless, we are aware of the fact that the amplitudinal variability of precession-related cycles could also be influenced by changes in sedimentation rates or internal processes of the climate system. Low sedimentation rates decrease the time resolution and the signal-to-noise ratio and thus may distort the original, amplitudinal climate response to orbital forcing. Internal processes of the climate system couple specific variables or mutually interact among them. These interactions

may either amplify anomalies of one of the interacting elements or damp them. Thus, we only set precession-based age control points, where the alignment with the orbital record is corroborated by both the precession component and the obliquity component of proxy records. A point of discussion is that we have no model linking the precessional response of the proxy records to orbital forcing. Precession insolation forcing is hemispherically asymmetric with northern hemisphere summers being 180° (11.5 k.y.) out of phase with southern hemisphere summers and we did not examine whether northern or southern hemisphere insolation exerted a stronger control on the precessional signal of the proxy records. We simply assumed that the observed correlation between benthic $\delta^{18}O$ warm stages and obliquity-related maxima or minima in proxy records is similar for precessional minima. For instance, if obliquity- related maxima in GRA density correlate with $\delta^{18}O$ warm stages (maxima in orbital obliquity), we also assumed that precession-related maxima in GRA density correspond to precession-controlled maxima in insolation. We used the summer insolation at 65°N as a target record and assumed an in-phase relationship between insolation and the proxy record. However, we did not tune to precession if the adjustment would lead to unrealistic large time lags between obliquity and glacial-bound variations in proxy-records indicative of global climate change.

4.5 Development of an orbitally derived age model for Site 1237

Sedimentation rates are relatively low (< 3 cm/k.y.) at Site 1237. For this reason, we first demonstrate that the quality of the logging data from Site 1237 is still appropriate for orbital tuning (**Fig. 4-2**). The depth interval from 60 – 80 mcd is especially suited for a test, because it has a well-constrained paleomagnetic age model that provides a first approximation of changes in sedimentation rates. Sedimentation rates range from 1.6 cm to 2 cm/k.y. between the Base of Mammoth and the Base of Cochiti. Within this interval, cyclic fluctuations of the GRA bulk density and magnetic susceptibility records are characterized by two major clusters of cycles, from 37 – 49 cm and from 77 – 114 cm (**Fig. 4-2**). These two clusters clearly identify the response to precession (19 k.y. and 23 k.y. cycles) and obliquity (41 k.y. cycle), whereas the range of the clusters is defined by the variability of sedimentation rates.

Spectral analyses in the depth domain suggested that the records of benthic $\delta^{13}C$, magnetic susceptibility, and GRA density are best suited for orbital tuning. The $\delta^{13}C$ and magnetic susceptibility records revealed significant variability at the obliquity frequency band. The GRA density record provided in addition also significant variability at precession-related frequencies (**Fig. 4-2**). Before tuning, we examined their relationships to obliquity-dominated changes in global climate as indicated by comparisons with the benthic $\delta^{18}O$ record. The GRA densities vary according to the nature of the sedimentary matrix, which is dominated by carbonate and smaller amounts of siliciclastics and biogenic opal. Maxima in GRA density reflect maxima in carbonate percentages. Obliquity-related maxima in GRA densities are associated with $\delta^{18}O$ warm stages and $\delta^{13}C$ maxima.

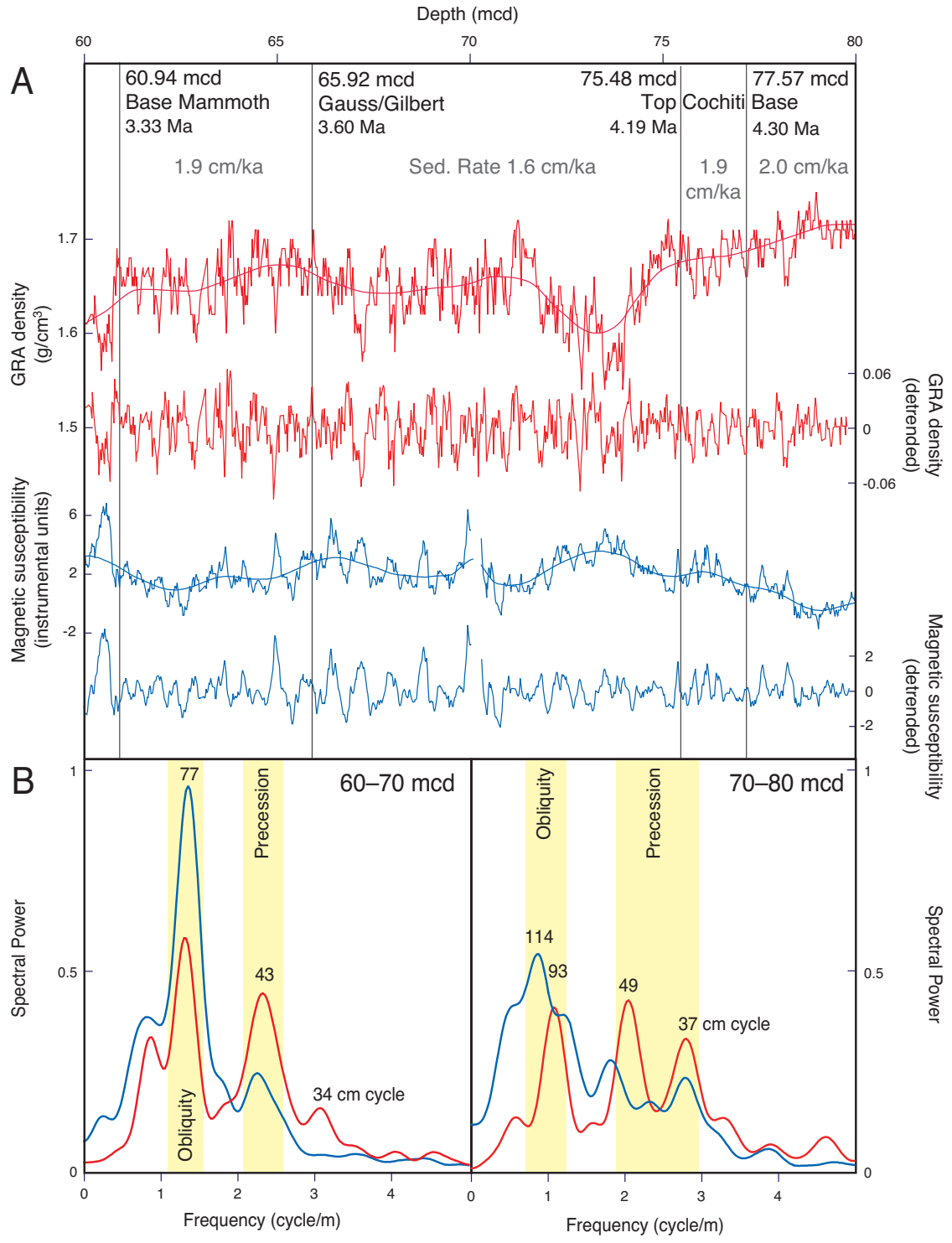

Fig. 4-2 Cyclic variations in gamma ray attenuation (GRA) density and magnetic susceptibility at Site 1237. **A.** Fluctuations in GRA density (red curve) and magnetic susceptibility (blue curve) between 60 and 80 mcd. Each record was detrended by subtraction of the Gaussian weighted smooth (thick lines). The detrended records were subjected to spectral analyses. Ages and depths of magnetic reversal boundaries are indicated. Sedimentation rates were estimated from magnetostratigraphy. **B.** Results from spectral analyses for the intervals from 60 – 70 mcd and 70 – 80 mcd. Cycle lengths are given in cm. Considering the sedimentation rates shown in A, cycles of 37 – 43 cm reflect precession cycles (23 k.y. and 19 k.y.) and cycles of 77 – 114 cm are related to obliquity cycles (41 k.y.).

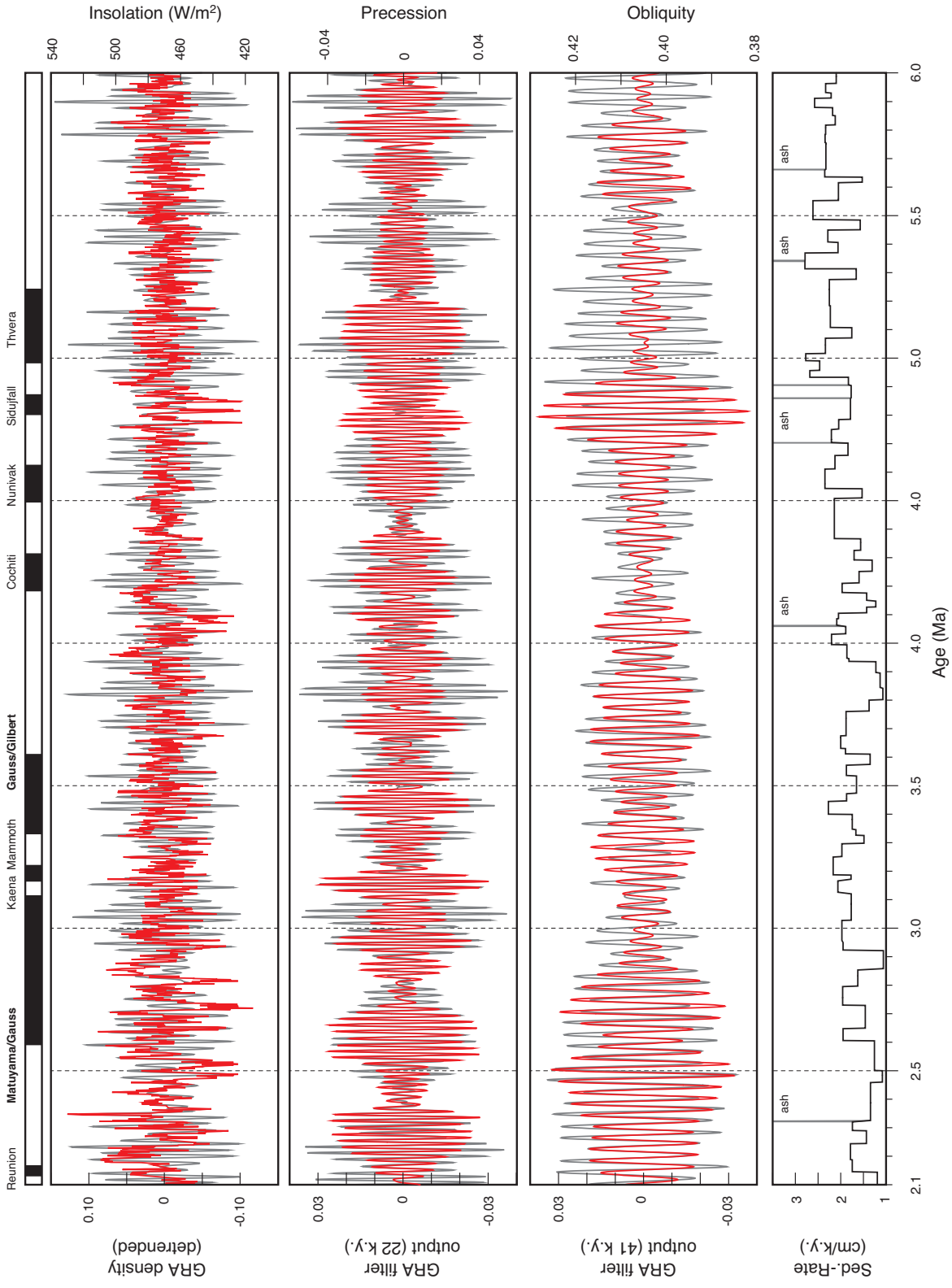

Fig. 4-3 Match between northern hemisphere summer insolation (65°N) and GRA density (detrended) at Site 1237 from 2.1 – 6.0 Ma. Comparison of orbital precession and obliquity with the 21 k.y. and 41 k.y GRA filter outputs, respectively. Sedimentation rates are corrected for ash layers (gray bars).

Tab. 4-1 Age model for Site 1237

Age (k.y.)	Depth (mcd)	Age (k.y.)	Depth (mcd)
2071	40.55	4210	76.00
2144	41.42	4252	76.67
2188	42.19	4291	77.18
2244	43.19	4325	77.76
2290	43.85	4366	78.40
2321	44.39	4508	81.44
2323	44.51	4542	81.96
2458	46.33	4611	83.58
2500	46.78	4658	84.58
2605	48.10	4702	85.39
2648	48.94	4703	85.57
2729	50.12	4751	86.63
2796	51.43	4784	87.30
2854	52.37	4858	88.63
2922	53.09	4859	88.76
2957	53.77	4904	89.56
3028	55.17	4905	89.71
3121	56.83	4932	90.21
3166	57.75	4956	90.84
3186	58.11	4990	91.69
3250	59.49	5015	92.38
3296	60.40	5069	93.64
3325	60.83	5106	94.29
3346	61.18	5183	96.00
3399	62.10	5275	98.07
3445	63.15	5313	98.70
3472	63.65	5338	99.40
3534	64.68	5343	99.90
3574	65.43	5369	100.63
3611	65.93	5406	101.39
3630	66.29	5449	102.37
3675	67.19	5485	102.94
3760	68.79	5552	104.68
3800	69.34	5615	105.99
3842	69.79	5635	106.28
3895	70.39	5660	106.88
3935	70.88	5662	107.03
3946	71.08	5755	109.19
3994	71.97	5784	109.87
4031	72.79	5817	110.64
4058	73.30	5850	111.34
4062	73.47	5878	111.95
4085	73.95	5911	112.80
4105	74.36	5930	113.22
4126	74.66	5963	113.99
4148	74.93	6013	115.04
4176	75.33		

The magnetic susceptibility record is negatively correlated to the carbonate record and represents the degree of magnetized sediment and hence approximates the ratio of siliciclastic versus biogenic material. Maxima in magnetic susceptibility reflect relatively higher amounts of siliciclastics during $\delta^{18}O$ cold stages. The siliciclastic fraction is mainly derived from eolian deposition, as Site 1237 underlies the modern path of dust that originates in the Atacama Desert of Chile (Mix et al. 2003). Accordingly, we correlated obliquity-related minima in magnetic susceptibility, maxima in GRA density, and maxima in benthic $\delta^{13}C$ with maxima in orbital obliquity (warm stages). We involve the benthic $\delta^{18}O$ record into this process in those intervals where obliquity-related cycles were clearly registered. We started our tuning from the Gauss/Matuyama boundary (47.9 ± 0.1 mcd), which has a well-constrained astronomical age of 2.59 ± 0.01 Ma (Shackleton et al., 1995; Lourens et al., 1996). Other magnetic reversal boundaries were not considered during the tuning process. An initial age model for the interval from 2.1 Ma to 6 Ma was derived by tuning the 41-k.y. component of the magnetic susceptibility record to orbital obliquity. The tuning was then verified *via* comparisons with the obliquity-related GRA density filter output. In a final approach, we matched the precessional component of the GRA record to the insolation record (**Fig. 4-3**) and reduced the number of tie points to an amount sufficient enough to keep the GRA density record approximately in phase with obliquity and precession (**Tab. 4-1**).

After tuning, we extracted the precession- and obliquity-related components from the proxy records by using Tukey band-pass filters. The filtered components are compared with the respective orbital time series in **Figures 4-3** and **4-4**. The 21-k.y. component of the GRA density record reveals a remarkably good resemblance with orbital precession in the intervals from 2.2 – 4.7 Ma and from 5.6 – 6.0 Ma, in particular with respect to the eccentricity

modulation as reflected in the amplitude variations. In addition, a very consistent relation is found between the 41-k.y. components in our proxy records (GRA density, benthic $\delta^{13}C$ and $\delta^{18}O$) and astronomical obliquity. The age model from 4.7 Ma to 5.6 Ma is mainly based on correlating the 41-k.y. signal of the isotope records to obliquity (**Fig. 4-4**), because the GRA density record provided a weak variability at the obliquity band, especially between 4.9 Ma and 5.5 Ma, and no clear similarity in amplitude fluctuations between orbital precession and the 21-k.y. GRA component.

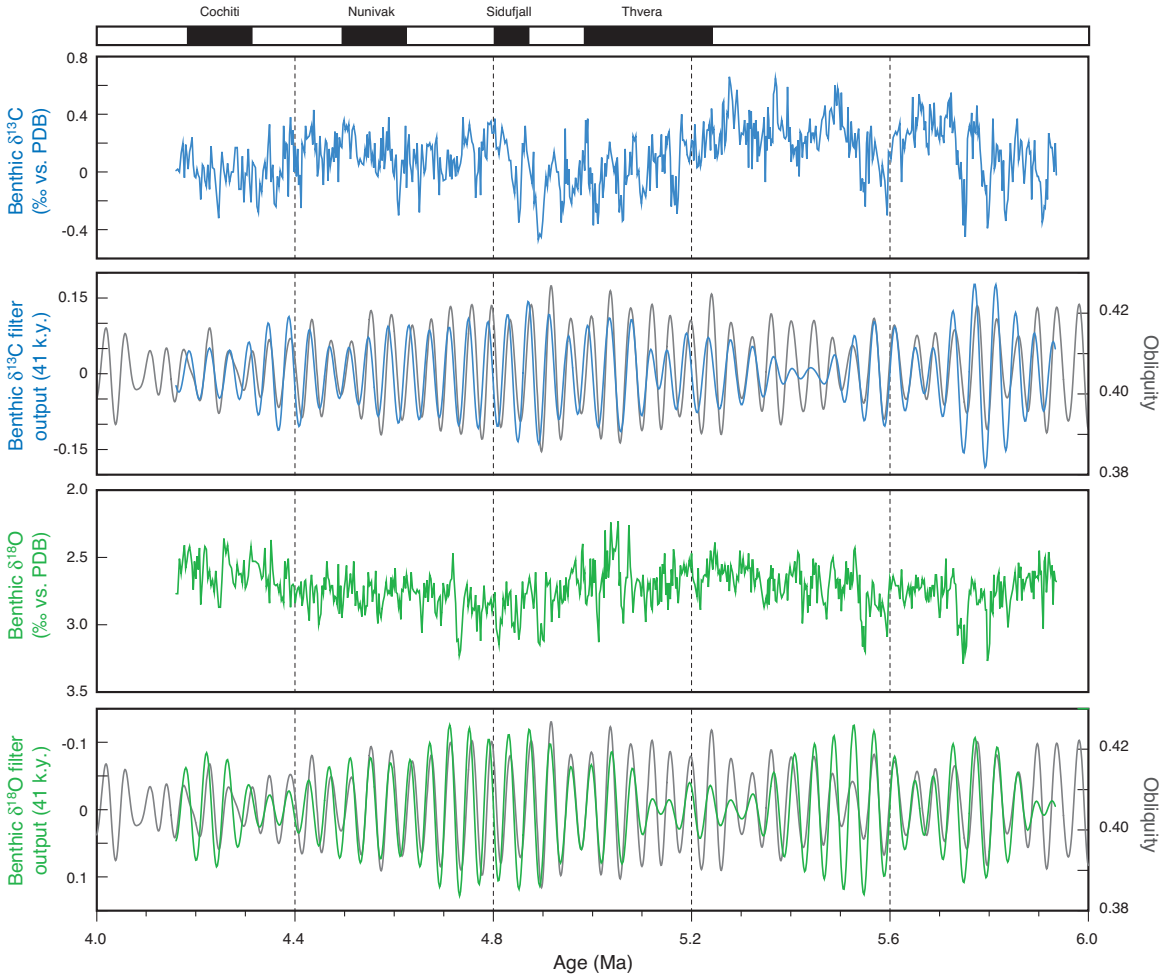

Fig. 4-4 Benthic $\delta^{13}C$ and $\delta^{18}O$ records from Site 1237 for the time interval from 4.2 – 6 Ma and overlays of filtered 41 k.y. components on orbital obliquity.

In addition, a convincing age model should not produce physically unreasonable changes in sedimentation rates, especially in pelagic regions. The sedimentation rates at pelagic Site 1237 were found to vary from 1.1 cm/k.y. to 2.8 cm/k.y., which seems reasonable. This range provides no evidence for distortions caused by the age model (**Fig. 4-3**) and is close to the values obtained from initial bio- and magnetostratigraphy.

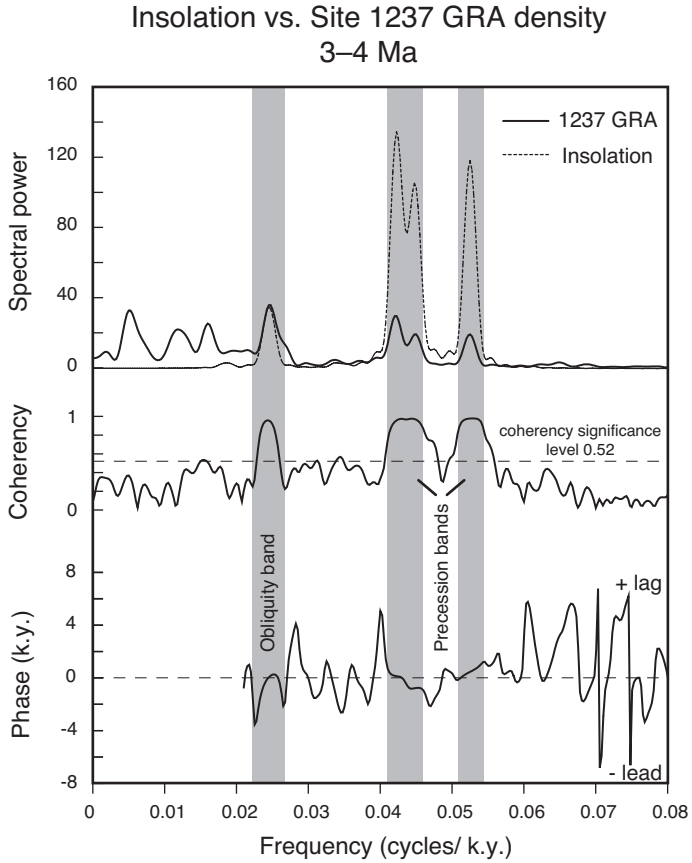

Fig. 4-5 Example of cross spectral analyses between northern hemisphere summer insolation (65°N) and the GRA density record from Site 1237 for the time interval from 3 – 4 Ma with power spectra, coherency spectrum and phase relationships. Both records were interpolated at 2 k.y. steps. The number of lags was set to 50 % of the time series (bandwidth = 0.003). All relationships are coherent above the 80 % confidence level (non-zero coherency level = 0.52). Positive phases (in k.y.) indicate that GRA density lags insolation forcing.

To further examine our time scale, we used cross-spectral analyses to determine the time lags and coherencies of the proxy records with respect to the orbital time series. Coherency between the geological data and the orbital target in the precession band is one of the fundamental methods by which a time scale may be evaluated (Shackleton et al., 1995). Separating the time interval from 2 Ma to 6 Ma into 4 succeeding intervals, cross-spectral comparison indicated that northern hemisphere summer insolation and GRA density were in phase (as requested by our tuning) and displayed high coherencies at the precession (mainly > 0.95) and obliquity (0.91 – 0.97) frequency bands (**Fig. 4-5, Tab. 4-2**). The benthic $\delta^{13}C$ record provided coherencies of 0.97 and 0.89 for the time intervals from 4.2 – 5 Ma and from 5 – 5.9 Ma, respectively. Brüggemann (1992) showed that high coherencies are very unlikely to appear by tuning a randomly fluctuating time series to the astronomical record. Thus, the very high coherencies at Site 1237 would not be obtained without a close coupling between changes in insolation and southeast Pacific paleoceanography. Cross-spectral analyses also indicated fairly constant phase relationships between variations in orbital obliquity and benthic

isotopes. For consistency of phase calculations, the $\delta^{18}O$ record was multiplied by -1, so that larger values indicate interglacial conditions along with maxima in northern hemisphere summer insolation. Variations in benthic $\delta^{13}C$ lag obliquity forcing by ~5 k.y., and obliquity-related variations in $-\delta^{18}O$ by ~2 k.y. Accordingly, the benthic $-\delta^{18}O$ signal, indicative of changes in ice volume, would lag obliquity forcing by about 3 k.y. As a consequence, the tuned ages at Site 1237 might be a few thousand years too old rather than too young, if the true phase lag was close to 6 k.y., as suggested by Chen et al. (1995).

Tab. 4-2 Cross-spectral coherencies and phase relationships between different proxies from Sites 1237, 1241, 925/926 and northern hemisphere summer insolation.

Spectral cross correlation	Time interval in Ma	41 k.y		23 k.y		19 k.y	
		Coh.	Phase	Coh.	Phase	Coh.	Phase
Insol. vs. GRA density (Site 1237)	2.2 – 3.0	0.94	1.7	0.95	0.3	0.77	-0.3
	3.0 – 4.0	0.96	0.1	0.97	0.0	0.98	0.5
	4.0 – 5.0	0.97	1.8	0.97	0.5	0.92	0.0
	5.0 – 6.0	0.91	-3.2	0.95	-0.3	0.98	-0.5
Insol. vs. benthic $\delta^{13}C$ (Site 1237)	4.2 – 5.0	0.97	5.1	0.83	6.7		
	5.0 – 5.9	0.89	2.5	0.65	5.1		
Benthic $\delta^{18}O$ (reversed) vs. benth. $\delta^{13}C$ (Site 1237)	4.2 – 5.0	0.94	1.7	0.84	6.9		
	5.0 – 5.9	0.91	2.2	0.67	3.0		
Insol. vs. benthic $\delta^{13}C$ (Site 1241)	2.5 – 3.5	0.98	4.5	0.82	0.6		
	3.5 – 4.5	0.96	5.0	0.80	7.0		
	4.5 – 5.5	0.95	6.0				
Insol. vs. % sand (Site 1241)	2.5 – 3.5	0.95	-3.0	0.94	-1.4	0.83	-0.9
	3.5 – 4.5	0.96	-1.3	0.94	0.0	0.93	0.6
	4.5 – 5.5	0.96	-1.5	0.94	0.0	0.93	-1.2
Benthic $\delta^{18}O$ (reversed) vs. benth. $\delta^{13}C$ (Site 1241)	2.5 – 3.5	0.94	3.3	0.82	2.9		
	3.5 – 4.5	0.96	3.0	0.68	4.8		
	4.5 – 5.5	0.92	3.2				
Benthic $\delta^{13}C$ (Site 1241) vs. benth. $\delta^{13}C$ (Site 1237)	4.2 – 5.5	0.98	-2.6	0.77	-2.2		
Benthic $\delta^{18}O$ (Site 1241) vs. benth. $\delta^{18}O$ (Site 1237)	4.2 – 5.5	0.92	-0.7	0.75	-3.6		
Benthic $\delta^{13}C$ (Site 1241) vs. benth. $\delta^{13}C$ (Site 925/926)	2.5 – 4.0	0.95	-1.2				
	4.0 – 5.7	0.96	2.5				
Benthic $\delta^{18}O$ (Site 1241) vs. benth. $\delta^{18}O$ (Site 925/926)	2.5 – 4.0	0.97	0.8	0.88	2.3		
	4.0 – 5.7	0.93	-3.5				

4.6 Development of an orbitally derived age model for Site 1241

The proxy records from Site 1241 contain significant distribution of variance at obliquity-related wavelengths of 100-200 cm. Accordingly, sedimentations rates vary from 2.5 cm to 5 cm and are higher than those at Site 1237. The primary signals that we used for tuning were benthic $\delta^{13}C$ and sand percentages of the carbonate fraction. Both records are highly coherent with $\delta^{18}O$ at the obliquity frequency band. Maxima in $\delta^{13}C$ and sand percentages are associated with $\delta^{18}O$ warm stages. The sand fraction record is in addition also marked by strong concentration of variance at precessional frequency bands. Carbonates and GRA density values show distinctly weaker correlations to $\delta^{18}O$, although obliquity-related minima in GRA density and carbonate percentages are mainly associated with $\delta^{18}O$ warm stages. This correlation is opposite to that found at Site 1237. These data were only considered for identifying obliquity or precession-related cycles in intervals, where the variance or the response to orbital forcing was less pronounced in the $\delta^{13}C$ and sand fraction records.

Before using the sand fraction data for tuning, we examined the type of paleoceanographic information provided by this record. Variations in the sand percentages of the carbonate fraction are often used as a proxy to reconstruct either changes in carbonate dissolution or differences in carbonate accumulation between foraminifers and calcareous nannoplankton. The sand fraction consists of nearly 100 % of foraminiferal shells at Site 1241. For such environments it has been shown that the sand content of deep-sea carbonates decreases as dissolution progresses (e.g. Bickert et al., 1997). Foraminiferal shells are weakened by dissolution and tend to break down in small fragments. As a result, material moves from the coarse fraction into finer fractions. At the shallow water depth of Site 1241 (2027 m), carbonate dissolution is expected to have been low. Therefore, it is not surprising that the Pliocene variability in sand fraction percentages does not correspond to the general pattern of Pacific carbonate dissolution. Over the past 4.5 Ma, carbonate dissolution in the equatorial Pacific was enhanced during interglacials (Farrell and Prell, 1991). Thus, Pliocene changes in carbonate dissolution mainly operated on 41-k.y. cycles. These relationships rather exclude changes in carbonate dissolution as a primary mechanism, because high sand percentages at Site 1241 are associated with interglacials and reveal in addition strong precession-related variability. As carbonate dissolution seems to be of secondary importance, changes in the ratio between nannofossil placoliths and foraminiferal shells are regarded as the primary mechanism that could change the relative portion of the coarse fraction (Bickert and Wefer, 1996). Hence, the sand fraction record is indicative of changes in carbonate productivity.

We used the oxygen isotope stages 96, 98 and 100 as a starting point for calibrating the time scale at Site 1241. These stages were easily recognized in the benthic oxygen isotope record (**Fig. 4-6**). Their age assignments to the orbital record are well constrained (e.g. Tiedemann and Franz, 1997) and identified the 3 corresponding obliquity cycles. We then tuned the 41-k.y. component of the benthic $\delta^{13}C$ record to orbital obliquity assuming no phase difference. This resulted in a preliminary time scale for the interval from 2.4 Ma to 5.7 Ma. In a next step, we compared the sand fraction record with the northern hemisphere summer

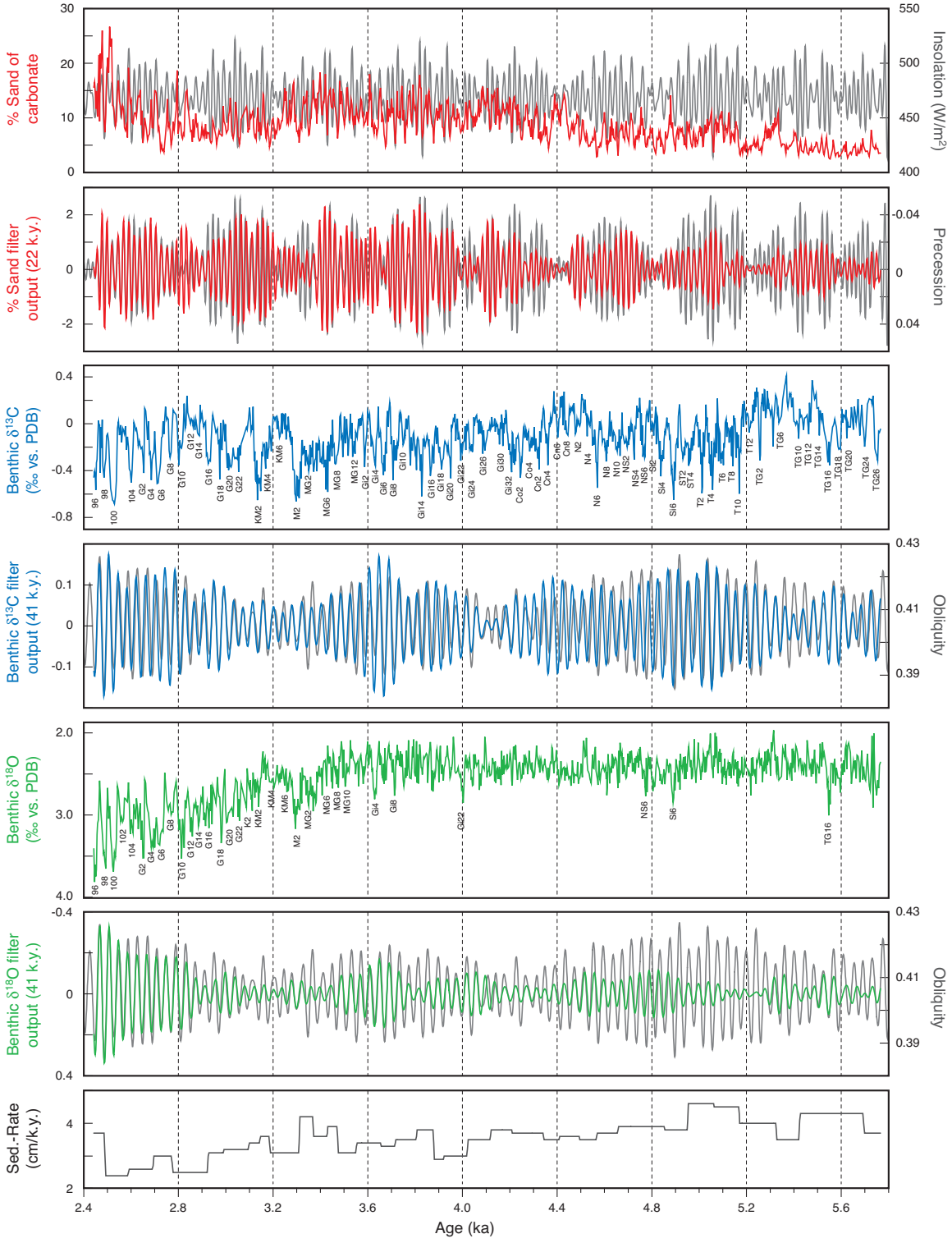

Fig. 4-6 Summary of Site 1241 records for the time interval from 2.4 Ma to 5.8 Ma: % sand of the carbonate fraction overlain on northern hemisphere summer insolation (65°N), benthic $\delta^{13}C$, $\delta^{18}O$, and sedimentation rates; overlays of filtered 21-k.y. and 41-k.y. components (% sand, $\delta^{13}C$, $\delta^{18}O$) on orbital precession and obliquity, respectively.

insolation record and tuned the precession-related maxima of the sand record to insolation maxima (**Fig. 4-6**). The new age model changed the phase relationship between the $\delta^{13}C$ record and orbital obliquity with $\delta^{13}C$ lagging obliquity insolation forcing relatively constant by about 5 k.y. and lagging $\delta^{18}O$ by about 3 k.y. during the interval from 2.5 – 5.5 Ma (**Tab. 4-2**). Mix et al. (1995) found a similar phase relationship for the Pliocene between benthic $\delta^{13}C$ and $\delta^{18}O$ at tropical east Pacific Site 849 (2 k.y.). Results from cross spectral analyses from Site 1241 imply that the benthic $\delta^{18}O$ signal, indicative of changes in ice volume, lagged obliquity forcing by about 2 k.y. For comparison, the tuning at Site 1237 yielded a similar phase lag of about 3 k.y. The tuned ages at Site 1241 might be a few thousand years too old rather than too young if a larger phase lag close to 6 k.y. is assumed (Chen et al., 1995). The age-depth control points for Site 1241 are given in **Table 4-3**.

Tab. 4-3 Age model for Site 1241

Age (k.y.)	Depth (mcd)	Age (k.y.)	Depth (mcd)
2443	58.21	4430	123.03
2489	59.92	4496	125.13
2589	62.35	4567	127.62
2693	65.05	4600	128.72
2753	66.76	4639	130.34
2795	67.77	4657	130.94
2924	71.25	4702	132.55
2991	73.31	4774	135.69
3107	76.87	4880	139.51
3185	79.76	4954	142.50
3211	80.46	5058	147.00
3287	82.87	5104	149.26
3361	85.65	5173	152.67
3429	88.16	5307	157.68
3463	89.53	5347	159.07
3587	93.42	5404	161.18
3666	96.02	5449	162.84
3716	97.72	5508	165.40
3912	104.72	5551	167.34
4021	107.84	5627	170.74
4136	111.76	5691	173.18
4252	116.42		
4313	118.74		

To evaluate our tuned age model and the match between the proxy records and the orbital record, we applied the same methods used for Site 1237. Tuning to precession resulted in a concentration of variance over all the main orbital frequencies. For statistical evaluation of the tuned time scale, we applied cross-spectral analyses to estimate the coherencies between the proxy records and the orbital target for the time intervals from 2.5 – 3.5 Ma, 3.5 – 4.5 Ma, and 4.5 – 5.5 Ma (**Fig. 4-7**). At the obliquity band, coherency estimates for the sand fraction, benthic $\delta^{13}C$ and $\delta^{18}O$ records are higher than 0.94. At the precession bands, the sand fraction record provided coherency estimates of > 0.9. **Table 4-2** summarizes the coherencies and phase estimates of the different proxies for Site 1241. The high coherencies also indicate that the physical linkage between changes in solar insolation and paleoceanography was strong through the entire interval from 2.5 – 5.5 Ma. Sedimentation rates were estimated and vary between 2 cm/k.y. and 5 cm/k.y. Higher sedimentation rates mark the older part of the record. This is reasonable because the depositional environment in the equatorial east Pacific was characterized by a late Miocene to early Pliocene biogenic bloom enhancing the sediment flux to the sea floor. Finally, we applied bandpass filtering to extract the orbital frequency components from the sand fraction, $\delta^{13}C$ and $\delta^{18}O$ time series and compared them with orbital precession and obliquity. We found a remarkable similarity between the amplitude variation in orbital precession and the precessional components in the sand fraction record (**Fig. 4-6**). This implies that we correctly

mapped the climate signal onto the orbital record. A mismatch of precession-related cycles, e.g., making one precession cycle too old or too young would be recognized by an out-of-phase relationship with orbital obliquity. The filtered 41-k.y. components in the sand fraction, $\delta^{13}C$ and $\delta^{18}O$ records show a very consistent relationship with orbital obliquity, with different but relatively constant phase offsets (**Tab. 4-2**). The mismatch between orbital obliquity and the 41-k.y. component of the sand fraction at ~2.9 Ma is caused by relatively high amounts of ash, although we deleted the corresponding interval of the ash layer (77.08 – 77.10 mcd, Mix et al., 2003) before tuning. Inspection of the sand fraction, however, revealed relatively high amounts of ash over an interval of ~1.5 m (76.27 – 77.77 mcd) that clearly distorted the primary signal of the sand fraction record.

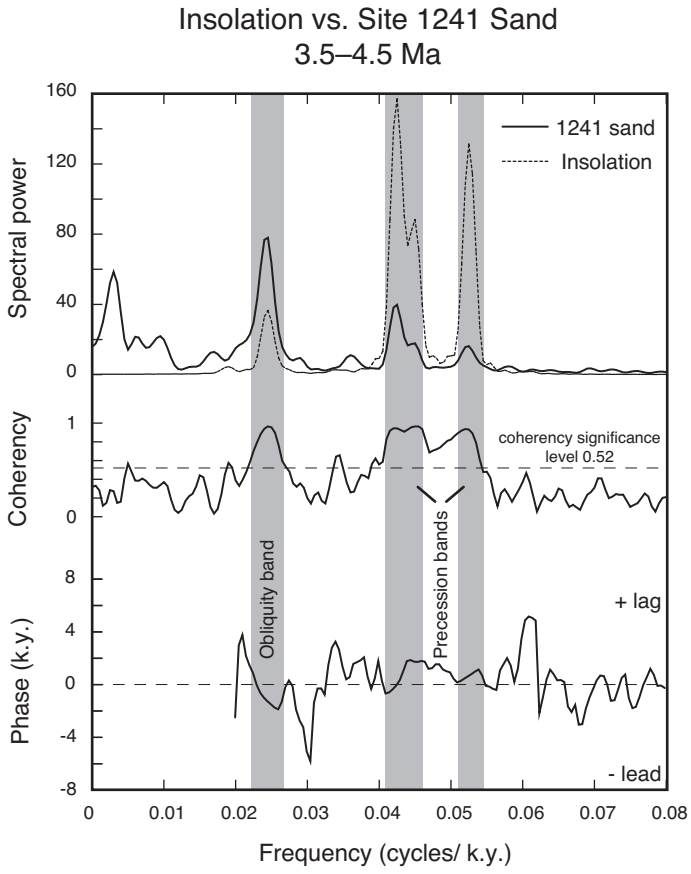

Fig. 4-7 Example of cross-spectral analyses between northern hemisphere summer insolation (65°N) and the percentage sand record from Site 1241 for the time interval from 3.5 – 4.5 Ma with power spectra, coherency spectrum and phase relationships. Both records were interpolated at 2 k.y. steps. The number of lags was set to 50 % of the time series (bandwidth = 0.003). All relationships are coherent above the 80 % confidence level (non-zero coherency level = 0.52). Positive phases (in k.y.) indicate that % sand lags insolation forcing.

4.7 Comparison of astronomically tuned age models

To further examine the quality of the astronomically calibrated time scales from Sites 1237 and 1241, we plotted the benthic $\delta^{18}O$ and $\delta^{13}C$ records from both sites versus age (**Fig. 4-8**). This allows the comparison of their age models for the time interval from 4.2 Ma to 5.7 Ma. The oxygen isotope records from the two sites are well correlated and are almost in phase at the precession- and obliquity-related frequency bands (**Tab. 4-2**). Several eye-catching structures and prominent isotope stages are easily recognized and have almost identical ages (within a range of ± 2 k.y). Accordingly, we numbered the unambiguously correlated isotope

stages in **Figure 4-8** following the numbering scheme developed by Shackleton et al. (1995). In several intervals, however, patches are seen where the signal-to-noise ratio in the $\delta^{18}O$ records is so low that isotope stages bear no clear resemblance. The comparison of the carbon isotope records further strengthens the stratigraphic correlation between the two sites, as the $\delta^{13}C$ records are exceptionally well correlated, which is also indicated by cross spectral analyses. Both $\delta^{13}C$ records are highly coherent with each other at the orbital periods of 41 k.y. and 23 k.y (**Tab. 4-2**). We used the excellent correlation to complete the numbering of isotope stages for the interval from 5.7 Ma to 4.2 Ma (**Fig. 4-8**). In summary, the correlation of isotope stratigraphies between Sites 1237 and 1241 demonstrated that their astronomically calibrated age models are identical within an error range of a few thousand years.

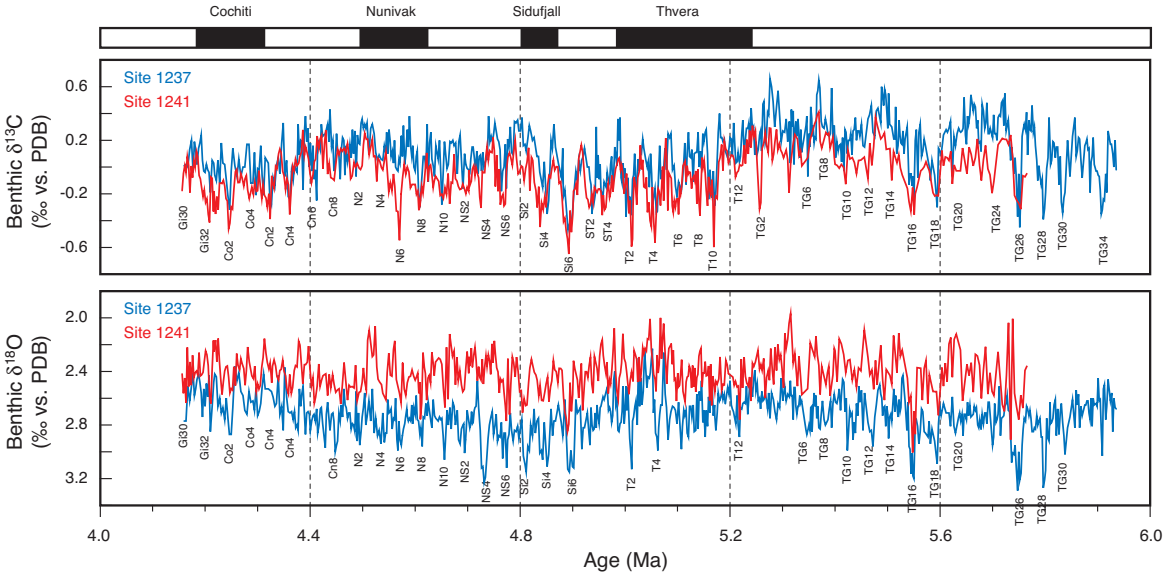

Fig. 4-8 Comparison of benthic $\delta^{18}O$ und $\delta^{13}C$ records from Sites 1237 and 1241 for the time interval from 4.0 – 6.0 Ma. Oxygen and carbon isotope stages are numbered following the numbering scheme of Shackleton et al. (1995), which is firmly linked to the underlying 41 k.y. isotope cycles. Even numbers indicate cold stages and odd numbers indicate warm stages. The letters in front of the marine isotope stages identify the magnetic polarity interval. For example, the first cold stage of the Sidufjall chron is called Si2 and the first cold stage occurring in the magnetic interval between the Sidufjall and Thvera is called ST2. These signatures indicate the match of isotope stages that correspond to the underlying and continuously numbered orbital obliquity cycles.

The comparison of the benthic $\delta^{18}O$ and $\delta^{13}C$ records from Pacific Site 1241 and Atlantic Site 925/926 provides another excellent opportunity to test our age model for the late Miocene to Pliocene interval from 5.7 Ma to 2.5 Ma (**Fig. 4-9**). The time scale at Atlantic Site 925/926 (Ceara Rise; Tiedemann and Franz, 1997; Shackleton and Crowhurst, 1997) was developed by tuning precession-related variations in magnetic susceptibility to the same target record used for calibrating Sites 1241 and 1237. The benthic isotope records were established by Tiedemann and Franz (1997), Billups et al. (1997) and Shackleton and Hall (1997). For the time interval from 4 – 2.5 Ma, cross spectral comparison between the $\delta^{18}O$ records from Sites

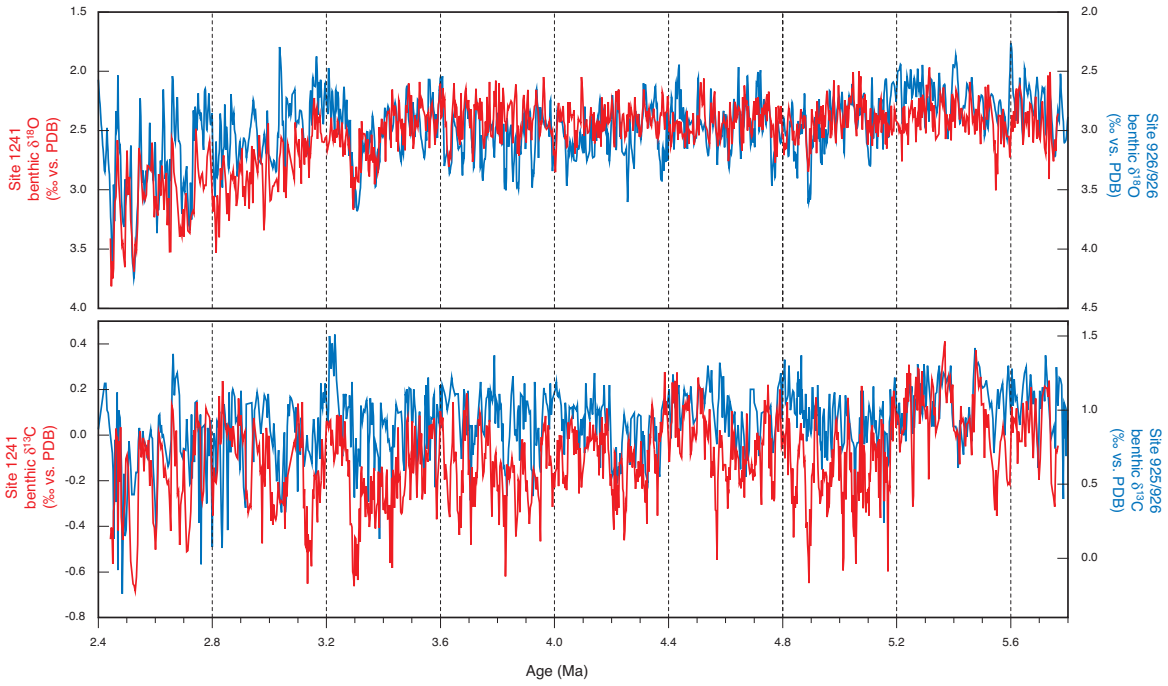

Fig. 4-9 Comparison of benthic $\delta^{18}O$ and $\delta^{13}C$ records from Sites 1241 (this study) and 925/926 (Tiedemann and Franz, 1997; Billups et al., 1997; Shackleton and Hall, 1997) for the time interval from 2.4–5.7 Ma.

1241 and 925/926 indicates that the spectral distribution of variance is very similar and coherent for cycles ≥ 41 k.y. (**Fig. 4-10**). The dominant obliquity-related variations are highly coherent and in phase (**Tab. 4-2**). In the time interval from 5.7 – 4 Ma, the distribution of spectral variance for cycles ≥41 k.y. is less similar but variations in $\delta^{18}O$ are highly coherent at the obliquity band. The visual comparison of the oxygen isotope records indicates a remarkably good correlation for the time intervals from 3.75 – 2.5 Ma and 5.1 – 4.5 Ma (**Fig. 4-9**), reflecting the global nature of the $\delta^{18}O$ ice volume signal and relatively uniform changes in deep water temperatures and/or salinity at the two sites. The correlation is less pronounced in the intervals from 5.7 – 5.1 Ma and from 4.5 – 3.75 Ma, because the $\delta^{18}O$ amplitude fluctuations are more different between both sites. These differences cannot be ascribed to differences in the time resolution as the sampling resolution and the sedimentation rates are similar at both sites. Thus, we attribute these deviations to larger local differences in deep-water temperature/salinity fluctuations. The regional overprint of the global $\delta^{18}O$ signal is expected to have been larger at Site 925/926 than at Site 1241, at least for the interval from 4.5 Ma to 3.75 Ma. This has been suggested by the isotope study of Billups et al. (1997). The bathymetric comparison of Pliocene benthic $\delta^{18}O$ records from Ceara Rise indicated anomalous high $\delta^{18}O$ values at Site 925 between 4.2 Ma and 3.7 Ma, which were interpreted to represent a stronger flux of relatively warmer and more saline North Atlantic Deep Water (NADW) at 3000 m water depth. This is consistent with other studies that attribute early Pliocene warmth and enhanced NADW production to an increased northward heat and salt transport, which

probably resulted from a critical threshold in the closure history of the Central American Isthmus (Haug and Tiedemann, 1998; Haug et al., 2001a).

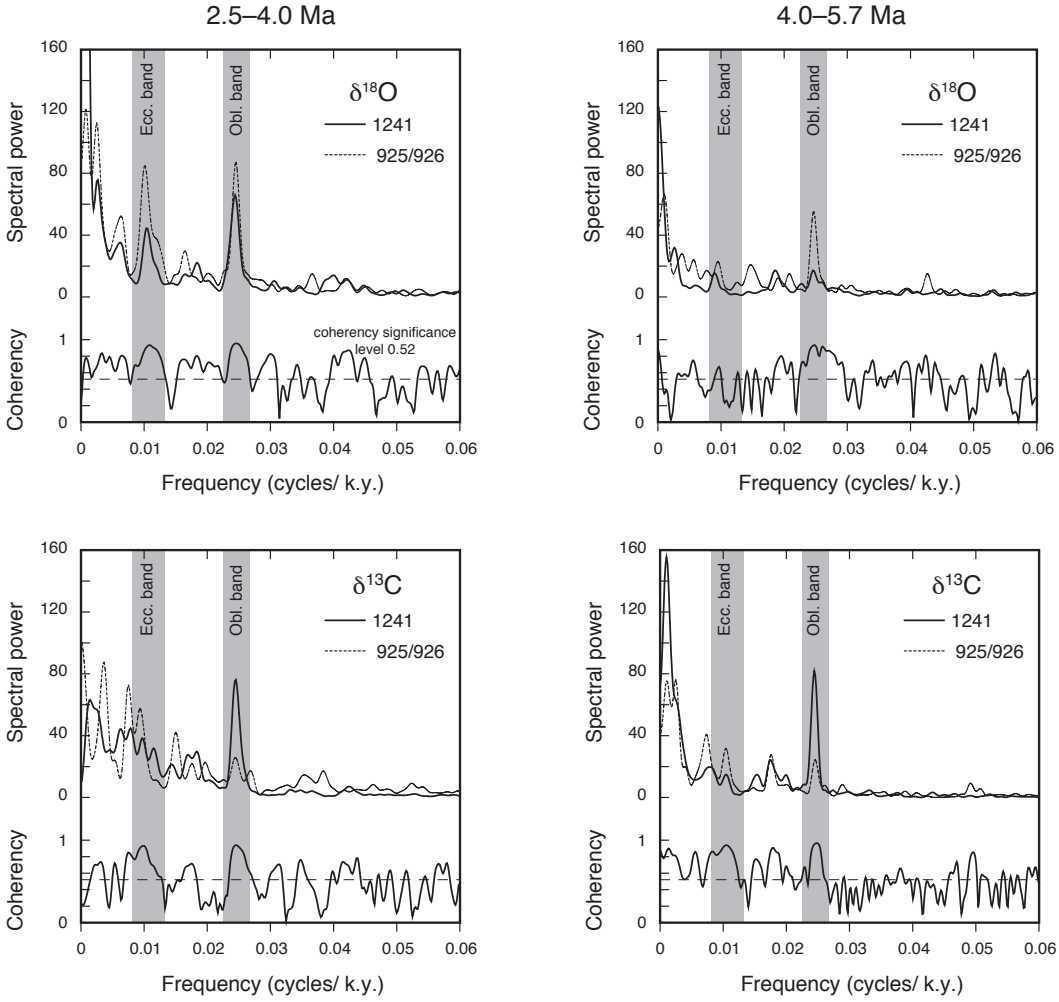

Fig. 4-10 Cross spectral analyses between benthic $\delta^{18}O$ and between $\delta^{13}C$ records from Sites 1241 and 925/926 for the time intervals from 2.5 – 4 Ma and 4 – 5.7 Ma with power and coherency spectra. Records were interpolated at 2 k.y. steps. The number of lags was set to 50 % of the time series. All relationships are coherent above the 80% confidence level (non-zero coherency level = 0.52).

The benthic $\delta^{13}C$ records from Sites 925 / 926 and 1241 are exceptionally well correlated between 5.7 Ma and 2.5 Ma (**Fig. 4-9**) and surprisingly good in those intervals, where the correlation of the $\delta^{18}O$ signal is relatively weak (5.7 – 5.1 Ma, 4.5 – 3.75 Ma). Cross spectral analyses between the $\delta^{13}C$ records indicate that the spectral distribution of variance is very similar and coherent for cycles ≥ 41 k.y., especially in the older time interval from 5.7 – 4 Ma (**Fig. 4-10; Tab. 4-2**). The remarkable similarity between the Pacific and Atlantic $\delta^{13}C$ deep-water signal (**Fig. 4-9**) with strongest concentration of variance at the 41-ky. cycle indicates a strong response to global variations in the carbon reservoirs and associated isotope

Tab. 4-4 Ages of the magnetic reversals between 2.1 Ma and 6 Ma, according to LHZHAV95 (Lourens et al., 1996), SCHPS95 (Shackleton et al., 1995), CK95 (Cande and Kent, 1995) and this study. The depth ranges of reversals (Site 1237) are from Mix et al. (2003). *Note: Depth ranges of reversals at Site 1237 are different from those in Mix et al. (2003). The reversals were determined at sections that did not belong to the mcd splice. Using core logging data, we more precisely matched these sections to the mcd splice.

Geomagnetic reversal boundary		Site 1237 range in mcd	Site 1237 this study	LHZHAV 96	SCHPS95	CK95
Reunion (Base)	Top	41.35	2142	2149		2150
	Mean	41.81	2166			
	Base	42.36	2198			
Gauss/Matuyama	Top	47.82	2583	2581	2600	2600
	Mean	47.93	2591			
	Base	48.04	2600			
Kaena (Top)*	Top	56.61	3109	3034	3046	3040
	Mean	56.70	3114			
	Base	56.80	3120			
Kaena (Base)*	Top	57.60	3159	3119	3131	3110
	Mean	57.73	3165			
	Base	57.86	3172			
Mammoth (Top)*	Top	58.80	3218	3215	3233	3220
	Mean	58.85	3220			
	Base	58.99	3227			
Mammoth (Base)	Top	60.60	3310	3333	3331	3330
	Mean	60.94	3332			
	Base	61.28	3351			
Gilbert/Gauss	Top	65.53	3581	3597	3594	3580
	Mean	65.92	3610			
	Base	66.31	3631			
Cochiti (Top)	Top	75.13	4162	4192	4199	4180
	Mean	75.48	4184			
	Base	75.83	4201			
Cochity (Base)	Top	77.37	4302	4304	4316	4290
	Mean	77.57	4314			
	Base	77.76	4325			
Nunivak (Top)	Top	81.00	4487	4499	4479	4480
	Mean	81.17	4495			
	Base	81.34	4503			
Nunivak (Base)	Top	83.68	4616	4637	4623	4620
	Mean	83.86	4624			
	Base	84.04	4633			
Sidufjall (Top)	Top	87.37	4787	4810	4781	4800
	Mean	87.65	4802			
	Base	87.93	4817			
Sidufjall (Base)	Top	88.70	4857	4901	4878	4890
	Mean	88.99	4872			
	Base	89.27	4886			
Thvera (Top)	Top	90.83	4956	5004	4977	4980
	Mean	91.50	4983			
	Base	92.17	5008			
Thvera (Base)	Top	96.64	5211	5239	5232	5230
	Mean	97.32	5242			
	Base	98.00	5272			

fractionations. The amplitudes and the clarity of the 41-k.y. cycles are stronger developed in the $\delta^{13}C$ than in the $\delta^{18}O$ records, especially in the late Miocene and early Pliocene intervals. This demonstrates that the benthic $\delta^{13}C$ records are not only a powerful medium for orbital tuning, but also a valuable tool for chronostratigraphic correlations that could assist the late Miocene and early Pliocene benthic oxygen isotope stratigraphy, as the $\delta^{13}C$ signal lags relatively constant behind $\delta^{18}O$ at the 41-k.y. period (2 – 3 k.y.). This opportunity may primarily become important when extending the isotope stratigraphy further back in time, particularly for those intervals where the $\delta^{13}C$ response to cyclic changes in global climate is more clearly developed than in the oxygen isotope signal. The comparison between the isotope records from Sites 1241 and 925/926 also suggests that their orbitally tuned age models are almost identical within an error range of a few thousand years.

Finally, the excellent paleomagnetic stratigraphy at Site 1237 with clear definitions of all Pliocene chrons allows an independent comparison of our age model to the Pliocene astronomical polarity time scale (APTS) that mainly resulted from the combined chronologies of Hilgen (1991a,b), Shackleton et al. (1995) and later refinements of Lourens et al. (1996). Our age assignments for the Pliocene magnetic reversal boundaries agree within their error ranges (depth range of magnetic reversals) with the APTS, except for the Kaena chron (**Tab. 4-4**). Our astronomical ages for the base and top of Kaena are about one and two obliquity cycles older, respectively. Apart from the general discrepancy in absolute age control, our age model suggests that the Kaena chron spans a time interval of 51 ± 12 k.y. As this interval is 103 ± 23 cm long, the appropriate sedimentation rate is ~2 cm/k.y. (**Fig. 4-3**). Considering the depth range for the top and base of Kaena, the interval of the reversal would be 22 – 46 k.y. shorter than previously estimated by other age models (**Tab. 4-4**). Expanding the interval by 22 – 46 k.y. would significantly drop the sedimentation rate and means that we misinterpreted one or two obliquity cycles as precession cycles. This is not very likely for the following reasons. First, the magnetic reversals of Kaena as well as the top of Mammoth are determined at the same core and the mcd in this interval is not affected by a switch point between holes. Therefore, we can exclude that we missed a sediment section over this interval. Second, the next older magnetic reversal, the top of Mammoth, is only ~1 m downcore and its assigned age agrees well with that from the APTS (**Tab. 4-4**). Our age model suggests a sedimentation rate of ~1.8 cm/k.y. for the interval between the top of Mammoth and the base of Kaena, which is similar to that found for the Kaena chron. Third, spectral variation in both GRA density and color reflectance reveals a dominant precession-related 44 cm-cycle for the interval from 54 – 59 mcd (2.97 – 3.23 Ma). In addition, the spectral variance of the color reflectance is also marked by a pronounced eccentricity-related 222 cm-cycle. One may argue that this cycle is statistically not convincing, as it occurs only twice in this short interval. On the other hand, its appearance between 2.97 Ma and 3.23 Ma is not very surprising, because the precession-related amplitudes of the color reflectance record may just reflect the strong eccentricity modulation of the astronomical precession record within this interval (**Fig. 4-3**).

Apart from the age discrepancy of the Kaena chron, the good agreement between the APTS and the orbitally-derived ages for the geomagnetic reversal boundaries at Site 1237 suggests

that our age model is very similar to those of Lourens et al. (1996) and Shackleton et al. (1995) given the error involved in reversal identification and orbital tuning. This result demonstrates the potential for developing an APTS at Site 1237, probably for the entire Neogene.

4.8 Stratigraphic adjustment of Sites 1236 and 1239

The records from Sites 1236 and 1239 are not directly tuned to variations in Earth's orbital parameters. At Site 1236, the main drawback is its poor time resolution. Sedimentation rates vary from 0.5 cm to 1 cm / k.y. and thus are not suited for orbital tuning. Although Site 1239 has high sedimentation rates of up to 10 cm/k.y., it still lacks a composite depth for the Miocene/Pliocene interval, a major precondition for orbital tuning. However, the opportunity for reconstructing such a composite section is excellent. High-resolution core logging data from two holes as well as high resolution borehole logging data cover the Miocene/Pliocene interval. Density and natural gamma ray intensity records from borehole and core logging data exhibit strong correlation of meter-scale variability and allow the construction of an equivalent logging depth (eld) scale for the XCB-cored intervals (Mix et al., 2003). Such an eld-based composite depth is under construction. The advantage of this depth scale is that it corrects for stretching and squeezing of cored sediment sections. Furthermore, it provides the best estimate of in situ depth and is ideal for estimating mass accumulation rates.

Instead of orbital tuning, we established an initial age model based on magnetostratigraphic (Site 1236) and biostratigraphic information (Site 1239) (Mix et al., 2003). In a second step, we matched the benthic $\delta^{18}O$ and $\delta^{13}C$ isotope records from Site 1236 and Hole 1239A with those from Site 1241 by visual identification of oxygen and carbon isotope stages. This procedure indirectly resulted in orbitally tuned age models for Sites 1236 and 1239, spanning the intervals from 2.5 – 5.3 Ma and 2.7 – 5 Ma, respectively. The comparison between benthic $\delta^{18}O$ and $\delta^{13}C$ records is shown in **Figures 4-10** and **4-11** and the age-depth control points for Site 1236 and Hole 1239A are given in **Tables 4-5** and **4-6**. The age model for Hole 1239A is regarded as very preliminary as our stratigraphic correlation to Site 1241 suggests significant gaps at core breaks. The detailed age model for Site 1236 could have never been achieved without using its $\delta^{13}C$ record as a tool for chronostratigraphic correlation with Site 1241. Although the $\delta^{13}C$ record from Site 1236 is indicative of isotope changes at the Pacific intermediate water level, it clearly resembles the general $\delta^{13}C$ structure of the Pacific central and deep-water sites. In contrast, the intermediate water $\delta^{18}O$ signal shows a relatively weak correlation to the "globally correlative" oxygen isotope stratigraphy, represented by Site 1241 in **Figure 4-10**. This again demonstrates the utility of early Pliocene benthic $\delta^{13}C$ records for stratigraphic correlations.

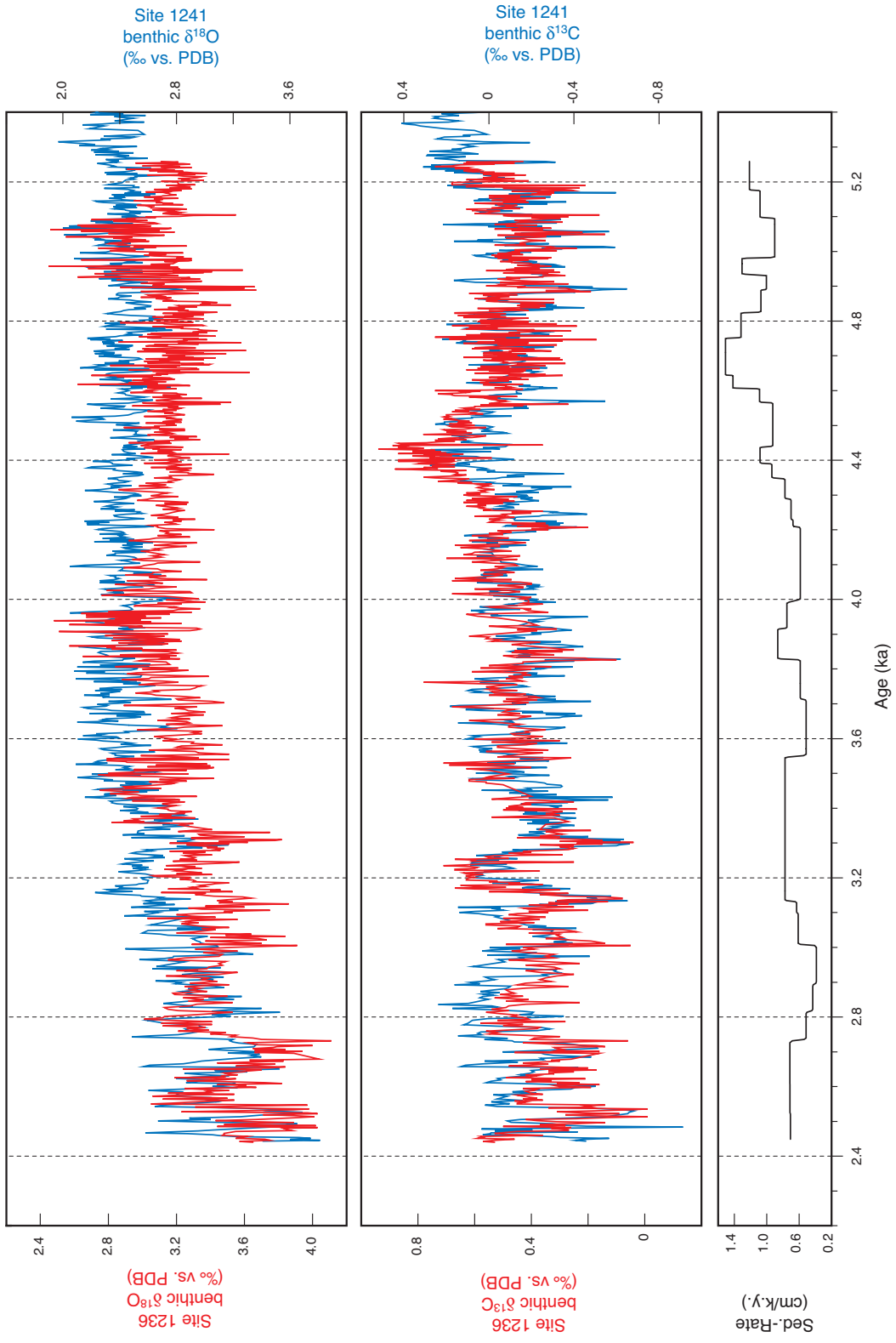

Fig. 4-11 Comparison of benthic $\delta^{18}O$ and $\delta^{13}C$ records from Sites 1241 and 1236 for the time interval from 2.4 – 5.3 Ma.

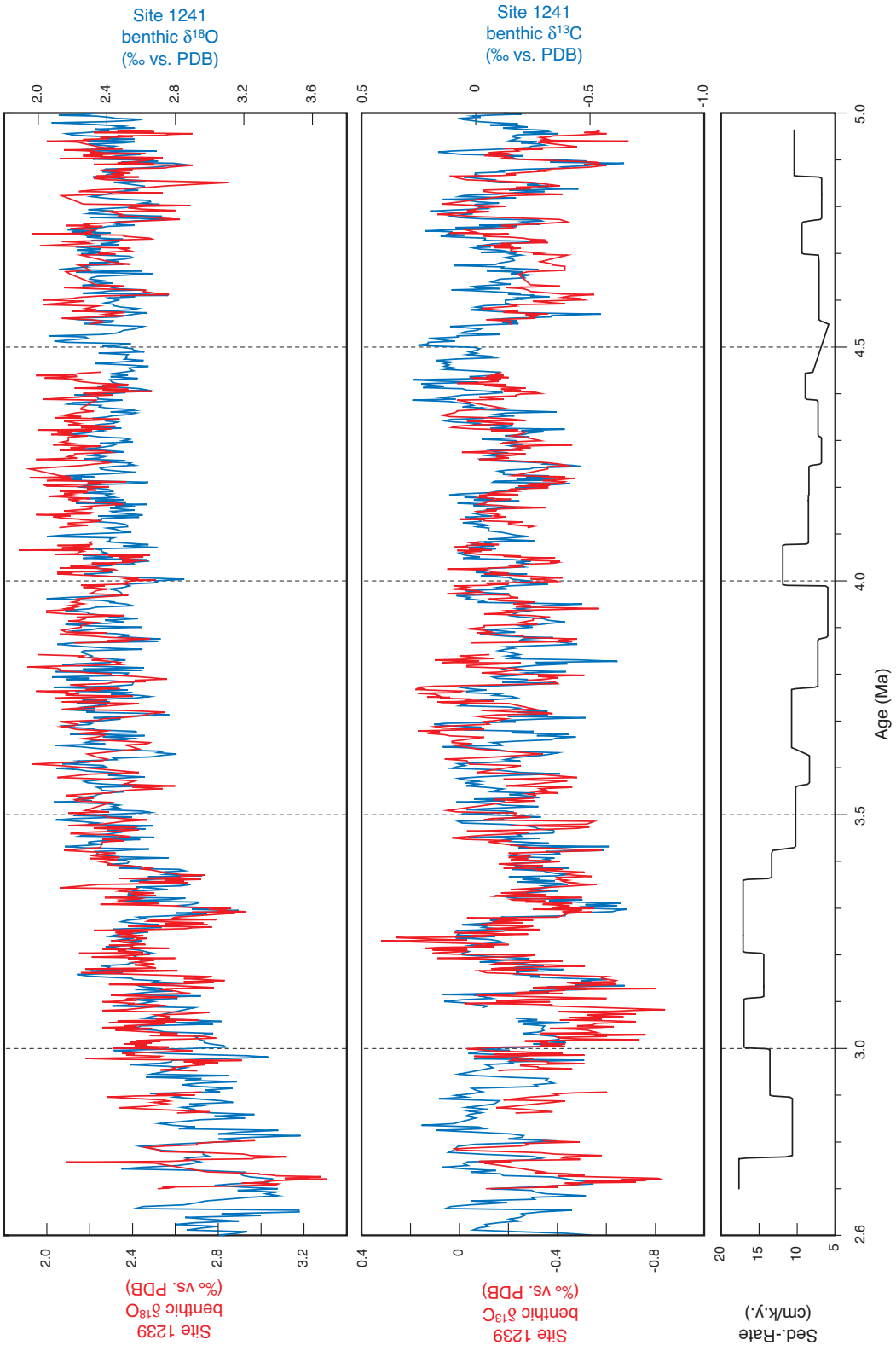

Fig. 4-12. Comparison of benthic $\delta^{18}O$ and $\delta^{13}C$ records from Sites 1241 and 1239 for the time interval from 2.7 – 5 Ma.

Tab. 4-5. Age model for Site 1236

Age (k.y.)	Depth (mcd)	Age (k.y.)	Depth (mcd)
2446	10.28	4288	22.20
2522	10.82	4347	22.66
2606	11.42	4390	23.06
2732	12.32	4438	23.58
2814	12.74	4565	24.76
2892	13.08	4605	25.20
3006	13.52	4644	25.74
3097	14.08	4751	27.36
3132	14.30	4824	28.32
3548	17.52	4889	29.02
3711	18.36	4933	29.46
3827	19.04	4980	30.08
3915	19.80	5096	31.12
3992	20.38	5175	31.98
4207	21.64	5244	32.82
4228	21.78		

Tab. 4-6 Age model for Site 1239

Age (k.y.)	Depth (mcd)	Age (k.y.)	Depth (mcd)
2700	150.73	4077	317.52
2766	162.29	4183	326.56
2896	176.15	4247	331.92
2999	190.18	4307	336.03
3107	208.51	4386	341.78
3204	222.41	4446	347.11
3361	249.34	4553	352.34
3424	257.70	4696	362.60
3561	271.77	4767	369.23
3630	277.48	4863	375.77
3769	292.48	4956	385.43
3876	300.24		
3989	307.04		

4.9 Conclusions

Here we present two consistent high resolution orbitally tuned age models for the Leg 202 Sites 1237 and 1241 as well as benthic isotope stratigraphies for Sites 1236, 1237, 1239 and 1241 that cover the time interval from 2.5 Ma to 6 Ma. The age models for Sites 1237 and 1241 were generated by correlating the high frequency variations in GRA density, percent sand of the carbonate fraction, and benthic $\delta^{13}C$ to the orbital solution of Laskar et al. (1993). Cross-spectral analyses revealed highly significant coherencies between their astronomically related frequency components and orbital obliquity and precession. The age models for Sites 1236 and 1239 were constructed by transferring ages from Site 1241 *via* correlation of isotope records. The establishment of astronomically calibrated isotope stratigraphies at Sites 1237 and 1241 with an average sampling interval of less than 3 k.y. along with the excellent paleomagnetic stratigraphy at Site 1237 with clear definitions of all Pliocene chrons allowed a direct comparison with previously published astronomical age models. The excellent correlation of benthic $\delta^{18}O$ and $\delta^{13}C$ stratigraphies between Pacific Site 1241 and Atlantic Site 925/926 (Ceara Rise) confirms the age model constructed at sediment sequences from Atlantic Leg 154. Furthermore, the ages of the Pliocene polarity reversals at Site 1237 agree well with those of the generally accepted astronomical polarity time scale (Hilgen, 1991a,b; Shackleton et al., 1995; Lourens et al., 1996). Hence, our work places the late Miocene to middle Pliocene sediment records from Leg 202 into a high resolution, globally correlative, and astronomically calibrated stratigraphic framework and provides an excellent basis for further paleoceanographic studies.

The Atlantic-Pacific comparison of benthic $\delta^{18}O$ and $\delta^{13}C$ records indicates that the late Miocene and early Pliocene $\delta^{13}C$ signal is globally correlative and better structured than the $\delta^{18}O$ signal. Although the spectral variability of both parameters is dominated by 41-k.y. cycles

with relatively constant phase relationships, the clarity and correlative nature of the 41-k.y. cycle is generally better developed in $\delta^{13}C$ records. This demonstrates that the benthic $\delta^{13}C$ records are not only a powerful medium for orbital tuning, but also a valuable tool for chronostratigraphic correlations that could assist the late Miocene and early Pliocene benthic oxygen isotope stratigraphy. This opportunity may primarily become important when extending the isotope stratigraphy further back in time, particularly for those intervals where the $\delta^{13}C$ response to cyclic changes in global climate is more clearly developed than in the oxygen isotope signal.

In summary, our results from Site 1237 and 1241 demonstrate the potential for expanding both the isotope stratigraphy and the astronomical polarity time scale to the base of the Neogene, as the composite depth of the APC-cored sequence at Site 1237 suggests a complete recovery of the last 30 Ma along with an excellent magnetic stratigraphy.

Acknowledgements

We are grateful to the Deutsche Forschungsgemeinschaft (DFG). The establishment of such a high-resolution stratigraphic framework for Leg 202 sediment records would have been impossible without the support of the DFG Grants Ti240/13 and Ti240/14. This work also provided an excellent stratigraphic basis for ongoing studies within the DFG supported Research Unit "Impact of Gateways on ocean circulation, climate, and evolution". We thank the crew of the Joides Resolution and the Leg 202 science party for an exceptionally successful expedition. We especially would like to acknowledge the quick aid of Pieter Grootes and Nils Andersen from the "Leibniz-Labor für Altersbestimmung und Isotopenforschung" for measuring the benthic isotopes from Site 1236, during a time when our isotope laboratory faced severe mass spectrometer problems. Stimulating discussions with Jeroen Groeneveld, Dirk Nürnberg and Joachim Schönfeld at different stages of this study were greatly appreciated. We thank Nicole Gau, Lulzim Haxhiaj, Agnes Heinemann, Anna Jesußek, Ulrike Nielsen, Janne Repschläger, and Kerrin Wittmaack for a great deal of help in sample preparation and isotope measurements. The manuscript benefited from reviews by ...

CHAPTER 5

CHANGES IN CARIBBEAN SURFACE HYDROGRAPHY DURING THE PLIOCENE SHOALING OF THE CENTRAL AMERICAN SEAWAY

Silke Steph[1], Ralf Tiedemann[1], Jeroen Groeneveld[1], Dirk Nürnberg[1], Lars Reuning[1], Gerald Haug[2]

[1]IFM-GEOMAR, Leibniz-Institut für Meereswissenschaften, Kiel, Germany

[2]GeoForschungsZentrum, Potsdam, Germany

submitted to Paleoceanography

Abstract

Pliocene planktonic $\delta^{18}O$ records (*G. sacculifer*) from Caribbean ODP Sites 999, 1000, equatorial east Pacific Site 851, Atlantic Sites 925 (Ceara Rise) and 1006 (western Great Bahama Bank) were used to examine Caribbean-Pacific and Caribbean-Atlantic atmospheric and oceanic linkages associated with the progressive closure of the Central American Seaway (5.5 – 3 Ma). Comparisons with planktonic Mg/Ca records suggest Caribbean salinity changes of about 2.6 salinity units on precessional periodicities, when the Pacific-Caribbean throughflow became significantly restricted after 4.4 Ma. This high-amplitude variability in SSS is also observed at Site 1006, monitoring the Caribbean outflow into the Atlantic. The comparison of Caribbean and Atlantic planktonic $\delta^{18}O$ records suggests the Atlantic subtropical gyre as the major source for high salinity surface waters. Precession-induced variations in the volume transport of Pacific surface water masses through the Panamanian Seaway are considered as a main factor to explain the observed Caribbean salinity minima.

5.1 Introduction

The closure of the Central American Seaway at about 2.7 Ma, and the intensification of the northern hemisphere glaciation since 3 Ma played a major role in modifying Pliocene climate and oceanography. Closure-induced changes in global thermohaline circulation have been invoked to be the cause either for the onset (Berggren and Hollister, 1974), or for the delay (Berger and Wefer, 1996), or for setting the preconditions of the northern hemisphere glaciation (Haug and Tiedemann, 1998; Driscoll and Haug, 1998). While the link between closure and climate is still a matter of debate, paleoceanographic studies suggest a close link between the formation of the isthmus and major oceanographic changes during the early Pliocene between 4.6 Ma and 4.2 Ma, when the shoaling of the Panamanian sill reached a critical threshold for upper ocean water mass exchange (Keigwin, 1982a; Haug et al. 2001a). The restricted exchange of surface water masses led to the establishment of the modern Atlantic/Pacific salinity contrast that is linked to the atmospherical net freshwater transport from the tropical Atlantic and Caribbean into the equatorial East Pacific (e.g. Broecker and Denton, 1989; Jousaumme et al., 1986). In addition, results from General Circulation Models and paleoceanographic studies suggest a reorganization of equatorial Pacific surface circulation, and an increased volume transport of heat and salt into the North Atlantic *via* an intensified Gulf Stream favoring North Atlantic Deep Water formation and Atlantic carbonate preservation (Maier-Raimer et al., 1990; Farrell et al., 1995; Tiedemann and Franz, 1997; Billups et al., 1997; Cannariato and Ravelo, 1997; Mikolajewicz and Crowley, 1997; Haug and Tiedemann, 1998; Billups et al., 1999; Haug et al., 2001a).

Here, we present a high-resolution planktonic foraminiferal $\delta^{18}O$ record (*G. sacculifer*) from Caribbean ODP Site 1000 located at Pedro Channel on the Northern Nicaragua Rise. This record spans the time interval from 5.6 – 3 Ma and will be compared with the recently published planktonic $\delta^{18}O$ record (*G. sacculifer*) from ODP Site 999 (Haug et al., 2001a), which is positioned farther south and thus closer to the Pliocene gateway region. Haug et al. (2001a) attempted to assess closure-related changes in Caribbean sea surface salinity (SSS) by comparing planktonic oxygen isotope records from Caribbean Site 999 and equatorial east Pacific Site 851. They interpreted the divergence between both records to reflect a salinity increase of one unit since 4.2 Ma, assuming no major change in sea surface temperature (SST) that would in turn affect the SSS estimate. Our new record from Site 1000 considers for the first time changes in SST and provides insights into Pliocene latitudinal gradients in Caribbean surface water hydrography. Major differences in Caribbean SSS developed after 4.6 – 4.2 Ma, suggesting strong local changes in addition to the general SSS increase. To further assess the Caribbean water mass exchange with the Pacific and the Atlantic, we compared the Caribbean records with records from the Pacific (Site 851) and Atlantic (Sites 925, 1006). Forcing mechanisms that might have controlled the Pliocene history of Caribbean SSS will be discussed, considering long-term tectonic feedbacks along with short-term changes in atmosphere-upper ocean interactions and solar radiation.

5.2 Modern Oceanography

As a major source region for the Gulf Stream, the Caribbean Sea plays an important role in the net export of heat and salt into high northern latitudes. Today, the uppermost water column in the southern part of the Caribbean is composed of relatively fresh Caribbean Water (CW, 0 – 80 m) and high-salinity Subtropical Under Water (SUW) approximately between 80 – 180 m that forms the permanent Caribbean thermocline (Wüst, 1964). The CW represents a mixture of the Amazon and Orinoco River outflow and equatorial Atlantic surface water that mainly enters the Caribbean *via* the Guyana Current through the Lesser Antilles Passages. The salinity enriched SUW originates from the subtropical gyre and mainly enters the Caribbean *via* the North Equatorial Current through the Greater Antilles Passages (Windward and Mona Passage) (Wüst, 1964; Johns et al., 2002). These water masses form the Caribbean Current that passes the Yucatan Channel and the Florida Straits, where it merges with the Antilles Current to form the northward flowing Western Boundary Current (**Fig. 5-1**).

The average flow through the Caribbean is estimated as 20 – 30 Sv (Sv = Sverdrup = 10^6 m^3s^{-1}) (e.g. Wüst, 1964; Müller-Karger et al., 1989; Johns et al., 2002). Results from numerical models (e.g. Johns et al., 2002) suggest that the volume of shallow Atlantic water masses transported into the Caribbean is controlled by both the strength of the meridional overturning in the N-Atlantic and by changes in the tropical wind field controlling the position of the Intertropical Convergence Zone (ITCZ). The Caribbean inflow through the southernmost passages of the Lesser Antilles is considered to balance the return flow for the modern export of North Atlantic Deep Water, while nearly all of the wind driven inflow occurs north of Martinique (ca. 15°N).

The modern Caribbean throughflow shows a strong wind-driven seasonality with maximum values in spring and summer, and minimum values in fall (Schott et al., 1988; Molinari et al., 1990; Larsen, 1992; Johns et al., 2002). From spring to summer, when the ITCZ moves northward, the inflow to the southern Caribbean appears to result from a strengthened Guyana Current entering through the southernmost Lesser Antilles Passages (Müller-Karger et al., 1989). This inflow is considered to contribute to lower SSS in the eastern Caribbean due to the admixture of waters from the Amazon and Orinoco rivers that reach their maximum discharge in June and August, respectively.

In August, when the ITCZ reaches its northernmost position at 6°N – 10°N (Philander and Pacanowski, 1986), the development of a cyclonic circulation cell southeast of the Lesser Antilles blocks the direct inflow of South Atlantic water to the Caribbean *via* the Guyana Current (Müller-Karger et al., 1989; Johns et al., 2002). Until January, the northward transport along the coast of South America is retroflected to the east and provides the western source of the North Equatorial Counter Current. In spite of the retroflection, a significant amount of Amazon freshwater is carried northwestward and can be traced into the central Caribbean Sea to about 70°W (Hellweger and Gordon, 2002), however, with a lag time of ca. 6 months. The largest river draining directly into the western Caribbean is the Magdalena River with a mean discharge of $6.9*10^3$ m^3s^{-1} which is two orders of magnitude lower than the average Amazon discharge of $1.6*10^5$ m^3s^{-1} (River Discharge Database, 2003).

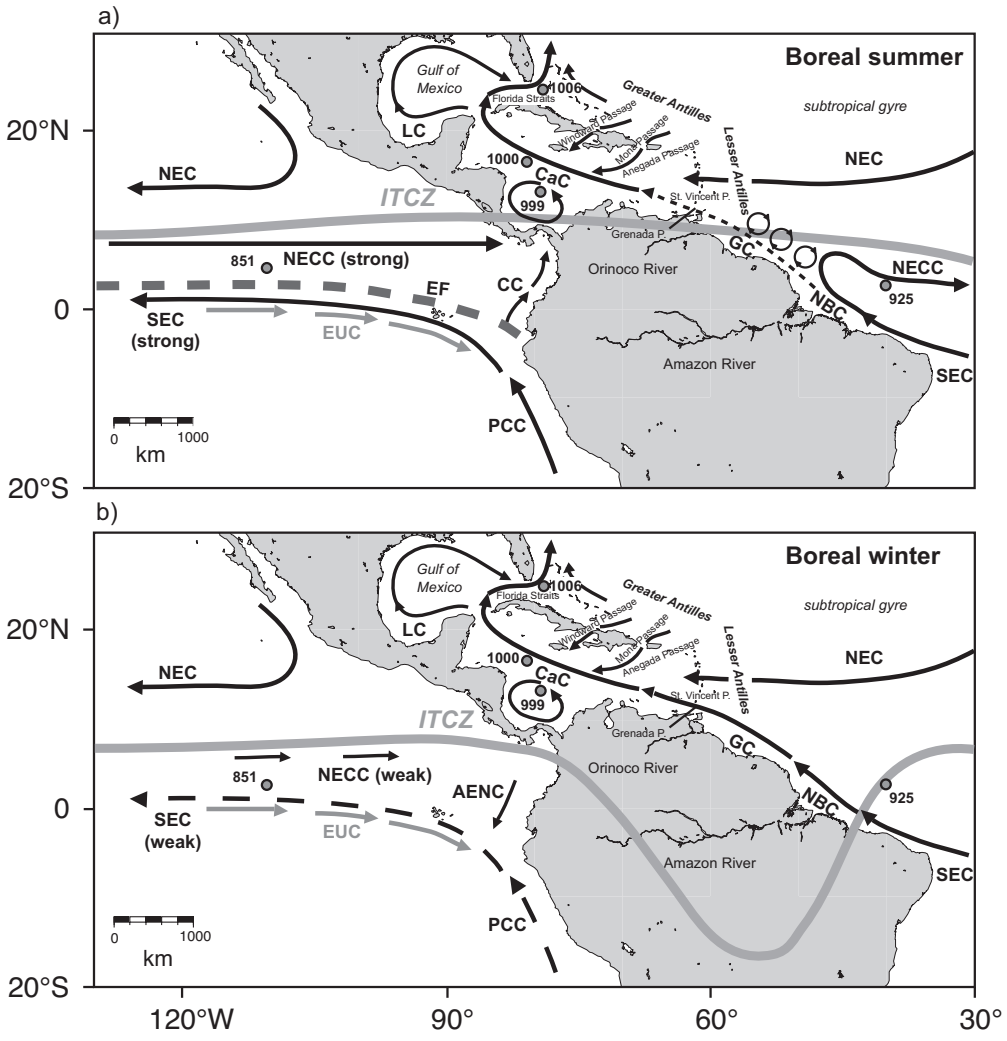

Fig. 5-1 Modern oceanographic setting of the tropical western Atlantic and eastern Pacific showing major surface current systems. The locations of ODP sites discussed in this study are indicated. **a**: Scenario during boreal summer with the ITCZ at its northernmost position. The Atlantic SEC is retroflected towards the east. **b:** Scenario during boreal winter with the ITCZ at its southern position. The Atlantic GC enters the Caribbean *via* the Lesser Antilles Passages. NEC: North Equatorial Current; NECC: North Equatorial Counter Current; SEC: South Equatorial Current; NBC: North Brazil Coastal Current; GC: Guyana Current; CAC: Caribbean Current; LC: Loop Current; PCC: Peru-Chile Current; CC: Colombia Current; EUC: Equatorial Undercurrent; AENC: Annual El Niño Current; EF: Equatorial Front; ITCZ: Intertropical Convergence Zone.

In addition to the freshwater supply from the Amazon and Orinoco rivers, Caribbean SSS is controlled by the seasonal position of the tropical rain belt that follows the ITCZ and determines the evaporation/precipitation ratio. The migration of the ITCZ leads to a dry (February – May) and a wet season (August – October) north of about 5°N (Müller-Karger et al., 1989). In the western Caribbean, these phases are roughly parallel to changes in SSS. According to Dessier and Donguy (1994), and Hellweger and Gordon (2002), modern evaporation/precipitation west of 70°W exerts a stronger control on SSS than the freshwater supply from the Amazon.

On average, modern Caribbean salinities at 50 m water depth (assumed main habitat depth of *G. sacculifer*) range between 35 and 37 salinity units and SSTs are usually warmer than 27 °C (Levitus and Boyer, 1994a,b). Local differences in SSS and SST between Site 1000 and 999 are very small at 50 m water depth. At Site 1000 (Pedro Channel), salinity varies between 35.7 salinity units (winter) and 36.2 salinity units (summer) and at Site 999 (Colombian Basin) between 35.9 salinity units (winter) and 36.6 salinity units (summer) (Levitus and Boyer, 1994b).

5.3 Material and Methods

Caribbean ODP Site 1000 is located in Pedro Channel between Nicaragua and Jamaica (16° 33'N, 79° 52'W) at a water depth of 916 m (Sigurdsson et al., 1997). Carbonate preservation is excellent according to the shallow site location far above the lysocline. The interval from 5.6 Ma to 2.4 Ma was sampled every 10 cm corresponding to a time resolution better than 3 kyr. A nearly complete late Miocene-Pliocene interval was cored at Hole 1000A with the advanced hydraulic piston corer system. In addition to reference Hole A, we sampled cores 1R and 2R from Hole B to stratigraphically splice across the drilling disturbed intervals of cores 1000A-10H and 1000A-13H, respectively.

For isotope analysis of the mixed-layer-dwelling foraminifera *G. sacculifer* (without sac-like final chamber), 10 specimens were picked from the 315 – 400 µm size fraction. For the benthic $\delta^{18}O$ record, one to three tests of the epibenthic species *C. wuellerstorfi* (> 400 µm size fraction) were analyzed. Prior to analysis, specimens were slightly crushed and ultrasonically cleaned with methanol. The excess liquid and mud were siphoned off and the samples were dried at 60 °C.

All isotope analyses were run at IFM-GEOMAR (Kiel) on a Finnigan MAT 252 Mass Spectrometer with automated Kiel carbonate preparation device. Analytical precision was better than 0.07 ‰ for $\delta^{18}O$ and 0.04 ‰ for $\delta^{13}C$. The values are reported relative to Pee Dee Belemnite (PDB), based on calibrations directly to National Bureau of Standards (NBS) 19. $\delta^{18}O$ values of *C. wuellerstorfi* were adjusted to seawater equilibrium by + 0.64 ‰ (Shackleton and Hall, 1984).

For Mg/Ca analysis, 20 specimens (approximately 0.5 – 1.2 mg of sample material) of *G. sacculifer* were selected from the 315 – 400 µm size fraction. Specimens visibly contaminated by ferromanganese oxides and specimens with a final sac-like chamber were discarded. The specimens were gently crushed between glass plates in order to open the chambers and were cleaned subsequently according to the cleaning protocol of Barker et al. (2003), including several rinses with distilled deionized water and methanol (suprapur) and in-between ultrasonic treatment, two times 10 minutes soaking of the samples in a hot (97°C) oxidizing 1 % $NaOH/H_2O_2$ solution (10 ml 0.1 N NaOH (analytical grade); 100 µl 30 % H_2O_2 (suprapur)), a weak acid leach (0.001 M QD HNO_3) and finally dissolved in QD 0.075 M HNO_3. Analyses were performed on an ICP-AES (ISA Jobin Yovin-Spex Instruments S.A. GmbH) at IFM-GEOMAR (Kiel).

We used the software package AnalySeries 1.2 from Paillard et al. (1996) for time series analyses and stratigraphic correlation in order to establish an age model for Site 1000.

5.4 Estimation of the calcification depth of *G. sacculifer*

In order to reconstruct changes in upper ocean water mass signatures as derived from planktonic $\delta^{18}O$ data, the habitat depth of planktonic foraminifers is of basic interest. Therefore, we tried to assess the calcification depth of *G. sacculifer* in the Caribbean. The present knowledge of the habitat depth of planktonic foraminifera is mainly based on tow studies. Most results consistently suggest a main abundance depth in the range of 0 – 80 m for *G. sacculifer* (Fairbanks et al., 1982; Hemleben and Spindler, 1983; Ottens, 1992; Kemle-von-Mücke and Oberhänsli, 1999; Schmuker and Schiebel, 2002), although living specimens are also found much deeper in the water column up to 1000 m water depth (e.g. Kemle-von-Mücke and Oberhänsli, 1999). It is well known, that *G. sacculifer* adds calcite in deeper and cooler water masses during gametogenesis accumulating ^{18}O (e.g. Duplessy et al., 1981; Lohmann, 1995). Therefore, it has to be considered that the $\delta^{18}O$ signal of *G. sacculifer* represents a mixture of shell parts that calcified at shallow and deeper water depths. We only measured *G. sacculifer* without a sac-like formed last chamber to largely reduce isotopic signals from gametogenic calcification (Duplessy et al., 1981).

To examine the relationship between expected habitat depth (0 – 80 m) and *G. sacculifer* $\delta^{18}O$ value, we measured stable isotopes from 15 Caribbean core top samples collected during *RV Sonne* Cruise SO 164 (Nürnberg et al., 2002). The comparison of measured $\delta^{18}O$ and calculated equilibrium calcite $\delta^{18}O$ ($\delta^{18}O_C$ as a function of habitat temperature and $\delta^{18}O_W$ water value) provides the deviation between expected habitat depth and the habitat depth as suggested from the $\delta^{18}O$ foraminiferal value. Equilibrium $\delta^{18}O_C$ was calculated from $\delta^{18}O_W$ and temperature using a rearrangement of the paleotemperature equation for *G. sacculifer* (Spero et al. 2003):

$$\delta^{18}O_C = [T-12.0-5.67*(\delta^{18}O_W-0.27)]/-5.67 \quad [1]$$

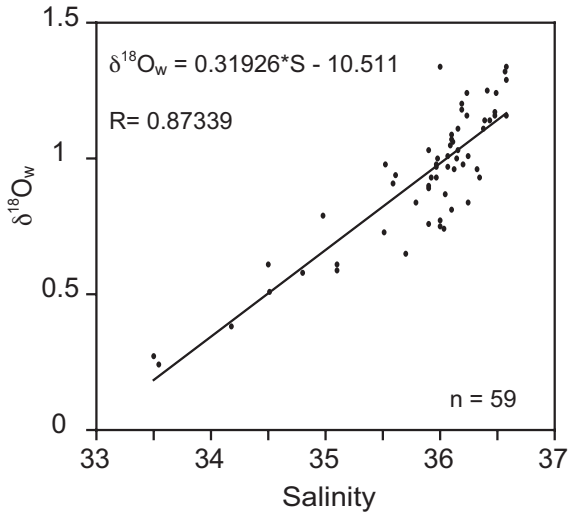

Fig. 5-2 $\delta^{18}O$-salinity relationship established for the modern southern Caribbean (0 – 100 m water depth, summer). Data are taken from Schmidt et al. (1999).

We chose the equation of Spero et al. (2003) instead of others, because the normalization factors derived from experimental and plankton tow data are *G. sacculifer*-specific. To determine $\delta^{18}O_W$, we established a $\delta^{18}O$-salinity relationship for the Caribbean (0 – 100 m water depth, summer; **Fig. 5-2**) using $\delta^{18}O_W$ and salinity data available from Schmidt et al. (1999):

$$\delta^{18}O_W \text{ (Caribbean)} = 0.319S-10.511 \quad [2]$$

Then, we calculated the $\delta^{18}O_W$ and the $\delta^{18}O_C$ for the Caribbean core top stations using annual mean salinity and temperature data from Levitus and Boyer (1994a,b). $\delta^{18}O_W$ values were converted from SMOW (standard mean oceanic

water) to PDB (Pee Dee Belemnite) by subtracting 0.27 ‰ as indicated in equation 1 (Hut, 1987). $\delta^{18}O_C$ was calculated for different water depths (0 – 200 m) and compared with measured core top *G. sacculifer* $\delta^{18}O_C$ values to estimate the isotope-derived habitat depth. As a result, the match between measured and calculated $\delta^{18}O_C$ suggests an average habitat depth of 95 ± 16 m (**Tab. 5-1**). We are aware of the fact that the estimates for each station (**Tab. 5-1**) represent a mean of different calcifying depths, although *G. sacculifer* may have lived predominantly within the upper 80 m of the water column. Hence, for paleoceanographic interpretations it has to be considered that the isotope signal from *G. sacculifer* is certainly not a pure upper mixed layer signal. The application of other paleotemperature equations (e.g. O'Neil et al., 1969; Shackleton, 1974) would lead to shallower habitat depths in the range of 30 – 50 m. An extended discussion and comparison of different paleotemperature equations is given in Mulitza et al. (2004).

Tab. 5-1 Isotope derived habitat depth (m) for *G. sacculifer* from Caribbean core top samples collected during *RV Sonne* Cruise SO 164 (May 22 – June 28, 2002).

Station Nr.	Latitude	Longitude	$\delta^{18}O_c$ measured (‰)	Isotope derived habitat depth (m)
SO16401-3	13°50.195 N	74°09.028 W	-1.35	81
SO16402-3	15°18.290 N	72°47.060 W	-1.39	102
SO16403-3	16°32.400 N	72°12.310 W	-1.58	103
SO16404-2	17°16.380 N	71°39.090 W	-1.63	100
SO16407-3	21°19.460 N	74°08.760 W	-1.53	78
SO16419-3	21°14.710 N	74°20.990 W	-1.37	103
SO16420-2	16°45.490 N	71°29.220 W	-1.37	120
SO16421-3	16°06.000 N	70°30.000 W	-1.42	103
SO16423-3	15°34.010 N	65°08.090 W	-1.25	108
SO16424-3	14°11.890 N	63°25.430 W	-1.50	79
SO16425-3	14°41.250 N	59°44.480 W	-1.48	85
SO16448-2	15°57.020 N	60°55.000 W	-1.74	64
SO16450-3	15°21.250 N	59°16.940 W	-1.22	111

5.5 Age Model

The age model at Site 1000 was mainly based on benthic (*C. wuellerstorfi*) isotope stratigraphy and biostratigraphy. The opportunity for an astronomical calibration of the Late Miocene to Pliocene timescale was limited as no composite depth exists, which would cover and identify coring gaps usually occurring at core breaks. The timescale was achieved by identifying eye-catching benthic oxygen isotope stages according to the Miocene-Pliocene isotope nomenclature of Shackleton et al. (1995). Then, we correlated the oxygen isotope events to the isotope standard time scale from Site 925/926, which was orbitally tuned to the astronomical solution of Laskar (1990) (Bickert et al., 1997; Tiedemann and Franz, 1997; Shackleton and Hall, 1997). The match between

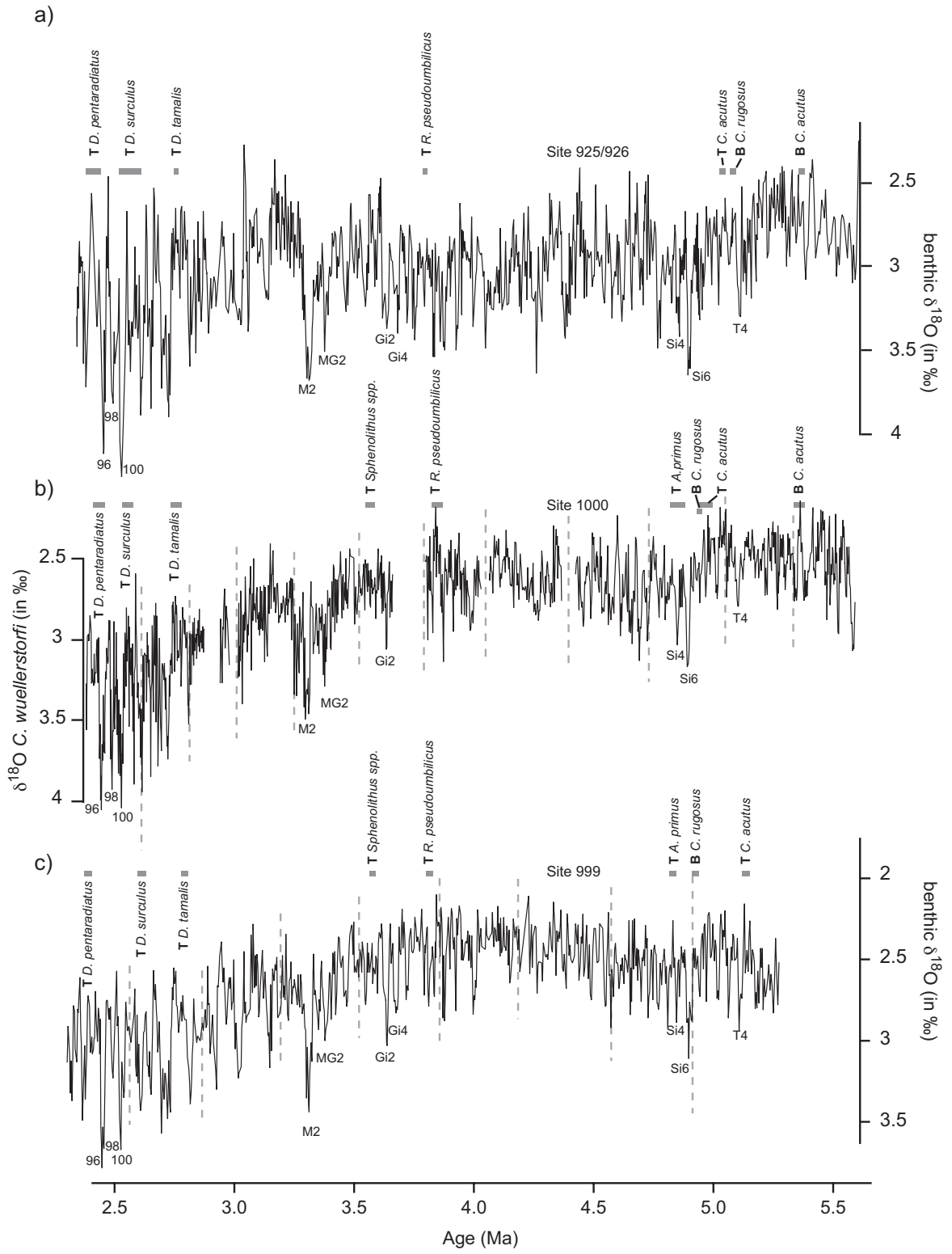

Fig. 5-3 Correlation of benthic $\delta^{18}O$ records for Caribbean Sites 1000 (**b**) and 999 (**c**) to the orbitally tuned $\delta^{18}O$ record of western Atlantic Sites 925/926 (**a**) (Bickert et al., 1997; Tiedemann and Franz, 1997; Shackleton and Hall, 1997). Pronounced isotope stages and biostratigraphic events are indicated. Dashed lines indicate core breaks in Caribbean sites.

both benthic $\delta^{18}O$ records resulted in an initial age model and displays the general dominance of Pliocene 41-kyr climate fluctuations (**Fig. 5-3**). This age model suggests that core breaks are associated with stratigraphic gaps of up to 70 kyrs. The relatively large gap between 3.66 Ma and 3.80 Ma represents drilling-disturbed intervals of overlapping cores 1000A-13H and 1000B-2R (sections 6-7) that were not sampled.

The correlation of benthic isotope records revealed the dominance of precessional periodicities (23 and 19 kyr) in the planktonic $\delta^{18}O$ record from 3.0 Ma to 4.4 Ma (cores 11, 12, 14, 15). Maxima in planktonic $\delta^{18}O$ match precessional maxima in northern hemisphere summer insolation (**Fig. 5-4**). To further amplify the precessional component of the planktonic $\delta^{18}O$ record, we subtracted the benthic $\delta^{18}O$ values from the *G. sacculifer* record, which largely reduced the 41-kyr cycle of the $\delta^{18}O$ ice volume signal in the planktonic isotope record. Spectral analyses in the depth domain provided dominant planktonic $\delta^{18}O$ cycles, e.g. ranging from 100 – 110 cm (cores 11 – 14) to 80 cm (core 15). Sedimentation rates derived from the initial age model identify these cycles as a response to orbital precession. The counting of precession-related cycles yielded the time span for each core. Accordingly, the appropriate time span for each core should be in agreement with the initial age model. In case of disagreements, we reassigned our correlation between the benthic isotope records but did not adjust the planktonic $\delta^{18}O$ signal to variations in orbital precession. This procedure improved the initial age model and helped to identify stratigraphical gaps associated with core breaks (**Figs. 5-3, 5-4**). Furthermore, the remarkable similarity between benthic $\delta^{13}C$ records (Sites 1000 and 925/926, (Tiedemann et al., manuscript in preparation, 2004) corroborated the robustness of the age model.

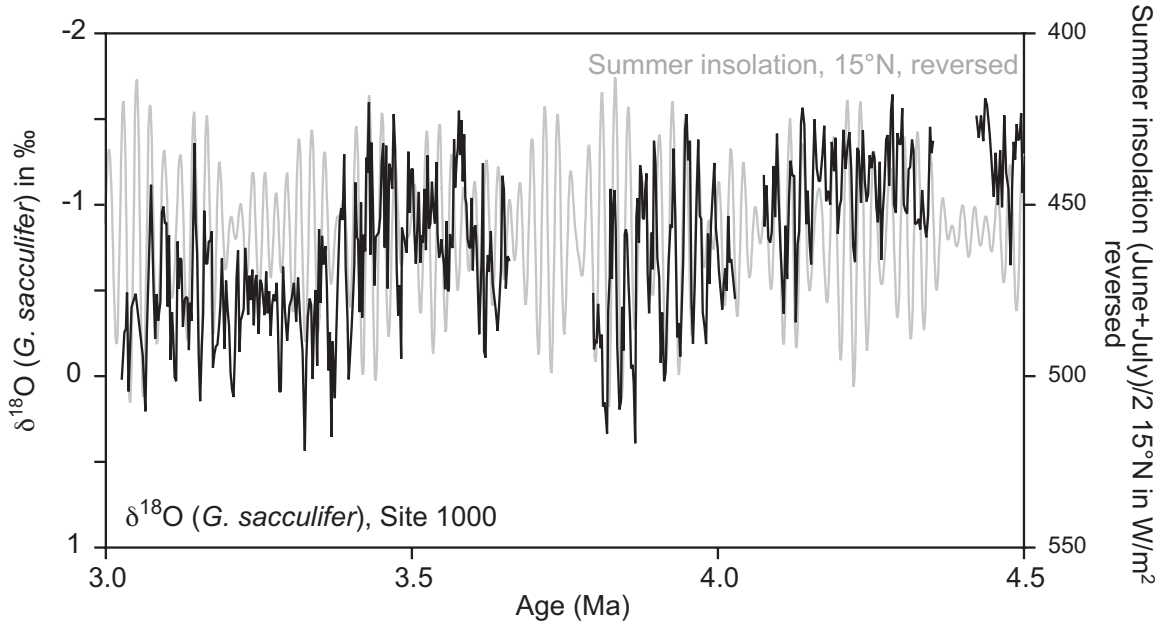

Fig. 5-4 Planktonic $\delta^{18}O$ record (*G. sacculifer*) from Caribbean Site 1000 compared to northern hemisphere summer insolation (June + July / 2; 15°N; reversed) (Laskar, 1990). In general, high $\delta^{18}O$ values (interpreted as high SSS) are linked to northern hemisphere summer insolation maxima.

The nannofossil age assignments obtained from our final age model correspond within their error range to those calculated by Raffi and Flores (1995), and Shackleton et al. (1995), except for the nannofossil events of Top (T). *C. acutus*, Base (B). *C. rugosus*, and T. *D. quinqueramus* around the Miocene/Pliocene boundary (Backman and Raffi, 1997) (**Fig. 5-3**). According to the biostratigraphic work of Backman and Raffi (1997) the base of *C. rugosus* was estimated to occur approximately one obliquity cycle before the top of *C. acutus*. In contrast, the biostratigraphy at Site 1000 (Kameo and Bralower, 2000) suggests that the top of *C. acutus* appears at greater sediment depth than the base of *C. rugosus*, leaving behind a stratigraphic problem that cannot be resolved within this study. At Site 1000, both events occur within core 17 and about 100 kyr later than suggested by Backman and Raffi (1997). The stratigraphic adjustment of core 17 is based on simple identification of pronounced marine isotope stages (MIS) Si4 and Si6 (**Fig. 5-3**), whereas the two events occur not more than two obliquity cycles later and therefore suggest a younger age. The age assignment of B. *C. acutus* is almost identical to the age calculated by Backman and Raffi (1997).

For direct comparisons with isotope records from Site 999 (Haug and Tiedemann, 1998) and 851 (Cannariato and Ravelo, 1997), we adjusted the benthic oxygen isotope record from Site 999 to Site 925/926 and used the correlation between planktonic $\delta^{18}O$ records from Sites 999 and 851 to adjust Site 851 (Haug et al., 2001a). The alignment of most nannofossil events between Sites 1000 and 999 correlates within an error range of less than half an obliquity cycle. Although MIS 96 - 100 are clearly recognized at both Sites, the associated stratigraphic position of T. *D. surculus*, and T. *D. pentaradiatus* deviates by up to two obliquity cycles. However, the estimated ages for T. *D. surculus*, and T. *D. pentaradiatus* at Sites 999 and 1000 are within the estimated time span given by Raffi and Flores (1995) for these events. A larger biostratigraphic uncertainty results from the position of T. *C. acutus* at Site 999. At Site 1000, the top of *C. acutus* overlaps with the base of *C. rugosus*, whereas at Site 999 both events are separated by about 170 kyr. This uncertainty cannot be ascribed to a coring gap, because both events are present within one core at each site. In addition to the lithostratigraphy (Siggurdson et al., 1997), the presence of 41-kyr isotope cycles in the benthic record, as well as the clear identification of MIS T4 provide no indication for a sediment slump at Site 999, which could explain the time offset. The supply of reworked older sediment material would have resulted in an opposite effect by moving the top of *C. acutus* upcore. Hence, the stratigraphic position of T. *C. acutus* remains a problem.

5.6 Evolution of Pliocene SSS in the Caribbean

The new planktonic oxygen isotope record from Site 1000 (**Fig. 5-5**) adds valuable information to the results from Haug et al. (2001a). Their study was based on a comparison of planktonic $\delta^{18}O$ records between Caribbean Site 999 and Pacific Site 851. The divergence between both records at 4.7 Ma and the 0.5 ‰ $\delta^{18}O$ increase at Site 999 since 4.2 Ma was interpreted to reflect an increase of one salinity unit in Caribbean SSS in response to the shoaling of the Central American Seaway. Caribbean Site 1000 reveals distinctly higher short-term isotope fluctuations with generally higher $\delta^{18}O$ values than the more southern Caribbean Site 999. $\delta^{18}O$ values vary from -1.8 ‰ to 0.5 ‰

compared to -2.1 ‰ to -0.5 ‰ at Site 999. During the late Miocene and early Pliocene (5.6 – 4.4 Ma), $\delta^{18}O$ values were about 0.2 ‰ higher at Site 1000 (**Fig. 5-5**). The amplitudes of $\delta^{18}O$ variations were relatively low and both records show similar patterns. A significant change in inner-Caribbean surface water conditions occurred after 4.4 Ma. $\delta^{18}O$ amplitudes at Site 1000 strongly increased from 4.4 Ma to 3.8 Ma (up to 1.3 ‰) and were considerably higher than those observed at Site 999. This increase in amplitudes is associated with the development of strong 23-kyr cycles (**Figs. 5-5, 5-6**). In contrast, the planktonic $\delta^{18}O$ record from Site 999 reflects no clear response to cyclic variations in orbital parameters. When $\delta^{18}O$ values at Site 1000 reach minima, the difference to Site 999 is smallest. Large differences of up to 1.5 ‰ are linked to $\delta^{18}O$ maxima at Site 1000. At 3.6 Ma, the difference in $\delta^{18}O$ between Caribbean sites decreased and increased again after 3.3 Ma. These strong local differences in $\delta^{18}O$ would suggest a pronounced regional and temporal variability in Caribbean SSS after 4.4 Ma, if temperature fluctuations were similar at both sites.

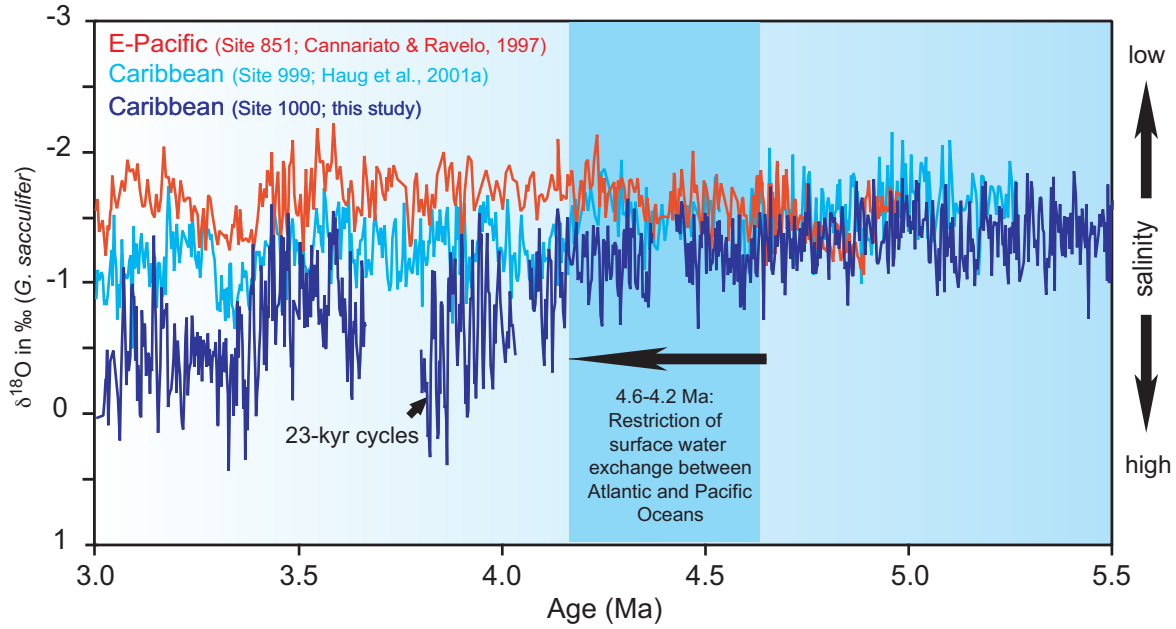

Fig. 5-5 Comparison of planktonic $\delta^{18}O$ records (*G. sacculifer*) from Caribbean Sites 1000 (dark blue, this study) and 999 (light blue) (Haug et al., 2001a) to tropical east Pacific Site 851 (red) (Cannariato and Ravelo, 1997). The time interval from 4.6 Ma to 4.2 Ma is marked by an overall increase in Caribbean SSS with strong local differences in Caribbean SSS after 4.2 Ma. The development of strong 23-kyr. cycles in planktonic $\delta^{18}O$ at Site 1000 starts at about 4.4 – 4.2 Ma ago.

To examine the relationship between SST and SSS at Site 1000 more precisely, we compared a short interval of the planktonic $\delta^{18}O$ record (4.6 – 3.8 Ma) with Mg/Ca measurements on the same species, *G. sacculifer* (**Fig. 5-7**). In general, high $\delta^{18}O$ values reflect low temperatures and/or high salinities. High Mg/Ca ratios are indicative of high SST (e.g. Nürnberg et al., 1996; Nürnberg et al., 2000; Nürnberg, 2000). Here we do not present absolute Mg/Ca-derived temperatures. This will be the topic of an extended forthcoming publication (Groeneveld et al., submitted b), which evaluates the influence of SSS on Mg/Ca-ratios. From 4.4 Ma to 3.8 Ma, when the progressive closure of the

isthmus led to the Pacific-Caribbean salinity contrast, fluctuations in Mg/Ca ratios, $\delta^{18}O$ and northern hemisphere summer insolation are clearly positively correlated, e.g. maxima in northern hemisphere summer insolation are associated with high Mg/Ca ratios and high $\delta^{18}O$ values at Site 1000. This implies that maxima in Caribbean SSS occurred during warm stages. Since a simultaneous increase in SST and SSS influences the $\delta^{18}O$ values in opposite directions, the effect of SST on the $\delta^{18}O$ signal is fully compensated by the strong overprint of SSS. Thus, $\delta^{18}O$ amplitude fluctuations of up to 1.3 ‰ exclusively represent minimum changes in salinity. According to the $\delta^{18}O$-salinity relationship for the modern Caribbean (**Fig. 5-2**), such fluctuations would correspond to a change in SSS of up to 4 salinity units. We are aware of the problem that the Pliocene $\delta^{18}O$-salinity relationship may have deviated from the modern one and possibly was closer to the general modern ocean $\delta^{18}O$-salinity relationship ($\delta^{18}O_W = 0.5*S$) (Broecker and Peng, 1982), which would reduce the amplitude of 4 salinity units to 2.6 salinity units.

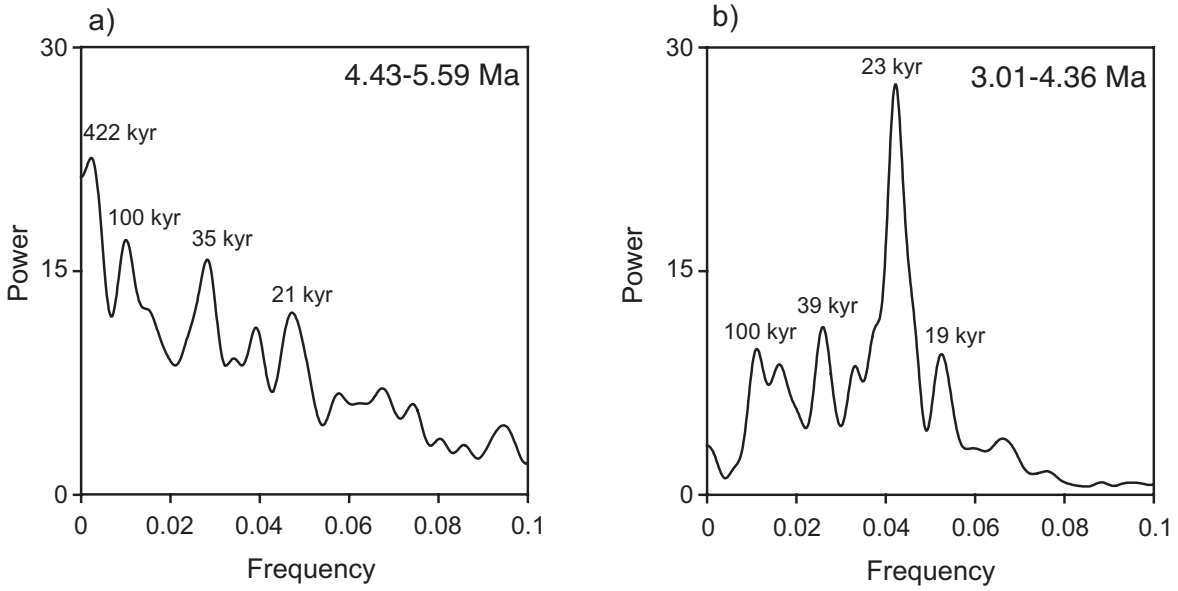

Fig. 5-6 Spectral analyses accomplished for different time slices of the planktonic $\delta^{18}O$ record (*G. sacculifer*) for Site 1000. (**a**) Time interval from 4.43 – 5.59 Ma, when the Panamanian Gateway was still open for surface water exchange. The response of planktonic $\delta^{18}O$ to orbital precession was weak. Time step: 2 kyr; Number of lags: 20 % of the series; Confidence interval: 80 %; Bandwith: 0.0064. (**b**) Time interval from 3.01 – 4.36 Ma, when the inflow of Pacific surface waters into the Caribbean was restricted. Variations in planktonic $\delta^{18}O$ were dominantly controlled by orbital precession. Time step: 2 kyr; Number of lags: 20 % of the series; Confidence interval: 90 %; Bandwidth: 0.0056.

The observed variability in both SSS and SST clearly follows a 23-kyr rhythm after 4.4 Ma as indicated by a comparison with changes in northern hemisphere summer insolation and spectral analyses (**Figs 5-4, 5-6**). It is well known that precession-related changes of the seasonal cycle at low latitudes significantly affect the strength and zonality of the trade winds and tropical SST conditions as shown by modeling experiments and paleoceanographic data (e.g. Kutzbach and Guetter, 1986; McIntyre et al., 1989). The strong response of the Site 1000 planktonic $\delta^{18}O$ record to orbital precession (23-kyr cycles) would imply a low-latitude climate forcing as the dominant trigger for changes in SST and SSS rather than a high-latitude forcing because of the absence of

pronounced 41-kyr cycles. The clear deviation between planktonic and benthic $\delta^{18}O$ records (**Figs. 5-3, 5-5**) also suggests a strong local forcing rather than a global forcing. The water mass signatures between Caribbean Sites 1000 and 999 seem to be decoupled from each other after 4.4 Ma, as Site 999 reveals no clear response to precessional forcing. During northern hemisphere summer insolation maxima, differences in $\delta^{18}O$ (~1.5 ‰) suggest a very strong salinity gradient towards the north. SSS increased over a distance of ~450 km (from Site 999 to Site 1000) by up to 3 salinity units. During northern hemisphere summer insolation minima, $\delta^{18}O$ values were similar at both sites, except for two time intervals, from 3.9 – 3.6 Ma and from 3.4 – 3 Ma, where differences in $\delta^{18}O$ were enlarged (0.6 ‰).

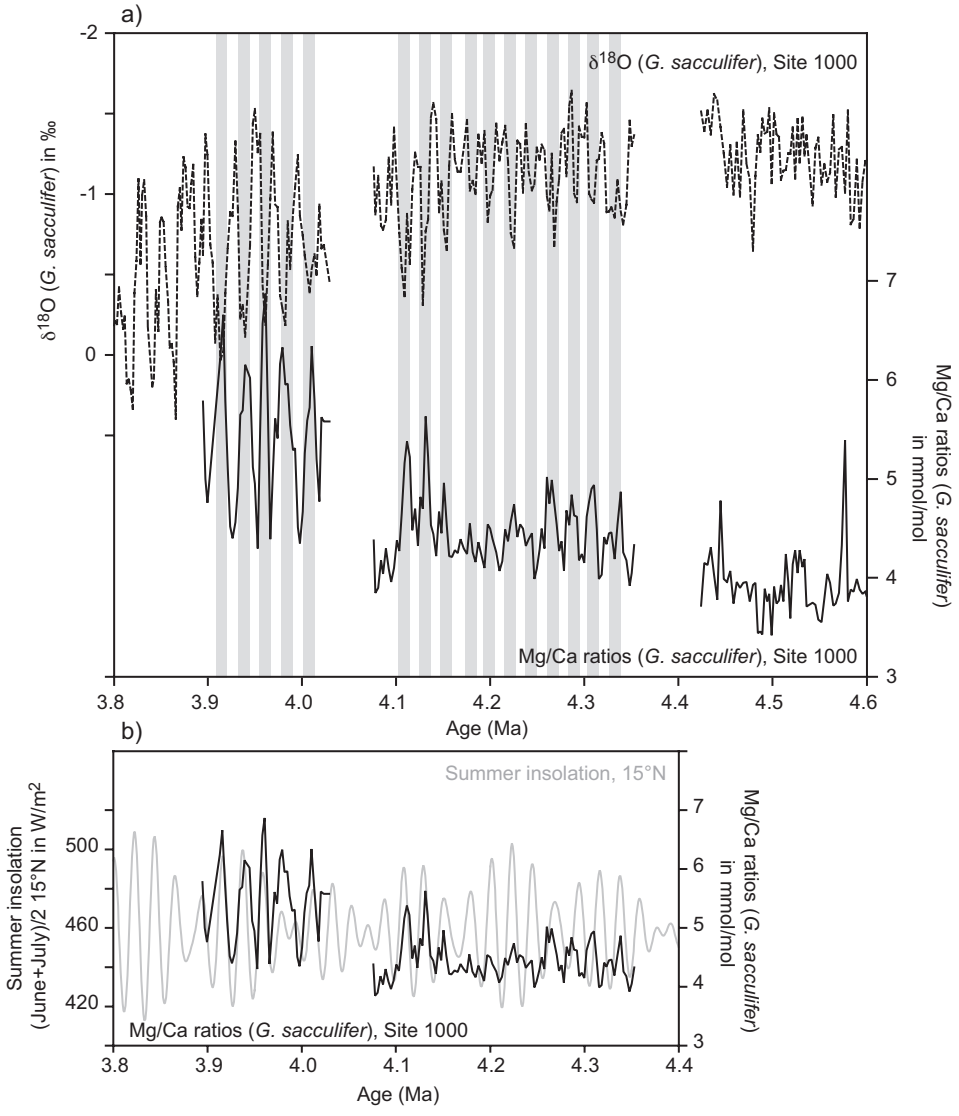

Fig. 5-7 Mg/Ca ratios (*G. sacculifer*) for Caribbean Site 1000 (Groeneveld et al., submitted b). (**a**) Mg/Ca ratios (black line) and $\delta^{18}O$ *G. sacculifer* (dashed line) for Site 1000. Gray bars indicate the correlation of high Mg/Ca ratios (high SST) with high $\delta^{18}O$ values (high SSS). (**b**) The comparison of Mg/Ca ratios and northern hemisphere summer insolation (June + July / 2, 15°N) (Laskar, 1990) demonstrates that high SST are generally linked to northern hemisphere summer insolation maxima.

5.7 What controls Caribbean SSS and SST during the Pliocene?

The local differences in Caribbean SSS as well as the presence of strong 23-kyr cycles in SSS and SST at Site 1000 paralleling the progressive closure of the Central American Seaway raise several questions concerning the climate forcing mechanisms. There is no doubt that tectonic feedbacks and atmosphere-upper ocean interactions are responsible for the observed pattern, but the mechanisms to be considered are manifold. This includes long-term tectonic processes like the shoaling of the Isthmus of Panama, the uplift of the northern Andes, as well as interactions between insolation, tropical wind field, hydrological cycle, ocean surface currents, and El Niño-Southern Oscillation (ENSO) fluctuations, affecting Caribbean surface hydrography also on shorter timescales. Below, these processes will be discussed to evaluate their significance.

5.7.1 Shoaling of the gateway

For the early Miocene pre-isthmian phase, paleobathymetrical reconstructions from benthic foraminiferal assemblages suggest a sill depth of about 2000 m (Duque-Caro, 1990), allowing for a free exchange between Pacific and Atlantic water masses down to intermediate depths (Keller and Barron, 1983). By ~12 Ma, the sill shoaled to a water depth of about 1000 m, blocking the deeper flow through the Panama-Costa Rica Strait (Duque-Caro, 1990; Coates et al., 1992). The first recorded intermingling of terrestrial faunas between North and South America at 8.0 – 9.3 Ma (Webb, 1985; Marshall, 1988) suggests the existence of an extended archipelago in Central America since the late Miocene. From about 12 – 6 Ma, the Panama sill shoaled to about 200 m water depth (Duque-Caro, 1990), but deeper leakages in the Panama isthmian strait from 200 – 500 m water depth may have persisted as indicated by bathyal benthic foraminifera from the Chargres Formation (Collins et al., 1996).

More recently, several studies documented that the progressive closure of the Central American Seaway reached a critical threshold for profound changes in ocean circulation and climate between 4.7 Ma and 4.2 Ma that was associated with a general increase in Caribbean SSS (Haug and Tiedemann, 1998; Haug et al., 2001a). With an open isthmus, numerical models suggest the inflow of Pacific surface water masses into the Caribbean rather than outflow of Caribbean/Atlantic water masses into the Pacific (e.g. Maier-Reimer, 1990; Mikolajewicz and Crowley, 1997) due to the regional differences in sea level. Similar planktonic $\delta^{18}O$ values at Caribbean and equatorial east Pacific sites reflect the free exchange of surface waters prior to 4.7 Ma. After 4.2 Ma, the progressive closure of the gateway restricted the Atlantic-Pacific surface water exchange, reducing the inflow of low-salinity Pacific water masses. At the same time, the zonal net atmospheric transport of water vapor from the Atlantic/Caribbean into the Pacific increased SSS in the Caribbean. This increase is inferred from planktonic $\delta^{18}O$ records (*G. sacculifer*, **Fig. 5-5**) and suggests that the atmospheric freshwater flux into the Pacific exceeds the low salinity return flow from the Pacific into the Caribbean. This does not necessarily imply that the Panamanian sill depth was shallower than the habitat depth of *G. sacculifer* (< 80 m) as suggested by Haug et al. (2001a), because the freshwater balance of atmospheric export from the Atlantic/Caribbean and oceanic import from the Pacific *via* the gateway tips the scale. A change in the volume transport of surface

waters in response to a narrowing of the gateway could also explain the long-term increase in Caribbean SSS, although a leakage in the gateway deeper than the habitat depth of *G. sacculifer* may still have existed.

In contrast to Site 1000, the southern Site 999 appears to be permanently affected by the throughflow of low salinity waters as indicated by generally lower planktonic $\delta^{18}O$ values and amplitudes. The most simple explanation is that Site 999 was closer to the final openings of the Panamanian Seaway (Savin and Douglas, 1985; Duque-Caro, 1990; and Collins et al., 1996). Site 1000, however, is more affected by relatively saline surface water masses originating from the tropical Atlantic as today. This makes the position of Site 1000 more sensitive for changes in the volume transport through the gateway and associated expansions of the Pacific low salinity tongue as indicated by a high variability in planktonic $\delta^{18}O$ since 4.2 Ma.

The northward increase in Caribbean salinity strengthened after 4.4 Ma in concert with northern hemisphere insolation maxima. Reduced inner-Caribbean salinity gradients occurred prior to 4.4 Ma (open isthmus), from 3.6 – 3.4 Ma, and during times of insolation minima, when both sites display similar $\delta^{18}O$ values. Precession-induced changes in the Caribbean salinity gradient most likely responded to variations in insolation, tropical wind field, and oceanography rather than to tectonic changes or sea level fluctuations. Benthic oxygen isotope records suggest that early Pliocene changes in sea level were relatively small and fluctuated on 41-kyr cycles probably on the order of 20 – 40 m (e.g. Lear et al., 2003). Changes on 23-kyr cycles are assumed to have been even smaller, because benthic isotope records show no clear response to precessional forcing. Hence, it is rather unlikely that precessional fluctuations in sea level triggered significant changes in the throughflow.

A remarkable return to lower SSS at Site 1000 with $\delta^{18}O$ values similar to those at Site 999 marks the time interval between 3.6 Ma and 3.3 Ma. This diminishing gradient may reflect a repeated long-term intensification of the throughflow associated with a change in the width or depth of the gateway, although we cannot exclude other factors as mentioned below. A significant sea level rise at 3.6 Ma is improbable, because benthic oxygen isotope records indicate no general decrease in global ice volume (e.g. Tiedemann et al., 1994; Shackleton et al., 1995; Tiedemann and Franz, 1997). However, the end of this event at 3.3 Ma is paralleled by an increase in global ice volume (culminating in MIS-M2 and MIS-MG2) and thus by a sea level drop.

5.7.2 Mountain uplift and river runoff

The Neogene uplift of the Andes presumably caused extensive changes in S-American climate and wind-driven oceanic surface circulation by reorganizing the pattern of atmospheric circulation and the hydrological cycle (Hay, 1996; Mix et al., 2003). But the timing and consequences for climate and ocean circulation, possibly responding to critical thresholds in the uplift history, are poorly constrained. The uplift of the Andes established a barrier for the southeast trade winds that is considered to have influenced the hydrological cycle. Today, this orographic interception results in a rain shadow on the western side and enhanced precipitation on the eastern side of the sub-equatorial northern Andes south of 3°S forming a major source for the Amazon River. North of

3°S, within the range of the Intertropical Convergence Zone (ITCZ) both sides receive heavy rainfall (Montgomery et al., 2001). A review of quantitative paleoelevation estimates (Gregory-Wodzicki, 2000) suggests that the Eastern Cordillera of the central Andes attained no more than half of the modern elevation by ~10 Ma and implies uplift on the order of 2000 – 3500 m since the late Miocene. Major uplift of the Colombian Andes has been assessed to occur at a later stage, reaching ~40 % of its modern elevation by ~4 Ma and a modern height by ~2.7 Ma. This timing corresponds roughly to changes in the erosion history of the Andes as detected in Atlantic sediment sequences from ODP Leg 154 (Ceara Rise). Increasing Amazon River supply and changes in clay mineralogy indicate major uplift phases from 9 – 8 Ma (Dobson et al., 1997) and since 4.6 Ma (Curry et al., 1995) as well as a substantial regional climate change (Tiedemann and Franz, 1997; Harris and Mix, 2002). Thus, the late Miocene and early Pliocene may represent the most dynamic episode of uplift in the northeastern Andes. According to Hoorn et al. (1995), the late Miocene paleogeographic evolution of northern South America redirected the outflow of the Orinoco River from the Caribbean into the Atlantic. This should have resulted in a net increase in Caribbean SSS, although enhanced drainage into the Atlantic and subsequent freshening of the Guyana Current may have partly compensated the Caribbean SSS increase. The influence of the Magdalena River discharge on late Neogene Caribbean water mass signatures is unknown. We surmise that an enhanced Pacific inflow of low salinity waters would overprint the fluvial signatures and the freshwater plume would be diverted eastwards. At this point, we cannot exclude a fluvial freshening at Site 999. If at all, the influence of the Magdalena River may have become more important during the final closure of the Isthmus.

5.7.3 Atlantic-Caribbean surface water exchange

In general, the progressive reduction in Pacific inflow should have amplified the Guyana Current and the Atlantic inflow of surface water masses into the Caribbean as the Gulf Stream and North Atlantic Deep Water formation intensified as suggested by General Circulation Models (Mikolajewicz and Crowley, 1997). A strengthening of meridional overturning in the North Atlantic is assumed to favor the flow of equatorial Atlantic water masses through the southernmost passages of the Lesser Antilles rather than forcing the advection of water masses from the North Atlantic subtropical gyre (Johns et al., 2002; see chapter 5.2).

To track early Pliocene changes in the $\delta^{18}O$ signature of upper ocean water masses that entered the Caribbean *via* the Guyana Current and left the Caribbean through the Florida Straits, we compared planktonic $\delta^{18}O$ records (*G. sacculifer*) from Site 925 (Ceara Rise) (Billups et al., 1998) and Site 1006 (Bahama Bank) with those from the Caribbean (**Fig. 5-8**). Today, Caribbean surface water masses originate from the equatorial Atlantic (Caribbean Water, CW, 0 – 80 m) and from the north Atlantic subtropical gyre (Subtropical Under Water, SUW, 80 – 180 m). The salinity of SUW is ~ one salinity unit higher than the salinity of CW (**Fig. 5-9**). The comparison between Sites 925 and 1000 monitors the influence of equatorial west Atlantic upper layer waters at the position of Caribbean Site 1000. At Site 1006, upper ocean water masses consist of two main components: the Caribbean outflow *via* the Florida Current and the western boundary flow of the subtropical

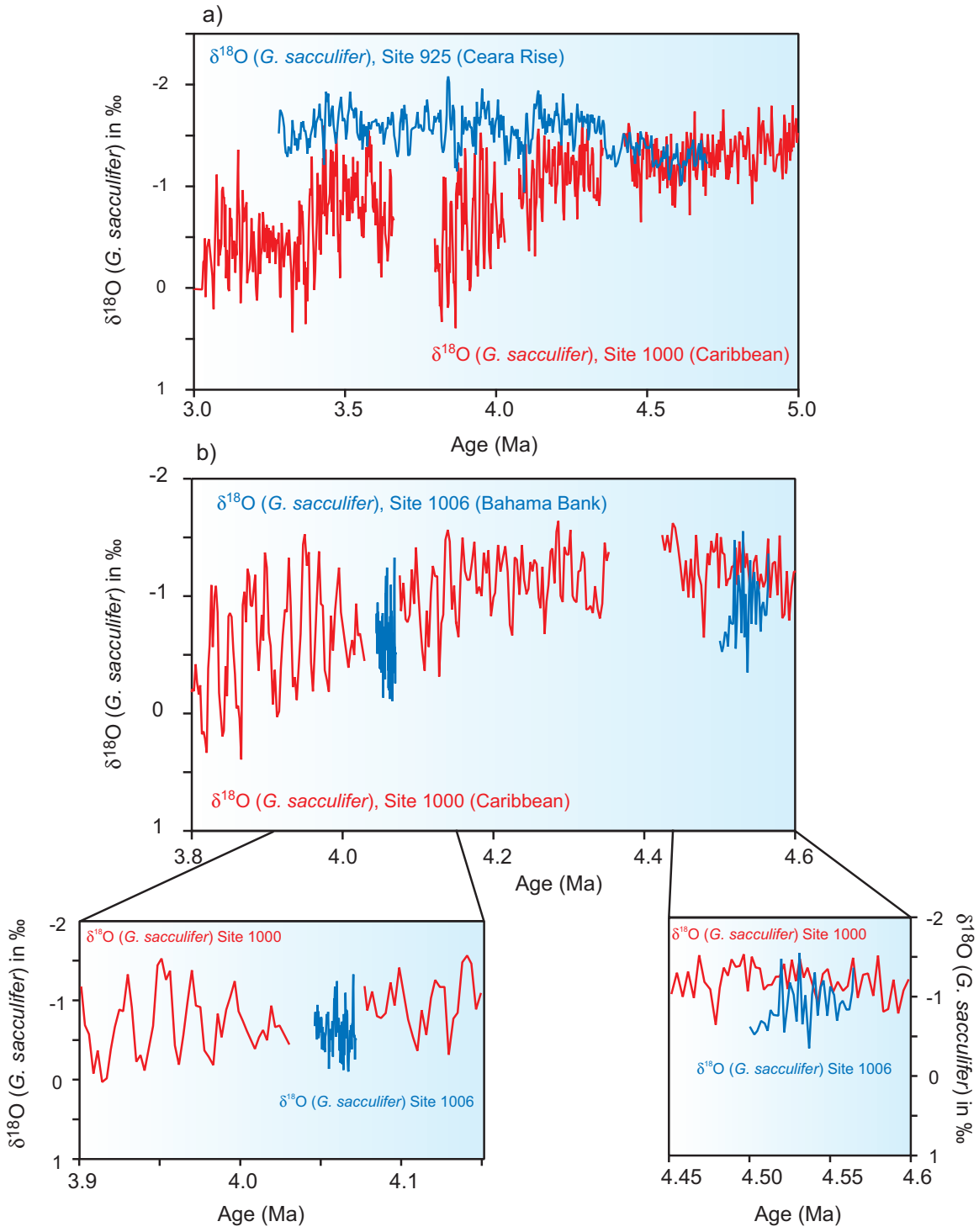

Fig. 5-8 Comparison between planktonic $\delta^{18}O$ records from Caribbean Site 1000 and Atlantic Sites 925 and 1006. (**a**) $\delta^{18}O$ records (*G. sacculifer*) from Sites 1000 (red line) and 925 (equatorial west Atlantic, Ceara Rise, blue line) (Billups et al., 1998 and 1999). At about 4.4 Ma, $\delta^{18}O$ values at Site 925 show a step like decrease at the same time when Caribbean $\delta^{18}O$ increased. (**b**) $\delta^{18}O$ record (*G. sacculifer*) from Site 1000 compared to $\delta^{18}O$ (*G. sacculifer*) for two short intervals (from 4 – 4.1 Ma and 4.5 – 4.6 Ma) from Site 1006 (western Great Bahama Bank, Caribbean outflow region) (Reuning et al., submitted). $\delta^{18}O$ values were generally higher at Site 1006 in the older interval, whereas $\delta^{18}O$ at Sites 1000 and 1006 shows similar values and amplitudes in the younger part.

gyre, which contributes approximately 10 % to the Florida Current (Leaman et al., 1995). Hence, Site 1006 should monitor general changes in Pliocene Caribbean salinities.

The comparison of Sites 925 and 1000 indicates that equatorial northwest Atlantic planktonic $\delta^{18}O$ values were similar to the Caribbean values prior to 4.4 Ma (**Fig. 5-8**). After 4.4 Ma the Caribbean trend towards higher $\delta^{18}O$ values is not reflected at Site 925. In contrast, $\delta^{18}O$ values decreased at 4.4 Ma and remained at a significantly lower level until 3.2 Ma. During times of extreme Caribbean salinity maxima (e.g. 3.8 – 4 Ma), the $\delta^{18}O$ values at Site 1000 were about 1.5 ‰ higher than at Site 925. Even though allowing for higher temperatures at Site 925, the large difference clearly suggests lower salinities in the equatorial northwest Atlantic. This excludes the transfer of water masses *via* the Guyana Current as a major Caribbean salinity source. We attribute the maxima in Caribbean SSS to an enhanced inflow of Atlantic surface waters originating from the subtropical gyre. This contradicts with model results from Johns et al. (2002) (see chapter 5.2) and suggests mechanisms other than enhanced thermohaline overturn to have controlled the source of Atlantic inflow during the early Pliocene.

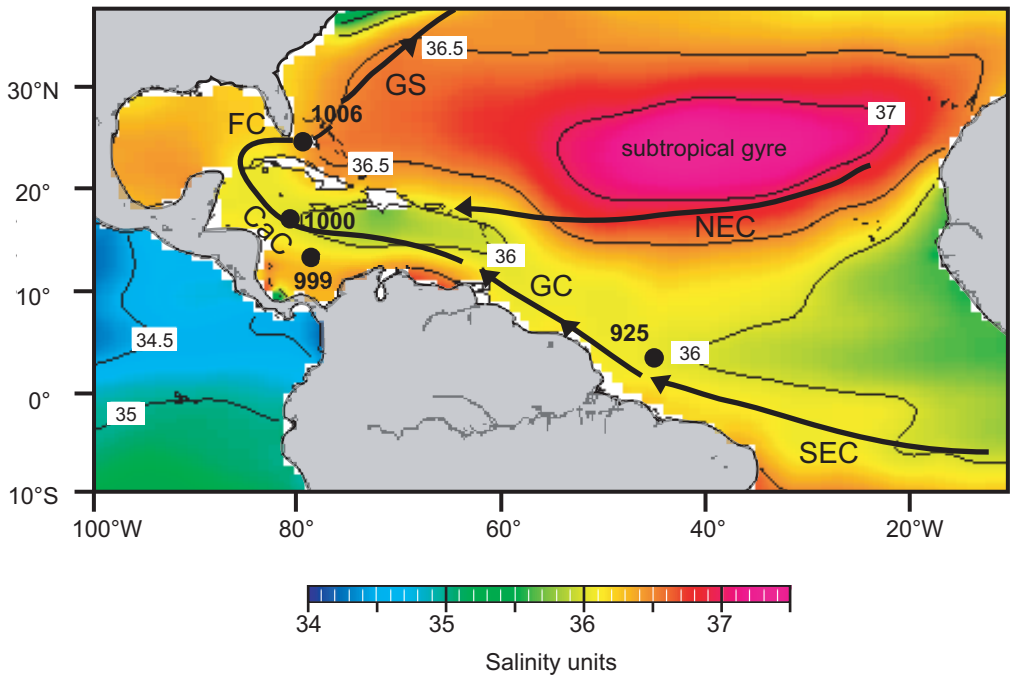

Fig. 5-9 Annual sea surface salinity (50 m water depth) in salinity units (Levitus and Boyer, 1994b) (colors and small numbers) and major surface currents in the tropical Atlantic/Caribbean. CaC: Caribbean Current; FC: Florida Current; GC: Guyana Current; GS: Gulf Stream; NEC: North Equatorial Current; SEC: South Equatorial Current. Black circles indicate locations of ODP Sites 925, 999, 1000 and 1006.

The planktonic $\delta^{18}O$ differences between Sites 1000 and 1006 are expected to monitor modifications in surface water signatures on their pathway through the Caribbean basins. For a comparison with Site 1000, we established planktonic $\delta^{18}O$ records with a time resolution better than 1 kyr for two short time intervals from ~4.5 – 4.6 Ma and ~4.0 – 4.1 Ma (Reuning et al.,

submitted). These two intervals cover the full range of orbital-scale $\delta^{18}O$ amplitude fluctuations prior to, and after the critical threshold in the closure history of the Central American Seaway. The comparison between Sites 1000 and 1006 (**Fig. 5-8**) is probably biased by minor stratigraphic uncertainties, as age control at Site 1006 is solely based on biostratigraphy (Kroon et al., 2000; Reuning et al., submitted). $\delta^{18}O$ values at Site 1006 are, on average, about 0.4 ‰ higher than at Site 1000 prior to the restriction of Pacific surface water inflow into the Caribbean (4.5 – 4.6 Ma). If temperatures were similar at both sites, as today, then SSS at the exit of the Caribbean would have been about 0.8 salinity units higher. Such an increase may have resulted from both, salinity enrichment of Caribbean surface waters caused by evaporation during their journey from Site 1000 to Site 1006, or the admixture of higher salinity waters from the subtropical Atlantic gyre.

The interval from ~4.0 – 4.1 Ma, unfortunately, includes a data gap at Site 1000 (see chapter 5.5). Nevertheless, both $\delta^{18}O$ records show similar values and the amplitudes at Site 1006 correspond to those observed at Site 1000 between 4.2 Ma and 4 Ma. Another important feature at Site 1006 is the strong response of the planktonic $\delta^{18}O$ record to orbital precession and the positive correlation to planktonic Mg/Ca-ratios (Reuning et al., submitted) as observed at Site 1000. From this we conclude that the observed changes in salinity at Site 1000 are transported *via* the Florida Current into the Atlantic, influencing the transfer of salt into the north Atlantic source regions of deep water formation, and thereby affecting the convection and strength of the thermohaline overturn probably also on precessional periods. The presence of a semi-precessional component in $\delta^{18}O$ (*G. sacculifer*) at Site 1006, which was not recorded at Site 1000, is interpreted as an overprint from low salinity waters originating in the Gulf of Mexico (Reuning et al., submitted).

5.7.4 What is the link between tropical wind field and Caribbean hydrography?

Early Pliocene changes in the tropical wind field and associated patterns of ocean surface currents are considered as the most important parameters to explain the observed inner-Caribbean variations in upper water mass signatures. The migration of the ITCZ and the associated precipitation pattern strongly influence SSS in the tropics. Thus, a general shift of the tropical rain belt should leave an imprint on SSS. In comparison to its modern average position at ~6°N (**Fig. 5-1**), the ITCZ is expected to be located farther north during the late Miocene to early Pliocene (~10°N) (Flohn, 1981), as the lack of a northern hemisphere ice cap strengthened the thermal asymmetry between both hemispheres. A weaker northern hemisphere pole-equator temperature gradient would pull the ITCZ northward. This is consistent with the fact that early Pliocene to mid-Pliocene climate was warmer than today and less variable than during the late Pliocene and Pleistocene due to the absence of large fluctuations in global ice volume (Crowley, 1991; Tiedemann et al., 1994; Mix et al., 1995). Microfaunal evidence from mid-Pliocene sediment records suggests warmer SST of 3 – 7 °C in middle to high latitudes and no significant difference in the tropics with respect to the present (e.g. Dowsett et al., 1996). Moreover, the intensification of the Gulf Stream enhanced North Atlantic heat piracy *via* strengthened cross-equatorial heat transport and intensified thermohaline overturn after ~4.6 Ma (Maier-Reimer et al., 1990; Crowley, 1992; Mikolajewicz and Crowley, 1997; Haug and Tiedemann, 1998). Southern Ocean SST reconstructions from silicoflagelates (Whitehead and Bohaty, 2003) indicate a temperature

decrease after ~4.2 Ma supporting the hypothesis of enhanced northern hemisphere heat piracy. At a first glance, the latter process would argue for a northward migration of the ITCZ as long as the heat flux to the north would exceed the thermohaline driven upwelling of relatively warm North Atlantic Deep Water in the Southern Ocean. Dust flux records off northwest Africa imply that the latitudinal summer position of the ITCZ has remained essentially in place over the course of the Pliocene (Tiedemann et al., 1989). As the position of the ITCZ strongly depends on atmospheric pressure gradients created by thermal differences, the relative stable position in the eastern Atlantic may result from continental influence, because northwest Africa attains a surface temperature always much higher than the adjacent ocean that stabilizes the minimum in surface pressure (Philander et al., 1996).

In contrast, strong support for an early Pliocene southward shift of the ITCZ comes from studies on Atlantic and Pacific changes in tropical wind field and surface hydrography (Hovan, 1995; Cannariato and Ravelo, 1997; Chaisson and Ravelo, 1997; Billups et al., 1999). Farrell et al. (1995) noted a dramatic decrease in carbonate and opal accumulation and a distinct southward shift in the locus of maximum opal accumulation rates in the eastern tropical Pacific at ~4.4 Ma. These changes were accompanied by a decrease in the thermocline depth of the eastern tropical Pacific (Cannariato and Ravelo, 1997). The observed shift in the geographical patterns of biogenic sediment accumulation and the shoaling of the thermocline are indicative of changes in the tropical wind field. This is consistent with a weakening of the southeast trade winds between 5 Ma and 4 Ma and a southward shift of the ITCZ in the east Pacific as deduced from eolian grain size and flux studies (Hovan, 1995). These changes document the reorganization of tropical Pacific circulation most probably in response to the restriction of the Panama seaway, because these shifts occurred as the Atlantic-Pacific salinity gradient established. In the tropical Atlantic, major changes in surface hydrography at 4.4 – 4.0 Ma (Chaisson and Ravelo, 1997; Norris, 1998) were also linked to a southward movement of the ITCZ (Billups et al., 1999).

In the Caribbean, the proposed southward shift of the ITCZ is elusive, because changes in the volume transport through the gateway may have fully overprinted Caribbean sea surface signatures that probably resulted from a southward shift of the tropical rain belt. However, a southward shift of the ITCZ is not in conflict with the general pattern of latitudinal salinity changes in the Caribbean. Prior to 4.4 Ma, planktonic $\delta^{18}O$ values were higher at Site 1006 than at Site 1000 (**Fig. 5-8**). This $\delta^{18}O$ gradient is interpreted to reflect a southward decrease in Caribbean SSS and would be consistent with a paleo-position of the ITCZ close to Site 1000. After 4.4 Ma, when high and similar $\delta^{18}O$ values characterized the northern Sites 1006 and 1000, the inner-Caribbean salinity gradient shifted southward between Sites 1000 (~16°N) and 999 (~12°N) (**Figs. 5-1, 5-5, 5-8**). SSS decreased from Site 1000 to Site 999 during northern hemisphere summer insolation maxima. This pattern would be in agreement with a position of the ITCZ always south of Site 1000 and is consistent with a sea surface freshening in the northwestern tropical Atlantic (~4°N) at 4.4 Ma as indicated by a step like 0.2 ‰ decrease in planktonic $\delta^{18}O$ at Site 925 (Billups et al., 1999) (**Fig. 5-8**).

On shorter timescales, the presence of dominant 23-kyr cycles in Caribbean SST and SSS suggests low latitude climate forcing to have played a crucial role in modulating surface hydrography after 4.4 Ma. Several studies suggest that the latitudinal position of the ITCZ is sensitive to changes in the seasonality of insolation associated with the precession band of Milankovitch forcing (Haug et al., 2001b). If northern hemisphere insolation becomes more seasonal, the heat capacity of the northern summer insolation is at a maximum and pulls both, the ITCZ and the high precipitation belt to the north. Hence, we infer that maxima in northern hemisphere summer insolation are associated with maxima in Caribbean SST and with minima in SSS along the rain belt of the ITCZ. Assuming the most likely scenario with the ITCZ to appear always south of Site 1000 (~16°N) raises fundamental problems to explain the observed variability in Caribbean SST and SSS. In this case, high SST should correlate with low SSS when the ITCZ approaches the position of Site 1000. However, observed maxima in SST correspond to maxima in SSS. If the ITCZ would have crossed Site 1000 twice during a full precession cycle, variations in SSS should respond to half-precession cycles, which are not observed. The extreme case, assuming a summer position of the ITCZ always north of Site 1000 could provide the observed correlation between high temperatures and high salinities but is in conflict with the data from Site 1006 (**Fig. 5-8**). At both sites, oxygen isotope values and amplitudes are similar and Mg/Ca ratios are positively correlated to the $\delta^{18}O$ records. This pattern excludes a latitudinal position of the ITCZ between Sites 1000 and 1006. Thus, latitudinal fluctuations in the tropical rain belt cannot explain the observed coupling between Caribbean SSS and SST. Moreover, we would not expect that spatial changes in the ratio of precipitation/evaporation induce planktonic $\delta^{18}O$ amplitudes of up to 1.3 ‰ at Sites 1000 and 1006, considering the habitat depth of *G. sacculifer*. Hence, the observed Caribbean pattern of SSS and SST suggests another forcing mechanism most probably associated with wind-driven changes in the volume transport through the gateway.

With the reorganization of Atlantic and Pacific surface water circulation after ~4.4 Ma precession-driven variations in the tropical wind field may have exerted a stronger influence on Caribbean surface hydrography by modifying the Pacific-Caribbean and Atlantic-Caribbean surface water exchange. The development of pronounced 23-kyr cycles in Caribbean SST and SSS paralleled the development of the Atlantic-Pacific salinity contrast. This indicates that the reduction in the volume transport of Pacific surface waters through the gateway made the Caribbean more sensitive for precession-driven changes in surface hydrography. Thus, we infer that variations in the tropical wind field along with changes in east Pacific surface hydrography triggered variations in the volume transport through the gateway on precessional periodicities. Reductions in the volume transport through the gateway during northern hemisphere summer insolation maxima would strengthen the influence of Atlantic surface waters from the subtropical gyre resulting in Caribbean SST and SSS maxima (Sites 1000, 1006). In turn, enhanced throughflow during northern hemisphere summer insolation minima would strengthen the influence of relatively cool, low salinity Pacific surface waters in the Caribbean leading to minima in SSS and SST. Considering a modern atmospherical configuration with an open isthmus, relatively cool water masses of the Pacific North Equatorial Counter Current (NECC) would enter the Caribbean. The modern difference in temperatures between the NECC in the eastern Pacific and the Caribbean is ~5 °C at

50 m water depth. Whether variations in the Pacific surface current system (**Fig. 5-1**) favored the inflow of less saline and cooler Pacific surface water masses *via* the NECC, the Columbia Current, or the California Current as suggested by Duque-Caro (1990) remains unsolved. Hence, early Pliocene temperature and salinity reconstructions from the tropical east Pacific are clearly needed to identify the major contributor and to further assess the mechanism controlling the volume transport through the gateway on precessional periodicities.

5.7.5 Links to El Niño-Southern Oscillation (ENSO) fluctuations

Today, the El Niño-Southern Oscillation is a major source of interannual climate variability with the most severe impact on the equatorial east Pacific ocean-atmosphere system. In a simple coupled ocean-atmosphere model Clement et al. (1999, 2000) suggested that precession-induced changes of the seasonal cycle influence the long-term behavior of ENSO, which in turn has the potential to modulate variations in ocean circulation and climate. These model results are consistent with paleoclimate records preserved in New Guinea corals that show a clear response of ENSO variability to seasonal insolation changes associated with orbital precession (Tudhope et al., 2001). Both studies demonstrated that the southeast trades weaken when aphelion falls in boreal summer or autumn (as today), favoring the development of warm El Niño events.

Modern El Niño events are associated with several changes in the equatorial eastern Pacific ocean-atmosphere system. The NECC strengthens, SST and precipitation increase, the thermocline deepens, and the ITCZ moves equatorward. Vice versa, when perihelion falls in boreal summer or autumn (as during the mid-Holocene), the southeast trade winds strengthen and inhibit the development of warm El Niño anomalies. Evidence for reduced mid-Holocene El Niño activity is provided by paleoclimatic studies of Ecuador Lake records (Rodbell et al., 1999), coral records from the West Pacific (Gagan et al., 1998) and pollen records from northern Australian lakes (McGlone et al., 1992).

Accordingly, changes in Pliocene ENSO activity may have amplified precessional variations in the Panamanian throughflow (discussed in chapter 5.7.4). Enhanced El Niño activity during minima in northern hemisphere summer insolation is expected to have increased the volume transport of Pacific surface waters into the Caribbean *via* a strengthened and more southerly NECC, whereas SSS of eastern equatorial Pacific surface waters was additionally lowered by enhanced precipitation.

Molnar and Cane (2002), Philander and Fedorov (2003) and others propose that the early to mid-Pliocene Pacific might have been characterized by a permanent El Niño-like state. Paleoceanographic evidence from Site 1239 off the coast of Ecuador suggests considerable variability in surface productivity on precessional cycles, indicative of changes in upwelling and wind strength (Mix et al., 2003). Thus, although tropical climate may have operated on a permanent El Niño-like mode, it does not exclude precession-induced changes in ENSO variability.

5.8 Conclusions

Pliocene planktonic stable isotope records from the Caribbean (Sites 999, 1000), the western Atlantic (Sites 925, 1006), and the Pacific (Site 851) have been used to reconstruct variations in Pacific-Caribbean and Atlantic-Caribbean surface water exchanges in response to the progressive closure of the Central American Seaway. Major changes occurred between 4.7 Ma and 4.2 Ma, when the reduction in volume transport through the gateway reached a critical threshold increasing Caribbean salinity and thus, affecting the ocean-atmosphere-climate system through increased thermohaline heat and salt transport to high northern latitudes. The main conclusions include the following:

1. The comparison of paired planktonic $\delta^{18}O$ and Mg/Ca data from Site 1000 suggests salinity fluctuations on precessional periodicities with amplitudes of about 2.6 salinity units (1.3 ‰ change in $\delta^{18}O$) after 4.4 Ma. These amplitudes represent minimum changes in salinity, as $\delta^{18}O$ and Mg/Ca data are positively correlated. Maxima in SSS and SST correspond to precessional maxima in northern hemisphere summer insolation. If the rain belt of the ITCZ did not directly influence the position of Site 1000, enhanced evaporation during SST maxima may have contributed to the increase in Caribbean SSS.

2. The differences in planktonic $\delta^{18}O$ between Sites 999 and 1000 identify a strong variability in Caribbean salinity gradients toward the north after 4.4 Ma. The more southern position of Site 999 is generally more affected by the admixture of low salinity Pacific surface waters. Expansions of the low salinity tongue influenced the more northern Site 1000 only during minima in northern hemisphere summer insolation, when $\delta^{18}O$ differences between Sites 999 and 1000 were smallest. Salinity differences (up to 1.5 ‰ in $\delta^{18}O$) are largest during insolation maxima. This is interpreted to reflect a stronger influence of relatively warm and saline Atlantic surface waters at Caribbean Site 1000 during times of reduced volume transport through the Panama seaway.

3. Atlantic-Caribbean differences in planktonic $\delta^{18}O$ (Sites 925, 1000) exclude the transfer of water masses from the Guyana Current through the southernmost Lesser Antilles Passages as a main source for the observed Caribbean salinity maxima. This suggests the North Atlantic subtropical gyre as the major player providing the Caribbean with high salinity water masses during maxima in northern hemisphere summer insolation.

4. Similar planktonic $\delta^{18}O$ values and amplitudes at Caribbean Site 1000 and Site 1006 (located within the Caribbean outflow region) reflect that the observed changes in Caribbean salinity are transported into the Atlantic *via* the Florida Current. This in turn should have influenced the transfer of salt into the north Atlantic source regions of deep water formation, thereby affecting the convection and strength of the thermohaline overturn probably also on precessional periods.

5. The weak response of Caribbean SSS and SST to changes in orbital obliquity in combination with a strong response to orbital precession suggests low latitude climate forcing to have played a crucial role in modulating the interbasin surface water exchange through ocean-

atmosphere interactions after 4.4 Ma. We surmise that changes in the volume transport through the gateway varied on precessional periodicities mainly driven by variations in the tropical wind field and related changes in east Pacific oceanography. Latitudinal shifts of the Caribbean rain belt (ITCZ) on precessional periods cannot explain the observed coupling between Caribbean SSS and SST after 4.4 Ma considering a paleo-summer position of the ITCZ slightly north of the modern one. In this case, high SST should correlate with low SSS, when the ITCZ approaches the position of Site 1000 during northern hemisphere summer insolation maxima, which is opposite to our observations.

Acknowledgements

We thank H. Kinkel, D. Crudeli, and M. Schulz for discussions and criticism, and L. Haxhiaj, U. Nielsen and A. Jesußek for technical assistance. We also thank the reviewers for valuable comments to the manuscript. This research used samples and data provided by the Ocean Drilling Program, which is sponsored by the U.S. National Science Foundation and participating countries under management of Joint Oceanographic Institutions. Funding for this research was provided by the Deutsche Forschungsgemeinschaft (projects Ti 240/7 and Ti 240/12, the latter being part of the DFG-Research Unit, FOR 451: Impact of Gateways on Ocean Circulation, Climate, and Evolution at Kiel University).

CHAPTER 6

PLIOCENE CHANGES IN TROPICAL EAST PACIFIC UPPER OCEAN STRATIFICATION: RESPONSE TO TROPICAL GATEWAYS?

Silke Steph[1], Ralf Tiedemann[1], Jeroen Groeneveld[1], Arne Sturm[1], and Dirk Nürnberg[1]

[1]IFM-GEOMAR, Leibniz-Institut für Meereswissenschaften, Wischhofstr. 1-3, 24148 Kiel, Germany

submitted to ODP Scientific Results, *Volume 202*

Abstract

A combination of high-resolution stable isotope records and Mg/Ca temperature estimates of four different planktonic foraminiferal species from ODP Site 1241 allows for the first time to differentiate between temperature and salinity changes in the tropical east Pacific upper water column during the Pliocene (5.5 – 2.5 Ma). An increase of the $\delta^{18}O$ gradient in the upper water column between 5.4 Ma and 3.3 Ma that is reflected by all deep-dwelling foraminifers was accompanied by a 6 °C temperature decrease at the bottom of the photic zone between 5.4 Ma and 4.0 Ma. This is interpreted to reflect an early Pliocene shoaling of the tropical east Pacific thermocline that was possibly triggered by changes in the configuration of low-latitude ocean gateways. Temperatures at the surface and within the thermocline, however, remained comparatively stable. The deviation of $\delta^{18}O$ records and Mg/Ca temperature estimates from thermocline-dwelling planktonic foraminifers suggests that local changes in salinity exerted a much stronger control on Pliocene tropical east Pacific upper ocean water mass signatures than previously assumed.

6.1 Introduction

The early to middle Pliocene includes the most recent period when Earth's climate was significantly warmer than present, as indicated by ocean temperature estimates from marine microfauna and by palynological data (e.g. Dowsett et al., 1992, 1994, 1996). This warm period was terminated by an irreversible global cooling trend after 3.2 Ma that was associated with the intensification of the Northern Hemisphere Glaciation (NHG).

Two recent hypotheses link the major onset of the NHG to modifications in ocean heat transport and thermohaline circulation that were attributed to the constriction of low-latitude ocean gateways. On one hand, it was suggested that the progressive closure of the Central American Seaway (CAS) has been the cause either for the onset (Berggren and Hollister, 1974) or for the delay (Berger and Wefer, 1996) or for setting preconditions for the NHG (Haug and Tiedemann, 1998; Driscoll and Haug, 1998). On the other hand, Cane and Molnar (2001) identified the narrowing of the Indonesian Gateway (IG), and associated changes in tropical Pacific oceanography as a mechanism that may have contributed to the Pliocene cooling. The ultimate causes for the late Pliocene-Pleistocene climate transition, however, are still under debate (e.g. Ravelo et al., 2004).

The closure history of the CAS (13 – 1.8 Ma) is intensely investigated and stratigraphically well constrained (e.g. Keigwin, 1982a,b; Webb, 1985; Lundelius, 1987; Duque-Caro, 1990; Coates et al., 1992; Collins et al., 1996; Haug and Tiedemann, 1998, Coates et al., 2004). The Pliocene time interval from 4.6 Ma to 4.2 Ma has been shown to represent a critical period in the closure history, when the restriction of Pacific-Atlantic surface water exchange resulted in profound changes in ocean circulation and chemistry. Closure-induced variations mainly affected the Atlantic Ocean as indicated by ocean model experiments (Maier-Reimer et al., 1990; Mikolajewicz and Crowley, 1997) and paleoceanographic studies (e.g., Keigwin, 1982a; Tiedemann and Franz, 1997; Haug and Tiedemann, 1998; Haug et al., 2001a; Steph et al.; submitted a, see chapter 5). The main changes include a strengthening of the Gulf Stream system, enhanced thermohaline overturn in the North Atlantic, as well as the development of the Caribbean Warm Pool, and an increase in Caribbean sea surface salinity. The closure-induced impact on tropical Pacific oceanography yet remains ambiguous, because of possible interactions resulting from the constriction of the IG.

The IG has narrowed gradually since 20 Ma due to the northward drift and collision of the Australia-New Guinea Block with Indonesian terranes (e.g. Hamilton, 1979). In contrast to the CAS, the Pliocene history of the IG is stratigraphically not well constrained and is not well enough characterized to relate oceanographic changes in the tropical Pacific and Indian Ocean directly to gateway-induced thresholds. By reevaluating plate tectonic models, Cane and Molnar (2001) proposed that the Pliocene narrowing of the passage after 5.0 – 3.0 Ma may have strengthened the West Pacific Warm Pool (WPWP) and enhanced the tropical trans-Pacific sea surface temperature gradient. These changes are corroborated by Ocean General Circulation Models that examined closure-related oceanographic changes in the Pacific and Indian Ocean (e.g. Hirst and Godfrey, 1993; Godfrey, 1996). The development of the trans-Pacific temperature gradient is expected to have modified the thermal structure of the tropical Pacific from an El Niño-like state into more

modern like conditions of a La Niña-like state. This would include the shoaling of the east Pacific thermocline. Indeed, tropical records indicate that significant tropical climate reorganization occurred twice, once between 4.5 Ma and 4.0 Ma, well before significant NHG, and once between 2.0 Ma and 1.5 Ma, well after the onset of significant NHG (Ravelo et al., 2004). Evidence for early Pliocene reorganizations in east Pacific surface water and atmospheric circulation towards more modern conditions comes from Farrell et al. (1995) and Hovan (1995). According to Farrell et al. (1995), carbonate and opal accumulation significantly decreased in the tropical east Pacific and the maximum of opal accumulation shifted more towards the east at about 4.4 Ma. Based on eolian grain size and flux studies, Hovan (1995) postulated a southward shift of the Intertropical Convergence Zone (ITCZ) between 5.0 Ma and 4.0 Ma, which would be consistent with observed changes in thermocline depth. Faunal assemblages and planktonic $\delta^{18}O$ records from tropical Pacific ODP Sites 806 and 847 suggest that the development of the modern trans-Pacific thermocline slope crossed a critical threshold between 5.0 Ma and 4.0 Ma (Chaisson and Ravelo, 2000). This change is characterized by a shoaling of the thermocline in the eastern tropical Pacific that was also recorded in multispecies planktonic stable isotope records from tropical east Pacific Site 851 as documented by Cannariato and Ravelo (1997). Their comparison of planktonic $\delta^{18}O$ records from the tropical east and west Pacific suggested that sea surface temperatures (SST) in the WPWP were cooler than in the tropical east Pacific before ~4.0 Ma. The development of the more modern-like trans-equatorial SST gradient with higher temperatures in the WPWP and lower temperatures in the east Pacific, however, was not observed to start before 2.0 – 1.5 Ma (Cannariato and Ravelo, 1997; Ravelo et al., 2004). Other studies of Wang (1994) and Andersson (1997) examined the Pliocene evolution of SSTs in the WPWP by applying planktonic foraminiferal transfer functions. Their results suggest that early Pliocene SSTs in the WPWP were similar or only slightly cooler than modern ones. If tropical east Pacific mixed layer temperatures were significantly cooler during the early Pliocene, this would imply an early development of the trans-equatorial temperature gradient.

This study sheds new light onto the thermal structure of the tropical east Pacific, as our strategy considers combined information from planktonic stable isotopes and Mg/Ca temperature reconstructions. This allows for the first time to differentiate between temperature and salinity changes in the upper water column. Therefore, we established stable isotope and Mg/Ca records of shallow- and deep-dwelling planktonic foraminifers from Site 1241, spanning the time interval from 5.5 – 2.5 Ma. In addition, the position of Site 1241 close to Panama, and the comparison with planktonic $\delta^{18}O$ records from tropical east Pacific Site 851 (Cannariato and Ravelo, 1997) allowed to further assess the regional variability in Pliocene tropical east Pacific upper ocean water mass signatures.

6.2 Tropical east Pacific oceanography

Today, the tropical east Pacific shows a steep thermocline with a temperature gradient of up to 15 °C in the upper 100 m of the water column (Fairbanks et al., 1982). Modern variations in surface currents and winds are closely coupled to the latitudinal position of the ITCZ (e.g. Donguy and Meyers, 1996; Johnson et al., 2001) (**Fig. 6-1**).

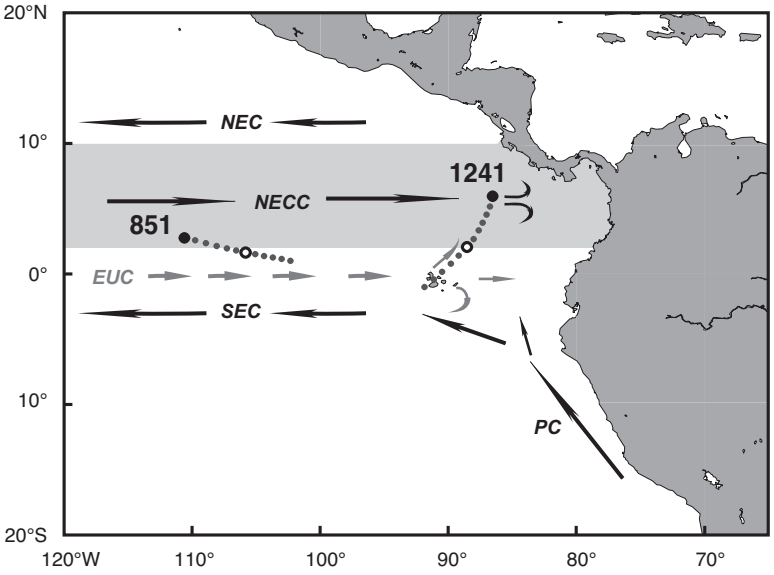

Fig. 6-1 Map of the tropical east Pacific showing major surface currents. The locations of ODP Sites 851 and 1241 and their plate tectonic backtracks (in 1 M.y. steps, Mix et al., 2003) are indicated. Large black dots: modern position, white dots: paleoposition of these Sites at 6 Ma ago. NEC = North Equatorial Current, NECC = North Equatorial Counter Current, EUC = Equatorial Under Current, SEC = South Equatorial Current, PC = Chile Current.

The North Equatorial Current (NEC, north of 10°N) and the South Equatorial Current (SEC, south of 3°N) transport surface waters westward, driven by the northeast and southeast trade winds, respectively. Between 10°N and 3°N, within the ITCZ region, the North Equatorial Counter Current (NECC) carries the return flow of warm, low saline surface waters (S < 34.5) eastward out of the WPWP region (Wyrtki, 1981; Delcroix et al., 1987; Donguy and Meyers, 1996). The east equatorial tongue of the SEC consists of relatively cool and salt-rich South Pacific water masses that are transported equatorwards *via* the Peru-Chile Current (PC) (Wyrtki, 1966; Strub et al., 1998). Cool surface water temperatures within the cold tongue are maintained by equatorial upwelling. The maximum difference in SST between the cold tongue of the SEC and the warm tongue of the NECC is up to 6 °C (Levitus and Boyer, 1994a). Between 2°N and 2°S, the Equatorial Under Current (EUC) flows eastward along the equator in 30 - 300 m depth beneath the SEC (Wyrtki, 1966; Philander, 1973; McPhaden, 1986). The EUC is a geostrophic current driven by the Coriolis force, and by west-east pressure gradients. It rises with the thermocline as it flows across the Pacific, bringing relatively cool, high-saline and nutrient-enriched water to the surface layer west of Galapagos Islands and extending into the Panama Bight (Wyrtki, 1981; Bryden and Brady, 1985). Therefore, equatorial upwelling in the tropical east Pacific partially consists of cool, nutrient-enriched waters of the EUC (Stevenson and Taft, 1971; Pak and Zaneveld, 1973; Leetma, 1982). Near the Galapagos Islands, EUC water is deflected northward between 2°N and 4°N and 92°W to 95°W at 75 – 100 m depth (Lukas, 1986; Steger et al., 1998). The water column in this region thus exhibits a strong halocline and thermocline (Millero et al., 1998).

The thermocline depth and structure in the modern tropical east Pacific are mainly controlled by seasonal variations in the depth and strength of the EUC and the NECC. The NECC and the cold tongue of the SEC strengthen during northern hemisphere summer and autumn, when southeast trade winds are strong. Hence, enhanced eastward transport of warm surface water within the NECC depresses the thermocline in the tropical east Pacific (Donguy and Meyers, 1996). When the southeast trade winds are weak in northern hemisphere winter and spring, the transport within the NECC and the SEC is diminished. The tropical east Pacific thermocline is shallow during this time (Halpern and Weisberg, 1989).

6.3 Strategy

Past studies demonstrate that the isotopic offset between different species of planktonic foraminifers reflects the temperature range within the photic zone in the tropics (e.g. Ravelo and Fairbanks, 1992; Ravelo and Shackleton, 1995; Cannariato and Ravelo, 1997; Ravelo and Andreasen, 1999; Chaisson and Ravelo, 2000; Faul et al., 2000). The temperature range and thus the isotopic differences in $\delta^{18}O$ between species are large, when the thermocline is shallow, and are small, when the thermocline is deep. Since oxygen isotope values are biased by both, temperature changes and variations in $\delta^{18}O_{seawater}$, we established low-resolution Mg/Ca records in order to assess the temperature signal. We also considered the benthic $\delta^{18}O$ record to distinguish local changes in $\delta^{18}O_{seawater}$ from global variations that result from changes in global ice volume. Furthermore, the $\delta^{13}C$ values of planktonic foraminifers were included for the evaluation of changes in upper water mass signatures. Changes in the $\delta^{13}C$ signal of planktonic foraminifers are primarily indicative of the variations in the nutrient distribution within the upper water column but are, however, not necessarily linked to changes in upper ocean stratification.

In addition to this approach, we also considered variations in the paleo-position of Site 1241, because the plate tectonic movement of the Cocos Plate significantly displaced Site 1241 northward from its original position at the Galapagos Hotspot during the last 12 Ma (Mix et al., 2003).

6.3.1 Selection of planktonic foraminifers

In order to assess vertical gradients in upper ocean water mass signatures, we measured the stable isotope composition and Mg/Ca ratios of four planktonic foraminiferal taxa with different habitat depths: *Globigerinoides sacculifer* (without sac-like final chamber), *Neogloboquadrina dutertrei*, *Globorotalia limbata* (dextral variety) and *Globorotalia tumida* (**Fig. 6-2**).

The distribution and abundance of planktonic foraminiferal species is strongly related to vertical variations in hydrograhic parameters such as temperature, food availability, chlorophyll concentration and light levels (e.g. Fairbanks et al., 1980; Fairbanks and Wiebe, 1980; Fairbanks et al., 1982; Curry et al., 1983; Ganssen and Sarnthein, 1983; Sautter and Thunell, 1991; Thunell and Sautter, 1992; Ortiz et al., 1995, 1996, 1997; Watkins and Mix, 1998). These factors result in

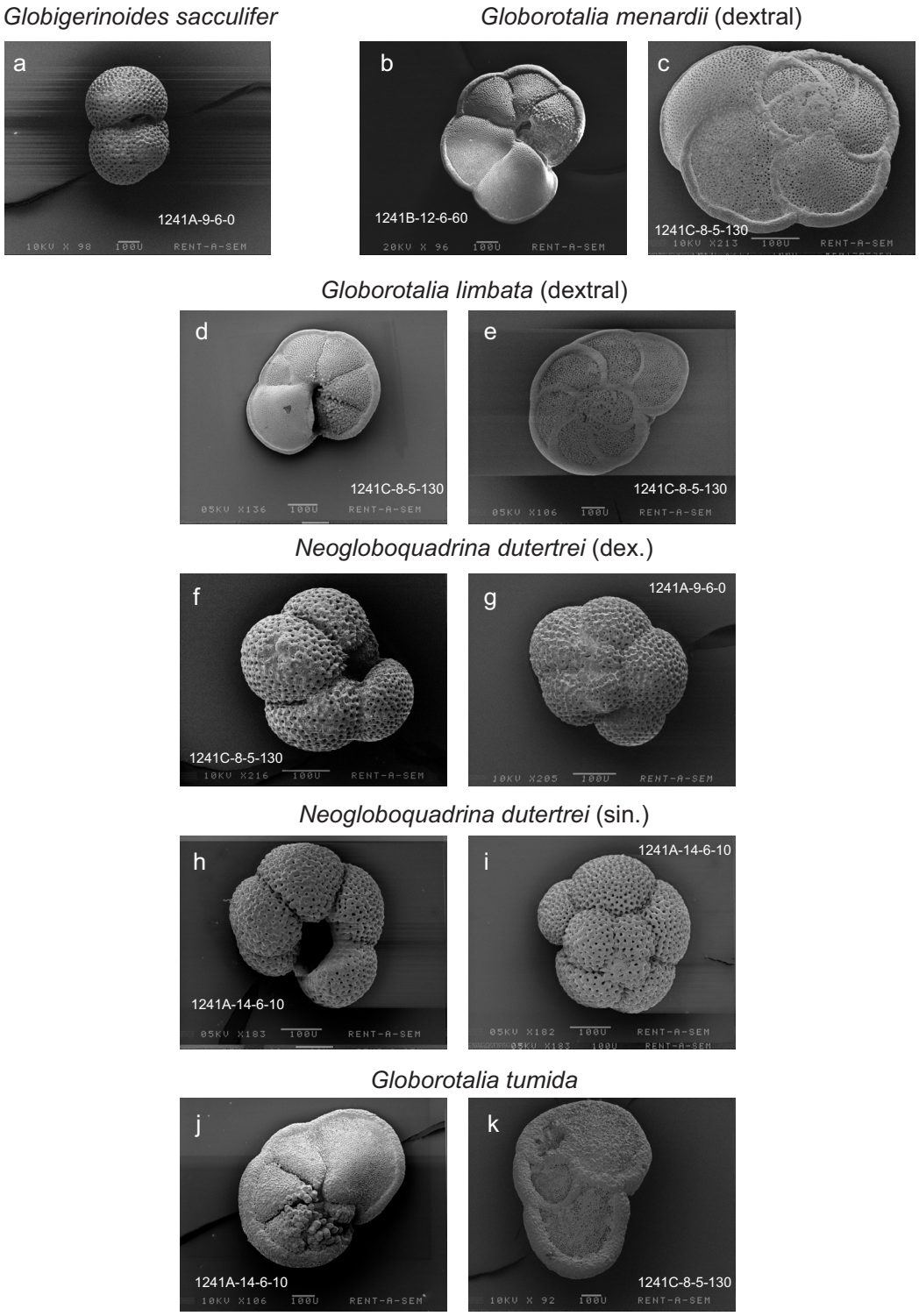

Fig. 6-2 SEM pictures of the planktonic foraminiferal taxa used in this study. **a**: *Globigerinoides sacculifer* (without sac-like final chamber), **b, c**: *Globorotalia menardii*, **d, e**: *Globorotalia limbata* (dextral), **f, g**: *Neogloboquadrina dutertrei* (dextral), **h, i**: *Neogloboquadrina dutertrei* (sinistral), **j, k**: *Globorotalia tumida*. The samples from which the specimens originate are indicated in each picture.

a predictable living-depth range of the different species that can be deciphered by the stable isotope composition of test calcite (Fairbanks and Wiebe, 1980; Ravelo et al., 1990; Ravelo and Fairbanks, 1992; Niebler et al., 1999; **Fig. 6-3**).

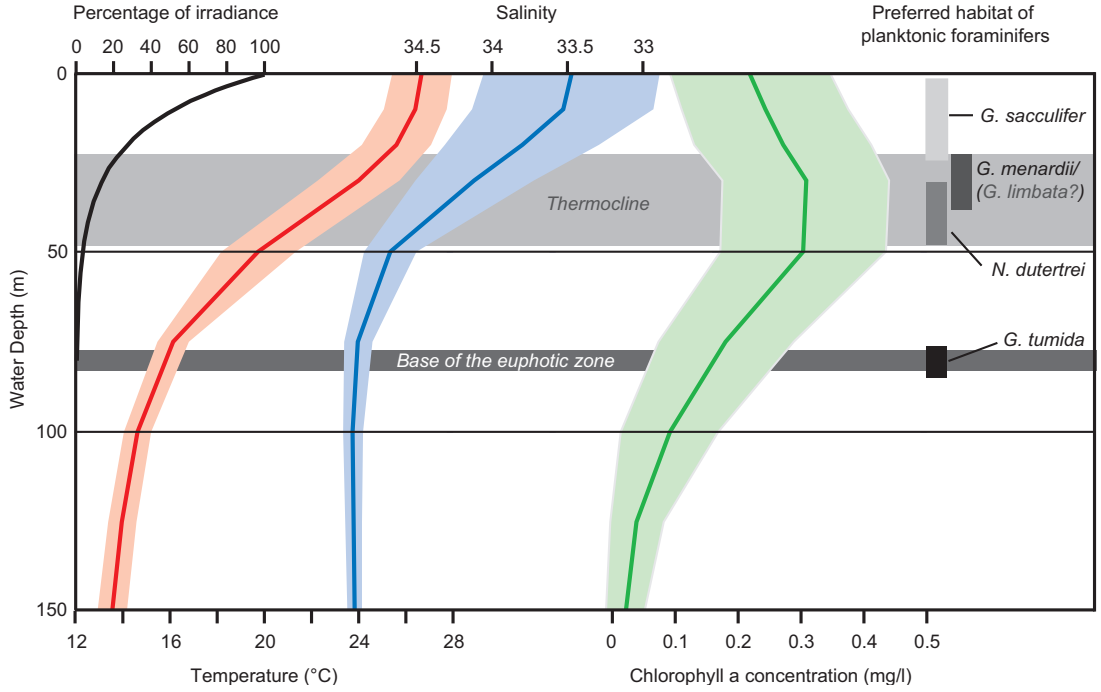

Fig. 6-3 Modern annual-average properties of the upper water column for the tropical east Pacific and assumed habitat depths for the species used in this study. Atlas data on physical and chemical properties are from the Ocean Climate Laboratory (2001), squares 7008 and 7009 (10°N, 100°W-0°N, 80°W). Data from the Caribbean were excluded. Thick lines indicate the mean values, and shaded areas show the range of standard deviation. Red: temperature, blue: salinity, green: chlorophyll a concentration. Black line: percentage of irradiance, data taken from Enfield and Lee (submitted); the 0.1 % irradiance level is defined as the base of the euphotic zone. The gray area indicates the thermocline as zone with the highest vertical temperature gradient. Bars to the right indicate the range of preferred habitat depths for *G. sacculifer*, *G. menardii* (equal to *G. limbata*?), *N. dutertrei*, and *G. tumida*.

G. sacculifer and *G. tumida* are foraminifers whose calcification depth is considered as being nearly constant within the tropics (e.g. Ravelo and Andreasen, 1999, and references therein). The spinose, symbiont-bearing *G. sacculifer* has been found living and calcifying within the warm, nutrient depleted surface mixed layer and upper thermocline (Fairbanks et al., 1982; Curry et al., 1983). Hence, it mainly records the isotopic composition of near surface water. However, the adult tests of *G. sacculifer* include a substantial proportion of gametogenetic calcite that is added slightly deeper in the thermocline and may alter $\delta^{18}O$ values (e.g. Duplessy et al., 1981; Lohmann, 1995). The isotopic composition of *G. tumida* reflects the hydrographic conditions at the bottom of the photic zone (Ravelo and Fairbanks, 1992; Ravelo and Shackleton, 1995). This is a nearly constant depth level in tropical waters. The $\delta^{18}O$ values and Mg/Ca ratios of *G. tumida* are thus primarily considered to register any change of the thermocline depth since the temperature at the bottom of the photic zone is in part regulated by the depth of the thermocline. Other deep-dwelling species

are found at different depths within the thermocline, associated with the maximum in chlorophyll concentration and primary productivity (e.g. Curry et al., 1983; Sautter and Thunell, 1991; Ravelo and Fairbanks, 1992; Ravelo and Andreasen, 1999). Thus, their isotopic composition reflects the temperature and chemical composition at the depth of the thermocline as temperature transition layer in a whole. Since the thermocline depth varies through time, the absolute calcification depth of those species cannot be determined from their isotopic composition alone (e.g., Curry et al., 1983; Sautter and Thunell, 1991; Ravelo and Fairbanks, 1992; Ravelo and Andreasen, 1999). When hydrographic conditions change, thermocline-dwelling species may migrate to shallower or deeper levels (e.g. Ravelo and Fairbanks, 1992; Faul et al., 2000). As these species calcify within a steep thermal gradient, only slight changes in the living depth may have a significant influence on the isotopic composition of their tests. We therefore compared stable isotope records of *G. limbata* (dextral) and *N. dutertrei*, two non-spinose, thermocline-dwelling species with presumably overlapping habitat depths, to assess indications of their vertical migration.

Neogloboquadrina dutertrei, the modern representative of the Neogloboquadrinid lineage (*N. acostaensis, N. humerosa,* and *N. dutertrei*) (e.g., Parker, 1967; Blow, 1969; Srinivasan and Kennett, 1976) was selected for the time interval from 5.25 Ma to 2.4 Ma. *N. dutertrei* has the tendency to calcify within a narrow temperature range in the tropics (Curry et al., 1983; Ravelo and Fairbanks, 1992; Billups and Spero, 1996; Faul et al., 2000). It inhabits the middle to deep thermocline today, and it is supposed to be closely coupled to the chlorophyll maximum (Fairbanks et al., 1982; Watkins et al., 1998; Spero et al., 2003). **Figures 6-2f** and **6-2g** show the morphotype we commonly used for isotopic and Mg/Ca measurements.

G. limbata, a late Miocene to late Pliocene *Globorotalia* (*Menardella*) species (e.g. Banner and Blow, 1960; Kennett and Srinivasan, 1983), was chosen to resemble the middle Miocene to modern *Globoratalia menardii*, because *G. menardii* did not occur in sufficient numbers in the early to middle Pliocene section of Site 1241 (Mix et al., 2003). In the eastern equatorial Pacific, *G. menardii* today lives within the upper to middle thermocline (Spero et al., 2003). The isotopic offset between *G. limbata* (dextral) and *G. menardii* (dextral) appears to be small but systematic during the Pliocene, with approximately 0.17 ‰ higher $\delta^{13}C$ values and 0.14 ‰ higher $\delta^{18}O$ values in *G. limbata* (**Tab. 6-1**). This is less than a half of short-term variations in down core records. Though the exact ecological preference of *G. limbata* remains elusive for the Pliocene, their test morphology is similar. Therefore, we suggest that *G. limbata*, like the modern *G. menardii*, reflects thermocline conditions.

Together, the stable isotopic composition of the four species used in this study is supposed to reflect the physical and chemical structure of the entire photic zone in the eastern equatorial Pacific (**Fig. 6-3**). The $\delta^{18}O$ difference between *G. tumida* and either *N. dutertrei* or *G. sacculifer* has been suggested to be a measure of the relative depth of the thermocline (Ravelo and Fairbanks, 1992; Ravelo and Shackleton, 1995; Cannariato and Ravelo, 1997; Chaisson and Ravelo, 2000). For instance, when the thermoline is shallow, large temperature gradients within the photic zone create higher $\delta^{18}O$ and Mg/Ca temperature differences between shallow- and deep-dwelling planktonic foraminifers.

Tab. 6-1 Isotope values of *G. limbata* (dextral) and *G. menardii* (dextral) from four selected samples, and offsets between the species: **a**) for $\delta^{18}O$ **b**) for $\delta^{13}C$.

a

Sample Nr.	Age	$\delta^{18}O$ *G. limbata* (dex)	$\delta^{18}O$ *G. menardii* (dex)	$\delta^{18}O$ difference
1241C-3-4-0	2443	-0.422	-0.599	+0.177
1241C-5-6-60	3264	-0.147	-0.212	+0.065
1241A-11-5-30	4011	-1.065	-1.274	+0.209
1241C-8-3-100	4110	-0.545	-0.658	+0.113
				+0.141

b

Sample Nr.	Age	$\delta^{13}C$ *G. limbata* (dex)	$\delta^{13}C$ *G. menardii* (dex)	$\delta^{13}C$ difference
1241C-3-4-0	2443	1.775	1.507	+0.268
1241C-5-6-60	3264	1.266	1.106	+0.160
1241A-11-5-30	4011	1.763	1.595	+0.168
1241C-8-3-100	4110	1.367	1.269	+0.098
				+0.174

6.3.2 Plate tectonic backtrack of the Cocos Plate

Today, ODP Site 1241 is located in the Panama Basin within the relatively warm and low saline water masses of the NECC (Levitus and Boyer, 1994a, 1994b; **Fig. 6-1**). Considering the tectonic backtrack path of the Cocos Plate (Pisias et al., 1995; Mix et al., 2003), Site 1241 would move southwestward, closer to its origin at the Galapagos Hotspot (**Fig. 6-1**).

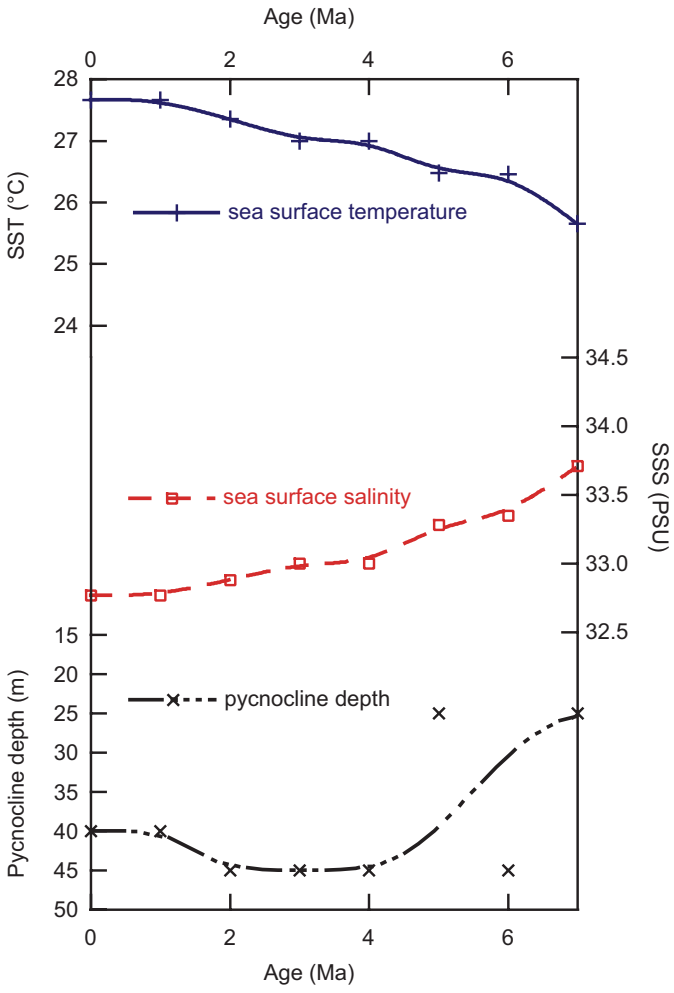

Fig. 6-4 Modern annual-average properties of the upper ocean at paleolocations of Site 1241 for the last 7 Ma, based on plate-tectonic backtracking and an assumption of no temporal changes in regional oceanographic properties. Atlas data on physical and chemical properties are from WOA98 (Ocean Climate Laboratory, 1999). Pycnocline depth is calculated to the nearest 5 m, based on the shallowest maximum in the vertical density gradient. Symbols are average values extracted from the nearest 1° latitude-longitude box in each atlas. Lines: smoothed trends of each property along the backtrack path. SST= sea-surface temperature, SSS= sea-surface salinity. Figure modified from Mix et al. (2003).

This implies that 12 Ma ago, Site 1241 was positioned close to the equator, probably below the SEC and EUC. If we suppose that the overall conditions in the equatorial east Pacific remained constant over the past 7 Ma, the paleogeographic displacement of Site 1241 can be used to predict features of oceanographic change. Assuming the modern oceanographic conditions, we would expect a deepening of the pycnocline and the thermocline, a rise of sea surface temperature (SST), and a decrease of sea surface salinity (SSS), as Site 1241 moved out of the SEC and the equatorial upwelling region and into the NECC during the last 7 Ma (Mix et al., 2003) (**Fig. 6-4**). Significant differences from these predicted trends would imply substantial changes in regional oceanographic conditions during the Pliocene.

6.4 Material and Methods

We used tropical east Pacific ODP Site 1241 (Cocos Ridge; 5° 50.570'N, 86° 26.676'W; 2027 m water depth) for the present study. The depth interval from 58 mcd to 178 mcd (5.7 – 2.5 Ma) was sampled at a mean distance of 10 cm above 162 mcd and a mean distance of 15 cm below. The time resolution of this series is generally better than 3 k.y. (Tiedemann et al., submitted; see chapter 4). The samples were freeze-dried and washed through a 63 μm mesh. From each sample, ten well-preserved tests of *Globigerinoides sacculifer* (without sac-like final chamber) were picked from the 355 – 400 μm fraction for stable isotope measurements. From the same size fraction, ten specimens of *Globorotalia limbata* (dextral) and *Globorotalia tumida* were picked from every second sample. As *Neogloboquadrina dutertrei* is not present in sufficient numbers in the 355 – 400 μm fraction, we picked 15 – 20 specimens from the 250 – 355 μm fraction of every second sample. For species determination, we followed the taxonomic concepts of Kennett and Srinivasan (1983). Measurements of *G. limbata* (dextral) and *G. menardii* (dextral) were performed on four samples where the two coexisted in order to assess the isotopic signature of *G. limbata* (**Tab. 6-1**).

Isotope analyses were run at IFM-GEOMAR (Kiel) using a Finnigan Delta-Plus-Advantage mass spectrometer coupled to a Finnigan/Gas Bench II. Accuracy as revealed from replicate measurements of National Bureau of Standards (NBS) 19 was better than ± 0.07 ‰ for $\delta^{18}O$ and ± 0.05 ‰ for $\delta^{13}C$ (± 1σ). The isotope values are reported relative to Pee Dee Belemnite (PDB).

Paleotemperatures were reconstructed from Mg/Ca ratios of *G. sacculifer*, *G. tumida*, *N. dutertrei*, and *G. limbata*. Twenty to twenty-five specimens of *G. sacculifer*, *G. tumida*, *G. limbata* (dextral) and *N. dutertrei* (approximately 0.5 – 1.2 mg of shell material) were picked from the same size fraction as used for stable isotope measurements, when enough specimens were available. For temperature estimation, *G. sacculifer* was picked from every second sample in the time interval from 2.5 Ma to 3.7 Ma, and from every sample between 3.7 Ma and 4.8 Ma. For samples with low numbers of *G. sacculifer*, we picked up to 35 specimens from the 250 – 355 μm fraction to obtain additional material. We only considered one sample per section for *G. tumida* and *N. dutertrei*. The average time resolution of these records is better than 45 k.y. For the Mg/Ca record of *G. limbata*, we used one sample every second section, corresponding to a time resolution better than than 90 k.y. This preliminary record has two gaps between 2.9 –

3.4 Ma and 4.6 – 5.1 Ma. We avoided specimens visibly contaminated by ferromanganese oxides for Mg/Ca analysis. The specimens were gently crushed between glass plates in order to open the chambers. The shell debris was subsequently cleaned according to Barker et al. (2003). Sample treatment includes several rinses with distilled deionized water and methanol (suprapur) and in-between ultrasonic treatment, two times 10 minutes soaking of the samples in a hot (97 °C) oxidizing 1% $NaOH/H_2O_2$ solution (10 ml 0.1 N NaOH (analytical grade); 100 µl 30% H_2O_2 (suprapur)), a weak acid leach (0.001M subboiled distilled HNO_3) and finally dissolution in subboiled distilled 0.075 M HNO_3. Analyses were performed on the ICP-OES (Ciros CCD SOP, Spectro A.I., Germany) at the Institute of Geosciences, University of Kiel (see Groeneveld et al., submitted a).

For *G. sacculifer* the conversion of Mg/Ca ratios into SSTs was carried out by applying the equation of Nürnberg et al. (2000) (SST = (Log (Mg/Ca) - Log 0.491)/0.033). For *G. tumida*, *N. dutertrei* and *G. limbata*, Mg/Ca temperatures were calculated by using the paleotemperature equation of Anand et al. (2003) (SST = (Log (Mg/Ca) - Log 0.38)/0.09). As this equation is based on a multispecies approach, it allows for the use of the same calibration for the three different species of deep-dwelling foraminifers.

The age model of Site 1241 is based on orbital tuning (Tiedemann et al., submitted, see chapter 4). The authors used the percent sand of carbonate fraction and benthic $\delta^{13}C$ records for the correlation of high frequency variations to the orbital solution of Laskar et al. (1993). The astronomical time scale of Site 1241 is in agreement with that from Atlantic Sites 925/926 as indicated by a comparison of benthic $\delta^{13}C$ records.

6.5 Results

6.5.1 Oxygen isotope records

Figure 6-5 shows the Pliocene planktonic oxygen isotope records of *G. sacculifer*, *G. limbata* (dextral), *N. dutertrei* and *G. tumida* together with the benthic $\delta^{18}O$ record from Site 1241 (Tiedemann et al., submitted, see chapter 4). In general, the $\delta^{18}O$ differences between the planktonic species indicate a clear depth ranking, consistent with their assumed ecology. The relatively low $\delta^{18}O$ values of *G. sacculifer* reflect warmer surface water masses as it calcifies predominantly within the surface mixed layer. Generally higher $\delta^{18}O$ values of *G. tumida* result from its deep habitat at the bottom of the photic zone within cool subsurface waters below the thermocline. The thermocline-dwellers *G. limbata* and *N. dutertrei* display intermediate values between those of *G. sacculifer* and *G. tumida.* Lower $\delta^{18}O$ values within the thermocline than at the bottom of the photic zone most likely indicate that a comparatively warm thermocline prevailed above the bottom of the photic zone in the tropical east Pacific during the Pliocene.

Two outstanding features were determined in the long-term $\delta^{18}O$ records:

1. The $\delta^{18}O$ values of deep-dwellers increased between 5.4 Ma and 3.3 Ma (Marine Isotope Stage (MIS) M2). This trend is shown by all deep-dwelling species, but it appears to be more distinct in the $\delta^{18}O$ records of thermocline-dwellers. The $\delta^{18}O$ values of *G. limbata* and *N. dutertrei* rise gradually by about 1 ‰, whereas the $\delta^{18}O$ increase in the *G. tumida* record is only about 0.5 ‰ with a major step of 0.3 ‰ between 4.7 Ma and 4.2 Ma. In contrast, the $\delta^{18}O$ record of the mixed layer-dweller *G. sacculifer* is marked by a long-term decrease of about 0.8 ‰ from 5.7 Ma to 3.4 Ma with a transient maximum at MIS Si6 (*ca.* 4.9 Ma). The following increase in $\delta^{18}O$ *G. sacculifer* values from 3.4 Ma to 3.3 Ma culminates at 3.3 Ma (MIS M2). A similar trend is observed in the deep-dweller records. This increase was either associated with an increase in global ice volume, a decrease in deep-water temperature, or both as suggested by the benthic $\delta^{18}O$ record (**Fig. 5**). The long-term $\delta^{18}O$ increase in the deep-dweller records and the $\delta^{18}O$ decrease in the *G. sacculifer* record between 5.4 Ma and 3.3 Ma reveal an enhancement of the $\delta^{18}O$ gradient in the upper water column (**Figs. 6-5, 6-6**).

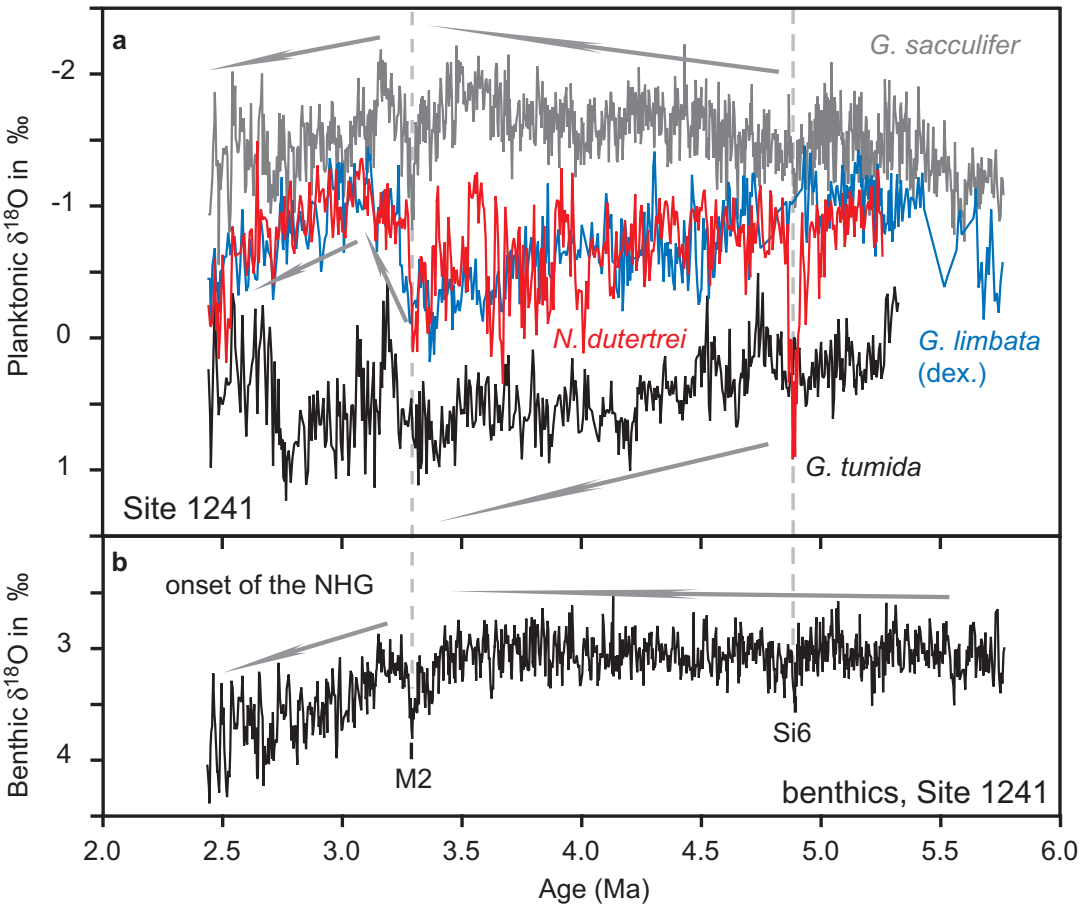

Fig. 6-5 Multispecies planktonic $\delta^{18}O$ records (**a**) compared to the benthic $\delta^{18}O$ record of Site 1241 (**b**), (Tiedemann et al., submitted, see chapter 4). In **a**: gray line: *G. sacculifer*; red line: *N. dutertrei*; blue line: *G. limbata* (dextral); black line: *G. tumida*. Important marine isotope stages (MIS) Si6 (ca. 4.9 Ma) and M2 (ca. 3.3 Ma) are indicated. Gray arrows mark major trends in planktonic and benthic $\delta^{18}O$ records. Note the exceptionally high $\delta^{18}O$ values of *N. dutertrei* (left-coiling) during MIS Si6.

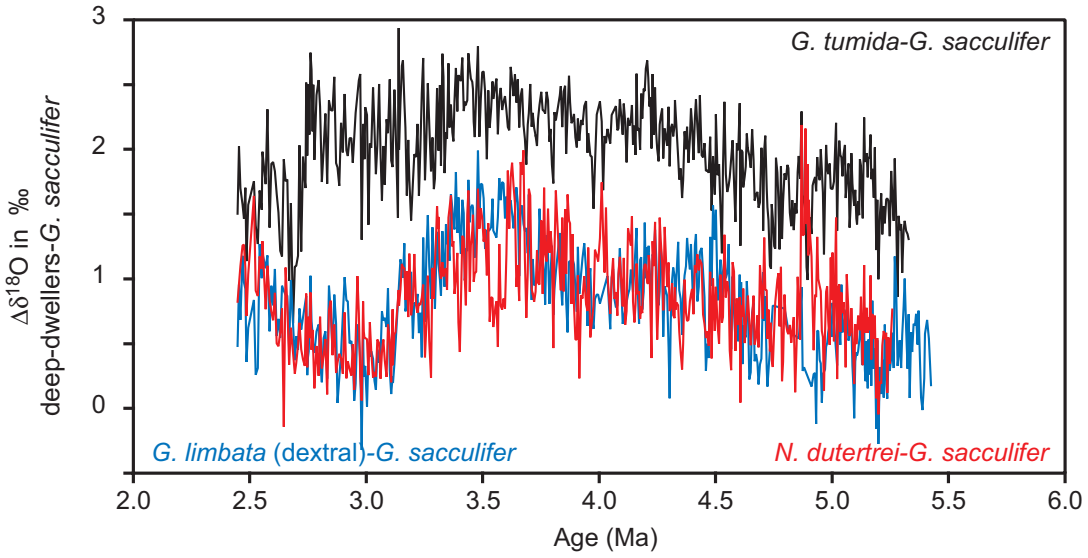

Fig. 6-6 Differences in $\delta^{18}O$ between deep-dwelling planktonic foraminifers and *G. sacculifer* at Site 1241. Black line: *G. tumida-G. sacculifer*; red line: *N. dutertrei-G. sacculifer*; blue line: *G. limbata* (dextral)-*G. sacculifer.* In general, $\Delta\delta^{18}O$ deep-dwellers-*G. sacculifer* increases gradually between 5.4 Ma and 3.3 Ma, indicating an increase in the $\delta^{18}O$ gradient of the upper water column.

In order to distinguish global $\delta^{18}O$ signals from local variations, we compared the planktonic $\delta^{18}O$ records to the benthic $\delta^{18}O$ record of Site 1241 (Tiedemann et al., submitted, see chapter 4) (**Fig. 6-5**). We consider the benthic $\delta^{18}O$ record to reflect global climatic changes, as it shows a dynamic that is comparable to global ice volume changes and temperature variability in the source regions of deep-water formation at high latitudes (e.g. Tiedemann et al., 1994; Shackleton et al., 1995; Tiedemann et al., submitted, see chapter 4). Major long-term deviations between benthic and planktonic records occurred between 5.7 Ma and 3.3 Ma (**Fig. 6-5**). The benthic isotope record shows no long-term trend, whereas the $\delta^{18}O$ values of deep-dwellers increased by about 1 ‰ and the *G. sacculifer* $\delta^{18}O$ values decreased by about 0.8 ‰. Thus, the trends in the planktonic $\delta^{18}O$ records point to significant changes of the surface structure and properties (being temperature and/or salinity) in the tropical east Pacific.

2. After 3.3 Ma (MIS M2), the $\delta^{18}O$ records of *G. sacculifer* and *G. tumida* were characterized by similar trends, whereas the records of the thermocline-dwellers *G. limbata* and *N. dutertrei* deviated significantly from those of *G. sacculifer* and *G. tumida*. The time interval between 3.2 Ma and 3.1 Ma, often referred to as the "Mid-Pliocene Warmth" (e.g. Crowley, 1996; Raymo et al., 1996), is marked by a $\delta^{18}O$ minimum in *G. tumida* and *G. sacculifer* that is not apparent in the $\delta^{18}O$ records of *G. limbata* and *N. dutertrei*. Thereafter, the $\delta^{18}O$ values of both *G. tumida* and *G. sacculifer* increased by about 1 ‰, followed by a $\delta^{18}O$ decrease after 2.7 Ma. This decrease is more pronounced in the $\delta^{18}O$ record of *G. tumida*. The oxygen isotope values of the thermocline-dwellers, however, show an opposite trend. They decreased by about 0.8 ‰ between 3.3 Ma and 3.0 Ma, and increased again by about 0.7 ‰ between 3.0 Ma and 2.5 Ma (**Figs. 6-5, 6-6**).

A comparison of planktonic $\delta^{18}O$ records with the benthic $\delta^{18}O$ record suggests that a significant portion of the variability within planktonic $\delta^{18}O$ records between 3.3 Ma and 2.5 Ma depended on changes in global ice volume. Benthic $\delta^{18}O$ values increased gradually after 3.2 Ma, indicating an increase in global ice volume due to the intensification of the NHG. Hence, the general $\delta^{18}O$ increase that is reflected by the planktonic $\delta^{18}O$ records after 3.2 – 3.0 Ma primarily mirrors the global cooling trend.

The short-term variability of $\delta^{18}O$ is generally highest in the record of *N. dutertrei*, showing fluctuations of up to 1.5 ‰, especially in the time interval between 4 Ma and 3.3 Ma. Such strong variations in $\delta^{18}O$ could account for small changes in calcification depth within the steep thermal gradients of the thermocline (Cannariato and Ravelo, 1997), although it was previously suggested that *N. dutertrei* generally calcifies close to the same temperature, regardless of oceanographic changes (Curry et al., 1983; Ravelo and Fairbanks, 1992; Billups and Spero, 1996). One remarkable feature in the *N. dutertrei* $\delta^{18}O$ record is the short (40 k.y) excursion to extremely high $\delta^{18}O$ values at about 4.9 Ma, during MIS Si6. $\delta^{18}O$ of *N. dutertrei* increased abruptly by approximately 1.5 ‰ (**Fig. 6-5**). This would equal a cooling of about 4 °C or a salinity increase of *ca*. 2 units, assuming that 0.4 ‰ of the $\delta^{18}O$ increase was coupled to an increase in global ice volume during MIS Si6 as indicated by the benthic $\delta^{18}O$ record. Evidence for the $\delta^{18}O$ shift was also found within the *N. dutertrei* / *N. humerosa* record of Site 851 (Cannariato and Ravelo, 1997), implying that the $\delta^{18}O$ shift was a regional rather than a local phenomenon. During MIS Si6, only left-coiling *N. dutertrei* are present in the samples of Site 1241, whereas *N. dutertrei* is otherwise dominantly dextral in the Pliocene section of Site 1241. The change in coiling-direction and the shift in the $\delta^{18}O$ composition may point to a species offset between left- and right-coiling morphotypes or a short-term change in the habitat depth, rather than reflecting an extreme change in oceanography. *G. limbata* (dextral) is rare during this time interval. Hence, a comparison between the two thermocline-dweller records that could point to a habitat change is not possible.

If the observed $\delta^{18}O$ signals of planktonic foraminifers primarily reflected Pliocene temperature variations, the observed long-term trends in vertical $\delta^{18}O$ gradients at Site 1241 might be interpreted straightforward as changes in the thermocline depth and structure (e.g. Ravelo and Fairbanks, 1992; Cannariato and Ravelo, 1997; Chaisson and Ravelo, 2000). Increasing $\delta^{18}O$ gradients between shallow- and deeper-dwelling foraminifers between 5.4 Ma and 3.3 Ma therefore would account for a shoaling or steepening of the tropical east Pacific thermocline, whereas the decrease in the gradient between the thermocline-dwellers and *G. sacculifer* after 3.3 Ma (MIS M2) would suggest a deepening of the tropical east Pacific thermocline just after the intensification of the NHG, as recorded in benthic $\delta^{18}O$ records. However, interpreting the planktonic $\delta^{18}O$ records simply in terms of temperature changes would have resulted in a misinterpretation as suggested by the Mg/Ca records of deep-dwellers.

6.5.2 Implications from Mg/Ca temperature estimates for deep-dwellers

The Mg/Ca-derived temperature estimates from the different planktonic foraminifers enable for the first time to quantify the thermal structure of the tropical east Pacific upper water column (**Fig. 6-7**). Moreover, these temperature estimates are used to assess the $\delta^{18}O$ salinity signal for the different habitat depths of the planktonic foraminifers.

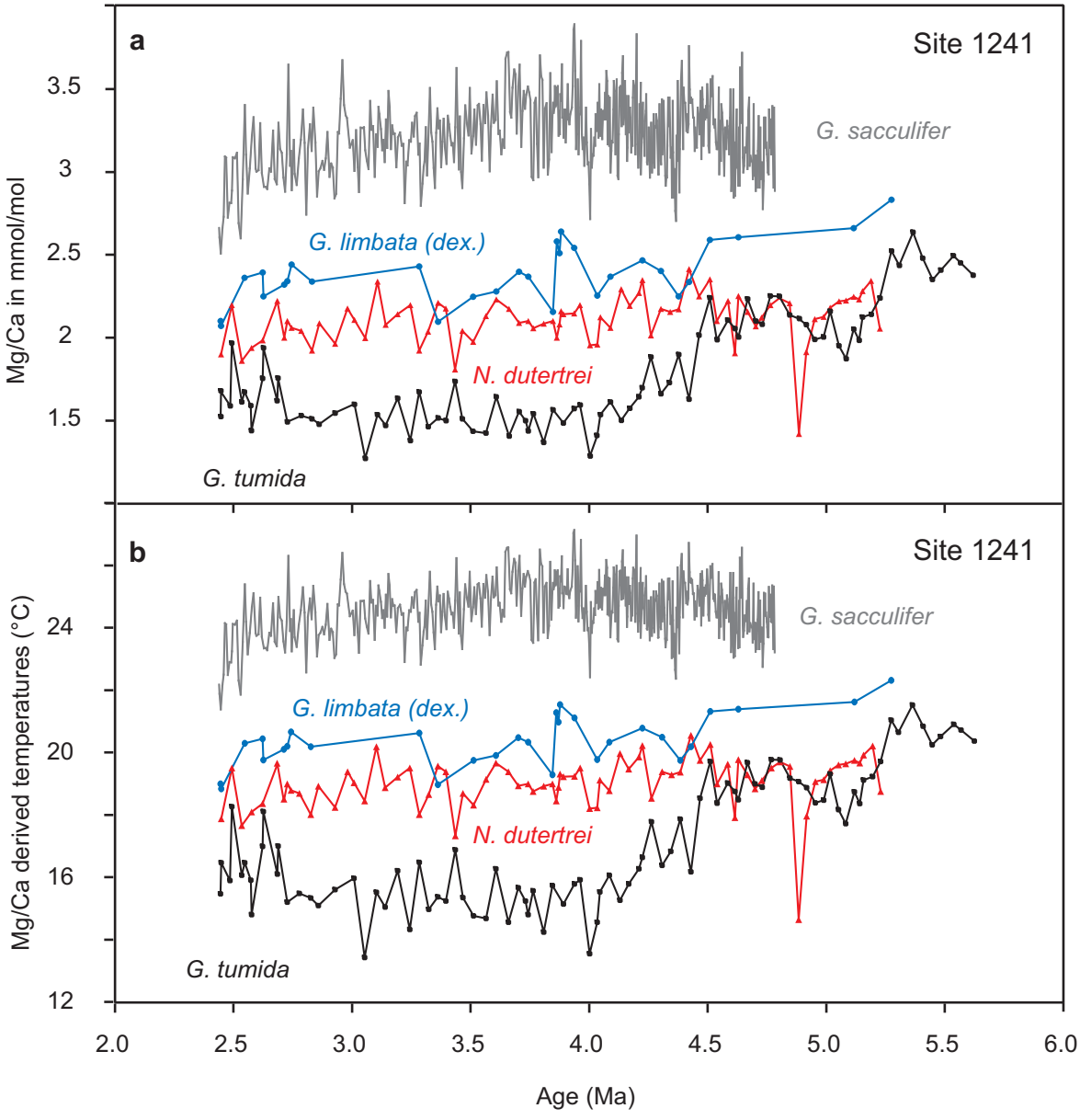

Fig. 6-7 Mg/Ca ratios and Mg/Ca derived temperatures of planktonic foraminifers from Site 1241. **a**: Mg/Ca in mmol/mol. Gray line: *G. sacculifer* (Groeneveld et al., submitted a); red line: *N. dutertrei*; blue line: *G. limbata* (dextral); black line: *G. tumida*. **b**: Mg/Ca derived temperatures. Temperatures for *G. sacculifer* (gray line) were calculated by applying the equation of Nürnberg et al. (2000). Temperatures for the deep dwellers *N. dutertrei* (red line), *G. limbata* (blue line) and *G. tumida* (black line) were calculated by using the paleotemperature equation of Anand et al. (2003).

Paleotemperatures of *G. sacculifer* vary between 21.4 °C and 27.2 °C (Groeneveld et al., submitted a). From 4.8 Ma to 3.7 Ma, the temperature record of *G. sacculifer* reveals a long-term increase of about 1 °C, from 24.5 °C to 25.5 °C. As such, surface mixed layer temperatures at Site 1241 were similar to those observed today in a water depth of about 30 – 40 m (Levitus and Boyer, 1994a). From 3.7 Ma to 2.5 Ma, temperatures decreased by up to 3 °C, reflecting a tropical cooling trend in the east Pacific (Groeneveld et al., submitted a). The salinity record shows no long-term trend from 4.8 to 3.7 Ma, but a $\delta^{18}O$ salinity decrease of approximately 0.8 ‰ from 3.7 Ma to 2.5 Ma (for further discussions see Groeneveld et al., submitted a).

The *G. tumida* Mg/Ca temperatures covary roughly with the trends observed in the $\delta^{18}O$ record of this species. *G. tumida* displays temperatures at the bottom of the photic zone which decreased by about 6 °C (from 21 °C to 15 °C) between 5.4 Ma to 4.0 Ma. This long-term trend is marked by two main steps in temperature decrease at 5.3 Ma and 4.5 Ma, and supports the $\delta^{18}O$ evidence for an early Pliocene shoaling of the tropical east Pacific thermocline. Temperatures remained relatively stable from 4.0 Ma to 2.7 Ma and varied between 13 °C and 16 °C (**Fig. 6-7**). This is in agreement with modern temperatures at depths of about 90 - 100 m, i.e. the modern bottom of the photic zone, at the position of Site 1241 (Levitus and Boyer, 1994a). Accordingly, Pliocene temperature conditions between 4.0 Ma and 2.7 Ma were close to the modern ones at this water depth. After 2.7 Ma, *G. tumida* shows a warming to maximum temperatures of 18 °C at *ca.* 2.6 Ma and 2.5 Ma, that may point to a slight deepening of the thermocline. In general, salinity changes seem to have exerted only minor control on these subsurface water mass signatures, as the trends in $\delta^{18}O$ and temperature are comparable at the bottom of the photic zone.

The Pliocene temperature variations within the thermocline, as recorded by *N. dutertrei* and *G. limbata*, were relatively stable from 5.4 to about 2.4 Ma, within a range of 18 – 19°C for *N. dutertrei* and 19 – 21 °C for *G. limbata* (**Fig. 6-7**). This would compare to modern temperatures in a water depth of 60 – 70 m and 40 – 50 m, respectively (Levitus and Boyer, 1994a). The modern thermocline and chlorophyll maximum, being the preferred habitat of *N. dutertrei*, are located at 25 – 37 m water depth in the Panama Basin (Fairbanks et al., 1982). Since temperatures within the modern thermocline are about 22 °C, and the Pliocene mixed layer temperature was close to the modern one, we assume that the absolute paleotemperature estimates for *N. dutertrei* and *G. limbata* appear to be slightly too cool. The remarkable temperature excursion of *N. dutertrei* (left-coiling) at MIS Si6 (4.9 Ma) resembles the $\delta^{18}O$ excursion and can almost fully account for the observed change in $\delta^{18}O$ (**Figs. 6-5, 6-7**). We ascribe this feature to a different habitat for the left-coiling *N. dutertrei*, because all other Mg/Ca and isotope values were measured on *N. dutertrei* dextral. The long-term variations of the Mg/Ca temperature and $\delta^{18}O$ records from *N. dutertrei* and *G. limbata*, however, differ significantly from each other. Neither the 1 ‰ $\delta^{18}O$ increase in *G. limbata* and *N. dutertrei* between 5.4 Ma and 3.3 Ma (MIS M2), nor the 0.8 ‰ decrease in $\delta^{18}O$ after 3.3 Ma was reflected by their paleotemperature records. The long-term $\delta^{18}O$ changes display relatively strong variations in salinity, because their general trend deviates from both the local temperature record, and the evolution of global climate as indicated by the benthic $\delta^{18}O$ record. Thus, salinity changes might have exerted a more important control on tropical east Pacific upper ocean hydrography during the Pliocene than previously assumed (Cannariato and Ravelo, 1997;

Chaisson and Ravelo, 2000). The 1 ‰ $\delta^{18}O$ increase between 5.4 Ma and 3.3 Ma refers to a salinity increase of approximately 2 units within the thermocline, if the global $\delta^{18}O$-salinity equation of Broecker and Peng (1982, 0.5 ‰ $\delta^{18}O$ = 1 salinity unit) is applied. The 0.8 ‰ decrease in $\delta^{18}O$ after 3.3 Ma, however, indicates a salinity decrease of 1.5 units in the thermocline. It parallels the first cooling steps associated with the intensification of the NHG (Haug and Tiedemann, 1998). We have to point out that this suggestion is only valid if the depth habitat of *G. limbata* and *N. dutertrei* is always coupled to the thermocline.

The presumed salinity changes could also be affected by changes in the calcification depth of *N. dutertrei* and *G. limbata*. The temperature estimates for these thermocline-dwellers suggest relatively stable temperatures during the Pliocene. The temperature decrease and the $\delta^{18}O$ increase of *G. tumida*, however, indicate an increase of the temperature gradient within the photic zone during the early Pliocene. This could be effected by a shoaling of the tropical east Pacific thermocline, as a shallow thermocline results in a shoaling and compression of the isotherms in the upper water column. If this had happened, a migration to a shallower habitat of *N. dutertrei* and *G. limbata* between 5.4 Ma and 4.0 Ma, i.e. closer to the surface mixed layer, may be anticipated.

The evidence for a thermocline shoaling between 5.4 Ma and 4.0 Ma at the position of Site 1241 contradicts the presumed changes in upper ocean hydrography due to the plate tectonic movement of the Cocos Plate (Mix et al., 2003) (**Figs. 6-1, 6-4**). Assuming that regional oceanographic properties did not change substantially over the last 7 Ma, the pycnocline depth should have increased between 6 Ma and 4 Ma. Site 1241 moved from the equatorial upwelling region with a shallow thermocline northward into the NECC with a deep thermocline (**Fig. 6-4**). Thus, the shoaling of the thermocline reflects indeed large-scale changes in upper ocean hydrography and not the migration of the site location.

6.5.3 Assessment of salinity gradients in the upper water column

To further examine the salinity changes in the upper water column, we estimated the salinity gradients from the mixed layer (*G. sacculifer*) to the thermocline (*N. dutertrei*) and to the bottom of the photic zone (*G. tumida*). **Figure 6-8** schematically illustrates these changes (ΔS) for the time interval younger than 4.8 Ma. In a first step, we estimated the temperature difference between *G. sacculifer* and the deep-dwellers ($\Delta T_{sac\text{-}deep}$) and transferred the difference into $\delta^{18}O$ values, assuming that a temperature increase of 1 °C equals a $\delta^{18}O$ decrease of 0.23 ‰ (e.g. Shackleton, 1974). Then, we subtracted the resulting $\delta^{18}O$ (temperature) difference from the measured $\delta^{18}O$ deep-dweller values ($\delta^{18}O_{deep}$). In other words, we corrected the $\delta^{18}O$ signals of *G. tumida* and *N. dutertrei* for their temperature offset to *G. sacculifer*. In a final step, we subtracted the $\delta^{18}O$ *G. sacculifer* signal ($\delta^{18}O_{sac}$) from these temperature-corrected records. This eliminates the $\delta^{18}O$ ice volume signal and provides the salinity related $\delta^{18}O$ differences with respect to *G. sacculifer*. Applying the global $\delta^{18}O$-salinity equation of Broecker and Peng (1982; 0.5 ‰ $\delta^{18}O$ = 1 salinity unit) yields a rough estimate of salinity change. The differences were derived by the following equation:

$$\Delta S = (\delta^{18}O_{deep} - (\Delta T_{sac\text{-}deep} * 0.23) - \delta^{18}O_{sac})*2 \qquad [1]$$

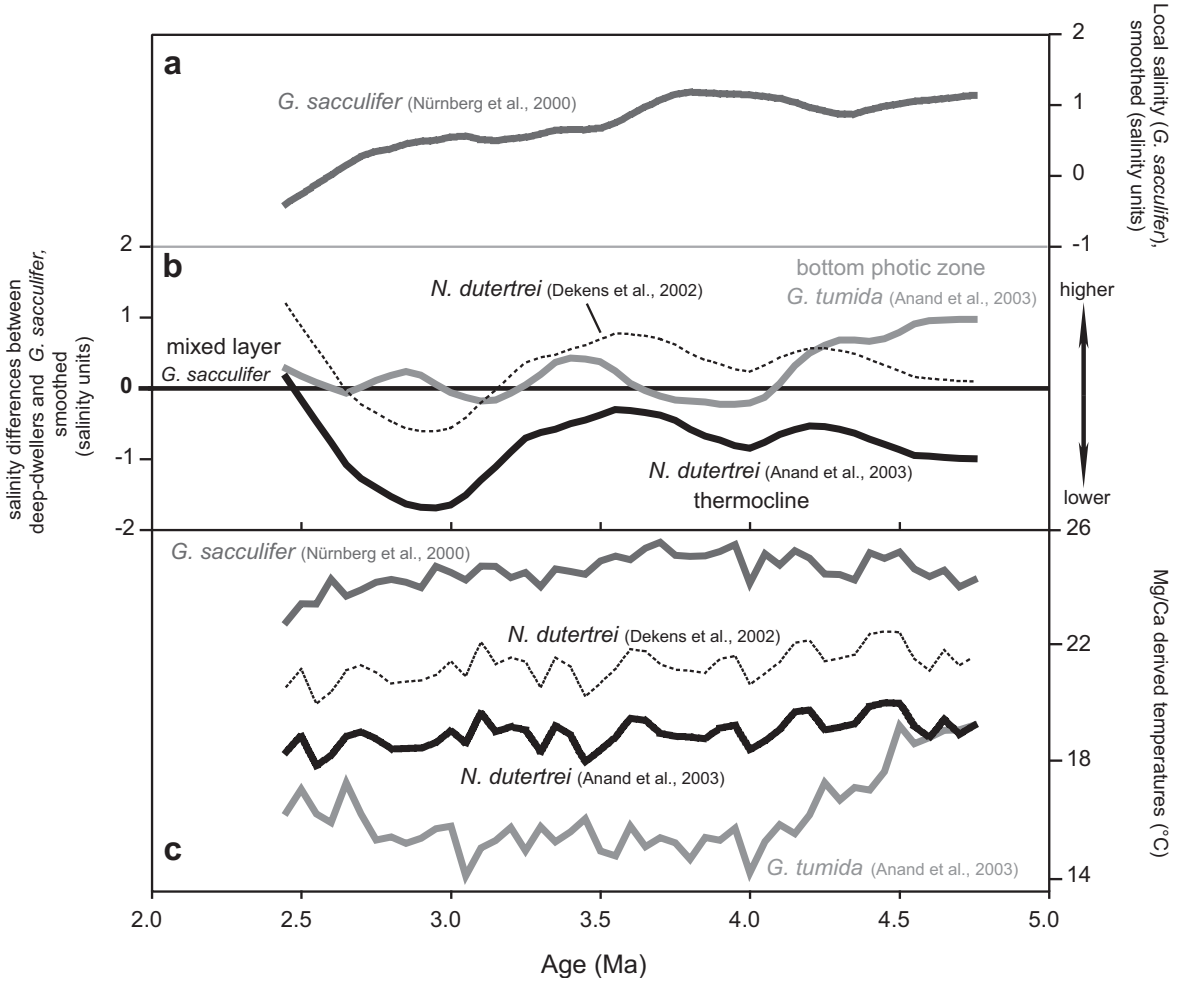

Fig. 6-8 $\delta^{18}O$-derived salinity of *G. sacculifer* (**a**), salinity estimates for *G. tumida* and *N. dutertrei* in relation to *G. sacculifer* (**b**), and Mg/Ca temperature estimates (**c**). For direct comparisons of the records, we interpolated the curves at 50-k.y. steps. The curves in figures **a**, and **b** were smoothed using a 20% weighted curve fit. **a**: Salinity of *G. sacculifer* was calculated by correcting $\delta^{18}O_{G.\ sacculifer}$ for changes in temperature and global ice volume (Groeneveld et al., submitted a). **b**: the salinity differences between deep-dwellers and *G. sacculifer* were calculated using equation 1. The equations used for temperature estimates are indicated for each curve. In this figure, the salinity of *G. sacculifer* is given as 0. Values > 0 indicate higher salinities, and values < 0 indicate lower salinities for the deep-dwellers with respect to the mixed layer (*G. sacculifer*). **c**: paleotemperature estimates for the different planktonic foraminifers in low resolution (50 k.y. steps). Paleotemperature equations used for the conversion of Mg/Ca values into temperatures are indicated.

Groeneveld et al. (submitted a) estimated the local $\delta^{18}O$ salinity signal for the mixed layer by correcting the $\delta^{18}O$ *G. sacculifer* values for changes in temperature and global ice volume, applying the equation from Shackleton (1974). The resulting salinity record from *G. sacculifer* suggests relatively constant values from 4.7 – 3.7 Ma, followed by a long-term decrease from 3.7 – 2.5 Ma (**Fig. 6-8**). These changes have to be considered when interpreting the salinity gradients between the *G. sacculifer* record and the deep-dweller records.

The relative salinity differences between the deep-dwellers and *G. sacculifer* provide the following information (**Fig. 6-8**): From 4.8 – 4.0 Ma, salinity decreased at the bottom of the photic

zone and increased within the thermocline, probably in response to the shoaling of the thermocline. The salinity increase at the level of the thermocline reached a maximum at about 3.6 Ma. After 3.6 Ma, salinity decreased until 2.9 Ma and then increased again from 2.9 Ma to 2.5 Ma. The relative increase in salinity after 2.9 Ma is interpreted to result from the salinity change in the mixed layer (*G. sacculifer*), as the local salinity within the mixed layer decreased significantly after 2.9 Ma (**Fig. 6-7a**). This decrease parallels the major intensification of the NHG.

If we try to interpret the observed relationships (**Fig. 6-8**) in terms of absolute changes in salinity, we are faced with severe problems that most likely result from uncertainties in estimating deep-dweller temperatures. The salinity values at the bottom of the photic zone appear to be higher than in the mixed layer prior to 4.1 Ma, and relatively similar after 4.1 Ma. Applying the temperature equation of Anand et al. (2003), the record of *N. dutertrei*, indicative of changes at the thermocline level, would provide the lowest salinities. This would suggest a permanent salinity minimum at the thermocline depth and higher salinities above and below. This is not very likely because the salinity at the thermocline depth should be on the mixing line between salinities of the mixed layer (*G. sacculifer*) and the bottom of the photic zone (*G. tumida*). Applying the Pacific temperature equations of Dekens et al. (2002) for *G. sacculifer* and *N. dutertrei* would result in nearly identical temperatures for both species, suggesting similar habitats (not shown in **Fig. 6-8**). The $\delta^{18}O$ values of the two species, however, are offset by up to 1.5 ‰. Assuming a relatively deep thermocline, and taking into account that *N. dutertrei* may have lived within the mixed layer as *G. sacculifer* did, this would suggest extreme differences in salinities for approximately the same water depth, which is physically unrealistic. In contrast, applying the Atlantic temperature equations of Dekens et al. (2002) for *G. sacculifer* and *N. dutertrei* would provide reasonable temperature and salinity distributions for the upper water column. The temperature estimates of *G. sacculifer* are similar to those derived from the equation of Nürnberg et al. (2000) within a range of ± 0.2°C. The Pliocene record of *N. dutertrei* indicates an average temperature of 21.5 °C that is close to the modern thermocline temperature at Site 1241 and about 3 °C cooler than the Pliocene calcification temperature of *G. sacculifer* (**Fig. 6-8**). Accordingly, the salinity at the thermocline would be slightly higher than in the mixed layer. However, this would introduce a new problem related to the salinities of *G. tumida*, especially in those intervals, where the salinity of *N. dutertrei* is higher than that of *G. sacculifer* and *G. tumida*, which is also not very likely. These relationships demonstrate that we are close to quantifying absolute temperature and salinity changes in the upper water column, but the accurracy of temperature estimates for deep-dwellers seems to be the limiting factor.

6.5.4 Carbon isotope trends

Figure 6-9 illustrates the comparison between planktonic carbon isotope records and the benthic $\delta^{13}C$ record of Site 1241 (Tiedemann et al., submitted, see chapter 4). As Site 1241 is located outside the equatorial upwelling region during the Pliocene, $\delta^{13}C_{DIC}$ (DIC = dissolved inorganic carbon) is expected to decrease with depth. Phytoplankton elevates surface $\delta^{13}C_{DIC}$ as it discriminates against $^{13}CO_2$ during photosynthesis, and heterotrophic organisms reintroduce ^{13}C-depleted CO_2 back into the DIC pool *via* respiration at depth (Kroopnick, 1974; Spero et al.,

2003). It is thus commonly assumed that the most positive $\delta^{13}C$ values correspond to the nutrient-depleted surface mixed layer, and that the lowest $\delta^{13}C$ values occur at depths of the thermocline, where the nutrient supply and recycling is highest.

Our results support this assumption, as the carbon isotopic values of the mixed layer-dweller *G. sacculifer* are generally higher than those of *N. dutertrei*, *G. limbata* (dextral) and *G. tumida*. The deep-dwelling foraminifers have $\delta^{13}C$ values between those of *G. sacculifer* and the benthic foraminiferal $\delta^{13}C$ record, indicative of relatively nutrient-enriched subsurface waters. $\delta^{13}C$ gradients between *G. sacculifer* and the deep-dwellers are up to 2 ‰ and are thus comparable to the modern $\delta^{13}C$ gradient within the upper 100 m of the water column within the Panama Basin (Fairbanks et al., 1982). In general, *N. dutertrei* shows the lowest $\delta^{13}C$ values as it probably calcified within the chlorophyll maximum, a layer that is marked by the recycling of organic matter and is thus enriched in ^{12}C. However, we will not compare the absolute values, as the species-specific offsets to $\delta^{13}C_{seawater}$ equilibrium are not well constrained. Therefore, we only considered the long-term trends for our interpretations.

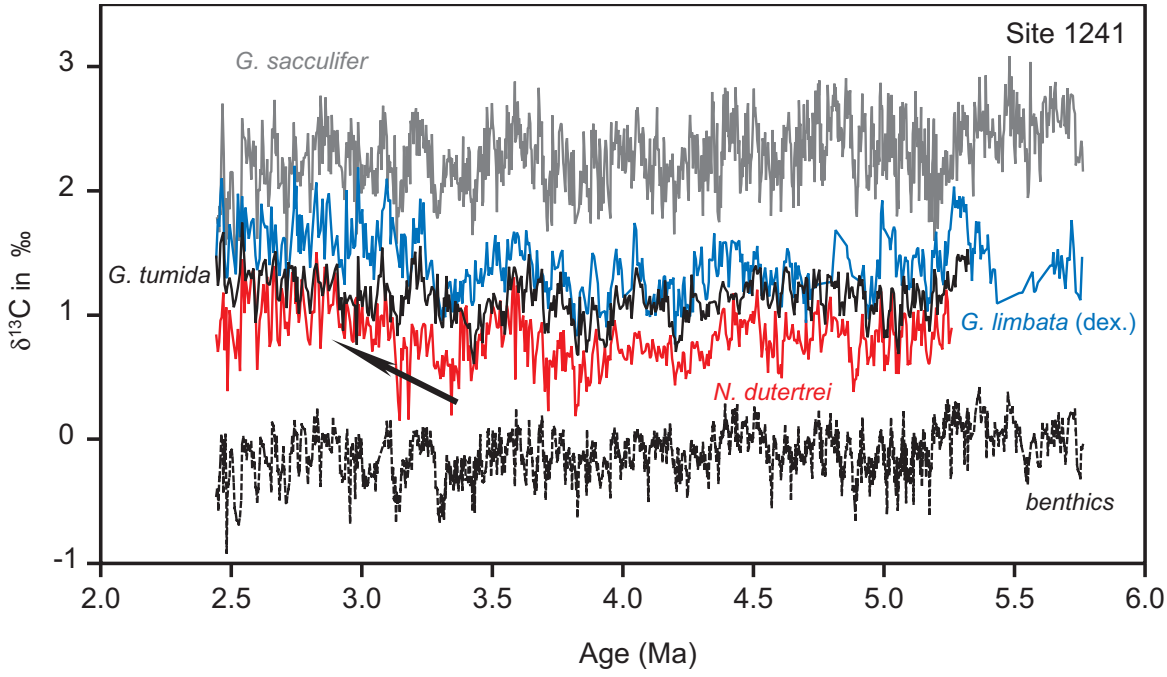

Fig. 6-9 $\delta^{13}C$ records of planktonic foraminifers (Site 1241) compared to the benthic $\delta^{13}C$ record of Site 1241 (Tiedemann et al., submitted, see chapter 4). Gray line: *G. sacculifer*; red line: *N. dutertrei*; blue line: *G. limbata* (dextral); black line: *G. tumida*; black dashed line: benthic $\delta^{13}C$. $\delta^{13}C$ values of the deep-dwelling foraminifers *N. dutertrei*, *G. limbata*, and *G. tumida* increase after 3.3 Ma (marked by the black arrow), whereas the $\delta^{13}C$ values of the mixed-layer-dweller *G. sacculifer* follow the global trend of the benthic record.

From 5.4 Ma to 3.3 Ma, all planktonic carbon isotope records were roughly parallel to each other and followed the general trend of the benthic $\delta^{13}C$ record at Site 1241 that is interpreted to reflect global changes in $\delta^{13}C$ (Tiedemann et al., submitted, see chapter 4) (**Fig. 6-9**). Accordingly,

the planktonic $\delta^{13}C$ records display changes in the global carbon reservoir between 5.4 Ma and 3.3 Ma, and do not indicate major changes in nutrient supply or utilization within the photic zone.

Between 3.3 Ma and 2.4 Ma, the $\delta^{13}C$ record of *G. sacculifer* and the benthic $\delta^{13}C$ record remained parallel, indicating that surface mixed layer water masses still reflected global changes in the $\delta^{13}C_{seawater}$. In contrast, the $\delta^{13}C$ records of deeper dwelling foraminifers show a gradual increase of 0.5 ‰ after 3.3 Ma (MIS M2) that deviates from the benthic $\delta^{13}C$ record (**Fig. 6-9**). This shift to higher $\delta^{13}C$ values within the thermocline and at the bottom of the photic zone decreases the $\delta^{13}C$ gradient between surface mixed layer and underlying water masses. Since this change in the carbon isotopic composition is not a global phenomenon, it indicates a change in nutrient supply or utilization, or a change in the thermocline source waters within the tropical east Pacific that was paralleled by global cooling as indicated by benthic $\delta^{18}O$ (Cannariato and Ravelo, 1997). The shift in the carbon isotopic composition of the deep-dwellers at 3.3 Ma is paralleled by the 0.8 ‰ shift in the $\delta^{18}O$ records of the thermocline-dwellers *G. limbata* and *N. dutertrei*, that suggests a salinity decrease within the tropical east Pacific thermocline. Other possible explanations for the observed shift in $\delta^{13}C$ can be a small change in habitat depth of the deep-dwellers or a shift in the $\delta^{13}C_{DIC}$ chemocline that may be related to subtle changes in the structure of the thermocline or pycnocline (Loubere, 2001). As the factors that control the $\delta^{13}C$ signal of planktonic foraminifers are manifold, additional productivity proxies would have to be taken into account for a more detailed determination of changes in upper ocean nutrient contents.

6.6 Discussion

6.6.1 Pliocene changes in the thermal structure of the tropical east Pacific upper water column and possible links to tectonics and climate

The Mg/Ca temperature records of shallow- and deep-dwelling planktonic foraminifers provided new insights into the Pliocene thermal structure of the upper water column at tropical east Pacific Site 1241. In general, the temperature estimates are in good agreement with the assumed ecological preferences of the foraminiferal species, as Mg/Ca temperatures decrease with increasing habitat depth (**Fig. 6-3, 6-7**).

The temperature reconstructions point to a marked shoaling of the tropical east Pacific thermocline between 5.4 Ma and 4.0 Ma. This is indicated by a temperature decrease of about 6 °C at the bottom of the photic zone, as reflected by the paleotemperature record of *G. tumida*. Major cooling steps occurred after 5.3 Ma and after 4.5 Ma (**Fig. 6-7**). Since mixed layer temperatures were relatively stable (~25 °C) as revealed by the Mg/Ca temperature record of *G. sacculifer*, the temperature gradient in the upper water column increased from about 5 °C to 10 °C during this time interval. Although the temperature gradient between surface mixed layer and the bottom of the photic zone was subject to strong changes, this did not affect the Mg/Ca temperature records of the thermocline-dwellers (*N. dutertrei* and *G. limbata*). We surmise that the temperatures within the thermocline would not vary strongly if thermocline depth changes, as long as SST remains stable. Indeed, the Mg/Ca temperatures of *N. dutertrei* and *G. limbata* remained relatively stable during

the Pliocene, because their habitat was always coupled to the thermocline level, as suggested. These records provide for the first time the opportunity to document the temperature adaptation of the thermocline-dwellers for the Pliocene.

The timing of the observed thermocline shoaling in the tropical east Pacific is in agreement with the results of Cannariato and Ravelo (1997). Their results, however, were based on planktonic stable isotope records and thus did not allow the quantification of Pliocene temperature gradients. This, unfortunately, led to a misinterpretation of the $\delta^{18}O$ record from *N. dutertrei*/ *N. humerosa* at tropical east Pacific Site 851.

The late Miocene to early Pliocene shoaling of the thermocline was completed by 4.0 Ma and represents a new stage in the thermal structure of the upper water column in the tropical east Pacific that persisted until 2.7 Ma, with slight modifications after 3.7 Ma. This new stage in thermal structure was already close to the modern one, if considering our temperature estimates as reasonable. In this context, of course, the application of Mg/Ca paleotemperature equations is a point of discussion. Our temperature estimates for *G. sacculifer* are based on the species-related equation of Nürnberg et al. (2000) and those for the deep-dwellers are based on the multi-species approach of Anand et al. (2003). The application of the Pacific species-related equations from Dekens et al. (2002) for *G. sacculifer* and *N. dutertrei* would result in nearly identical temperatures for both species, with temperatures about 2 °C higher than our estimates for *G. sacculifer*. This would suggest extreme differences in salinity at approximately the same water depth, which is regarded as unrealistic (see chapter 6.5.3). The Atlantic formula of Dekens et al. (2002) would suggest temperature estimates of *G. sacculifer* that are similar to those presented here. Their Atlantic species-related equation for *N. dutertrei* would provide thermocline temperatures about 3 °C warmer than our estimates for *N. dutertrei*. This would perfectly match the modern average thermocline temperature of about 22 °C and would, in addition, solve a problem concerning the salinity gradient between the mixed layer and the thermocline (chapter 6.5.3). The multi-species temperature equation from Elderfield and Ganssen (2000) would lead to generally lower temperatures for all habitats (6 °C cooler for *G. sacculifer*, 5 °C cooler for *N. dutertrei*, 4 °C cooler for *G. tumida*). As a result, the temperature gradient between the mixed layer and the bottom of the photic zone would approximate 8 °C in comparison to 10 °C as suggested by this study. We regard these temperature estimates derived from the Elderfield and Ganssen (2000) equation as too cold, because then Pliocene mixed-layer temperatures of 18.5 °C would have been significantly cooler than modern ones during a period when Earth's climate was generally warmer than today. On the one hand, these comparisons demonstrate the recent uncertainty in absolute temperature reconstructions. On the other hand, including the planktonic $\delta^{18}O$ values into the process of interpretation (associated relative changes in the $\delta^{18}O$ salinity signal) helps to identify temperature equations that provide physically realistic approaches for the temperature-salinity distribution in the upper water column, at least (see chapter 6.5.3). Although the temperature equations used in this study are afflicted with problems arising from the assessed $\delta^{18}O$ salinity signals, we regard our results as the most reasonable approximation. With the exception of the Pacific temperature equations of Dekens et al. (2002), all other temperature equations would suggest that the observed

new stage in the thermal structure of the tropical east Pacific upper water column between 4.0 Ma and 2.7 Ma was close to the modern one.

Slight thermal modifications resulted from a gradual cooling of about 1 °C in the mixed layer between 3.7 Ma and 2.7 Ma. After 2.7 Ma, the temperature gradient in the upper water column decreased significantly, caused by an additional drop in mixed layer temperatures of up to 2 °C and a warming of about 3 °C at the bottom of the photic zone after 2.7 Ma (**Fig. 6-7**). This suggests a deepening of the thermocline, probably in response to the intensification of the NHG and the development of significant cyclic variations in global ice volume after 2.75 Ma, as inferred from benthic $\delta^{18}O$ records (**Fig. 6-5b**). This finding contradicts the most recent assumption that the tropical climate was relatively stable during the mid-Pliocene intensification of global cooling (Ravelo et al. 2004).

Possible forcing mechanisms that come into question concerning the Pliocene development of the tropical east Pacific thermal structure of the upper water column are manifold. The long-term shoaling of the thermocline from 5.4 – 4.0 Ma (although accompanied by stepwise changes at 5.3 Ma and 4.5 Ma), and the gradual cooling of the mixed layer since 3.7 Ma imply a slow forcing mechanism. This suggests tectonic processes like the constriction of tropical gateways and mountain uplift as well as high latitude processes, like the development of the northern hemisphere ice cap, possible coupled to a reduction in atmospheric CO_2, as major candidates.

As the tropical Pacific is bordered by the IG to the west and by the CAS to the east, it is likely that changes in the configuration of these low-latitude gateways left a significant imprint on its surface hydrography. Although the timing of the constriction of the IG remains speculative, it was suggested that major changes in west Pacific surface hydrography associated with the constriction of the IG occurred during the middle to late Miocene and possibly close to the Pliocene/Pleistocene boundary (e.g. Hamilton, 1979; Kennett et al., 1985; Chaisson, 1995). More recently, Cane and Molnar (2001) and Molnar and Cane (2002) suggested that the constriction of the IG after 5.0 – 3.0 Ma may have played a major role for climate change during the Pliocene by strengthening the Walker Circulation over the Pacific and the trans-Pacific thermocline slope. These changes would be consistent with the shoaling of the thermocline in the east Pacific and with the gradual cooling in the mixed layer.

The timing of the stepwise changes in the thermocline shoaling, however, also suggests a close link to a critical threshold in the closure history of the CAS. Between 4.6 Ma and 4.2 Ma, surface water exchange between the Pacific and the Caribbean became significantly restricted (Keigwin, 1982a; Haug et al., 2001a; Steph et al., submitted a, see chapter 5). This is paralleled by a major step in subsurface cooling at Site 1241 after 4.5 Ma. The relationship between the emergence of the CAS and hydrographic changes in the tropical east Pacific is still a matter of debate. In case of an open Isthmus, General Circulation Model results predict a 10 Sverdrup (1 Sv = 10^6 m^3/sec) flow of low-saline NECC waters from the Pacific into the Caribbean due to higher Pacific sea level (Maier-Reimer et al., 1990). This is opposed by one Sverdrup of wind-driven surface water flow from the Caribbean into the Pacific. It was previously assumed that the inflow of warm, saline Caribbean surface water masses possibly maintained a deep thermocline in the east Pacific before the final

closure of the CAS (Farell et al., 1995). Although the exact timing of the final closure is still arguable, it did not occur significantly earlier than 2.7 Ma (e.g. Lundelius, 1987; Kameo and Sato, 2000). Accordingly, we do not expect that the wind driven inflow of Caribbean surface waters into the Pacific entirely ceased between 5 Ma and 4 Ma, thereby causing a significant thermocline shoaling in the tropical east Pacific during the early Pliocene. More recently, however, numerical model results provided a global mechanism that may link the early Pliocene thermocline shoaling to the changes in the configuration of the CAS. Oceanographers suggested that changes in rate of NADW production trigger global adjustments of the thermocline depth (e.g. Huang et al., 2000). The signal is carried from ocean to ocean by Kelvin and Rossby waves, inducing an upward (downward) movement of the main thermocline, when NADW formation is strong (weak). For example, model results predicted a 50 m thermocline shoaling in the Pacific for a 10 Sverdrup increase in NADW formation. In most modeling studies adressing the closure of the CAS, the closure-induced restriction of Pacific inflow into the Atlantic is associated with a salinity increase in the tropical Atlantic and with an intensification of the Gulf Stream system that introduces warm and saline waters to high northern latitudes, thereby favoring the production of North Atlantic Deep Water (NADW) and strengthening the meridional overturning (Maier-Reimer et al., 1990; Mikolajewicz and Crowley, 1997; Nisancioglu et al., 2003, Prange and Schulz, 2004). A strengthening of the NADW formation after the restiction of surface water exchange may thus have facilitated a shoaling of the tropical east Pacific thermocline. Indeed, considerable evidence from proxy data exists for enhanced NADW formation after 4.6 Ma (e.g. Haug and Tiedemann, 1998), thus parallel to the sea surface salinity increase in the Caribbean (4.7 – 4.2 Ma; e.g. Keigwin, 1982a; Haug et al., 2001a; Steph et al., submitted a, see chapter 5), and the major step of the observed thermocline shoaling in the tropical east Pacific (4.5 – 4.0 Ma).

Furthermore, the progressive shoaling of the CAS should have led to changes in atmospherical circulation, such as a strengthening of the Walker Circulation over the Pacific and changes in the trade wind strength that might have influenced Pacific surface current systems and the structure of the upper water column, as suggested by Hovan (1995), Cannariato and Ravelo (1997), Billups et al. (1999), and Chaisson and Ravelo (2000). A closure-induced warming of the Caribbean Basins after 4.6 – 4.4 Ma (Steph et al., submitted a, see chapter 5) may have caused the development of a pressure contrast between the western tropical Atlantic and the eastern tropical Pacific (Chaisson and Ravelo, 2000). This in turn was suggested to have strengthened the Walker Circulation over the tropical Pacific and increased the west-east thermocline tilt (Chaisson and Ravelo, 2000). Model results indicate an increase in sea level height within the WPWP region after the closure of the CAS (Maier-Reimer et al., 1990). A large hydraulic head in the WPWP due to more effective piling-up of warm surface waters may have increased the volume and velocity of the eastward flowing EUC (Maier-Reimer et al., 1990) that transports relatively cool, high saline waters into the tropical east Pacific at the thermocline level. This may have contributed to a shoaling of the thermocline as well. Moreover, strong support for an early Pliocene southward shift of the ITCZ comes from studies that investigated Atlantic and Pacific changes in tropical wind field and surface hydrography (Hovan, 1995; Farrell et al., 1995; Cannariato and Ravelo, 1997; Chaisson and Ravelo, 1997; Norris, 1998; Billups et al., 1998; 1999). Similar to the modern seasonal cycle, a

shift to a more southern position of the ITCZ in the tropical east Pacific would have weakened the southeast trades and thus significantly reduced the strength of the NECC and the SEC. A decrease in the return flow of warm water from the WPWP and a strengthened EUC thus may have allowed for the observed thermocline shoaling in the tropical east Pacific and in turn triggered the development of stronger tropical Pacific east-west gradients (Cannariato and Ravelo, 1997; Chaisson and Ravelo, 2000). In addition, this scenario is expected to cool the tropical east Pacific mixed layer, which however, is not observed in the interval between 4.8 Ma and 3.7 Ma (**Fig. 6-7**). Hence, it is not clear to what extent this mechanism may have contributed to a shoaling of the thermocline during the early Pliocene.

6.6.2 Salinity changes within the tropical east Pacific upper water column

The comparison of $\delta^{18}O$ records and Mg/Ca temperature estimates of planktonic foraminifers from tropical east Pacific Site 1241 (**Figs. 6-5, 6-7**) documents that local variations in salinity have exerted a much stronger influence on tropical east Pacific upper ocean hydrography than previously assumed (Cannariato and Ravelo, 1997; Chaisson and Ravelo, 2000). The shoaling of the thermocline from 5.4 – 4.0 Ma, as indicated by Mg/Ca temperatures, was associated with a salinity increase in the thermocline and a decrease at the bottom of the photic zone, whereas the salinity in the mixed layer remained relatively constant. The shoaling of the thermocline was probably associated with a strengthened influence of the EUC on the thermocline, if the EUC was saltier than the NECC, as it is today. This may explain the salinity increase at the thermocline level. However, we then would also expect a salinity increase at the bottom of the photic zone, which is not observed. Whether the shoaling of the CAS and the reduced exchange of surface waters possibly influenced the salinity structure in the tropical east Pacific remains speculative. The salinity decrease in the mixed layer from 3.7 Ma to 2.5 Ma is interpreted to reflect the development of the modern low salinity tongue, expanding from the Panama Basin towards the west. Today, low SSS in the Panama Basin is coupled to high precipitation/evaporation ratios within the ITCZ region, whereas a significant portion of the net freshwater flux originates in the Atlantic and Caribbean and is transported to the Panama Basin *via* the trade winds (Jousaumme et al., 1986). The ultimate cause for the freshening of the tropical east Pacific after 3.7 Ma is elusive, but possible mechanisms include the gradual shoaling of the CAS, northern hemisphere cooling, a southward shift of the ITCZ as well as changes in the net moisture flux. The freshening should have increased the stratification in the upper water column, especially after 3.3 Ma, when the decrease in salinity was also registered by the thermocline-dwellers. However, *G. tumida* also registered a salinity decrease at the bottom of the photic zone and thus, we cannot exclude an influence from sub-thermocline waters. This change in sub-thermocline salinity was associated with a $\delta^{13}C$ shift towards higher values at the bottom of the photic zone and at the thermocline.

6.6.3 Regional variations in tropical east Pacific upper ocean signatures

The modern tropical east Pacific is marked by pronounced climatic and oceanographic gradients over only a few degrees of latitude (**Fig. 6-1**). To examine regional variations in Pliocene tropical east Pacific upper ocean signatures, we compared planktonic stable isotope records from Site 1241 with those from Site 851 (Cannariato and Ravelo, 1997). Today, Site 851 is located about 3° southward of Site 1241 and about 26° further to the west. Site 1241 lies within the relatively warm, low saline waters of the NECC, whereas Site 851 is positioned at the NECC/SEC boundary with the EUC in its subsurface. About 6 Ma ago, the position of Site 1241 was ca. 2.5° further to the south and Site 851 was located ca. 0.5° further to the south, as suggested by their tectonic backtrack paths (Duncan and Clague, 1985; Pisias et al., 1995; Mix, et al., 2003) (**Fig. 6-1**). If the late Miocene oceanic surface circulation was similar to the recent pattern, both sites were then located close to the boundary of the SEC/NECC. Accordingly, late Miocene to early Pliocene latitudinal changes in surface hydrography would have affected both sites in similar ways. On the other hand, differences in upper ocean water mass signatures between Sites 1241 and 851 would rather indicate longitudinal changes, possibly in response to the progressive closure of the CAS. During the last 7 Ma, Site 1241 moved out of the equatorial upwelling region into the NECC, whereas Site 851 remained close to the SEC/NECC boundary (**Fig. 6-1**). Therefore, latitudinal differences in upper ocean hydrography between both sites may have left a stronger imprint in more recent times.

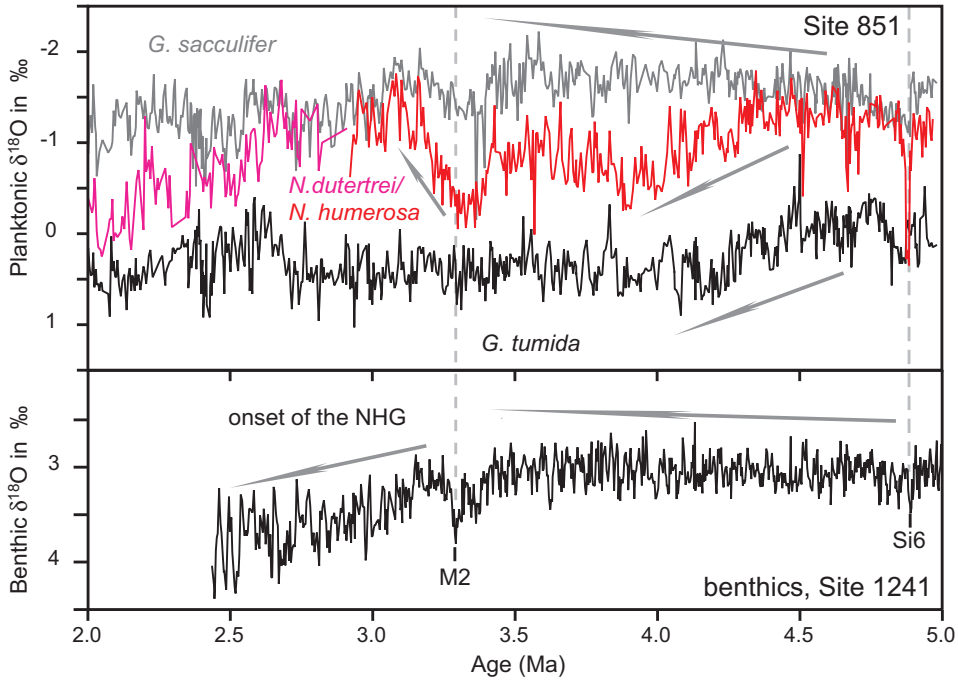

Fig.6-10 Multispecies planktonic $\delta^{18}O$ records from Site 851 (top; Cannariato and Ravelo, 1997) compared to the benthic $\delta^{18}O$ record of Site 1241 (bottom), (Tiedemann et al., submitted, see chapter 4). Top: gray line: *G. sacculifer*, red line: *N. humerosa*, pink line: *N. dutertrei*, black line: *G. tumida*. Values for *N. humerosa* were not corrected to the *N. dutertrei* record (see Cannariato and Ravelo, 1997). Marine Isotope Stages (MIS) Si6 (ca. 4.9 Ma) and M2 (ca. 3.3 Ma) are indicated. Gray arrows mark major trends in planktonic and benthic $\delta^{18}O$ records. Note the exceptionally high $\delta^{18}O$ values of *N. humerosa* during MIS Si6.

Figures 6-5, 6-10, 6-11, and **6-12** compare the planktonic stable isotope records of Sites 1241 (5.7 – 2.5 Ma) and 851 (5.0 – 2.0 Ma). In general, oxygen isotope patterns and trends of *G. sacculifer*, *N. dutertrei*/*N. humerosa* and *G. tumida* were similar at both sites between 5 Ma and 2.5 Ma (**Figs. 6-5, 6-10**). The increase in the $\delta^{18}O$ gradient within the upper water column was observed at both sites during the time interval between 4.7 Ma and 4.2 Ma, indicating that the early Pliocene shoaling of the tropical east Pacific thermocline was a regional phenomenon.

The use of similar size fractions of *G. sacculifer* and *G. tumida* for stable isotope analyses at Site 1241 and Site 851 (Cannariato and Ravelo, 1997) allows for the direct comparison of the absolute $\delta^{18}O$ and $\delta^{13}C$ values. We did not directly compare the *N. dutertrei* record of Site 1241 with the *N. dutertrei*/*N. humerosa* record of Site 851 because of uncertainties concerning species-specific and size-related isotopic offsets between the two sites.

The comparison of $\delta^{18}O$ and $\delta^{13}C$ records of *G. sacculifer* from Sites 851 (Cannariato and Ravelo, 1997) and 1241 indicates that surface mixed layer conditions were almost identical at both sites between 5.0 Ma and 2.5 Ma showing equal absolute values, isotope patterns and amplitude variations with respect to the error range of the analyses and stratigraphic uncertainties (**Figs. 6-11, 6-12**). Assuming that temperature differences between the two sites did not play a significant role, this would imply that both sites were located within similar surface water masses.

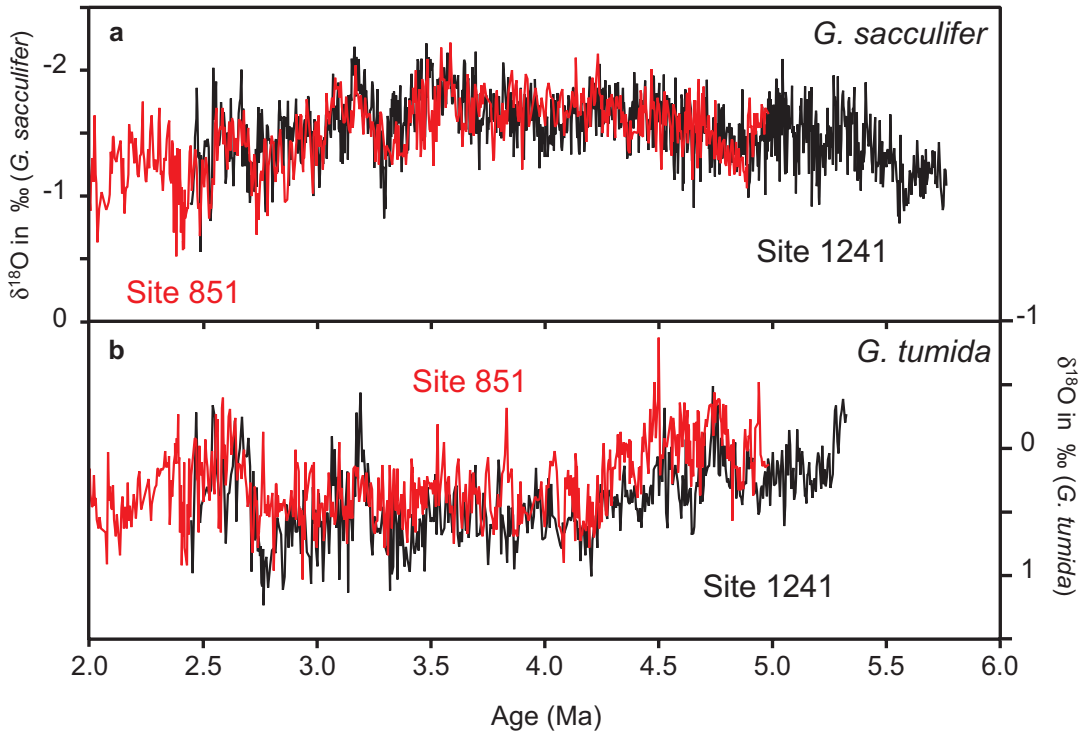

Fig. 6-11 Comparison between planktonic $\delta^{18}O$ records from Sites 1241 (this study) and Site 851 (Cannariato and Ravelo, 1997). **a**: *G. sacculifer* records. Black line: Site 1241; red line: Site 851. **b**: *G. tumida* records. Black line: Site 1241; red line: Site 851.

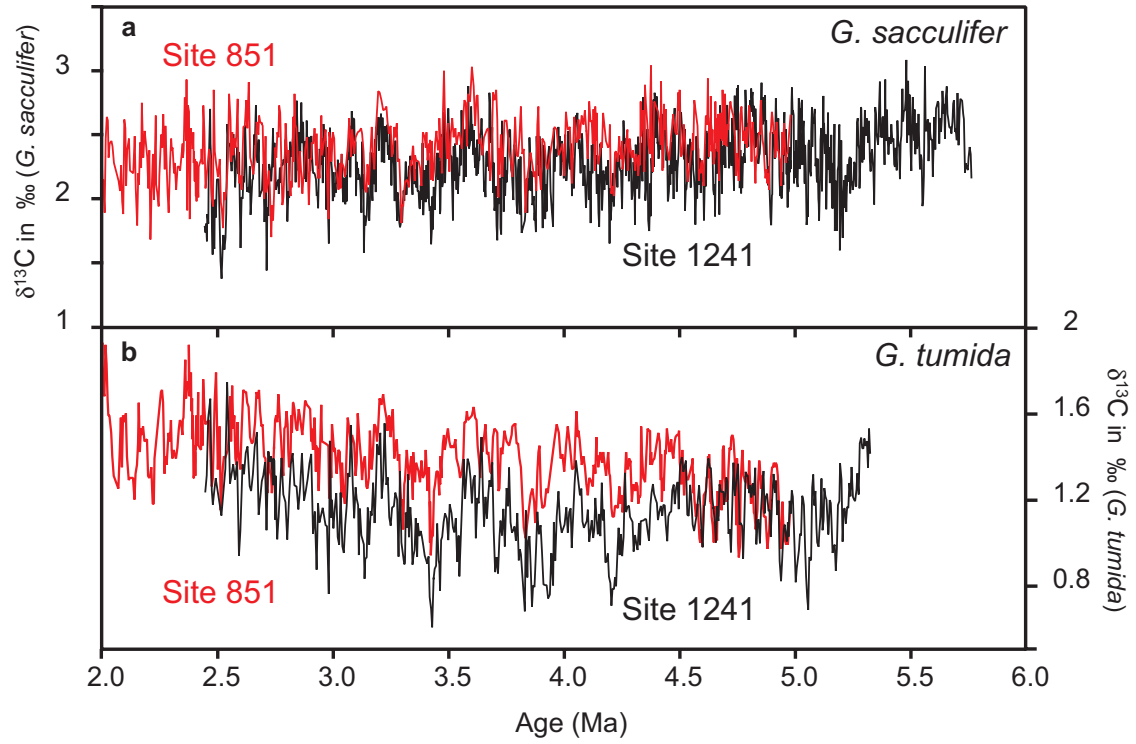

Fig. 6-12 Comparison between planktonic $\delta^{13}C$ records from Sites 1241 (this study) and Site 851 (Cannariato and Ravelo, 1997). **a**: *G. sacculifer* records. Black line: Site 1241; red line: Site 851. **b**: *G. tumida* records. Black line: Site 1241; red line: Site 851.

Considering the similarity of the *G. sacculifer* stable isotope records from Sites 1241 and 851, the warm, low saline waters of the NECC probably reached slightly further south during the early Pliocene, so that both sites were equally influenced by NECC waters between 5.0 Ma and 2.5 Ma. If the SEC exerted a major control on both sites during the late Miocene and early Pliocene, we would expect a warming of the mixed layer temperatures at Site 1241 due to the northward movement of Site 1241 away from the SEC/NECC boundary (**Fig. 6-4**). This should lead to the development of a $\delta^{18}O_{G.\ sacculifer}$ gradient between both sites, if not fully compensated by salinity changes. The SST estimates for *G. sacculifer* at Site 1241 indicate a slight warming of about 1 °C between 4.8 Ma and 3.7 Ma (Groeneveld et al., submitted a) (**Fig. 6-7**), whereas the expected development of $\delta^{18}O$ gradients between both sites after 5 – 4 Ma was not observed (**Fig. 6-11**). In addition, the absence of $\delta^{18}O_{G.\ sacculifer}$ gradients between both sites contradicts a distinct influence of Caribbean surface waters on Pliocene tropical east Pacific surface hydrography. Significant inflow of warm, high saline Caribbean surface waters would have had a stronger imprint at Site 1241 than at Site 851, as it was located closer to the final openings of the CAS (Savin and Douglas, 1985; Duque-Caro, 1990; Collins et al., 1996; Coates et al., 2004).

Small regional differences occur between Sites 851 and 1241, when comparing the stable isotope records of *G. tumida* (**Figs. 6-11, 6-12**). The general increase of $\delta^{18}O_{G.tumida}$ at both sites is supported by a decrease of Mg/Ca temperatures of *G. tumida* at Site 1241, indicating the early Pliocene shallowing of the tropical east Pacific thermocline with a major $\delta^{18}O$ increase between

4.7 Ma and 4.2 Ma. However, the $\delta^{18}O$ values of *G. tumida* were generally lower at the more western Site 851 before 4.2 Ma, indicating either higher temperatures or lower salinities at the bottom of the photic zone (**Fig. 6-11**). This may point to a slightly deeper thermocline at the more western Site 851 due to longitudinal variations in upper ocean hydrography. After 4.2 Ma, no major latitudinal or longitudinal differences in $\delta^{18}O$ signatures at the bottom of the photic zone are displayed by the comparison of $\delta^{18}O_{G.\ tumida}$ records from Sites 851 and 1241. The $\delta^{13}C$ values of *G. tumida* were enriched by up to 0.5 ‰ at Site 851 with respect to Site 1241 during the interval between 4.5 Ma and 2.5 Ma (**Fig. 6-12**). Higher $\delta^{13}C$ values may indicate either an enhanced influence of nutrient depleted water masses, or lower nutrient contents at the bottom of the photic zone at Site 851. To explain these differences in $\delta^{13}C$ by regional differences in oceanography is difficult. Since Site 851 was constantly located closer to the SEC/NECC boundary with the nutrient-enriched EUC in the subsurface (**Fig. 6-1**), we would rather expect the nutrient contents in the subsurface to be higher and the $\delta^{13}C$ values to be lower. The observed shift to generally higher $\delta^{13}C$ values in the deep-dweller records at Site 1241 after 3.3 Ma to 3.2 Ma (MIS M2) was also reported for Site 851 by Cannariato and Ravelo (1997). They interpreted the $\delta^{13}C$-shift as a change in the source of upwelling intermediate waters after 3.2 Ma.

6.6.4 $\delta^{13}C$-shift in tropical Pacific subsurface waters after 3.3 Ma

The $\delta^{13}C$ records of the deep-dwelling planktonic foraminifers (Sites 1241 and 851) indicate a gradual increase of 0.5 ‰ after 3.3 – 3.2 Ma (MIS M2) (**Fig. 6-9**). This increase is neither reflected in the global signal of the benthic $\delta^{13}C$ record nor in the $\delta^{13}C$ of the mixed layer-dweller *G. sacculifer* at Site 1241. The timing of this shift is closely linked to the first cooling steps of the intensification of the NHG. As similar changes were also observed in a deep-dweller record from the western tropical Pacific (Whitman and Berger, 1993), it is likely that these variations in $\delta^{13}C$ are a regional phenomenon affecting the entire tropical Pacific thermocline, rather than resulting from local changes in upper-ocean nutrient cycling. Accordingly, Cannariato and Ravelo (1997) interpreted the increase in tropical Pacific thermocline ventilation to indicate a change in the high-latitude source of upwelled intermediate water, or increased productivity in the source region of intermediate water.

The Southern Ocean is thought to be an important source for tropical thermocline ventilation, as intermediate water masses formed in high latitudes become entrained into the thermocline on their way north and feed the EUC near the equator (Toggweiler, 1991). Paleoceanographic studies demonstrated that the tropical thermocline $\delta^{13}C$ signal originates partly in high latitudes and is transferred to the low-latitude thermocline as a preformed signal (Oppo and Fairbanks, 1989; McKenna et al., 1995; Ninnemann and Charles, 1997; Spero and Lea, 2002; Spero et al., 2003). Antarctic Intermediate Water (AAIW) and Subantarctic Mode Water (SAMW) provide the necessary conduit by which these two areas are linked, as first suggested by Oppo and Fairbanks (1989). The intermediate water is injected into the thermocline at the northern edge of the Antarctic Circumpolar Current and moves northward, becoming entrained in, and transported to the east by the EUC. In a general sense, the tropical thermocline-dweller *N. dutertrei* may therefore record changes in the Pliocene nutrient and carbon isotopic chemistry of waters at the Polar Front and/or

Subantarctic Front, as the source of the EUC is derived from SAMW/AAIW (Toggweiler et al., 1991; Loubere, 2000, 2001). Spero and Lea (2002) and Spero et al. (2003), for instance, interpreted Pleistocene $\delta^{13}C$ records of *N. dutertrei* near the Galapagos Islands to reflect high latitude $\delta^{13}C$ changes.

Recently, Carter et al. (2004) suggested more, shallower and faster intermediate water flow at the Canterbury Drift in the southwest Pacific after 3.25 Ma. They attributed these changes to the development of the Subantarctic Front and/or to an enhanced formation of SAMW. To detect possible links between Pliocene changes in $\delta^{13}C$ signatures of southeast Pacific AAIW and the $\delta^{13}C$ increase within the tropical Pacific thermocline at about 3.3 Ma, we compared the $\delta^{13}C$ record of the thermocline-dwelling foraminifer *N. dutertrei* from Site 1241 to the benthic $\delta^{13}C$ record of Site 1236 (Tiedemann et al., submitted, see chapter 4) (**Fig. 6-13**). Today, Site 1236 is located on the Nazca Ridge in a water depth of 1323 m. During the early Pliocene, it may have been a few hundred meters shallower due to its subsidence history (Mix et al., 2003). The relatively shallow depth of the site makes it suitable for monitoring intermediate water chemistry in the open ocean. From 5.3 Ma to 2.3 Ma, high benthic $\delta^{13}C$ values (0 – 0.8 ‰) at Site 1236 indicate the presence of AAIW. However, the $\delta^{13}C$ signature of the AAIW indicates no major change after 3.3 Ma. It is thus unlikely that the Pliocene $\delta^{13}C$ shift within the tropical Pacific thermocline monitored by *N. dutertrei* at Site 1241 was transferred to the tropics by AAIW formed in the southeast Pacific sector of the Southern Ocean. If Pliocene changes in Southern Ocean intermediate water composition can account for the observed changes in ventilation of the tropical Pacific thermocline, their source either derived from the shallower SAMW component of intermediate waters, or the source region was located in the high-latitude southwest Pacific and was marked by different preformed $\delta^{13}C$ values.

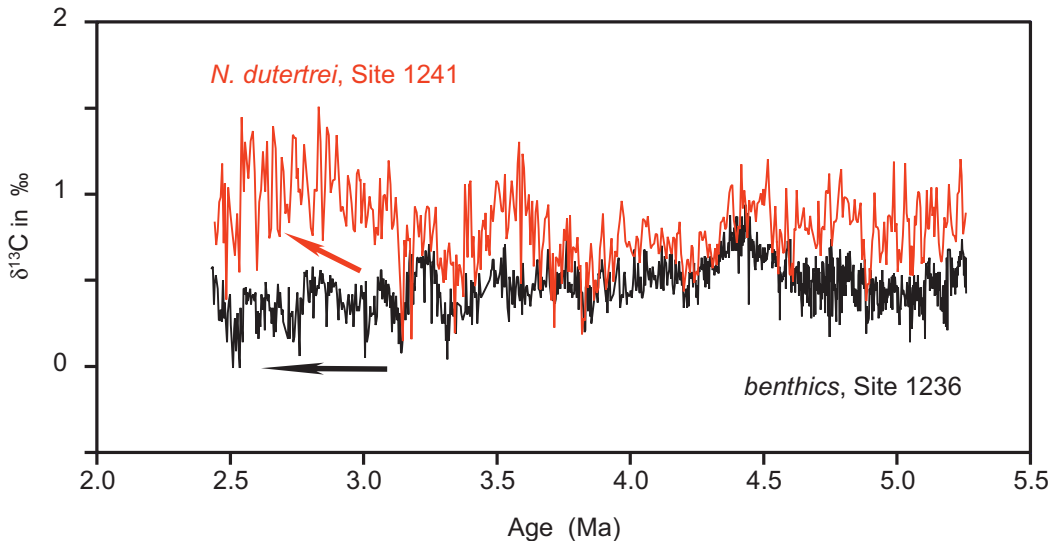

Fig. 6-13 $\delta^{13}C$ record of the thermocline-dweller *N. dutertrei* (red line) from Site 1241 plotted with the benthic $\delta^{13}C$ record (black line) from Site 1236 (Nazca Ridge; 1323 m water depth, Tiedemann et al., submitted, see chapter 4). The relatively shallow position of Site 1236 makes it suitable for monitoring changes in intermediate water composition. Arrows indicate that the $\delta^{13}C$ shift in the tropical east Pacific thermocline (*N. dutertrei*, Site 1241) is not mirrored in the intermediate water $\delta^{13}C$ record from Site 1236.

6.7 Summary and Conclusions

In comparison to other planktonic stable isotope studies that examined the Pliocene tropical east Pacific (Cannariato and Ravelo, 1997), this study provides for the first time both Mg/Ca temperature estimates, and stable isotope records from shallow- and deep-dwelling planktonic foraminifers that span the time interval from 5.5 - 2.5 Ma. This allows for the differentiation between temperature and salinity changes in the upper water column and sheds new light on variations in the thermal structure of the tropical east Pacific upper water column. The main conclusions include the following:

1. From 4.8 Ma to 3.7 Ma, the Mg/Ca-derived mixed-layer temperatures remained relatively constant (Groeneveld et al., submitted a). At the bottom of the photic zone, however, *G. tumida* records a temperature decrease of 6 °C from 21 °C to 15 °C between 5.4 Ma and 4 Ma. Major cooling steps occurred after 5.3 Ma and 4.5 Ma. The associated increase of the temperature gradient between the mixed layer and the bottom of the photic zone documents the early Pliocene shoaling of the east Pacific thermocline. Temperatures within the thermocline remained relatively stable over this interval, as implied by the Mg/Ca records of *N. dutertrei* (18 – 19°C) and *G. limbata* (19 – 21 °C). The temperature gradient between the mixed layer dweller *G. sacculifer* and the thermocline-dweller *N. dutertrei* was relatively constant with 6 – 7 °C. The shoaling of the thermocline was associated with a salinity increase in the thermocline and a decrease at the bottom of the photic zone, whereas the salinity in the mixed layer remained relatively constant. The early Pliocene shoaling of the thermocline was probably associated with a reorganization of tropical east Pacific surface water circulation in response to tropical gateway dynamics (IG, CAS). The timing of the shoaling, however, suggests a link to the critical threshold in the closure history of the CAS that significantly restricted the Caribbean-Pacific surface water exchange between 4.6 Ma and 4.2 Ma.

2. The time interval from 3.7 Ma to 2.5 Ma was marked by a long-term cooling trend in the mixed layer of ~3 °C. This decrease did not affect thermocline temperatures. The temperature at the bottom of the photic zone remained relatively stable until 2.7 Ma but shows a slight warming trend from 2.7 Ma to 2.5 Ma. This warming may suggest a slight deepening of the thermocline. The tropical cooling of the mixed layer is paralleled by a decrease in SSS and is interpreted to reflect the development of the modern low salinity tongue, expanding from the Panama Basin towards the west. The gradual cooling and freshening of tropical east Pacific surface waters suggests slow tectonic forcing as a possible cause, although other mechanisms like northern hemisphere cooling, a southward shift of the ITCZ, as well as changes in the net moisture flux across the Isthmus of Panama may have contributed to the observed changes.

The decrease in SSS since 3.7 Ma was paralleled by a salinity decrease within the thermocline after 3.3 Ma. Whether this change reflects a freshening from the mixed layer or from sub-thermocline waters is not clear for the interval from 3.3 – 3.1 Ma, as the salinity at the bottom of the photic zone also decreased during this period.

3. Regional variations in Pliocene tropical east Pacific upper ocean hydrography were weak, as indicated by the comparison of planktonic stable isotope records from Sites 1241 and 851. The similarity of their *G. sacculifer* $\delta^{18}O$ and $\delta^{13}C$ records implies that both sites were affected by the same surface water masses from 5 Ma to 2.5 Ma. This was most likely the NECC, as no latitudinal gradients developed between the two sites when Site 1241 moved out of the SEC/NECC boundary and the equatorial upwelling region.

4. The $\delta^{13}C$ increase in deep-dweller records of Sites 1241 and 851 (Cannariato and Ravelo, 1997) after 3.3 – 3.2 Ma was previously interpreted to reflect changes in the source region of high-latitude intermediate waters that feed the EUC and the tropical Pacific thermocline (Cannariato and Ravelo, 1997). The timing of this shift parallels an increase and a shoaling of intermediate water flow close to New Zealand after 3.25 Ma (Carter et al., 2004). However, these changes in $\delta^{13}C$ were not registered in the benthic $\delta^{13}C$ record from intermediate water Site 1236, reflecting AAIW signatures from the southeast Pacific sector of the Southern Ocean.

Acknowledgements

We like to thank J. Schönfeld, H. Kinkel, L. Reuning and M. Regenberg for stimulating discussions and criticism at different stages of this study. The manuscript benefited significantly from reviews by……. We also thank W.P. Chaisson and A. Holbourn for help with species determination, H. Kinkel for providing the SEM pictures, and U. Nielsen, A. Jesußek, L. Haxhiaj and S. Koch for technical assistance. We thank the crew of the Joides Resolution and the Leg 202 science party for an exceptionally successful expedition. This study was performed within the DFG Research Unit FOR 451 (Impact of Gateways on Ocean Circulation, Climate and Evolution; funding under Ti240/12).

CHAPTER 7

IMPACT OF PANAMA UPLIFT ON CHANGES IN CARIBBEAN AND TROPICAL EAST PACIFIC UPPER OCEAN STRATIFICATION –

COMPARISON OF PALEOCEANOGRAPHIC RECONSTRUCTIONS AND NUMERICAL MODEL RESULTS

This short outline represents the current status of a planned publication (Steph, Groeneveld, Schmittner, Tiedemann and Nürnberg, in prep.) that will combine results from modeling studies (Schmittner) and paleoceanographic reconstructions (Steph, Groeneveld) to further assess and to understand the role of Panama uplift on observed changes in Pacific-Caribbean upper ocean water mass signatures. This comparison is especially important for interpreting marine proxy records from the equatorial east Pacific, as possible overlapping effects from changes in the configuration of the Indonesian Gateway may also have influenced the Pliocene tropical east Pacific surface water signal. The modeling experiments adressed scenarios for an open and closed Central American Seaway, without considering possible changes in the Indonesian throughflow. Thus, major discrepancies between paleoceanographic reconstructions and modeling results may provide hints for additional forcing mechanisms, possibly resulting from Pliocene changes in the source region and/or the volume transport of the Indonesian throughflow and associated changes in atmospheric and upper ocean circulation (as suggested by Cane and Molnar, 2001).

7.1 Paleoceanographic evidence

$\delta^{18}O$ and Mg/Ca temperature records of planktonic foraminifers with different habitat depths from tropical east Pacific Site 1241 (**Fig. 7-1,** Steph et al., submitted b; see chapter 6) and Caribbean Sites 999, 1000 (**Fig. 7-2 a, b**) were used to compare and evaluate Pliocene changes in Caribbean and tropical east Pacific upper ocean stratification. At tropical east Pacific Site 1241, the mixed layer-dweller *G. sacculifer*, the thermocline-dwellers *G. limbata* (dextral), and *N. dutertrei*, and the deep-dweller *G. tumida* (preferably living at the bottom of the photic zone) were used for analyses (see chapter 6). In general, an increase in the temperature difference between shallow- and deep-dwelling species is considered to reflect a shoaling of the thermocline (e.g. Ravelo and Fairbanks, 1992; see chapter 6). This interpretation postulates that the planktonic foraminiferal species did not

significantly change their habitat depth over time. Unfortunately, the deep-dweller *G. tumida*, whose habitat depth is considered as being nearly constant within the tropics, is absent in the Pliocene section of Caribbean Sites 999 and 1000. Thus, the investigation had to be solely based on the shallow-dweller *G. sacculifer*, and the thermocline-dwelling species *G. limbata* and *N. dutertrei*. *G. limbata*, as the modern *G. menardii*, is considered to have calcified in the upper to middle thermocline, whereas *N. dutertrei* presumably calcified in the middle to lower thermocline, probably coupled to the chlorophyll maximum (see chapter 6). The study of Caribbean Sites 999 and 1000 is thus biased by the fact that the thermocline-dwelling species probably migrated to deeper habitats when the thermocline deepened, or to shallower depths when the thermocline shoaled. If the habitat of these species was indeed coupled to the depth of the thermocline, we would expect that their calcification temperature remained relatively constant, as long as sea surface temperature did not change significantly. This is for example valid for tropical east Pacific Site 1241 throughout the Pliocene, where especially the calcification temperature of *N. dutertrei* remained relatively stable, although the thermocline shoaled through time (between 5.3 Ma and 4.0 Ma), as documented by a temperature decrease at the bottom of the photic zone that is recorded by *G. tumida* (**Fig. 7-1**, see chapter 6 for extended discussion). Thus, we assume that strong variations in the thermocline temperature only occur if the sea surface temperature underlies significant changes.

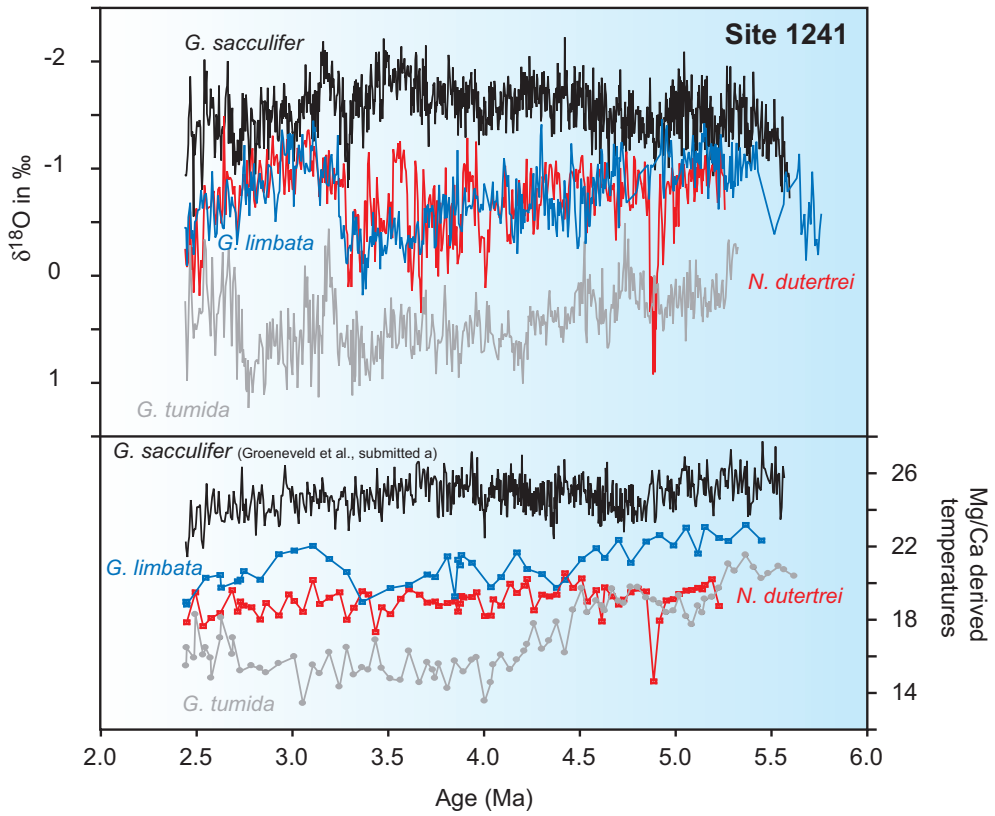

Fig. 7-1 Pliocene planktonic $\delta^{18}O$ (top) and Mg/Ca records (bottom) from planktonic foraminifers living in different habitat depths, Site 1241: black line: *G. sacculifer* (mixed layer); Red line: *N. dutertrei* (lower thermocline), Blue line: *G. limbata* (upper thermocline), Gray line: *G. tumida* (bottom of the photic zone).

Pliocene variations in tropical east Pacific upper ocean water mass signatures were extensively discussed in chapter 6. The most important change that was observed is the increase of the $\delta^{18}O$ gradient in the upper water column between 5.4 Ma and 3.3 Ma that was accompanied by a 6 °C temperature decrease at the bottom of the photic zone between 5.4 Ma and 4.0 Ma (**Fig. 7-1**). This is interpreted to reflect an early Pliocene shoaling of the thermocline in the tropical east Pacific. The timing of this event suggests a close link to changes in the configuration of the CAS, as the thermocline shoaling almost parallels the development of the modern Atlantic-Pacific salinity contrast that marks the restriction of Pacific-Caribbean surface water exchange (Haug et al., 2001a; see chapter 5 for extended discussion). The forcing mechanisms for thermocline shoaling in the tropical east Pacific are still arguable, but may e.g. include changes in the tropical wind field (Cannariato and Ravelo, 1997; Chaisson and Ravelo, 2000) or an increase in North Atlantic Deep Water (NADW) formation (Haug and Tiedemann, 1998) that may have triggered a global shoaling of the thermocline (e.g. Huang et al., 2000; see chapter 6). Temperatures within the mixed layer and at the thermocline level, however, remained comparatively stable at tropical east Pacific Site 1241. The deviation of $\delta^{18}O$ records and Mg/Ca temperature estimates from thermocline-dwelling foraminifers aditionally suggests that local changes in salinity exerted a much stronger control on Pliocene tropical east Pacific upper ocean water mass signatures than previously assumed by Cannariato and Ravelo (1997).

The Pliocene development of Caribbean upper ocean water mass signatures differed significantly from that in the tropical east Pacific, as indicated by $\delta^{18}O$ and Mg/Ca data from shallow- and deep-dwelling planktonic foraminifers from Caribbean Sites 999 and 1000. **Figures 7-2 a and 7-2 b** show the $\delta^{18}O$ and Mg/Ca temperature records of *G. sacculifer*, *G. limbata* (dextral) and *N. dutertrei* from these sites for the time interval from 5.5 – 2.5 Ma (Mg/Ca data for *G. sacculifer* were provided by the PhD thesis of J. Groeneveld). The $\delta^{18}O_{G.\ sacculifer}$ records from Caribbean Sites 999 (Haug et al., 2001a) and 1000 are discussed in detail in chapter 5. The $\delta^{18}O$ increase within the Caribbean mixed layer after 4.6 – 4.2 Ma was attributed to an increase in Caribbean sea surface salinity (SSS) due to the restriction of surface water exchange between Pacific and Caribbean (e.g. Haug et al., 2001a). Higher $\delta^{18}O$ values at northern Site 1000 thereby suggest a much stronger salinity increase towards the north, indicating strong local gradients in Caribbean SSS (see chapter 5 for an extended discussion).

Mixed layer temperatures at southern Caribbean Site 999 (Groeneveld et al., in prep.; **Fig. 7-2 a**) show no major trend over the course of the Pliocene, and absolute values (~22 – 27 °C) are similar to those observed at tropical east Pacific Site 1241 (Groeneveld et al., submitted a; **Fig. 7-1**). This implies that Site 999, located close to the final openings of the CAS, was still under the influence of relatively cool Pacific surface waters (Groeneveld et al., in prep.). Mg/Ca temperatures of *G. sacculifer* at northern Caribbean Site 1000, however, indicate a warming of the mixed layer after 4.4 Ma, with a timing coeval to the increase in Caribbean SSS (Groeneveld et al., submitted b, **Fig. 7-2 b**). The temperature increase within the mixed layer at northern Site 1000 is paralleled by a warming of ~4 – 5 °C at the lower thermocline level (*N. dutertrei*) at both Caribbean Sites, 999 and 1000, after 4.5 Ma. This warming at the thermocline level may either have been associated with the increase in Caribbean SST (only documented at Site 1000), or caused

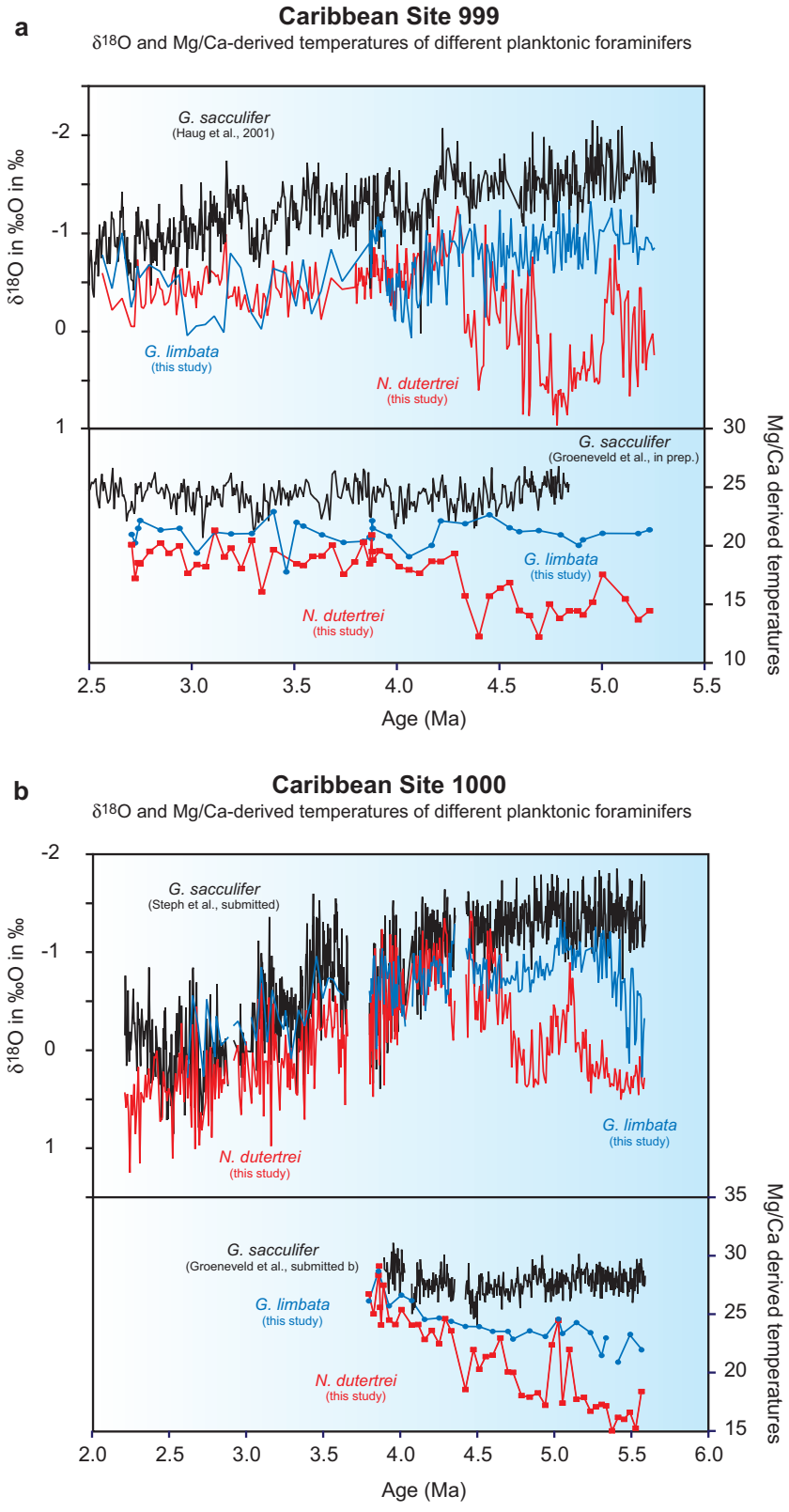

Fig. 7-2 Planktonic $\delta^{18}O$ and Mg/Ca records from planktonic foraminifers living in different habitat depths, **a**:Site 999; **b**: Site 1000: black line: *G. sacculifer* (mixed layer); Red line: *N. dutertrei* (lower thermocline), Blue line: *G. limbata* (upper thermocline).

by a deepening of the Caribbean thermocline, possibly related to the strengthening of the Caribbean/West Atlantic Warm Pool. However, the warming is not mirrored by the Mg/Ca temperature record of *G. limbata* (upper thermocline) at Site 999, and only weakly expressed in the Mg/Ca temperature record of *G. limbata* at Site 1000 (**Figs. 7-2 a, b**). This may indicate that the lower thermocline (habitat of *N. dutertrei*) was subject to stronger temperature changes than the upper thermocline (habitat of *G. limbata*), or may point to pronounced habitat changes of *G. limbata* and/or *N. dutertrei*. The early Pliocene subsurface warming in the Caribbean is in strong contrast to the thermal evolution of the Pacific upper water column, as it parallels the observed thermocline shoaling at Site 1241.

Furthermore, the deviation of Mg/Ca temperatures and $\delta^{18}O$ records of the thermocline-dwelling species indicates that Caribbean thermocline waters were also biased by strong changes in salinity. The ~1 ‰ decrease in $\delta^{18}O$ of *N. dutertrei* after 4.5 Ma is observed at both Caribbean sites and can more or less account for the Mg/Ca derived warming of 4 – 5 °C (**Fig. 7-2 a, b**). After 4.3 Ma, however, thermocline temperatures at Site 999 remained relatively stable, whereas the thermocline temperatures at Site 1000 increased slightly until 3.8 Ma. In contrast, the $\delta^{18}O$ records of the thermocline-dwellers from both Caribbean sites show an increase that is comparable to the $\delta^{18}O$ increase observed within the mixed layer at each site after 4.6 – 4.2 Ma (**Fig. 7-2 a, b**). This implies that analogue to the mixed layer salinity, the thermocline salinity also increased at both sites. The $\delta^{18}O$ increase at the thermocline level was again stronger at the more northern Site 1000, suggesting a salinity gradient between both Caribbean sites at the thermocline level comparable to that recorded in the mixed layer (see chapter 5).

Figure 7-3 summarizes shallow- and deep-dweller Mg/Ca temperature and $\delta^{18}O$ records from Caribbean Site 999 and tropical east Pacific Site 1241, emphasizing the paleoceanographic evidence for an opposite development of the Caribbean and tropical east Pacific upper water column during the restriction of surface water exchange between Pacific and Caribbean. This is documented by a thermocline shoaling in the tropical east Pacific, and a concomitant warming and/or deepening of the Caribbean thermocline that may point to a strengthening of the Caribbean/West Atlantic Warm Pool.

7.2 Implications from modeling experiments

The modeling experiments (**Fig. 7-4**) were carried out with the UVic Earth System Climate Model (UVic-ESCM Version 2.6). The UVic ESCM is a coarse resolution model of intermediate complexity. The ocean general circulation model is based on MOM-2 (Pacanowski, 1995) with eddy-induced tracer mixing paramerterized according to Gent and McWilliams (1990). The horizontal resolution of the model is 1.8 x 3.6 degrees, with 19 vertical layers of 50 – 500 m thickness (increasing with depth). In the model setup, the vertical diffusion (Kv) increases from 0.3 cm^2s^{-1} at the surface to about 1.3 cm^2s^{-1} at 5000 m depth (Schneider and Schmittner, submitted). The ocean model component is coupled to a vertically integrated energy-moisture balance model of the atmosphere and to a dynamic-thermodynamic sea ice component (Bitz et al., 2001).

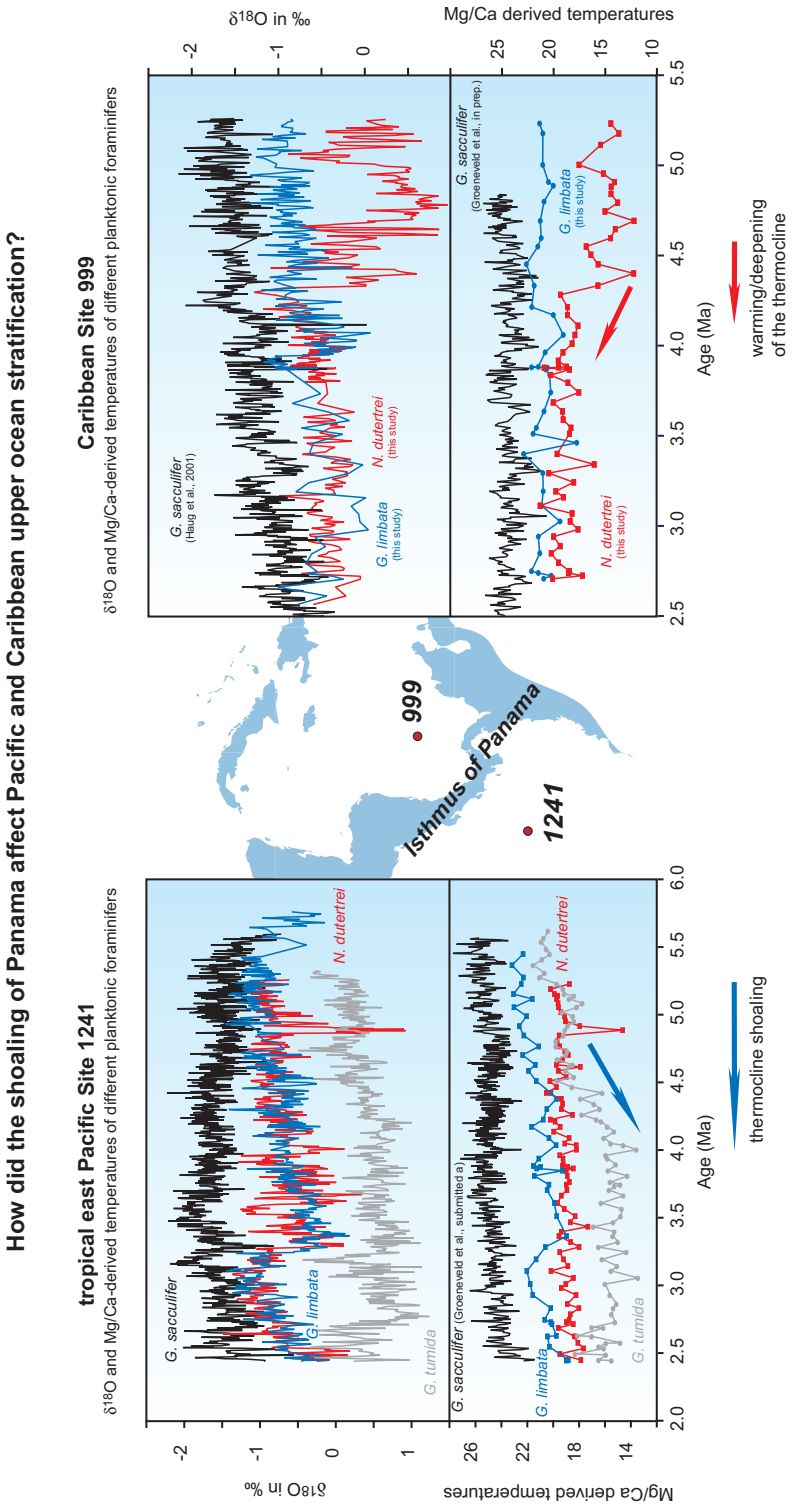

Fig.7-3 Comparison of Pacific (Site 1241) and Caribbean (Site 999) $\delta^{18}O$ and Mg/Ca-temperature records for planktonic foraminifers with different habitat depths: *G. sacculifer*: mixed layer; *N. dutertrei*, *G. limbata* (dextral): thermocline, *G. tumida*: bottom of the photic zone. The increase in $\delta^{18}O$ and Mg/Ca temperature gradients in the upper water column at tropical east Pacific Site 1241 between 5.3 – 4.0 Ma was interpreted as an early Pliocene thermocline shoaling. The decrease in $\delta^{18}O$ and Mg/Ca temperature gradients at Caribbean Site 999 between 4.5 Ma and 4.0 Ma has been interpreted as a warming/deepening of the thermocline. The timing of these changes suggests a close link to the closure history of the Central American Seaway.

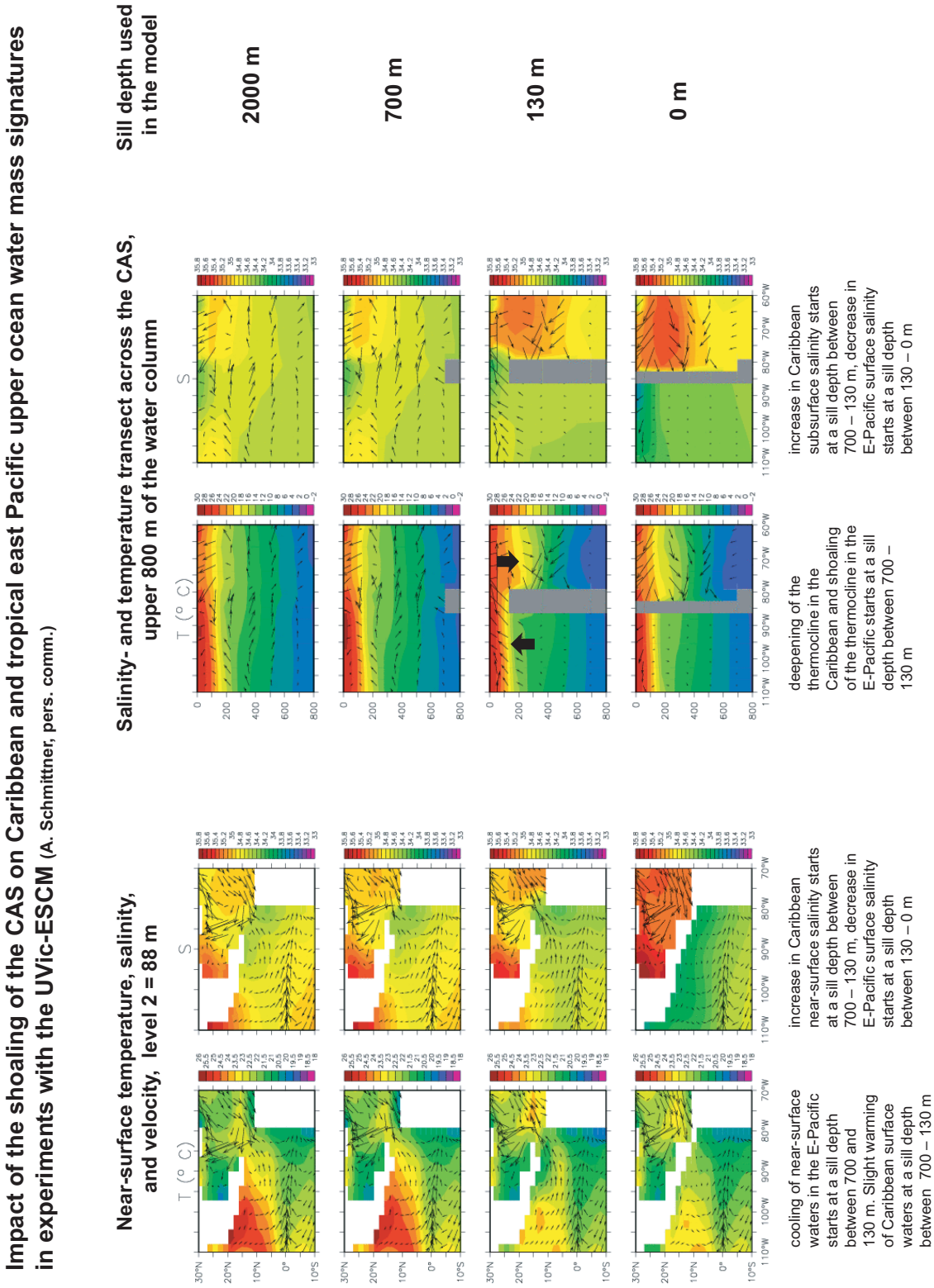

Fig. 7-4 .Model output showing salinity and temperature (annual means) for different sill depths of the Central American Seaway. Left: temperature and salinity maps encompassing the Caribbean and the tropical east Pacific (30°N – 10°S; 110°W – 70°W) at a depth level of 88 m. Right: East-west sections across the Panama gateway (from 110°W to 60°W at 11°N) illustrating the simulated changes in the vertical temperature and salinity structure. The arrows represent the velocity of the grid point at the beginning of the arrow.

Atmospheric wind-velocities used in the momentum transfer to the ocean and sea ice as well as for moisture advection and in the calculation of surface heat fluxes are prescribed using a present day climatological mean seasonal cycle and do not change in the different experiments. Orbital parameters (eccentricity, obliquity and precession) are set to present day values. The atmospheric pCO_2 is set to a constant preindustrial value of 280 ppm. A more detailed description of the model version used in this study is given by Weaver et al. (2001).

Four experiments with different Panama sill depths have been carried out in order to simulate different stages in the closure history of the CAS. The first experiment served as a control run for the preindustrial situation (closed seaway), whereas in the other experiments, the sill depth was set to 130 m, 700 m and 2000 m, respectively (Schneider and Schmittner, submitted). Each experiment was integrated for 2000 years to reach equilibrium. In order to investigate changes in ocean circulation, horizontal and vertical stream functions as well as water mass transports through the gateway were analyzed (Scheider and Schmittner, submitted).

With regard to changes in the Panamanian throughflow, the results of the model experiments with the UVic ESCM are in good agreement with those from earlier modeling studies (e.g. Maier-Reimer et al., 1990; Mikolajewicz and Crowley, 1997; Prange and Schulz, 2004), as presented by Schneider and Schmittner (submitted). In all experiments with an open isthmus, the net transport of water masses is directed from the Pacific into the Caribbean, but the total amount of the throughflow is decreasing from 10.6 Sv at a sill depth of 2000 m to 5 Sv at a sill depth of 130 m. Although the annual mean transport is always from the Pacific into the Atlantic, near-surface transport shows seasonal reversals during winter and spring, with Atlantic inflow into the Pacific. Furthermore, the gradual closure of the seaway leads to an intensification of North Atlantic Deep Water (NADW) formation and a related strengthening of the Gulf Stream and the North Atlantic drift (Schneider and Schmittner, submitted). Consequently, after the closure, the modern pattern of ocean circulation establishes, leading to higher SST and SSS in the North Atlantic. This is also in accordance with previous modeling studies (e.g. Maier-Reimer et al., 1990; Mikolajewicz and Crowley, 1997).

In order to compare closure-induced changes in Pacific and Caribbean upper ocean stratification as implied by the model experiments (**Fig. 7-4**) to those inferred from proxy data (**Fig. 7-3**), temperature and salinity maps derived from model results for different sill depths were generated for an area that encompasses the Caribbean and the tropical east Pacific (30°N – 10°S; 110°W –70°W) at a depth level of 88 m (**Fig. 7-4**). Moreover, east-west sections across the Panama gateway (from 110°W to 60°W at 10°N) were compiled in order to illustrate the simulated changes in the vertical temperature and salinity structure (**Fig. 7-4**).

In the Caribbean, the model simulates subsurface warming and a deepening of the thermocline with a shallowing sill (700 – 130 m), consistent with the Mg/Ca temperature records of *N. dutertrei* at Sites 999 and 1000. In agreement with the planktonic $\delta^{18}O$ records, a strong increase in Caribbean sub-surface salinities is simulated by the model that starts at a sill depth between 700 – 130 m and enhances when the sill shoals from 130 m to 0 m (**Fig. 7-4**). In the tropical east Pacific the model shows a subsurface cooling of up to 3 °C when the sill depth shoals from 700 m to

130 m. This is weaker than the cooling implied by the Mg/Ca temperature record of *G. tumida* (5 – 6 °C temperature decrease). In the model, freshening in the tropical east Pacific mixed layer occurs only for sill depths shallower than 130 m, and thus after the thermocline shoaling, and also after the major Caribbean salinity increase (between 700 – 130 m; **Fig. 7-4**). This sequence is supported by the proxy data, also suggesting that the SSS decrease in the tropical east Pacific (~3.6 Ma; Groeneveld et al., submitted a) lags the Caribbean salinity increase (after 4.6 – 4.2 Ma) by almost 1 Ma. An overview of paleoceanographic and modeling evidence for changes in Caribbean and tropical east Pacific upper ocean water mass signatures is provided in **Table 7-1**. In summary, the general consent between model experiments and proxy data confirms the assumption that most of the observed changes in Caribbean and tropical east Pacific upper ocean water mass signatures were indeed caused by the progressive closure of the CAS.

Tab. 7-1 Comparison between paleoceanographic and modeling evidence for changes in Caribbean and tropical east Pacific upper ocean water mass signatures.

Event	Paleoceanographic evidence	Implications from model results
Shoaling of the thermocline in the tropical east Pacific	5 – 6 °C decrease of T's at the bottom of the photic zone (Mg/Ca, *G. tumida*) at tropical east Pacific Site 1241 between 5.4 – 4.0 Ma.	Cooling of subsurface waters off the coast of Central America by up to 3 °C for a shoaling of the sill from 700 m to 130 m (**Fig 7-4**, left).
Deepening of the thermocline in the Caribbean	~4 – 5 °C increase of T's within the thermocline (Mg/Ca, *N. dutertrei*) at Caribbean Sites 999 and 1000 after 4.5 Ma.	Warming of Caribbean sub-surface waters (~4 – 5 °C at 200 m water depth) between 700 m –130 m sill depth.
Increase in Caribbean upper ocean salinity	Indicated by an increase in $\delta^{18}O$ within the mixed layer (*G. sacculifer*) and at the thermocline level (*N. dutertrei, G. limbata*) at Sites 999, 1000 after 4.6 – 4.2 Ma.	Increase in Caribbean salinity of ~0.5 salinity units starting between 700 – 130 m sill depth, and increasing between 130 – 0 m sill depth. Strongest salinity increase in the sub-surface, at ~200 m water depth.
Warming of the Caribbean mixed layer	Increase in Mg/Ca temperatures of *G. sacculifer* at northern Caribbean Site 1000 after 4.4 Ma, no mixed-layer warming at southern Caribbean Site 999 (Groeneveld et al., in prep.).	No pronounced evidence for mixed layer warming. Only slight T-increase (< 1 °C) in the upper 50 m between 700 – 130 m sill depth.
Development of inner-Caribbean salinity gradients (mixed layer and thermocline)	Strong differences in $\delta^{18}O$ of *G. sacculifer, G. limbata*, and *N. dutertrei* between Caribbean Sites 999 and 1000 after 4.2 Ma (stronger salinity increase towards northern Site 1000).	The model resolution is not suffiscient to resolve inner-Caribbean salinity gradients.
SSS-decrease in the tropical E-Pacific	Indicated by the comparison between Mg/Ca and $\delta^{18}O$ of *G. sacculifer* at tropical east Pacific Site 1241 after 3.6 Ma (Groeneveld et al., submitted a).	Freshening of ~one salinity unit in the upper 100 m of the water column at a sill depth between 130 – 0 m.

CHAPTER 8

PERMANENT EL NIÑO-LIKE STATE DURING THE PLIOCENE WARM PERIOD?

EVIDENCE FROM EQUATORIAL EAST PACIFIC PLANKTONIC STABLE ISOTOPE RECORDS (SITE 1239)

Recently, results from numerical models and theoretical studies have suggested that the Pliocene epoch may have reflected a permanent El Niño-like state (e.g.; Molnar and Cane, 2002; Philander and Fedorov, 2003). In the equatorial east Pacific, such a scenario would have been characterized e.g. by relatively high SSTs, a deepening of the thermocline, reduced southeast trade wind strength, weak or no coastal and equatorial upwelling, increased precipitation, and an equator-movement of the ITCZ (Wallace, 1998). So far, the paleoceanographic evidence for a Pliocene El Niño-like state is controversial (see chapter 1.2). This outline summarizes new information concerning this enigma that was derived from a planktonic stable isotope study at equatorial east Pacific Site 1239.

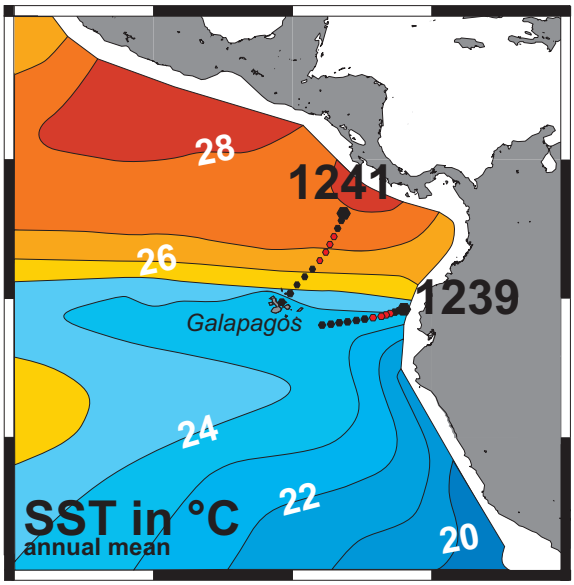

Modern sea surface temperatures in the tropical east Pacific (annual means; Levitus and Boyer, 1994). The positions of Sites 1239 and 1241 and their plate teconic backtrack paths are indicated.

The position of Site 1239 (located at the Carnegie Ridge, about 200 km off the coast of Ecuador) provides an excellent opportunity to further examine the role of ENSO during the early Pliocene, and to verify the hypothesis of a "permanent El Niño-like state" during the Pliocene warm period. Today, Site 1239 is located in the south equatorial upwelling area off Ecuador, which is characterized by a shallow thermocline, by relatively low SSTs, and by high surface productivity. Proxy data from this site in combination with those from more northern Site 1241, positioned within the North Equatorial Counter Current (NECC) (**Fig. 8-1**), are especially important to assess whether a permanent El Niño-like climate state persisted during the early Pliocene.

In a modern La Niña scenario, the North Equatorial Counter Current (NECC) transports warm, low saline water masses derived from the West Pacific Warm Pool (WPWP) towards the east north of the equator (Site 1241). South of the equator, a strong South Equatorial Current (SEC) transports cool, relatively saline water masses from the coast of Peru and Ecuador westward. Between these two surface currents, close to Site 1239, the equatorial front (EF) system divides warm, low saline NECC waters from cool, more saline SEC waters (Strub et al., 1998). This results in significant differences of surface water signatures between Sites 1239 (cooler, more saline, more nutrients) and 1241 (warmer, less saline, less nutrients). During El Niño, the weakening of the SEC generally induces the breakdown of the EF that becomes weak and unpredictable. As Site 1239 is located close to the EF, upwelling and surface productivity at the site location decrease, the thermocline deepens, and SSTs increase. Further north, at the position of Site 1241, the NECC also strengthens during El Niño, caused by an enhanced eastward transport of warm, low saline waters from the WPWP. A permanent early Pliocene El Niño-like state should thus strongly reduce the gradients in surface water signatures between Sites 1239 and 1241, resulting in similar planktonic stable isotope signatures at both site locations.

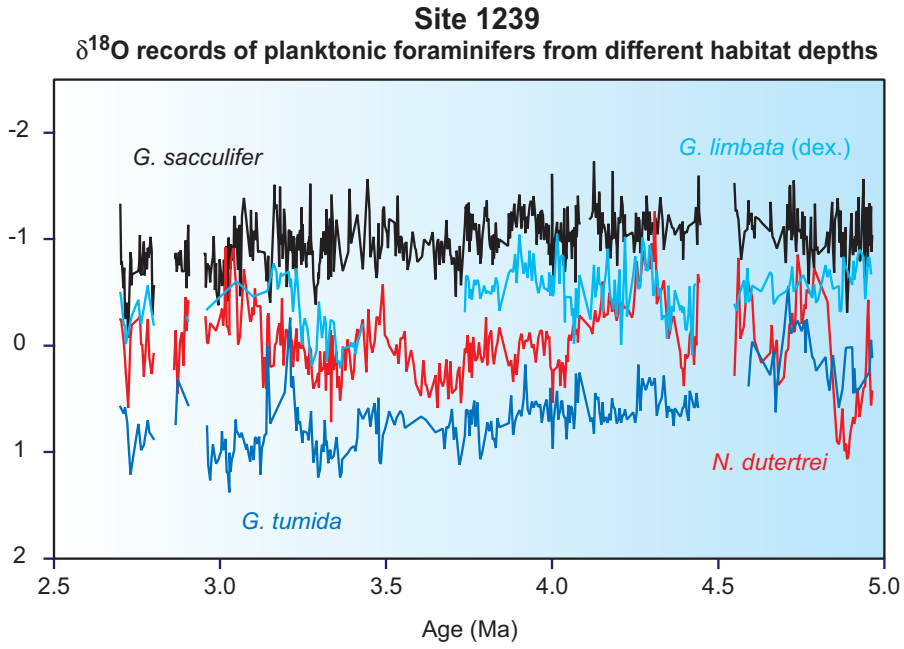

Fig. 8-2 $\delta^{18}O$ records of shallow- and deep-dwelling planktonic foraminifers from equatorial east Pacific Site 1239 for the time interval from 5.0 – 2.7 Ma. Black: *G. sacculifer* (mixed layer), light blue: *G. limbata* dextral (upper thermocline), red: *N. dutertrei* (lower thermocline) dark blue: *G. tumida* (bottom of the photic zone).

Within this study, stable isotope records ($\delta^{13}C$, $\delta^{18}O$) of four planktonic foraminiferal species with different habitat depths (*G. sacculifer*, *G. limbata* (dex), *N. dutertrei*, and *G. tumida*) were established for Site 1239 that span the time interval from 5.0 – 2.7 Ma. **Figure 8-2** summarizes the present status of available proxy records. At Site 1239, the creation of high-resolution stable isotope and Mg/Ca temperature records is limited by the low content of planktonic foraminifers in

the samples. It was thus necessary to cut down the fractionation of the samples to three size fractions, being < 125 µm, 125 – 250 µm, and > 250 µm. All specimens were picked from the > 250 µm fraction, so that the broad range of shell sizes may induce larger errors in stable isotope and Mg/Ca measurements.

In general, the $\delta^{18}O$ pattern of planktonic foraminifers at Site 1239 is similar to that observed at Site 1241 during the Pliocene (see chapters 6, 7). The mixed layer-dweller *G. sacculifer* shows the lowest $\delta^{18}O$ values, *G. tumida*, living at the bottom of the photic zone, displays the highest $\delta^{18}O$ values, and the $\delta^{18}O$ values of the thermocline-dwellers *G. limbata* and *N. dutertrei* are intermediate to those of *G. sacculifer* and *G. tumida*.

The comparison of $\delta^{18}O$ records (Sites 1241 *vs.* 1239) from the mixed layer-dwelling foraminifer *G. sacculifer* shows the lowest difference in absolute values between 5 Ma and 4.5 Ma (**Fig. 8-3 a**). After 4.5 Ma, the $\delta^{18}O$ gradient between the two *G. sacculifer* records increased significantly, whereas at ~3.5 Ma, the $\delta^{18}O$ difference reached a maximum of about 1 ‰. Interpreting the differences in $\delta^{18}O_{G.\ sacculifer}$ only in terms of temperature would suggest a gradual decrease in the mixed layer temperature at equatorial Site 1239 after 4.5 Ma. This implies that, if at all, a permanent El Niño may have existed in the interval older than 4.5 Ma. The $\delta^{18}O$ records from the deep-dweller *G. tumida* (bottom of the photic zone) provide almost identical values and trends for both sites from 5.0 Ma to 2.7 Ma (**Fig. 8-3 c**) This indicates that the early Pliocene thermocline shoaling in the tropical east Pacific (major subsurface cooling between 4.5 Ma and 4.0 Ma; see chapters 6, 7) was a regional phenomenon that affected both sites in the same way. The timing of this event is consistent with the increase in $\delta^{18}O_{G.\ sacculifer}$ gradients between Sites 1239 and 1241, and would aditionally argue against a permanent El Niño scenario after 4.5 Ma. The $\delta^{18}O$ values of *N. dutertrei* were significantly higher at the equator (Site 1239) than within the NECC (Site 1241), especially after 4.9 Ma (**Fig 8-3 b**). This may be interpreted in terms of lower Pliocene thermocline temperatures at Site 1239 with respect to Site 1241, and generally supports the $\delta^{18}O$ evidence from the mixed layer-dweller *G. sacculifer*. Planktonic Mg/Ca temperature reconstructions at Site 1241, however, have indicated that the Pliocene $\delta^{18}O$ records of planktonic foraminifers were strongly biased by salinity changes (see chapter 6). Hence, the interpretation of the $\delta^{18}O$ records at Site 1239 remains rather speculative as long as no Mg/Ca temperature data exists for this site.

The comparison of the *G. sacculifer* $\delta^{13}C$ records from Sites 1239 and 1241 provides additional insights into the question whether the Pliocene Pacific was characterized by a permanent El Niño-like state. These records are indicative of the nutrient concentrations in the mixed layer, whereas lower $\delta^{13}C$ values indicate higher nutrient concentrations (see chapter 6 for additional information). The $\delta^{13}C$ values of *G. sacculifer* are constantly by about 0.5 – 1 ‰ lower at the equatorial Site 1239 (**Fig. 8-3 d**). This may point to higher mixed layer productivity at the equatorial Site 1239, most probably triggered by the upwelling of nutrient-enriched subsurface waters. Higher equatorial surface productivity would argue against a permanent El Niño-like state, because coastal or equatorial upwelling at Site 1239 is assumed to be weak during an El Niño scenario. Thus, the gradients in mixed layer $\delta^{13}C$ between Site 1241 and Site 1239 should have been significantly

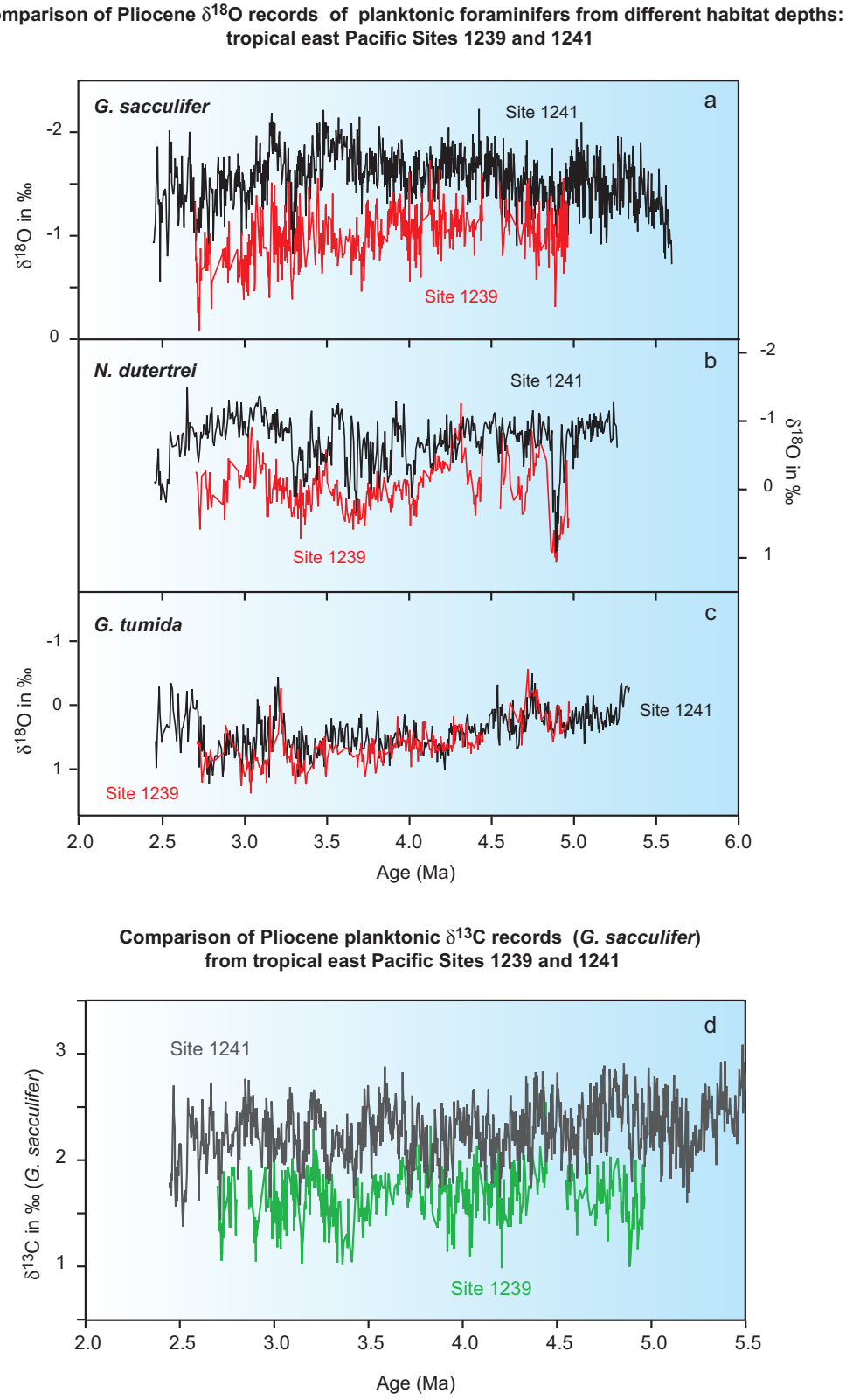

Fig. 8-3 a-c: Comparison of planktonic $\delta^{18}O$ records from Sites 1239 (red line) and 1241 (black line). **a**: *G. sacculifer*, **b**: *N. dutertrei*, **c**: *G. tumida*. **d**: $\delta^{13}C$ records of *G. sacculifer* for Sites 1239 (green line) and 1241 (gray line).

reduced. Unfortunately, the factors that control the $\delta^{13}C$ signal of planktonic foraminifers are manifold, making it only a rough indicator for changes in upper ocean productivity.

Finally, we are left with several questions concerning the hypothesis of an El Niño-like state, changes in equatorial east Pacific upper ocean stratification, upwelling, and productivity during the Pliocene. Although we cannot exclude the existence of a permanent El Niño at this point, the evidence derived from planktonic stable isotope records alone would rather argue against it – at least for the time interval younger than 4.5 Ma. In summary, these interpretations await the establishment of supplementary proxy records, such as opal accumulation rates, coccolith assemblages and Mg/Ca temperatures.

CHAPTER 9

RECONSTRUCTION OF PLIOCENE CHANGES IN CARIBBEAN INTERMEDIATE WATER VENTILATION – CONSTRAINTS ON ATLANTIC THERMOHALINE CIRCULATION

This chapter presents a short outline of a manuscript in preparation (Tiedemann, Steph and Haug) that will focus on Pliocene changes in Atlantic thermohaline circulation. Results from general circulation models (e.g Maier-Reimer et al., 1990; Mikolajewicz and Crowley, 1997) and paleoceanographic evidence (Haug and Tiedemann, 1998; Haug et al., 2001a) demonstrated that the Pliocene closure of the CAS led to an intensification of North Atlantic deep-water formation after 4.7 – 4.2 Ma. This intensification most likely resulted from a closure-induced salinity increase in the Caribbean and an intensification of the Gulf Stream that transported more salt into the source regions of NADW formation. This study (Steph et al., submitted a, see chapter 5), and the PhD study of J. Groeneveld (Uni Kiel), who quantified the salinity increase in the Caribbean, showed that the increase in Caribbean SSS started gradually after 4.7 – 4.6 Ma, but major steps occurred at 4.4 Ma and 4.2 Ma. Thus, the timing of these steps lags the observed increase in North Atlantic thermohaline circulation.

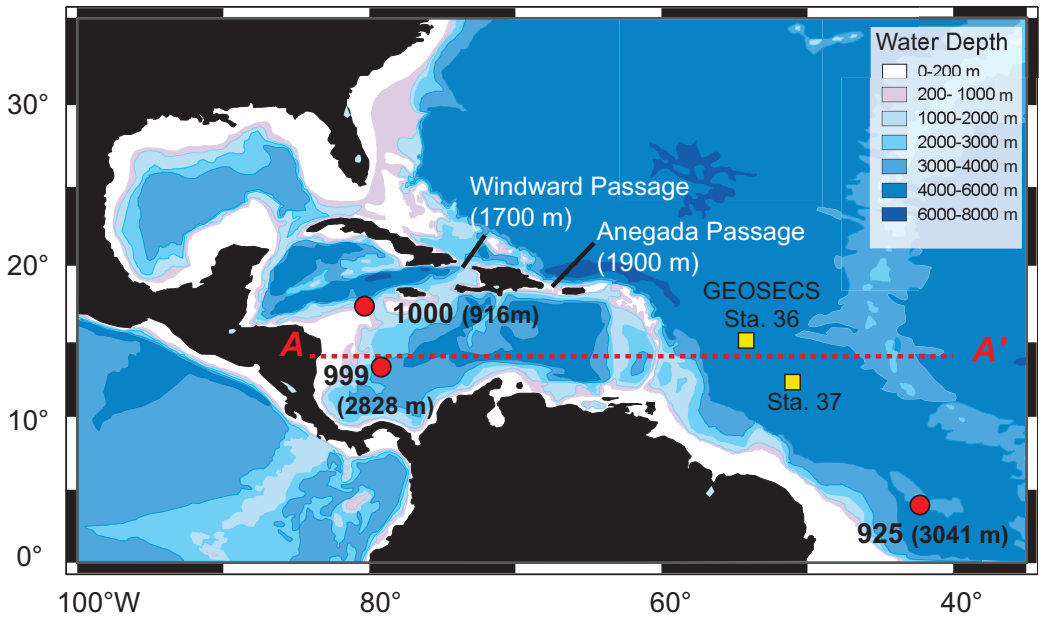

Fig. 9-1 Bathymetric map of the Caribbean. Red line indicates the section used in Figure 9-2.

Paleoceanographic evidence for the Pliocene increase in North Atlantic thermohaline circulation is mainly based on records of benthic $\delta^{13}C$ and percentage sand of the carbonate fraction from Caribbean Site 999, indicative of changes in deep water ventilation and carbonate preservation. Although Site 999 is located at a water depth of 2828 m, it reflects to a large part the chemical signature of upper NADW (UNADW). This is because Atlantic water masses have to enter the Caribbean above a sill depth of 1600 – 1900 m to fill the deep Caribbean basins (**Figs. 9-1, 9-2 a**). The gradual increase in benthic $\delta^{13}C$ and in the sand fraction after 4.7 – 4.6 Ma suggests an increase in UNADW ventilation (less nutrients, young water mass) that was associated with an increase in carbonate preservation. Before 4.6 Ma, low benthic $\delta^{13}C$ values and low sand contents indicate a poorly ventilated deep Caribbean and severe carbonate dissolution. In the early Pliocene, similar low $\delta^{13}C$ values (ca. 0.2 ‰) have only been documented at subantarctic South Atlantic Site 704 (2532 m water depth, Hodell and Venz, 1992), in contrast to higher NADW values (ca 1 ‰, e.g. at Sites 659 and 552; Tiedemann et al., 1994, Shackleton and Hall, 1984). This suggests that the Caribbean deep water was dominated by $\delta^{13}C$-depleted and nutrient-enriched Southern Ocean water masses (Antarctic Intermediate Water, AAIW) before 4.6 Ma (Haug and Tiedemann, 1998).

This study provides a new benthic $\delta^{13}C$ record from shallow Caribbean Site 1000. This site is positioned in a water depth of 916 m, and thus serves as a window into the Atlantic intermediate water level. Today, less ventilated, relatively nutrient-enriched (< $\delta^{13}C$) AAIW enters the Caribbean between 300 – 1000 m water depth (Site 1000) whereas oxygen-enriched, nutrient-depleted (> $\delta^{13}C$) UNADW ventilates the deep Caribbean further below (Site 999, **Fig. 9-2 a**). This configuration has been suggested to be typical of Pleistocene interglacial stages, but differed during glacial episodes. Several studies demonstrated that the formation of nutrient-poor lower NADW (LNADW) was reduced during Pleistocene and late Pliocene glacial maxima, whereas the production of good ventilated UNADW was intensified and dominated the N-Atlantic above a water depth of 2000 m (Boyle and Keigwin, 1982; Raymo et al., 1989, Flower et al., 2000). This should have resulted in good ventilated Caribbean water masses at 916 m water depth (Site 1000) during glacials, as suggested by the study of Zahn and Stüber (2002). They examined two cores from the tropical West Atlantic, positioned well above the Atlantic-Caribbean sills (cores OC205-2-103GGC and M35003 at 965 m and 1300 m water depth, respectively). Their benthic Cd/Ca and $\delta^{13}C$ records demonstrate that these cores bathed in good ventilated water masses during the last glacial maximum. Slowey and Curry (1995) investigated benthic foraminifers at the margins of the Bahama Bank for the Holocene and for the Last Glacial Maximum. They found that at all depths above 1500 m, glacial $\delta^{13}C$ values were higher than those for the late Holocene. This suggests the reduction of nutrient concentrations in the uppermost 1500 m, and indicates the absence of southern-source water masses. Below 2000 m water depth, however, poorly ventilated Southern Ocean Deep Water (SODW) filled the deep Atlantic and penetrated farther north than today. Oppo et al. (1995) and deMenocal et al. (1992) examined the Atlantic inflow into the deep Caribbean for the time interval of the last 2.6 Ma by comparing benthic $\delta^{13}C$ records from the deep Caribbean and the deep Atlantic (below the sill depth). They demonstrated that the deep Caribbean was better ventilated than the deep Atlantic during glacials. This implies that the boundary between

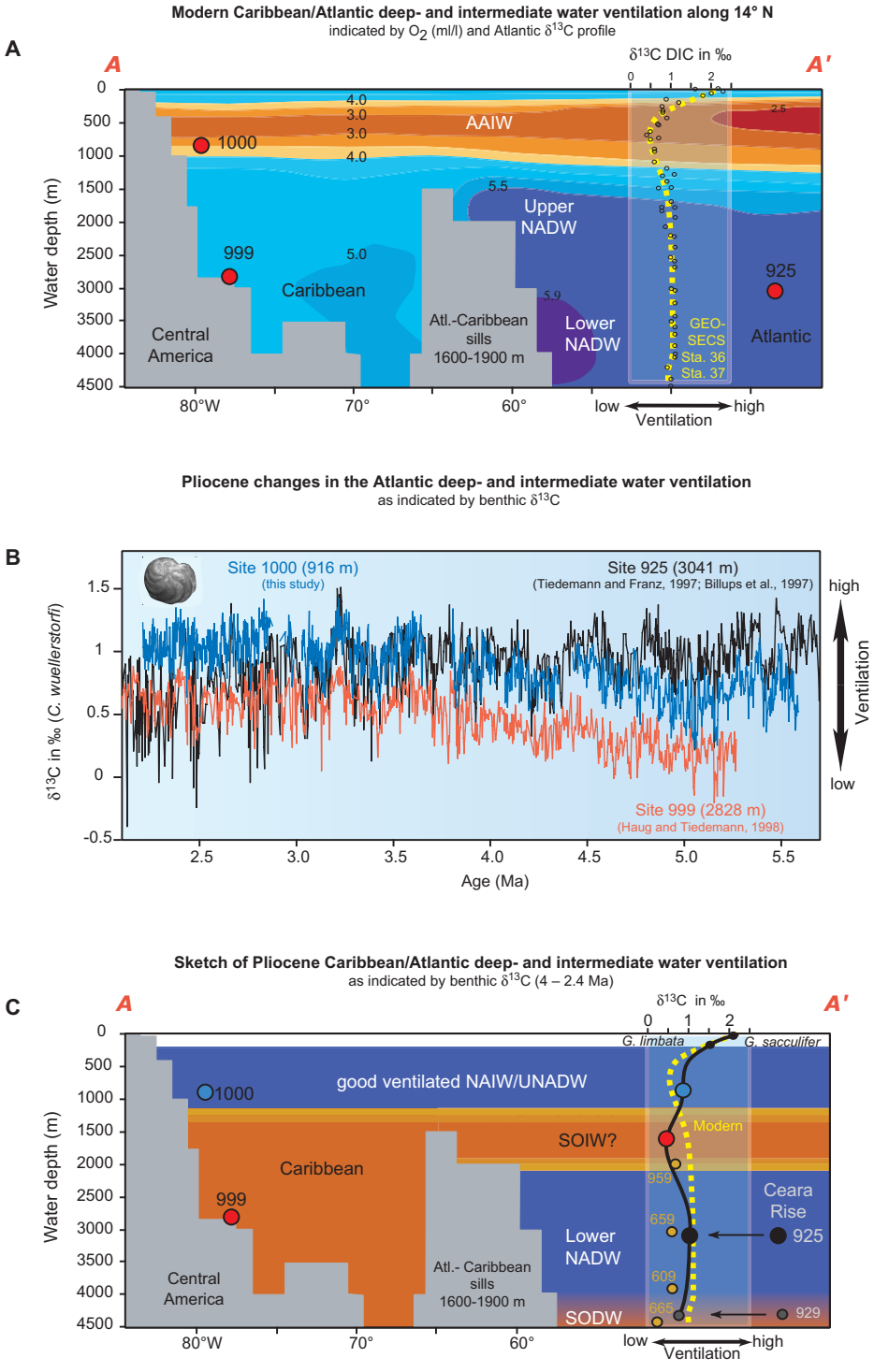

Fig. 9-2 a: Modern bathymetric transect of dissolved oxygen (ml/l) along 14°N and Atlantic $\delta^{13}C$ DIC profile from GEOSECS-stations (yellow line). **b:** Pliocene benthic $\delta^{13}C$ records from Caribbean Sites 999 (Haug and Tiedemann, 1998), 1000 (this study), and W-Atlantic Site 925 (Tiedemann and Franz, 1997; Billups et al., 1997). **c:** Working hypothesis of Pliocene Atlantic deep- and intermediate water ventilation and comparison of modern and Pliocene vertical $\delta^{13}C$ profiles. The red dot on the Pliocene $\delta^{13}C$ profile corresponds to Site 999, as it represents water masses that enter the Caribbean just above the sill depth. Additional Pliocene $\delta^{13}C$ values from other Atlantic Sites are marked by orange dots. NADW: North Atlantic Deep Water, AAIW: Antarctic Intermediate Water, SOIW: Southern Ocean Intermediate Water, SODW: Southern Ocean Deep Water, NAIW: North Atlantic Intermediate Water.

glacial UNADW and Southern Ocean Deep Water (SODW) was generally deeper than the Atlantic-Caribbean sills.

The $\delta^{13}C$ record from Site 1000 (916 m water depth), spanning the time interval from 5.6 Ma to 2.2 Ma, is the only tropical record that provides insights into the Pliocene low-latitude Atlantic intermediate water chemistry. The time interval from 5.6 – 2.2 Ma yields information on both, the impact of the closure of the CAS on UNADW and North Atlantic Intermediate Water (NAIW) formation, and variations in intermediate water ventilation related to the intensification of the NHG. At Site 1000, Pliocene benthic $\delta^{13}C$ values fluctuated between 0.4 – 1.3 ‰. From 5.4 – 5.0 Ma, $\delta^{13}C$ values decreased, reaching their lowest level between 5.2 Ma and 4.9 Ma (average $\delta^{13}C$ = 0.7 ‰). After 4.9 Ma, $\delta^{13}C$ values increased by about 0.5 ‰ until 4.4 Ma, and then decreased again between 4.4 Ma and 4.2 Ma. After 4.2 Ma, benthic $\delta^{13}C$ values increased on average from 0.7 ‰ to 1.1 ‰ until 2.2 Ma. The overall trend suggests an increase in intermediate water ventilation since 4.9 Ma (**Fig. 9-2 b**).

The comparison with equatorial Atlantic Site 925 at about 3000 m water depth provides informations about the initiation and enhancement of UNADW (NAIW) formation and the interplay between UNADW and LNADW formation, if the source regions of both water masses in the Labrador and Norwegian-Greenland Seas were characterized by similar $\delta^{13}C$ values. Today, Site 925 is located within the modern core depth of LNADW. The Atlantic $\delta^{13}C$ record shows relatively high values, on average 1 ‰, during the time interval from 5.5 Ma to 3.2 Ma, indicating the presence of good ventilated LNADW throughout this interval (**Fig. 9-2 b**). In the earliest Pliocene, the $\delta^{13}C$ values at Site 1000 are about 0.25 ‰ lower that those at Site 925. This suggests that the intermediate Atlantic was influenced by more nutrient-enriched water masses probably originating from the Southern Ocean. By 4.0 Ma, the long-term $\delta^{13}C$ increase at Site 1000 led to values that are identical with those at Site 925. This points to a first maximum in UNADW production at 4.0 Ma (**Fig. 9-2 b**), which is about 400 kyr earlier than postulated by Haug and Tiedemann (1998). Nearly identical values persisted until about 3.2 Ma and suggest a "super-conveyor" with strong UNADW and LNADW formation from 4.0 Ma to 3.2 Ma (**Fig. 9-2 b**). In concert with the intensification of the northern hemisphere glaciation, the $\delta^{13}C$ records start to diverge from each other with decreasing values at Site 925, whereas the $\delta^{13}C$ values remained high at Site 1000 (**Fig. 9-2 b**). Hence, global cooling resulted in a strong UNADW and weakened LNADW formation. This characterizes the beginning of the well-known Late Pliocene to Pleistocene relationship between UNADW and LNADW (deMenocal et al., 1992): During harsh climate episodes, production of LNADW was reduced, allowing bottom waters from the Southern Ocean to expand to shallower water depths and farther to the north.

The comparison of Caribbean $\delta^{13}C$ records from Sites 999 and 1000 provides surprising insights into the Pliocene pattern of Caribbean intermediate water ventilation. In general, the Pliocene Caribbean/Atlantic water masses at 916 m water depth (Site 1000) were always better ventilated (about 0.5 ‰ higher $\delta^{13}C$ values) than the water masses that entered the Caribbean above 1900 m water depth and filled the deep basins (Site 999) (**Fig. 9-2 b**). This pattern is in contrast with the modern pattern (poorly ventilated AAIW at Site 1000 and good ventilated UNADW at Site 999)

(**Fig. 9-2 a**). This implies the entrance of southern-source water masses below 900 m water depth and above 1900 m water depth (Caribbean-Atlantic sill depth), at least during the time interval from 5.3 Ma to 2.4 Ma (**Fig. 9-2 c**). After 2.4 Ma, the deep Caribbean was as good ventilated as the deep Atlantic during interglacials, associated with enhanced LNADW formation. During glacials, the pronounced $\delta^{13}C$ minima in the deep Atlantic indicate an increased influence of SODW in the Atlantic. This glacial-interglacial variability resulted in high $\delta^{13}C$ amplitude variations. At the deep Caribbean Site 999, the amplitudes remained low, and $\delta^{13}C$ minima were less pronounced. We interpret this to reflect the absence of Southern Ocean water masses in the Caribbean below 900 m water depth between 2.4 Ma and 2.0 Ma.

CHAPTER 10

SUMMARY AND CONCLUSIONS

This study established and examined Pliocene proxy records from the Caribbean (Sites 999, 1000) and the low-latitude east Pacific (Sites 1237, 1239, 1241) that span the time interval from ~6 Ma to 2.4 Ma. The main objectives were (1) to develop a consistent Pliocene orbitally tuned $\delta^{18}O$ stratigraphy, and (2) to reconstruct changes in Caribbean and tropical east Pacific hydrography that were presumably linked to the Pliocene closure of the CAS. The major results of this study are briefly summarized in the following paragraphs.

Stratigraphy

This thesis resulted in a consistent orbitally tuned benthic $\delta^{18}O$ stratigraphy for the Caribbean and the low-latitude tropical east Pacific. Comparisons with other orbitally tuned isotope stratigraphies from the equatorial western Atlantic (Ceara Rise, Sites 925/926; Tiedemann and Franz, 1997; Billups et al., 1997; Shackleton and Crowhurst, 1997) and with the most recently published "LR04" global benthic $\delta^{18}O$ isotope stack (Lisiecki and Raymo, 2005) suggest nearly identical ages for the numbered oxygen isotope stages between 2.4 Ma and 5.7 Ma. However, larger deviations between the $\delta^{18}O$ stack of Lisiecki and Raymo (2005) and the Pacific/Atlantic reference records (1241, 1237, and 925/926) occur in the time interval older than 5.0 Ma.

Sites 1237 and 1241 yielded a complete Pliocene sediment section and were selected as reference records, as their combination also provided a complete magnetostratigraphy. Their tuning was based on correlating high frequency variations in the GRA density, percent sand of the carbonate fraction, and benthic $\delta^{13}C$ to the orbital solution of Laskar et al. (1993). Hence, this study considers a lot more proxy records and their cyclic variations to develop an astronomical time scale than the "LR04" benthic $\delta^{18}O$ stack of Lisiecki and Raymo (2005). This is especially important as the signal-to-noise ratio in the $\delta^{18}O$ records is significantly reduced in the time interval older than 3.0 Ma.

The opportunity for orbital tuning was limited at Pacific Site 1239 and at Caribbean Sites 999 and 1000, as no composite depth exists that identifies and covers gaps at core breaks. The age model for tropical east Pacific Site 1239 is thus based on the direct correlation of benthic stable isotope records to the orbitally tuned benthic isotope records of Site 1241. The stratigraphies of Caribbean Sites 999 and 1000 were established by correlating their benthic stable isotope records to those from Atlantic Site 925/926. The consistency of the derived age models provided an excellent opportunity for comparisons of Pliocene proxy records from Caribbean and tropical east Pacific ODP sites.

Pliocene changes in Caribbean upper ocean hydrography

As already known from previous studies (e.g. Keigwin, 1982a; Haug et al., 2001a), significant changes in Caribbean near-surface water mass signatures occured after 4.7 – 4.2 Ma when the reduction in volume transport through the CAS reached a critical threshold, thereby increasing Caribbean salinity and thus affecting the ocean-atmosphere-climate system by increased thermohaline heat- and salt-transport to high northern latitudes. Additional Pliocene stable isotope and Mg/Ca temperature records for shallow- and deep-dwelling planktonic foraminifers from Caribbean Ocean Drilling Program (ODP) Sites 999 and 1000 were established and compared to $\delta^{18}O$ records from the tropical Atlantic (ODP Sites 925, 1006) and Pacific (ODP Sites 851, 1241) to further assess the Pacific-Caribbean and Atlantic-Caribbean water mass exchange, and to detect variations in Caribbean thermocline depth that may indicate the intensification of the Caribbean/West Atlantic Warm Pool in response to decreasing Pacific surface water inflow. The results provide new insights into Pliocene changes in Caribbean upper ocean hydrography:

- The comparison of $\delta^{18}O_{G.\ sacculifer}$ records between Caribbean Sites 999 and 1000 and Pacific Sites 851 and 1241 indicates that the increase in Caribbean SSS after 4.7 – 4.2 Ma was accompanied by the development of significant inner-Caribbean mixed-layer salinity gradients. The salinity increased with larger distance to the gateway region. Accordingly, mixed-layer salinities were higher at northern Site 1000.
- After 4.4 Ma, the differences in $\delta^{18}O_{G.\ sacculifer}$ between Caribbean Sites 999 and 1000 identify a strong variability of inner-Caribbean salinity gradients on orbital timescales. This was mainly caused by pronounced salinity changes at Site 1000. At this site, paired $\delta^{18}O$ and Mg/Ca data of *G. sacculifer* suggest strong temperature and salinity fluctuations on precessional periodicities. Thereby, maxima in SST and SSS correspond to precessional maxima in northern hemisphere summer insolation. This suggests that expansions of the Pacific low salinity tongue into the Caribbean influenced the more northern Site 1000 only during minima in northern hemisphere summer insolation, when $\delta^{18}O$ differences between both sites were smallest. Large salinity differences during northern hemisphere summer insolation maxima are interpreted to reflect a stronger influence of relatively warm and saline Atlantic surface waters at northern Site 1000 during times of reduced volume transport through the CAS.
- The Pliocene Atlantic-Caribbean differences in $\delta^{18}O_{G.\ sacculifer}$ (Sites 925, 1000) exclude the transfer of water masses from the Guyana Current through the southernmost Antilles passages as a main source for Caribbean high salinity waters, because the $\delta^{18}O$ values at tropical western Atlantic Site 925 were about 1.5 ‰ too low. The comparison of Caribbean Site 1000 to Site 1006, which is located at the Great Bahama Bank in the tropical western Atlantic, provides similar $\delta^{18}O_{G.\ sacculifer}$ values at both sites. This indicates that high-salinity surface waters left the Caribbean and fed the Gulf Stream, as Site 1006 is located under the Florida Current in the Caribbean outflow region. Thus, the combination of both results indicates the north Atlantic subtropical gyre to be a major player in providing the Caribbean with high salinity water masses during maxima in northern hemisphere summer insolation.

- $\delta^{18}O$ and Mg/Ca records of *N. dutertrei* indicate a warming of ca. 4 – 5 °C within the thermocline at both Caribbean Sites, 999 and 1000, after 4.5 Ma. This warming was paralleled by an increase in mixed-layer temperatures at northern Caribbean Site 1000 (Groeneveld et al., submitted b). Combining the results, a strengthening of the Caribbean/Atlantic Warm Pool after 4.5 Ma is suggested.

Pliocene changes in tropical east Pacific upper ocean hydrography

On the tropical east Pacific side of the CAS, this study focused on Site 1241 that is located relatively close to the final gateway region. $\delta^{18}O$ and Mg/Ca records of planktonic foraminifers from this site suggest that the response of tropical east Pacific upper ocean stratification to the progressive shoaling of the CAS differed significantly from that observed in the Caribbean.

- Mixed-layer temperatures were relatively stable at Site 1241 between 4.8 Ma and 3.7 Ma (Groeneveld et al., submitted a). In contrast, the temperatures at the bottom of the photic zone decreased by about 6 °C (from 21 °C to 15 °C) between 5.4 Ma and 4.0 Ma, with major cooling steps after 5.3 Ma and 4.5 Ma, as indicated by the Mg/Ca temperature record of *G. tumida* (this study). The associated increase of the temperature gradient within the photic zone documents a shoaling of the tropical east Pacific thermocline during the early Pliocene. The timing of this event is consistent with a critical threshold in the closure history of the CAS, when surface water exchange between Pacific and Caribbean became significantly restricted (Keigwin, 1982a; Haug et al., 2001a). The forcing mechanisms for this thermocline shoaling remain ambiguous, but may include an increase in NADW production after 4.6 Ma, and/or closure-related changes in the tropical wind field.
- After 3.7 Ma, the mixed-layer temperatures at Site 1241 decreased gradually (Groeneveld et al., submitted a). The temperatures at the bottom of the photic zone, however, did not vary much between 4.0 Ma and 2.7 Ma, but developed a weak warming trend from 2.7 Ma to 2.5 Ma. This warming may suggest a slight deepening of the thermocline in the tropical east Pacific after the intensification of NHG.
- Temperatures within the thermocline remained relatively stable throughout the Pliocene, as implied by the Mg/Ca records of *G. limbata* and *N. dutertrei*. The temperature gradient between *G. sacculifer* and *N. dutertrei* was fairly constant (6 – 7 °C).
- The comparison of planktonic $\delta^{18}O$ and Mg/Ca records indicates that salinity changes in the upper water column also played an important role in the tropical east Pacific. The early Pliocene thermocline shoaling was associated with an increase in thermocline salinity and a salinity decrease at the bottom of the photic zone. In contrast, mixed-layer salinities remained relatively stable until 3.7 Ma (Groeneveld et al., submitted a). However, the calculation of absolute salinity values for the deep-dwelling foraminifers revealed strong uncertainties with regard to the existing Mg/Ca paleotemperature equations.

Comparisons between proxy data and numerical model results

In order to further assess the role of Panama uplift on observed changes in Pacific and Caribbean changes in upper ocean water mass signatures during the early Pliocene, paleoceanographic proxy data (planktonic $\delta^{18}O$ and Mg/Ca) were compared to results from numerical modeling studies. Four experiments with different Panama sill depths (2000 m, 700 m, 130 m, 0 m) were carried out with the UVic-ESCM (Schmittner, pers. comm.). The generally good agreement of implications from proxy data and results from numerical modeling studies indicates that the shoaling of the CAS indeed was the main forcing factor for Pliocene variations in Pacific and Caribbean upper ocean stratification.

- The observed warming/deepening of the Caribbean thermocline (after 4.5 Ma) and an increase in Caribbean salinities (after 4.7 – 4.2 Ma) are also indicated by the model output, with the most significant changes occurring between model runs with a sill depth of 700 m and 130 m: A warming of 4 – 5 °C in 200 m water depth, and a salinity increase of 0.5 (significantly smaller than suggested by the $\delta^{18}O_{G.sacculifer}$ values from Site 1000).
- The thermocline shoaling in the tropical east Pacific (major step after 4.5 Ma) was also detected between model runs with a sill depth of 700 m and 130 m, and thus coeval to the Caribbean changes. Pacific subsurface cooling is weaker in the model output (3 °C) than suggested by Mg/Ca temperature data of *G. tumida* at Site 1241 (6 °C).

Permanent El Niño during the Pliocene?

To test the hypothesis whether a "permanent El Niño-like state" existed during the Pliocene, one focus of the study was the comparison of stable isotope records from equatorial Pacific Site 1239 and Site 1241, located farther north within the NECC. A permanent El Niño scenario should result in relatively similar surface water signatures at both sites due to a deepening of the thermocline, an increase in SSTs, and reduced equatorial upwelling at Site 1239. Although we cannot exclude a "permanent El Niño-like state" during the Pliocene at this stage, evidence from tropical east Pacific planktonic stable isotope records would rather argue against it – at least for the time interval younger than 4.5 Ma. However, supplementary proxy records (e.g. Mg/Ca temperatures; nutrient proxy data) are clearly needed to verify these initial results:

- The comparison of $\delta^{18}O$ records for the shallow-dweller *G. sacculifer* (1239 *vs.* 1241) indicates an increase in mixed-layer $\delta^{18}O$ gradients between both sites after 4.5 Ma. Interpreting the $\delta^{18}O$ records only in terms of temperature would thus imply a mixed-layer cooling at equatorial Site 1239 after 4.5 Ma.
- The similarity of $\delta^{18}O_{G.\ tumida}$ records from Sites 1239 and 1241 suggests that the early Pliocene thermocline shoaling observed at Site 1241 (main step after after 4.5 Ma) was a regional phenomenon that affected both sites in the same way. The timing is consistent with the increase in mixed-layer $\delta^{18}O$ gradients between both sites.
- The difference in $\delta^{13}C$ of *G. sacculifer* (1239 *vs.* 1241), with 0.5 – 1 ‰ lower values at the equatorial Site 1239 between 5.0 – 2.7 Ma, indicates higher nutrient concentrations in the equatorial mixed-layer, probably caused by equatorial upwelling.

Pliocene changes in Atlantic intermediate water circulation

This study provides a new Pliocene benthic $\delta^{13}C$ record from shallow Caribbean Site 1000 (916 m water depth) that serves as a window into the Atlantic intermediate water layer.

- The comparison of benthic $\delta^{13}C$ records from shallow Caribbean Site 1000 to deep western Atlantic Site 925 (3041 m water depth, modern core depth of LNADW) suggests a first maximum in UNADW formation at 4.0 Ma. Nearly identical $\delta^{13}C$ values at both sites between 4.0 Ma and 3.2 Ma indicate the existence of a "super-conveyor", with strong production of both, UNADW and LNADW. After 3.2 Ma, lower $\delta^{13}C$ values at deep Atlantic Site 925 than at Site 1000 suggest that global cooling resulted in a strengthened UNADW formation and a weakened LNADW formation. This characterizes the onset of the well-known late Pliocene-Pleistocene relationship between LNADW and UNADW, i. e. reduced LNADW formation during harsh climate episodes (deMenocal et al., 1992; Oppo et al., 1995).
- The comparison of Caribbean benthic $\delta^{13}C$ records from Sites 999 (2828 m water depth) and Site 1000 (916 m water depth) indicates that the shallow Site 1000 was better ventilated than the deep Caribbean Site 999 throughout the Pliocene. This result is rather astonishing, as it contradicts the modern pattern of Caribbean ventilation: Better ventilated deep basins, filled with UNADW (Site 999) and a less ventilated intermediate water level, penetrated by nutrient-enriched AAIW (Site 1000). Thus, the Pliocene pattern implies the entrance of a less ventilated southern-source water mass below 900 m (Site 1000) and above 1900 m (Atlantic-Caribbean sill depth), at least until 2.4 Ma.
- After 2.4 Ma, the deep Caribbean (Site 999, 2828 m water depth) was as good ventilated as the deep Atlantic (Site 925, 3041 m water depth) during interglacials, and better ventilated during glacials, indicating the absence of a southern-source water mass in the Caribbean below 900 m.

CHAPTER 11

REFERENCES

Ahrens, C.D., Horne, N., and Alvelais, R., 2001. *Essentials of Meteorology: An invitation to the Atmosphere (3rd Edition)*. Brooks Cole, 464 pp.

Anand, P., Elderfield, H. and Conte, M., 2003. Calibration of Mg/Ca thermometry in planktonic foraminifera from a sediment trap time series. *Paleoceanography,* 18–2: 15, doi: 10.1029/2002PA000846.

Andersson, C., 1997. Transfer function vs. modern analog technique for estimating Pliocene sea-surface temperatures based on planktic foraminiferal data, western equatorial Pacific Ocean. *J. Foram. Res.,* 27–2: 123–132.

Banner, F.T. and Blow, W.H., 1960. Some primary types of species belonging to the superfamily Globigerinaceae, Cushman Found. *Foram. Res. Contr.*, 11, pt. 1: 1–41.

Backmann, J. and Raffi, I., 1997. Calibration of Miocene nannofossil events to orbital tuned cyclostratigraphy from Ceara Rise. *In:* Curry, W.B., Shackleton N.J., and Richter, C. (Eds.), *Proc. Ocean Drill. Program Sci. Results,* 154: 83–100, College Station, TX (Ocean Drilling Program).

Barker, S., Greaves, M. and Elderfield, H., 2003. A study of cleaning procedures used for foraminiferal Mg/Ca paleothermometry. *Geochem. Geophys. Geosyst.*, 4–9, doi: 10.1029/2003GC000559.

Berger, A. and Loutre, M.F., 1991. Insolation values for the climate of the last 10 million years. *Quat. Sci. Rev.*, 10: 297–317.

Berger, W.H., Vincent, E. and Thierstein, H., 1981. The deep-sea record: major steps in Cenozoic ocean evolution. *In:* Warme, J.E., Douglas, R.E., Winterer, E.L., (Eds.), *The Deep Sea Drilling Project: a decade of progress. Soc. Econom. Paleontol. Mineral. Spec. Publ.,* 32: 489–504.

Berger, W.H. and Wefer, G., 1996. Expeditions into the Past: Paleoceanographic studies in the South Atlantic. *In:* Wefer, G., Berger, W.H., Siedler, G., Webb, D.J. (Eds.), *The South Atlantic: Present and Past Circulation.* Springer-Verlag, Berlin, pp. 363–410.

Berggren, W.A. and Hollister, C.D., 1974. Paleogeography, paleobiogeography, and the history of circulation of the Atlantic Ocean. *In*: Hay, W.W. (Ed.), *Studies in Paleoceanography*, *Soc. Econ. Paleontol. Mineral. Spec. Publ.*, vol. 20: 126–186.

Bickert, T. and Wefer, G., 1996. Late Quaternary deep water circulation in the South Atlantic: Reconstruction from carbonate dissolution and benthic stable isotopes. *In:* Wefer, G., Berger, W.H., Siedler, G., and Webb, D.J. (Eds.), *The South Atlantic: Present and Past Circulation.* Springer-Verlag, Berlin: 599–620.

Bickert, T., Curry, W.B. and Wefer, G., 1997. Late Pliocene to Holocene (2.6 – 0 Ma) western Equatorial Atlantic deep-water circulation; inferences from benthic stable isotopes. *In:* Curry, W.B., Shackleton N.J., Richter, C. (Eds.), *Proc. Ocean Drill. Program Sci. Results,* 154: 239–253, College Station, TX (Ocean Drilling Program).

Billups K. and Spero, H.J., 1996. Reconstructing the stable isotope geochemistry and paleotemperatures of the Equatorial Atlantic during the last 150,000 years: Results from individual foraminifera. *Paleoceanography,* 11: 217–238.

Billups, K., Ravelo, A.C. and Zachos, J.C., 1997. Early Pliocene deep-water circulation; stable isotope evidence for enhanced northern component deep water. *In:* Curry, W.B., Shackleton N.J., Richter, C. (Eds.), *Proc. Ocean Drill. Program Sci. Results,* 154: 319–330, College Station, TX (Ocean Drilling Program).

Billups, K., Ravelo, A.C. and Zachos, J.C., 1998. Early Pliocene deep-water circulation in the western equatorial Atlantic: Implications for high-latitude climate change. *Paleoceanography*, 13: 84–95.

Billups, K., Ravelo, A.C., Zachos, J.C. and Norris, R.D., 1999. Link between oceanic heat transport, thermohaline circulation, and the Intertropical Convergence Zone in the early Pliocene Atlantic. *Geology*, 27: 319–322.

Bitz, C.M., Holland, M.M., Weaver, A. J. and Eby, M., 2001. Simulating the ice-thickness distribution in a coupled climate model. *J. Geophys. Res.,* 106: 2441–2464.

Blackman, R.B. and Tukey, J.W., 1958. *The Measurement of Power Spectra From the Point of View of Communication Engineering*. New York (Dover Publications), 190 pp.

Blow, W.H., 1969. Late middle Eocene to Recent planktonic foraminiferal biostratigraphy. *In:* Brönnimann, P. and Renz, H.H. (Eds.), *Proc. First Int. Conf. Planktonic Microfossils*, *Geneva, 1967*. Leiden (E.J. Brill), pp. 199–422.

Boyle E.A. and Keigwin L.D., 1982. Deep circulation of the North Atlantic over the last 200,000 years: Geochemical evidence. *Science* 218: 784–787.

Broecker, W.S. and Peng, T.H., 1982. *Tracers in the Sea.* Lamont-Doherty Geol. Observ., Palisades, New York, 699 pp.

Broecker, W.S. and Denton, G.H., 1989. The role of ocean-atmosphere reorganizations in glacial cycles. *Geochim. Cosmochim. Acta*, 53: 2465–2501.

Broecker, W.S., 1997. Thermohaline circulation, the Archilles heel of our climate system: will man-made CO_2 upset the current balance? *Science*, 278: 1582–1589.

Brüggemann, W., 1992. A minimal cost function method for optimizing the age-depth relation of deep-sea sediment cores. *Paleoceanography*, 7: 467–487.

Bryden, H.L. and Brady, E.C., 1985. Diagnostic model of the three-dimensional circulation in the upper equatorial Pacific ocean. *J. Phys. Oceanogr.*, 15: 1255–1273.

Burton, K.W., Ling, H.F. and O'Nions, R.K., 1997. Closure of the Central American Isthmus and its effect on deep-water formation in the North Atlantic. *Nature*, 386: 382–385.

Cande, S.C. and Kent, D.V., 1995. Revised calibration of the geomagnetic polarity timescale for the Late Cretaceous and Cenozoic. *J. Geophys. Res., B,* 100: 6093–6095.

Cane, M. and Molnar, P., 2001. Closing of the Indonesian Seaway as a precursor to East African aridification around 3 – 4 million years ago. *Nature*, 411: 157–162.

Cannariato, K.G. and Ravelo, A.C., 1997. Pliocene-Pleistocene evolution of eastern tropical Pacific surface water circulation and thermocline depth. *Paleoceanography*, 12: 805–820.

Carter, R.M., Fulthorpe, C.S. and Lu, H., 2004. Canterbury Drifts at Ocean Drilling Program Site 1119, New Zealand: Climatic modulation of southwest Pacific intermediate water flows since 3.9 Ma. *Geology*, 32–11: 1005-1008.

Chaisson, W.P., 1995. Planktonic foraminiferal assemblages and paleoceanographic change in the trans-tropical Pacific Ocean: A comparison of West (Leg 130) and East (Leg 138), latest Miocene to Pleistocene. *In*: Pisias, N.G., Mayer, L.A., Janecek, T.R., Palmer-Julson, A. and van Andel, T.H. (Eds.), *Proc. Ocean Drill. Program Sci.Results*, 138: 555–581, College Station, TX (Ocean Drilling Program).

Chaisson, W.P. and Ravelo, A.C., 1997. Changes in upper water-column structure at Site 925, Late Miocene-Pleistocene: Planktonic foraminifer assemblage and isotopic evidence. *In:* Curry, W.B., Shackleton N.J., Richter, C. (Eds.), *Proc. Ocean Drill. Program Sci. Results,* 154: 255–268, College Station, TX (Ocean Drilling Program).

Chaisson, W.P. and Ravelo, A.C., 2000. Pliocene development of the East-West hydrographic gradient in the Equatorial Pacific. *Paleoceanography*, 15: 497–505.

Chandler, M., Rind, D. and Thompson, R., 1994. Joint investigations of the middle Pliocene climate II: GISS GCM Northern Hemisphere results. *Global Planet. Change*, 9: 197–219.

Chen, J., Farrell, J.W., Murray, D.W. and Prell, W.L., 1995. Timescale and paleoceanographic implications of a 3.6 m.y. oxygen isotope record from the Northeast Indian Ocean (Ocean Drilling Program Site 758). *Paleoceanography*, 10: 21–47.

Clemens, S.C., 1999. An astronomical tuning strategy for Pliocene sections; implications for global-scale correlation and phase relationships. *In:* Shackleton N.J., McCave, I.N., and Graham, P.W. (Eds.), *Astronomical (Milankovitch) calibration of the geological time-scale*. London (Royal Society of London), 1949–1973.

Clement, A.C., Seager, R. and Cane, M.A., 1999. Orbital Controls on the El Niño/Southern Oscillation and the tropical climate. *Paleoceanography*, 14: 441–456.

Clement, A.C., Seager, R. and Cane, M.A., 2000. Suppression of El Niño during the mid-Holocene by changes in the Earth's orbit. *Paleoceanography*, 15: 731–737.

Coates, A.G., Jackson, J.B.C., Collins, L.S., Cronin, T.M., Dowsett, H.J., Bybell, L.M., Jung, P. and Obando, J.A., 1992. Closure of the Isthmus of Panama: The near-shore marine record of Costa Rica and western Panama. *Geol. Soc. Am. Bull.*, 104: 814–828.

Coates, A.G., and Obando, J.A., 1996. The geological evolution of the Central American Isthmus. *In:* Jackson, J.B.C., Budd, A.F., and Coates, A.G., (Eds.): *Evolution and environment in tropical America.* University of Chicago Press, Chicago, Illinois, pp. 21–56.

Coates, A.G., Collins, L.S., Aubry, M-P. and Berggren, W.A., 2004. The Geology of the Darien, Panama, and the late Miocene-Pliocene collision of the Panama arc with northwestern South America. *Geol. Soc. Am. Bull,* 116: 1327–1344.

Collins, L.S., Coates, A.G., Berggren, W.A., Aubry, M-P. and Zhang, J., 1996. The late Miocene Panama Isthmian Strait. *Geology*, 24: 687–690.

Craig, H., 1957. Isotopic standards for carbon and oxygen and correction factors for mass-spectrometric analysis of carbon dioxide. *Geochim. Cosmochim. Acta*, 12: 133-149.

Cronin, T.M., Whatley, F., Wood, A., Tsukagoshi, A., Ikeya, N., Brouwers, E.M. and Briggs, W.M. Jr., 1993. Microfaunal evidence for elevated Pliocene temperatures in the Arctic Ocean. *Paleoceanography*, 8: 161–173.

Crouch, R.W. and Poag, W.C., 1979. *Amphistegina gibbosa* d'Orbigny from the California borderlands: The Caribbean connection. *J. Foram. Res.*, 9: 85–105.

Crowley, T.J., 1991. Past CO_2 changes and tropical sea surface temperatures. *Paleoceanography*, 6: 387–394.

Crowley, T.J., 1992. North Atlantic Deep Water cools the Southern Hemisphere. *Paleoceanography*, 7: 489–497.

Crowley, T.J., 1996. Pliocene climates: The nature of the problem. *Mar. Micropaleontol.*, 27: 3–12.

Curry, W.B., Thunell, R.C. and Honjo, S., 1983. Seasonal changes in the isotopic composition of planktonic foraminifera collected in Panama Basin sediment traps. *Earth Planet. Sci. Lett.*, 64: 33–43.

Curry, W.B., Shackleton, N.J., Richter, C. et al., 1995. *Proc. Ocean Drill. Program, Initial Report*, vol. 154, Ocean Drilling Program, College Station, Texas.

Dekens, P.S., Lea, D.W., Pak, D.K. and Spero, H.J., 2002. Core top calibration of Mg/Ca in tropical foraminifera: Refining paleotemperature estimation. *Geochem. Geophys. Geosyst.*, 3–4: doi: 10.1029/2001GC000200.

Delcroix, T., Eldin, G. and Hénin, C., 1987. Upper ocean water masses and transports in the western tropical Pacific (165°E). *J. Phys. Oceanogr.*, 17: 2248–2262.

deMenocal, P.B., Oppo, D.W. and Fairbanks, R.G., 1992. Pleistocene $\delta^{13}C$ variability of North Atlantic Intermediate Water. *Paleoceanography*, 7: 229–250.

Dengo, G., 1985. Tectonic setting for the Pacific margin from southern Mexico to Northwestern Columbia. *In:* Nairn, A.E., Stehli, F.G. and Uyeda, S. (Eds.), *The Pacific Ocean: The ocean basins and margins, 7A.* Plenum Press, New York, pp. 123–180.

Dessier, A. and Donguy, J.R., 1994. The sea-surface salinity in the tropical Atlantic between 10°S and 30°N-seasonal and interannual variations (1977–1989). *Deep-Sea Res. Part I*, 41: 81–100.

Dobson, M.D., Dickens, G.R. and Rea, D.K., 1997. Terrigenous sedimentation at Ceara Rise. *In:* Curry, W.B., Shackleton N.J., Richter, C. (Eds.), *Proc. Ocean Drill. Program Sci. Results,* 154: 465–473, College Station, TX (Ocean Drilling Program).

Donguy, J.R. and Meyers, G., 1996. Mean annual variation of transport of major currents in the tropical Pacific Ocean. *Deep-Sea Res. Part I*, 43: 1105–1122.

Dowsett, H.J. and Cronin, T.M., 1990. High eustatic sea level during the middle Pliocene: Evidence from the southeastern U.S. Atlantic Coastal Plain. *Geology*, 18: 435–438.

Dowsett, H.J. and Poore, R.Z., 1991. Pliocene sea-surface temperatures of the North Atlantic Ocean at 3.0 Ma. *Quat. Sci. Rev.*, 10: 189–204.

Dowsett, H.J., Cronin, T.M., Poore, R.Z., Thompson, R.S., Watley, R.C. and Wood, A.M., 1992. Micropaleontological evidence for increased meridional heat transport in the North Atlantic during the Pliocene. *Science*, 258: 1133–1135.

Dowsett, H.J., Thompson, R.S., Barron, J.A., Cronin, T.M., Fleming, R.F., Ishman, S.E., Poore, R.Z., Willard, D.A. and Holtz, T.R., 1994. Joint investigations of the middle Pliocene climate I: PRISM paleoenvironmental reconstructions. *Global Planet. Change*, 9–4: 169–195.

Dowsett, H.J., Barron, J. and Poore, R.Z., 1996. Middle Pliocene sea surface temperatures: A global reconstruction. *Mar. Micropaleontol.*, 27: 13–25.

Dowsett, H.J., Barron, J.A., Poore, R.Z., Thompson, R.S., Cronin, T.M., Ishman, S.E. and Willard, D.A., 1999. Middle Pliocene paleoenvironmental reconstruction: PRISM2, *U.S. Geol. Surv. Open File Rep.*, 99–535, 13 pp.

Driscoll, N.W. and Haug, G.H., 1998. A short circuit in the Thermohaline Circulation: A cause for Northern Hemisphere Glaciation? *Science*, 282: 436–438.

Duncan, R.A. and Clague, D.A., 1985. Pacific plate motion recorded by linear volcanic chains. *In:* Nairn, A.E.M., Stehli, F.G., and Uyeda, S. (Eds.), *The Oceans Basins and Margins: The Pacific Ocean, 7A*. Plenum Press, New York, 89–121.

Duplessy, J.C., Blanc, P.L. and Bé, A.W.H., 1981. $\delta^{18}O$-enrichment of planktonic foraminifera due to gametogenetic calcification below the euphotic zone. *Science*, 213: 1247–1250.

Duque-Caro, H., 1990. Neogene stratigraphy, paleoceanography and paleobiogeography in northwest South America and the evolution of the Panama Seaway. *Palaeogeogr. Palaeoclimatol. Palaeoecol.*, *77*: 203–234.

Eberli, G.P., Swart, P.K., and Malone, M., (Eds.), 1997. *Proc. Ocean Drill. Program, Initial Report*, vol. 166, Ocean Drilling Program, College Station, Texas.

Elderfield, H. and Ganssen, G., 2000. Past temperature and $\delta^{18}O$ of surface ocean waters inferred from foraminiferal Mg/Ca ratios. *Nature*, 405: 442–445.

Enfield, D.B. and Lee, S submitted. The heat balance of the Western Hemisphere Warm Pool, *J. Clim.*

Fairbanks, R.G. and Wiebe, P.H., 1980. Foraminifera and chlorophyll maximum: Vertical distribution, seasonal succession, and paleoceanographic significance. *Science,* 209: 1524–1526.

Fairbanks, R.G., Wiebe, P.H. and Bé, A.W.H., 1980. Vertical distribution and isotopic composition of living planktonic foraminifera in the western North Atlantic. *Science*, 207: 61–63.

Fairbanks, R.G., Sverdlove, M., Free, R., Wiebe, P.H. and Bé, A.W.H., 1982. Vertical distribution and isotopic fractionation of living planktonic foraminifera from the Panama Basin. *Nature*, 298: 841–844.

Farrell, J.W. and Prell, W.L., 1991. Pacific $CaCO_3$ preservation and $\delta^{18}O$ since 4 Ma; paleoceanic and paleoclimatic implications. *Paleoceanography*, 6: 485–498.

Farrell, J.W., Raffi, I., Janecek, T.R., Murray, D.W., Levitan, M., Dadey, K.A., Emeis, K.C., Lyle, M., Flores, J.A. and Hovan, S., 1995. Late Neogene sedimentation patterns in the eastern equatorial Pacific Ocean. *In*: Pisias, N. G., Mayer, L. A., Janecek, T. R., Palmer-Julson, A., and van Andel, T. H. (Eds.), *Proc. Ocean Drill. Program Sci. Results*, 138: 717–756, College Station, TX (Ocean Drilling Program).

Faul, K., Ravelo, A.C. and Delaney, M.L., 2000. Changes in upwelling, productivity, and photic zone depth in the eastern equatorial Pacific Ocean over the last 50,000 years: A foraminiferal isotopic and abundance study. *J. Foram. Res.*, 30: 110–125.

Flohn, H., 1981. A hemispheric circulation asymmetry during late Tertiary. *Geol. Rundsch.*, 70: 725–736.

Flower, B.P., Oppo, D.W., McManus, J.F., Venz, K.A., Hodell, D.A. and Cullen, J.L., 2000. North Atlantic intermediate to deep water circulation and chemical stratification during the past 1 Myr. *Paleoceanography*, 15: 388-403.

Frank, M., Reynolds, B.C. and O'Nions, R.K., 1999. Nd and Pb isotopes in Atlantic and Pacific water masses before and after closure of the Panama gateway. *Geology*, 27: 1147–1150.

Gagan, M., Ayliffe, L., Hopley, D., Cale, J., Mortimer, G., Chappell, J., McCulloch, M. and Head, M., 1998. Temperature and surface ocean water balance of the mid-Holocene tropical western Pacific. *Science*, 279: 1014–1018.

Ganssen, G. and Sarnthein, M., 1983. Stable-isotope composition of foraminifers: the surface and bottom water record of coastal upwelling. *In:* Suess, E. and Thiede, J. (Eds.), *Coastal Upwelling, Its Sediment record, Part A*. Plenum Press, New York, pp. 99–121.

Gartner, S., Chow, J. and Stanton, R.J., 1987. Late Neogene paleoceanography of the eastern Caribbean, the Gulf of Mexico and the eastern equatorial Pacific. *Mar. Micropaleontol.*, 12: 255–304.

Gent, P.R. and McWilliams, J.C., 1990. Isopycnal mixing in ocean circulation models. *J. Phys. Oceanogr.,* 20: 150–155.

Godfrey, J.S., 1996. The effect of the Indonesian Throughflow on ocean circulation and heat exchange with the atmosphere: A review. *J. Geophys. Res.*, 101: 12,217–12,237.

Gregory-Wodzicki, K.M., 2000. Uplift history of the Central and Northern Andes: A review. *Geol. Soc. Am. Bull.*, 112: 1091–1105.

Groeneveld, J., Steph, S., Tiedemann, R., Garbe-Schönberg, D., Nürnberg, D. and Sturm, A., submitted (a). Pliocene mixed-layer oceanography for Site 1241, using combined Mg/Ca and $\delta^{18}O$ analyses of *Globigerinoides sacculifer*. *Proc. Ocean Drill. Program Sci. Results,* 202.

Groeneveld, J., Nürnberg, D., Steph, S., Tiedemann, R., Reichart, G.J., Reuning, L. and Crudeli, D., submitted (b). Pliocene increase of Mg/Ca SSTs in the Caribbean: Western Atlantic Warm Pool formation, salinity influence, or diagenetical overprint? *Geochem. Geophys. Geosyst.*

Halpern, D. and Weisberg, R., 1989. Upper ocean thermal flow fields at 0°N, 28°W (Atlantic) and 0°N, 140°W (Pacific) during 1983-1985. *Deep Sea Res. Part I*, 36: 407–408.

Hamilton, W., 1979. *Tectonics of the Indonesian region. U.S. Geological Survey Prof. Paper* 1078: 345 pp.

Haq, B.U., 1981. Paleogene paleoceanography: early Cenozoic oceans revisited. *Oceanol. Acta*, 4 (Suppl.): 71–82.

Harris, S. and Mix, A.C., 2002. Climate and tectonic influences on continental erosion in tropical South America. *Geology*, 30: 447–450.

Haug, G.H. and Tiedemann, R., 1998. Effect of the formation of the Isthmus of Panama on Atlantic Ocean thermohaline circulation. *Nature*, 393: 673–676.

Haug, G.H., Tiedemann, R., Zahn, R. and Ravelo, A.C., 2001a. Role of Panama uplift on oceanic freshwater balance. *Geology*, 29: 207–210.

Haug, G.H., Hughen, K.A., Sigman, D.M., Peterson, L.C. and Röhl, U., 2001b. Southward migration of the Intertropical Convergence Zone through the Holocene. *Science*, 293: 1304–1308.

Haug, G.H., Ganopolski, A., Sigman, D.M., Rosell-Mele, A., Swann, G.E.A., Tiedemann, R., Jaccard, S.L., Bollmann, J., Maslin, M.A., Leng, M. and Eglinton, G., 2005. North Pacific seasonality and the glaciation of North America 2.7 million years ago. *Nature*, 433: 821–825.

Hay, W.W., 1996. Tectonics and climate. *Geol. Rundsch.*, 85: 409–437.

Haywood, A.M., Sellwood, B.W. and Valdes, P.J., 2000. Regional warming; Pliocene (3 Ma) paleoclimate of Europe and the Mediterranean. *Geology,* 28: 1063–1066.

Haywood, A.M., Valdes, P.J. and Sellwood, B.W., 2002. Magnitude of Climate variability during middle Pliocene Warmth: A paleoclimate modeling study. *Palaeogeogr. Paleoclimatol. Palaeoecol.,* 188: 1–24.

Hellweger, F.L. and Gordon, A.L., 2002. Tracing Amazon River water into the Caribbean Sea. *J. Marine Res.*, 60–4: 537–549.

Heinze, C. and Crowley, T.J., 1997. Sedimentary response to ocean gateway circulation changes. *Paleoceanography*, 12–6: 742–754.

Hemleben, Ch. and Spindler, M., 1983. Recent advances in research on living planktonic foraminifera. *In:* Meulenkamp, J.E. (Ed.), *Reconstruction of Marine Paleoenvironments, Utrecht Micropaleontol. Bull.*, 30: 141–170.

Hilgen, F.J., 1991a. Astronomical calibration of Gauss to Matuyama sapropels in the Mediterranean and implication for the geomagnetic polarity time scale. *Earth Planet. Sci. Lett.*, 104: 226–244.

Hilgen, F.J., 1991b. Extension of the astronomically calibrated (polarity) time scale to the Miocene-Pliocene Boundary. *Earth Planet Sci. Lett.*, 107: 349–368.

Hilgen, F.J., Krijgsman, W., Langereis, C.G., Lourens, L.J., Santarelli, A. and Zachariasse, W.J., 1995. Extending the astronomical (polarity) time scale into the Miocene. *Earth Planet. Sci. Lett.*, 136: 495–510.

Hilgen, F.J., Aziz, H.A., Krijgsman, W., Langereis, C.G., Lourens, L.J., Meulenkamp, J.E., Raffi, I., Steenbrink, J., Turco, E., van Vugt, N., Wijbrans, J.R. and Zachariasse, W.J., 1999. Present status of the astronomical (polarity) time-scale for the Mediterranean Late Neogene. *Phil. Trans. Roy. Soc. of London Series a – Mathematical Physical and Engineering Sciences*, 357: 1931–1947.

Hilgen, F.J., Abdul Aziz, H., Krijgsman, W., Raffi, I. and Turco, E., 2003. Integrated stratigraphy and astronomical tuning of the Seravallian and lower Tortonian at Monte dei Corvi (Middle-Upper Miocene, Northern Italy). *Paleogeogr., Paleoclimatol., Paleoecol.*, 199: 229–264.

Hirst, A.C. and Godfrey, J.S., 1993. The role of Indonesian Throughflow in a Global Ocean GCM. *J. Phys. Oceanogr.*, 23: 1057–1086.

Hodell, D.A. and Venz, K., 1992. Toward a high resolution stable isotopic record of the Southern Ocean during the Pliocene-Pleistocene (4.8 – 0.8 Ma). *In:* Kennett, J.P., and Warnke, D.A. (Eds.), *The Antarctic Paleoenvironment: A perspective on Global Change (Pt.1). AGU, Antarctic Res. Ser.,* 56: 265–310.

Hoorn, C., Guerrero, J., Sarmiento, G.A. and Lorente, M.A., 1995. Andean tectonics as a cause for changing drainage patterns in Miocene South America. *Geology*, 23: 237–240.

Houghton, J.T., Meira Filho, L.G., Callander, B.A., Harris, N., Kattenberg, A. and Maskell, K., 1996. Climate Change 1995 – the Science of Climate Change*:* Contribution of WGI to the Second Assessment Report of the Intergovernmental Panel on Climate Change, Intergovernmental Panel on Climate Change. *Cambridge University Press.,* Cambridge (UK).

Houghton, J.T., 1997. Global Warming: The complete briefing. *Cambridge Univ. Press*, New York. 251 pp.

Hovan, S.A., 1995. Late Cenozoic atmospheric circulation intensity and climatic history recorded by aeolian deposition in the eastern equatorial Pacific, Leg 138. *In*: Pisias, N. G., Mayer, L. A., Janecek, T. R., Palmer-Julson, A., and van Andel, T. H. (Eds.), *Proc. Ocean Drill. Program Sci. Results*, 138: 615–625, College Station, TX (Ocean Drilling Program).

Huang, R.X., Cane, M.A., Naik, N. and Goodman, P., 2000. Global adjustment of the thermocline in response to deepwater formation. *Geophys. Res. Lett.*, 27–6: 759–762.

Hut, G., 1987. Stable isotope reference samples for geochemical and hydrological investigations. *Report to the Director General, Int. At. Energy Agency,* Vienna, 42 pp.

Intergovernmental Panel on Climate Change, (IPCC) 2001. Climate change 2001: The scientific Basis. *Cambridge Univ. Press*, New York, 2001. (Available at http://www.grida.no/-climate/ipcc_tar/wg1/index.htm).

Imbrie, J., Hays, J.D., Martinson, D.G., McIntyre, A., Mix, A.C., Morley, J.J., Pisias, N.G., Prell, W.L. and Shackleton, N.J., 1984. The orbital theory of Pleistocene climate: support from a revised chronology of the marine $\delta^{18}O$ record. *In:* Berger, A., Imbrie, J., Hays, J., Kukla G. and Satzman, B. (Eds.) *Milankovitch and Climate:* NATO ASI Ser. C, Math. Phys. Sci.,126: 269–305.

Imbrie, J. and Imbrie, J.Z., 1980. Modelling the climatic response to orbital variations. *Science*, 207: 943–953.

Jackson, J.B.C., Jung, P., Coates, A.G. and Collins, L.S., 1993. Diversity and Extinction of tropical American mollusks and Emergence of the Isthmus of Panama. *Science*, 260: 1624–1629.

Johns, W.E., Townsend, T.L., Fratantoni, D.M. and Wilson, W.D., 2002. On the Atlantic inflow to the Caribbean Sea. *Deep Sea Res. Part I*, 49: 211–243.

Johnson, G.C., McPhaden, M.J. and Firing, E., 2001. Equatorial Pacific Ocean horizontal velocity, divergence, and upwelling. *J. Phys. Oceanogr.*, 31: 839–849.

Joussaumme, S., Sadourny, R. and Vignal, C., 1986. Origin of precipitating water in a numerical simulation of the July climate. *Ocean-Air Interact.,* 1: 43–56.

Kaneps, A.G., 1970. Late Neogene (late Miocene – recent) biostratigraphy (planktonic foraminifers) biogeography and depositional history. Atlantic Ocean, Caribbean Sea, Gulf of Mexico (PhD Thesis, Columbia Univ.; New York).

Kameo, K. and Bralower, T. J., 2000. Neogene calcareous nannofossil biostratigraphy of sites 998, 999, and 1000, Caribbean Sea, *In:* Leckie, R.M., Sigurdsson, H., Acton, G.D., and Draper, G., (Eds.), *Proc. Ocean Drill. Program Sci. Results*, 165: 3–17, College Station, TX (Ocean Drilling Program).

Kameo, K. and Sato, T., 2000. Biogeography of Neogene calcareous nannofossils in the Caribbean and eastern equatorial Pacific – floral response to the emergence of the Isthmus of Panama. *Mar. Micropaleontol.*, 29: 201–218.

Keigwin, L.D., 1978. Pliocene closing of the Isthmus of Panama, based on biostratigraphic evidence from nearby Pacific Ocean and Caribbean Sea cores. *Geology*, 6: 630–634.

Keigwin, L.D., 1982a. Isotopic paleoceanography of the Caribbean and east Pacific: Role of Panama uplift in late Neogene time. *Science*, 217: 350–352.

Keigwin, L.D., 1982b. Neogene planktonic foraminifers from Deep Sea Drilling Project Sites 502 and 503. *In*: Prell, W.L., Gardner, J.V., et al. (Eds.), *Init. Repts. DSDP*, 68: 269–288, Washington (US. Gov. Printing Office).

Keller, G. and Barron, J.A., 1983. Paleoceanographic implications of Miocene deep-sea hiatuses. *Geol. Soc. Am. Bull.*, 94: 590–613.

Keller, G., Zenker, C.E. and Stone, S.M., 1989. Late Neogene history of the Pacific-Caribbean gateway. *J. South American Earth Sci.*, 2: 73–108.

Kemle-von-Mücke, S. and Oberhänsli, H., 1999. The distribution of living planktic foraminifera in relation to southeast Atlantic oceanography. *In:* Fischer, G. and Wefer, G. (Eds.), *Use of Proxies in Paleoceanography: Examples from the South Atlantic*. Springer-Verlag, Berlin, Heidelberg, pp. 91–115.

Kent, D.V., 1999. Orbital tuning of geomagnetic polarity time-scales. *Phil. Trans. Roy. Soc. London Series A-Mathematical Physical and Engineering Sciences*, 357:1995–2007.

Kennett, J.P. and Srinivasan, M.S., 1983. Neogene Planktonic Foraminifera. *Hutchinson Ross Publishing Company,* Stroudsburg, PA., 265 pp.

Kennett, J.P., Keller, G. and Srinivasan, M.S., 1985. Miocene planktonic foraminiferal biogeography and paleoceanographic development of the Indo-Pacific region. *In:* Kennett, J. P. (Ed.), *The Miocene Ocean: Paleoceanography and Biogeography, Mem. Geol. Soc. Amer.,* 163: 197–236.

Kim, S.-J. and Crowley, T.J., 2000. Increased Pliocene North Atlantic Deep Water: Cause or consequence of Pliocene warming? *Paleoceanography,* 15–4: 451–455.

Knowlton, N., Weight, L.A., Solorzano, L.A., Mills, D.K. and Bermingham, E., 1993. Divergence in proteins, mitochondrial DNA, and reproductive compatibility across the Isthmus of Panama. *Science*, 260: 1629–1632.

Krijgsman, W., Hilgen, F.J., Raffi, I., Sierro, F.J. and Wilson, D.S., 1999. Chronology, causes and progression of the Messinian salinity crisis. *Nature*, 400: 652–655.

Kroon, D., Williams, T.V., Pirmez, C., Spezaferri, S., Sato, T. and Wright, J.D., 2000. Coupled bio-cyclostratigraphy of Site 1006: evidence for orbitally induced carbonate platform production during the Mio- and Pliocene. *In:* Swart, P.K., Eberli, G.P., Malone, M.J., and Sarg, J.F. (Eds.), *Proc. Ocean Drill. Program Sci. Results*, 166: 155–166, College Station, TX (Ocean Drilling Program).

Kroopnick, P., 1974. The dissolved O_2 – CO_2 – ^{13}C system in the eastern Equatorial Pacific. *Deep Sea Res.*, 21: 211–227.

Kutzbach, J.E. and Guetter, P.J., 1986. The influence of changing orbital parameters and surface boundary conditions on climate simulations for the past 18,000 years, *J. Atmos. Sci.,* 43–16: 1726–1759.

Larsen, J.C., 1992. Transport and heat flux of the Florida Current at 27°N derived from the cross-steam voltages and profiling data: theory and observation. *Phil. Trans. Roy. Soc. London Series A-Mathematical Physical and Engineering Science*, 338: 169–236.

Laskar, J., 1990. The chaotic motion of the solar system: a numerical estimate of the size of the chaotic zones. *Icarus*, 88: 266–291.

Laskar, J., Joutel, F. and Boudin, F., 1993. Orbital, Precessional, and Insolation Quantities for the Earth from -20 Myr to +10 Myr. *Astronomy and Astrophysics*, 270: 522–533.

Laskar, J., 1999. The limits of Earth orbital calculations for geological time-scale use. *Phil. Trans. Roy. Soc. London Series A-Mathematical Physical and Engineering Sciences*, 357: 1735–1759.

Lawrence, K.T., Liu, Z. and Herbert, T.D., 2004. High latitude and tropical climates linked prior to the onset of the Northern Hemisphere Glaciation: Evidence from the eastern tropical Pacific. *EOS Trans*, AGU, 85–47: Fall Meeting Suppl., Abstract No.: PP23A–1397.

Lea, D.W., Mashiotta, T.A. and Spero, H.J., 1999. Controls of Magnesium and Strontium uptake in planktonic foraminifera determined by life culturing. *Geochim. Cosmochim. Acta*, 63: 2369–2379.

Leaman, K.D., Vertes, P.S., Atkinson, L.P., Lee, T.N. , Hamilton, P. and Waddell, E., 1995. Transport, potential vorticity, and current/temperature structures across Northwest Providence and Santaren Channels and the Florida Current off Cay Sal Bank. *J. Geophys. Res.*, (C5) 100: 8561–8570, 10.1029/94JC01436.

Lear, C.H., Rosenthal, Y. and Wright, J.D., 2003. The closing of a seaway: Ocean water masses and global climate change. *Earth Planet. Sci. Lett.*, 210: 425–437.

Leetma, A., 1982. Observations of near-equatorial flows in the eastern Pacific. *J. Mar. Res.*, 40 (Supplement): 357–370.

Levitus, S. and Boyer, T.P., 1994a. World Ocean Atlas 1994, vol. 4: Temperature. *US-Department of Commerce,* Washington DC., 99 pp.

Levitus, S. and Boyer, T.P., 1994b. World Ocean Atlas 1994, vol. 3: Salinity. *US-Department of Commerce*, Washington DC, 99 pp.

Lisiecki, L.E. and Raymo, M.E., 2005. A Pliocene-Pleistocene stack of 57 globally distributed benthic $\delta^{18}O$ records. *Paleoceanography*, 20: doi: 10.1029/2004PA001071.

Lohmann, G.P., 1995. A model for variations in the chemistry of planktonic foraminifera due to secondary calcification and selective dissolution. *Paleoceanography*, 10: 445–457.

Loubere, P., 2000. Marine control of biological production in the eastern equatorial Pacific Ocean. *Nature*, 406: 497–500.

Loubere, P., 2001. Nutrient and oceanographic changes in the eastern equatorial Pacific from the last full glacial to the present. *Global Planet. Change,* 29: 77–98.

Lourens, L.J., Antonarakou, A., Hilgen, F.J., Van Hoof, A.A.M., Grazzini, V.C. and Zachariasse, W.J., 1996. Evaluation of the Plio-Pleistocene astronomical timescale. *Paleoceanography*, 11: 391–413.

Lukas, R., 1986. The termination of the equatorial undercurrent in the eastern Pacific. *Prog. Oceanogr.,* 16: 63–90.

Lundelius, E.L. Jr., 1987. The North American Quaternary sequence. *In*: Woodburne, M.O., (Ed.) *Cenozoic mammals of North America,* University of California Press, 211–235.

Lyle, M., Dadey, K.A. and Farrell, J.W., 1995. The late Miocene (11 – 8 Ma) eastern Pacific carbonate crash: evidence for reorganization of deep-water circulation by closure of the Panama Gateway. *In:* Pisias, N.G., Mayer, L.A., Janecek, T.R., Palmer-Julson, A. and van Andel, T.H. (Eds.), *Proc. Ocean Drill. Program Sci. Results*, 138: 821–838, College Station, TX (Ocean Drilling Program).

Maier-Reimer, E., Mikolajewicz, U. and Hasselmann, K., 1990. Ocean general circulation model sensitivity experiments with an open Central American Isthmus. *Paleoceanography*, 5: 349–366.

Manabe, S., Stouffer, R.J., Spelman, M.J. and Bryan, K. 1991. Transient response of a coupled ocean-atmosphere model to gradual changes in CO_2, part I: Annual mean response. *J. Clim.,* 4: 785–818.

Marincovich, L. and Gladenkov, A.Y., 1998. An early opening of the Bering Strait. *Nature*, 307: 149–151.

Marshall, L.G., Webb, S.D., Sepkoski Jr., J.J., and Raup, D.M. 1982. Mammalian evolution and the great American interchange. *Science*, 215: 1351–1357.

Marshall, L.G., 1988. Land mammals and the Great American Interchange. *American Scientist*, 76: 380–388.

Mayer, L., Pisias, N., Janecek, T., et al., 1992. *Proc. Ocean Drill. Program, Initial Reports,* 138: College Station, TX (Ocean Drilling Program).

McCorkle, D.C. and Keigwin, L.D., 1994. Depth profiles of $\delta^{13}C$ in bottom water and core top *C. wuellerstorfi* on the Ontong Java Plateau and Emperor Seamounts. *Paleoceanography*, 9: 197–208.

McGlone, M., Kirshaw, A.P. and Margraf, V., 1992. El Niño/Southern Oscillation climatic variability in Australasian and South American paleoenvironmental records. *In:* Diaz, H. and Margraf, V. (Eds.), *El Niño. Historical and paleoclimatic aspects of the Southern Oscillation.* Cambridge University Press, New York, pp. 435–462.

McIntyre, A., Ruddiman, W., Karlin, K. and Mix, A.C., 1989. Glacial North Atlantic 18.000 years ago: A CLIMAP reconstruction. *In*: Cline, H.J. et al. (Eds.), *Investigations of Late Quaternary Paleoceanography and Paleoclimatology*. The Geological Society of America, Inc., pp. 43–76.

McKenna, V.S., Farrell, J.W., Murray, D.W. and Clemens, S.C., 1995. The foraminifer record of ODP Site 847: paleoceanographic response to late Pleistocene climate variability. *In*: Pisias, N.G., Mayer, L.A., Janecek, T.R., Palmer-Julson, A., and van Andel, T.H. (Eds.), *Proc. Ocean Drill. Program Sci. Results*, 138: 695–714, College Station, TX (Ocean Drilling Program).

McPhaden, M.J., 1986. The Equatorial Under Current: 100 years of Discovery. *EOS Trans.*, AGU, 67–40: 762–764.

Meschede, M. and Frisch, W., 1998. A plate-tectonic model for the Mesozoic and early Cenozoic history of the Caribbean plate. *Tectonophysics*, 296: 269–291.

Meschede, M., Zweigel, P. and Kiefer, E., 1999. Subsidence and extension at a convergent plate margin: evidence for subduction erosion off Costa Rica. *Terra Nova*, 11: 112–117.

Mikolajewicz, U., Santer, B.D. and Maier-Reimer, E., 1990. Ocean response to greenhouse warming. *Nature*, 345: 589–593.

Mikolajewicz, U., Maier-Reimer, E., Crowley, T. and Kim, K.-Y., 1993. Effect of Drake and Panamanian Gateways on the circulation of an ocean model. *Paleoceanography,* 8–4: 490–526.

Mikolajewicz, U. and Crowley, T.J., 1997. Response of a coupled ocean/energy balance model to restricted flow through the Central American Isthmus. *Paleoceanography*, 12: 429–441.

Milankovich, M., 1941. History of radiation on the earth and its use for the problem of the ice ages. *Serb. Akad. Beogr. Spec. Publ.* 132.

Millero, F.J., Yao, W., Lee, K., Zhang, J.-Z. and Campbell, D.M., 1998. Carbonate system in the waters near the Galapagos Islands. *Deep Sea Res. Part II*, 45: 1115–1134.

Mix, A.C., Pisias, N.G., Rugh, W., Wilson, J., Morey, A. and Hagelberg, T.K., 1995. Benthic foraminifer stable isotope record from Site 849 (0 – 5 Ma); local and global climate changes. *In:* Pisias, N.G., Mayer, L.A., Janecek, T.R. (Eds.), *Proc. Ocean Drill. Program Sci. Results,* 138: 371–412, College Station, TX (Ocean Drilling Program).

Mix, A.C., Tiedemann, R., Blum, P., et al., 2003. *Proc. Ocean Drill. Program Initial Reports,* vol. 202, College Station, TX (Ocean Drilling Program).

Molinari, R., Johns, E. and Festa, J.F., 1990. The annual cycle of meridional heat flux in the Atlantic Ocean at 26.5°N. *J. Phys. Oceanogr.*, 20: 476–482.

Molnar, P. and Cane, M.A., 2002. El Niño's tropical climate and teleconnections as a blueprint for pre-Ice Age climates. *Paleoceanography*, 17–2: doi: 10.1029/2001PA000663.

Montgomery, D.R., Balco, G. and Willett, S.D., 2001. Climate, tectonics, and the morphology of the Andes. *Geology*, 29: 579–582.

Moore, T.C.Jr., Shackleton, N.J. and Pisias, N.G., 1993. Paleoceanography and the diachrony of radiolarian events in the eastern equatorial Pacific. *Paleoceanography*, 8: 567–586.

Müller-Karger, F.E., McClain, C.R., Fisher, T.R., Esaias, W.E. and Varela, R., 1989. Pigment distribution in the Caribbean Sea: Observations from space. *Progr. Oceanogr.*, 23: 23–64.

Mulitza, S., Donner, B., Fischer, G., Paul, A., Pätzold, J., Rühlemann, C. and Segl, M., 2004. The South Atlantic oxygen-isotope record of planktic foraminifera. *In:* Fischer, G. and Wefer, G. (Eds.), *The South Atlantic in the Late Quaternary: Reconstruction of mass budget and current systems*. Springer Verlag, Berlin, Heidelberg, pp. 121–142.

Murdock, T.Q., Weaver, A.J. and Fanning, A.F., 1997. Paleoclimatic response of the closing of the Isthmus of Panama in a coupled ocean-atmosphere model. *Geophys. Res. Lett.*, 24–3: 253–256.

Niebler, H.-S., Hubberten, H.-W. and Gersonde, R., 1999. Oxygen isotope values of planktic foraminifera: A tool for the reconstruction of surface water stratification. *In*: Fischer, G. and Wefer, G. (Eds.), *Use of Proxies in Paleoceanography*. Springer-Verlag, New York, pp.165–189.

Ninnemann, U. and Charles, C., 1997. Regional differences in Quaternary subantarctic nutrient cycling: Link to intermediate and deep water ventilation. *Paleoceanography*, 12–4: 560–567.

Nisancioglu, K.H., Raymo, M.E. and Stone, P.H., 2003. Reorganization of Miocene deep-water circulation in response to the shoaling of the Central American Seaway. *Paleoceanography*, 18–1: doi: 10.1029/2002PA000767.

Nof, D. and van Gorder, S., 2003. Did an open Panama Isthmus correspond to an invasion of Pacific water into the Atlantic? *J. Phys. Oceanogr.,* 33–7: 1324–1336.

Norris, R.D., 1998. Miocene-Pliocene surface water hydrography of the eastern equatorial Atlantic. *In:* Mascle, J., Lohmann, G.P., and Moullade, M. (Eds.), *Proc. Ocean Drill. Program Sci. Results*, 159: 539–555, College Station, TX (Ocean Drilling Program).

Nürnberg, D., Bijma, J. and Hemleben, C., 1996. Assessing the reliability of magnesium in foraminiferal calcite as a proxy for water mass temperatures. *Geochim. Cosmochim. Acta,* 60: 803–814.

Nürnberg, D., 2000. Taking the temperature of past ocean surfaces. *Science,* 289: 1698–1699.

Nürnberg, D., Müller, A. and Schneider, R., 2000. Paleo-seasurface temperature estimations in the equatorial east Atlantic from Mg/Ca ratios in planktic foraminifers – A comparison to SST estimates from UK´37, oxygen isotopes, and foraminiferal transfer function. *Paleoceanography*, 15: 124–134.

Nürnberg, D., Schönfeld, J., Dullo, W.-Chr., Rühlemann, C. et al., 2002. Rapid Climate Changes in the Western Tropical Atlantic – Assessment of the biogenous and sedimentary record. *R/V Sonne Cruise Report SO164*, Geomar Rept., 109, Kiel, 151 pp.

Ocean Climate Laboratory, 1999. *World Ocean Atlas 1998 (WOA98)* [CD-ROM]. Available from: National Climatic Data Center, Asheville NC 28801–5001, USA.

Ocean Climate Laboratory, 2001. *World Ocean Atlas 2001 (WOA01)*. Available at: www.nodc.noaa.gov/OC5/WOD01/pacif_s.html.

O'Neil, J.R., Clayton, R.N. and Mayeda, T.K., 1969. Oxygen isotope fractionation in divalent metal carbonates. *J. Chem. Phys.*, 51: 5547–5558.

Oppo, D. and Fairbanks, R.G., 1989. Carbon isotope composition of tropical surface water during the past 22,000 years. *Paleoceanography,* 4–4: 333–352.

Oppo, D.W., Raymo, M.E., Lohmann, G.P., Mix, A.C., Wright, J.D. and Prell, W.L., 1995. A $\delta^{13}C$ record of upper North Atlantic Deep Water during the past 2.6 million years. *Paleoceanography*, 5: 43–54.

Ortiz, J.D., Mix, A.C. and Collier, R.W., 1995. Environmental control of living symbiotic and asymbiotic foraminifera of the California Current. *Paleoceanography,* 10: 987–1009.

Ortiz, J.D., Mix, A.C., Rugh, W., Watkins, J.M. and Collier, R.W., 1996. Deep-dwelling planktonic foraminifera of the northeastern Pacific Ocean reveal environmental control of oxygen and carbon isotopic disequilibria. *Geochim. Cosmochim. Acta*, 60: 4509–4523.

Ortiz, J.D., Mix, A.C., Hostetler, S. and Kashgarian, M., 1997. The California Current of the last glacial maximum: Reconstruction at 42°N based on multiple proxies. *Paleoceanography*, 12: 191–205.

Ottens, J. J., 1992. Spatial dynamics of planktic foraminifera in the Northeast Atlantic. *In*: Ottens, J. J. (Ed.), *Planktonic foraminifera as indicators of ocean environments in the Northeastern Atlantic.* Academisch Proefschrift, Vrije Universiteit te Amsterdam, pp. 109–147.

Pacanowski, R.C., 1995. MOM 2: Documentation, User's Guide and Reference Manual, *Tech. Rep. 3, Geophys. Fluid Dyn. Lab. Ocean Group,* Princeton, N.Y.

Paillard, D., Labeyrie, L.D. and Yiou, P., 1996. Macintosh program performs time-series analysis. *EOS Trans. AGU*, 77: 379.

Pak, H. and Zanefeld, J.R.V., 1973. The Cromwell Current on the east side of the Galapagos Islands. *J. Geophys. Res.*, 78: 7845–7859.

Parker, F.L., 1967. Late Tertiary biostratigraphy (planktonic foraminifera) of tropical Indo-Pacific deep-sea cores. *Bull. Am. Paleontol.*, 52: 112–208.

Pälike, H. and Shackleton, N.J., 2000. Constraints on astronomical parameters from the geological record for the last 25 Myr. *Earth Planet. Sci. Lett.*, 182: 1–14.

Pearson, P.N., and Palmer, M.R., 2000. Atmospheric carbon dioxide concentrations over the past 60 million years. *Nature*, 406: 695–699.

Philander, S.G.H., 1973. Equatorial Under Current: Measurements and Theories. *Rev. Geophys* 11–3: 513–570.

Philander, S.G.H. and Pacanowski, R.C., 1986. A model of the seasonal cyle in the tropical Atlantic. *J. Geophys. Res.*, C12, 91: doi: 14192–14206.

Philander, S.G.H., Gu, D., Halpern, D., Lambert, G., Lau, N.C., Li, T. and Pacanowski, R.C., 1996. Why the ITCZ is mostly north of the Equator. *J. Clim.*, 9: 2958–2972.

Philander, S.G.H. and Fedorov, A. V., 2003. Role of tropics in changing the response to Milankovich forcing some three million years ago. *Paleooceanography,* 18–2: doi: 10.1029/2002PA0008372003.

Pisias, N.G., Mayer, L.A. and Mix, A.C., 1995. Paleoceanography of the eastern equatorial Pacific during the Neogene: synthesis of Leg 138 drilling results. In: Pisias, N.G., Mayer, L.A., Janecek, T.R., Palmer-Julson, A., and van Andel, T.H. (Eds.), *Proc. Ocean Drill. Program Sci. Results,* 138: 5–21, College Station, TX (Ocean Drilling Program).

Prange, M. and Schulz, M., 2004. A coastal upwelling seasaw in the Atlantic Ocean as a result of the closure of the Central American Seaway. *J. Geophys. Res.,* 31: doi: 10.1029/2004GL020073.

Raffi, I. and Flores, J.A., 1995. Pleistocene through Miocene calcareous nannofossils from the eastern equatorial Pacific Ocean (Leg 138). *In:* Pisias, N.G., Mayer, L.A., Janecek, T.R. Palmer-Julson, A., and van Andel, T.H. (Eds.), *Proc. Ocean Drill. Program Sci. Results,* 138: 233–282, College Station, TX (Ocean Drilling Program).

Ravelo, A.C., Fairbanks, R.G. and Philander, S.G.H., 1990. Reconstructing tropical Atlantic hydrography using planktonic foraminifera and an ocean model. *Paleoceanography,* 5: 409–431.

Ravelo, A.C. and Fairbanks, R.G., 1992. Oxygen isotopic composition of multiple species of planktonic foraminifera: recorders of the modern photic zone temperature gradient. *Paleoceanography*, 7: 815–832.

Ravelo, A.C. and Shackleton, N.J., 1995. Evolution of surface water circulation in the east equatorial Pacific over the past 2.0 Ma: Isotopic measurements from ODP Site 851. *In:* Pisias, N.G., Mayer, L.A., Janecek, T.R., Palmer-Julson, A., and van Andel, T.H. (Eds.), *Proc. Ocean Drill. Program Sci. Results,* 138: 503–514, College Station, TX (Ocean Drilling Program).

Ravelo, A.C. and Andreasen, D.H., 1999. Using planktonic foraminifera as monitors of the tropical surface ocean. *In:* Abrantes, F. and Mix, A. (Eds.), *Reconstructing Ocean History - A window into the future*. Plenum Press, New York, 217–244.

Ravelo, A.C. and Andreasen, D.H., 2000. Enhanced circulation during a warm period. *Geophys. Res. Lett.*, 27: 1001–1004.

Ravelo, A.C., Andreasen, D.H., Lyle, M., Lyle, A.O. and Wara, M.W., 2004. Regional climate shifts caused by gradual global cooling in the Pliocene epoch. *Nature*, 429: 263–267.

Raymo, M.E., Ruddiman, W.F., Backman, J., Clement, B.M. and Martinson, D.G., 1989. Late Pliocene variations in northern hemisphere ice sheets and North Atlantic deep water circulation. *Paleoceanography*, 4: 413–446.

Raymo, M.E. and Ruddiman, W.F., 1992. Tectonic forcing of late Cenozoic climate. *Nature*, 359: 117–122.

Raymo, M.E., Hodell, D. and Jansen, E., 1992. Response of deep ocean circulation to initiation of Northern Hemisphere glaciation (3-2 Ma). *Paleoceanography*, 7: 645–672.

Raymo, M.E., Grant, B., Horowitz, M. and Rau, G.H., 1996. Mid-Pliocene warmth: stronger greenhouse and stronger conveyor. *Mar. Micropaleontol.*, 27: 313–326.

Raymo, M.E., 1997. Thermohaline circulation of the deep North Atlantic in the early Pliocene: No evidence for major changes. *EOS Trans.*, AGU, 78–46: 56

Reijmer, J.J.G., Betzler, C., Kroon, D., Tiedemann, R. and Eberli, G.P., 2002. Bahamian platform development in response to sea-level changes and the closure of the Isthmus of Panama. *Int. J. Earth Sciences*, 91: 482–489.

Reuning, L., Reijmer, J.J.G., Betzler, C., Timmermann, A. and Steph, S., submitted. The semiprecessional cycle of sea surface temperature (SST) as a modern analogue for the generation of semiprecessional cycles in the early Pliocene. *Paleoceanography*.

Rind, D. and Chandler, M., 1991. Increased ocean heat transports and warmer climate. *J. Geophys. Res.*, 96: 7437–7461.

River Discharge Database, 2003. Center for Sustainability and Global Environment, Gaylord Nelson Institute for environmental studies, University of Wisconsin-Madison, h*ttp://www.sage.wisc.edu/riverdata*

Rodbell, D.T., Seltzer, G.O., Anderson, D.M., Abbott, M.A., Enfield, D.B. and Newman, J.H., 1999. An ~15,000 year record of El Niño-driven alluviation in southwestern Equador. *Science*, 283: 516–520.

Roth, J.M., Droxler, A.W. and Kameo, K., 2000. The Caribbean Carbonate Crash at the middle to late Miocene transition: linkage to the establishment of the modern global ocean conveyor. *In:* Leckie, R.M., Sigurdsson, H., Acton, G.D., and Draper, G., (Eds.), *Proc. Ocean Drill. Program Sci. Results*, 165: 249–273, College Station, TX (Ocean Drilling Program).

Ruddiman, W.F., Backman, J., Baldauf, P., Hooper, L., Keigwin, L.D., Miller, K., Raymo, M. and E. Thomas, 1986. Leg 94 paleoenvironmental synthesis. *In:* Ruddiman, W.F., Kidd, R.B., et al. (Eds.) *Init. Rept. DSDP,* 94: 1207–1215, Washington (U.S. Gov. Printing Office*).*

Ruddiman, W.F., Cameron, D. and Clement, B.M., 1987. Sediment disturbance and correlation of offset holes drilled with the hydraulic piston corer; Leg 94. *In:* Ruddiman W.F., Kidd, R.B., Baldauf, J.G. (Eds.), *Proc. DSDP, Sci. Results,* 94: 615–634, College Station, TX (Ocean Drilling Program).

Ruddiman, W.F. and Raymo, M.E., 1988. Northern Hemisphere climate regimes during the past 3 Ma: Possible tectonic connections. *Phil. Trans. R. Soc. London*, B 318: 411–430.

Saito, T., 1976. Geologic significance of coiling direction in the planktonic foraminifer *Pulleniatina*. *Geology*, 4: 305–309.

Sautter, L.R. and Thunell, R.C., 1991. Planktonic foraminiferal response to upwelling and seasonal hydrographic conditions: Sediment trap results from San Pedro Basin, Southern California Bight. *J. Foram. Res.,* 21: 347–363.

Savin, S.M. and Douglas, R.G., 1985. Sea level, climate, and the Central American Land Bridge. *In:* Stehli, F.G. and Webb, S.D. (Eds.), *The Central American Land Bridge*. Plenum Press, New York, pp. 303–324.

Schmidt, G.A., Bigg, G.R. and Rohling, E.J., 1999. Global Seawater-$\delta^{18}O$ Database. *http://www.giss.nasa.gov/data/o18data/*.

Schmuker, B. and Schiebel, R., 2002. Planktic foraminifers and hydrography of the eastern and northern Caribbean Sea. *Mar. Micropaleontol.*, 46: 387–403.

Schneider, B. and Schmittner, A., submitted. Simulating the impact of the Panamanian Seaway closure on ocean circulation, marine productivity, and nutrient cycling. *Paleoceanography*.

Schott, F.A., Lee, T.N. and Zantopp, R., 1988. Variability of structure and transport of the Florida Current in the period range of days to seasonal. *J. Phys. Oceanogr.*, 18–9: 1209–1230.

Shackleton, N.J., 1974. Attainment of isotopic equilibrium between ocean water and the benthonic foraminifera genus *Uvigerina*: Isotopic changes in the ocean during the last glacial. *Colloq. Int. C.N.R.S*, 219.

Shackleton, N.J., 1977. Carbon-13 in *Uvigerina*; tropical rainforest history and the equatorial Pacific carbonate dissolution cycles. *In:* Andersen, N.R., and Malahoff, A. (Eds.), *The fate of fossil fuel CO_2 in the oceans*. Plenum Press, New York, pp. 401–427.

Shackleton, N.J. and Hall, M.A., 1984. Oxygen and Carbon isotope stratigraphy of Deep Sea Drilling Project Hole 552A: Plio-Pleistocene glacial history. *Init. Rept. DSDP*, 81: 599–629, College Station, TX (Ocean Drilling Program).

Shackleton, N.J., and Hall, M.A., 1995. Stable isotope records in bulk sediments (Leg138). *In:* Pisias, N. G., Mayer, L. A., Janecek, T. R., Palmer-Julson, A., and van Andel, T. H. (Eds.), *Proc. Ocean Drill. Program Sci. Results,* 138: 797–805, College Station, TX (Ocean Drilling Program).

Shackleton, N.J., Hall., M.A. and Pate, D., 1995. Pliocene stable isotope stratigraphy of Site 846. *In:* Pisias, N. G., Mayer, L. A., Janecek, T. R., Palmer-Julson, A., and van Andel, T. H. (Eds.), *Proc. Ocean Drill. Program Sci. Results,* 138: 337–355, College Station, TX (Ocean Drilling Program).

Shackleton, N.J. and Crowhurst, S.J., 1997. Sediment fluxes based on an orbitally tuned time scale 5 Ma to 14 Ma, Site 926. *In:* Curry, W.B., Shackleton N.J., Richter, C. (Eds.), *Proc. Ocean Drill. Program Sci. Results,* 154: 69–82, College Station, TX (Ocean Drilling Program).

Shackleton, N.J. and Hall, M.A., 1997. The late Miocene stable isotope record, Site 926. *In:* Curry, W.B., Shackleton N.J., Richter, C. (Eds.), *Proc. Ocean Drill. Program Sci. Results,* 154: 367–373, College Station, TX (Ocean Drilling Program).

Shackleton, N.J., Crowhurst, S.J., Weedon, G.P. and Laskar, J., 1999. Astronomical calibration of Oligocene-Miocene time. *Phil. Trans. Roy. Soc. London Series A-Mathematical Physical and Engineering Sciences*, 357: 1907–1929.

Sigurdsson, H., Leckie, R.M., Acton, G.D., et al., 1997. *Proc. Ocean Drill. Program, Initial Reports,* vol. 165, College Station, Tex.

Sloan, L.C., Crowley, T.J. and Pollard, D., 1996. Modeling of middle Pliocene climate with the NCAR GENESIS general circulation model. *Mar. Micropaleontol.*, 27: 51–61.

Slowey, N.C. and Curry, W.B., 1995. Glacial-interglacial differences in circulation and carbon cycling within the upper western North Atlantic. *Paleoceanography*, 10: 715–732.

Spero, H.J. and Lea, D.W., 2002. The Cause of Carbon Isotope Minimum Events on Glacial Terminations. *Science*, 296: 522–525.

Spero H.J., Mielke, K.M., Kalve, E.M., Lea, D.W. and Pak, D.K., 2003. Multispecies approach to reconstructing eastern equatorial Pacific thermocline hydrography during the past 360 kyr. *Paleoceanography,* 18–1: doi: 10.1029/2002PA000814.

Srinivasan M.S. and Kennett, J.P., 1976. Evolution and phenotypic variation in the Late Cenozoic *Neogloboquadrina dutertrei* plexus. *In:* Takayanagi, Y., and Saito, T. (Eds.), *Progress in Micropaleontology*, American Museum of Natural History Micropaleontology Press, pp. 329–355.

Steger, J.M., Collins, C.A. and Chu, P.C., 1998. Circulation in the Archipelago de Colon (Galapagos Islands), November, 1993. *Deep Sea Res., Part II,* 45: 1093–1114.

Steph, S., Tiedemann, R., Groeneveld, J., Nürnberg, D., Reuning, L. and Haug, G.H. submitted (a). Changes in Caribbean surface hydrography during the Pliocene shoaling of the Central American Seaway. *Paleoceanography.*

Steph, S., Tiedemann, R., Groeneveld, J., Sturm, A. and Nürnberg, D., submitted (b). Pliocene changes in tropical east Pacific upper ocean stratification: Response to tropical gateways? *Proc. Ocean Drill. Program Sci. Results,* 202.

Stevenson, M.R. and Taft, B.A., 1971. New evidence of the Equatorial Undercurrent east of the Galapagos Islands. *J. Marine Res.*, 29: 103–115.

Strub, P.T., Mesias, J.M., Montecino, V., Rutllant, J. and Salinas, S., 1998. Coastal ocean circulation off western South America. *In:* Robinson, A.R. et al. (Eds.), *The Sea* (Vol. 11)*: Coastal Oceans*. New York (Wiley), 273–313.

Thunell, R.C. and Sautter, L.R., 1992. Planktonic foraminiferal faunal and stable isotopic indices of upwelling: A sediment trap study in the San Pedro Basin, Southern California Bight. *In:* Summerhayes, C.P., Prell, W.L., and Emeis, K.C. (Eds.), *Upwelling Systems: Evolution Since the Early Miocene*. *Geol. Soc. Spec. Publ.,* 64, London, pp. 77–91.

Tiedemann, R., Sarnthein, M. and Stein, R., 1989. Climatic changes in the western Sahara: Paleo-marine sediment record of the last 8 million years (Sites 657 – 661). *In:* Ruddiman, W., Sarnthein, M., et al. (Eds). *Proc. Ocean Drill. Program Sci. Results*, 108: 241–277, College Station, TX. (Ocean Drilling Program).

Tiedemann, R., Sarnthein, M. and Shackleton, N.J., 1994. Astronomic timescale for the Pliocene Atlantic $\delta^{18}O$ and dust flux records of Ocean Drilling Program Site 659. *Paleoceanography*. 9: 619–638.

Tiedemann, R. and Franz, S.O., 1997. Deep-water circulation, chemistry, and terrigenous sediment supply in the Equatorial Atlantic during the Pliocene, 3.3 – 2.6 Ma and 5 – 4.5 Ma. *In:* Curry, W.B., Shackleton N.J., Richter, C. (Eds.), *Proc. Ocean Drill. Program Sci. Results,* 154: 299–318, College Station, TX (Ocean Drilling Program).

Tiedemann, R., Franz, S.O. and Billups, K., 1997. A critical threshold in the Pliocene closure history of the Central American Isthmus. *EOS Trans.,* AGU, 78 – 46: 56.

Tiedemann, R., Sturm, A., Steph, S., Lund, S.P. and Stoner, J.S., submitted. Astronomically calibrated time scales from 6 – 2.5 Ma and benthic isotope stratigraphies of Sites 1236, 1237, 1239 and 1241. *Proc. Ocean Drill. Program Sci. Results,* 202.

Toggweiler, J.R., Dixon, K. and Broecker, W.S., 1991. The Peru upwelling and the ventilation of the South Pacific thermocline. *J. Geophys. Res.*, C11, 96: 20,467–20,497. doi: 10.1029/91JC02063.

Tudhope, A.W., Chilcott, C.P., McCulloch, M.T., Cook, E.R., Chappell, J., Ellam, R.M., Lea, D.W., Lough, J.M. and Shimmield, G.B., 2001. Variability in the El Niño-Southern Oscillation through a glacial-interglacial cycle. *Science*, 291: 1511–1516.

Van der Burgh, J., Visscher, H., Dilcher, D.L. and Kürschner, W.M., 1993. Paleoatmospheric signatures in Neogene fossil leaves. *Science*, 260: 1788–1790.

Wallace, J.M., Rasmusson, E.M., Mitchell, T.P., Kousky, V.E., Sarachik, E.S. and von Storch, H., 1998. On the structure and evolution of ENSO-related climate variability in the tropical Pacific: Lessons from Toga. *J. Geophys. Res.,* 103: 14,241–14,259.

Wang, L., 1994. Sea surface temperature history of the low latitude western Pacific during the last 5.3 million years. *Palaeogeogr., Palaeoclimatol., Palaeoecol.,* 108: 379–436.

Watkins, J. and Mix, A.C., 1998. Testing the effects of tropical temperature, productivity, and mixed-layer depth on foraminiferal transfer functions. *Paleoceanography* 13–1: 96–105.

Watkins, J.M., Mix A.C. and Wilson, J., 1998. Living planktic foraminifera in the central tropical Pacific Ocean: articulating the equatorial "cold tongue" during La Niña, 1992. *Mar. Micropaleontol.*, 33: 157–174.

Weaver, A.J.e.a., 2001. The UVic Earth System Climate Model: Model description, climatology, and applications to past, present and future climates. *Atmos. Ocean*, 4: 361–428.

Webb, S.D., 1985. Late Cenozoic mammal dispersals between the Americas. *In:* Stehli, F.G. and Webb, S.D. (Eds.), *The Great American Biotic Interchange*. Plenum Press, New York, pp. 357–386.

Weyl, P.K., 1968. The role of the oceans in climate change; a theory of the ice ages. *Meteorological Monographs*, 8: 37–62.

Whitehead, J.M. and Bohaty, S.M., 2003. Pliocene summer sea surface temperature reconstruction using silicoflagellates from Southern Ocean ODP Site 1165. *Paleoceanography,* 18–3: doi: 10.1029/2002PA000829.

Whitman, J.M. and Berger, W.H., 1993. Pliocene-Pleistocene Carbon Isotope Record - Site 586, Ontong Java Plateau. *In*: Berger, W.H., Kroenke, L.W., Mayer, L.A., et al. (Eds.), *Proc Ocean Drill. Program Sci. Results*, 130: 333–348, College Station, TX (Ocean Drilling Program).

Wüst G., 1964. *Stratification and Circulation in the Antillean-Caribbean Basins, Part 1: Spreading and Mixing of the Water Types with an Oceanographic Atlas*. Columbia University Press, London and New York.

Wyrtki, K., 1966. Oceanography of the eastern equatorial Pacific Ocean. *Oceanography and Marine Biology. An Annual Review*, 4: 33–68.

Wyrtki, K., 1981. An estimate of equatorial upwelling in the Pacific. *J. Phys. Oceanogr.,* 11: 1205–1214.

Zahn, R. and Stüber, A., 2002. Suborbital intermediate water variability inferred from paired benthic foraminiferal Cd/Ca and $\delta^{13}C$ in the tropical West Atlantic and linking with North Atlantic climates. *Earth Planet. Sci. Let.*, 200: 191–205.